12th INTERNATIONAL SYMPOSIUM

Advanced Display Technologies: Basic Studies of Problems in Information Display (FLOWERS'2003)

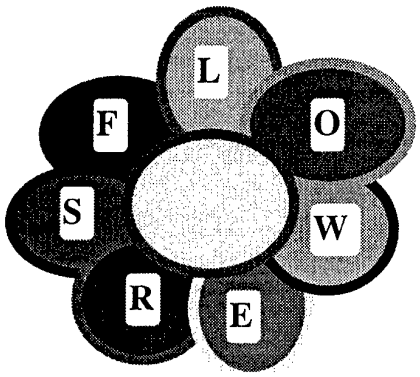

SYMPOSIUM PROCEEDINGS

August 25 –28, 2003
Korolev, Moscow Region, Russia

Organized by
SID Russia Chapter
SID Belorussia Chapter
SID Ukraine Chapter
Lebedev Physical Institute of Russian Academy of Sciences
Korolev City Administration
Mashpribor Institute, Korolev

Sponsored by
SID – The International Society for Information Display
Ministry of Industry, Science and Technology of the Russian Federation
European Office of Aerospace Research and Development of the USAF
SPIE – The International Society for Optical Engineering
SID Texas Chapter

REPORT DOCUMENTATION PAGE

Form Approved OMB No. 0704-0188

1. REPORT DATE *(DD-MM-YYYY)*	2. REPORT TYPE	3. DATES COVERED *(From – To)*
16-11-2004	Conference Proceedings	25 August 2003 - 27 August 2003

4. TITLE AND SUBTITLE

12th International Symposium Advanced Display Technologies: Basic Studies of Problems in Information Display (FLOWERS 2003)

5a. CONTRACT NUMBER
FA8655-03-1-5059

5b. GRANT NUMBER

5c. PROGRAM ELEMENT NUMBER

6. AUTHOR(S)

Conference Committee

5d. PROJECT NUMBER

5d. TASK NUMBER

5e. WORK UNIT NUMBER

7. PERFORMING ORGANIZATION NAME(S) AND ADDRESS(ES)

P. N. Lebedev Physical Institute of the Russian Academy of Sciences
Leninsky prospect, 53
Moscow 119991
Russia

8. PERFORMING ORGANIZATION REPORT NUMBER

N/A

9. SPONSORING/MONITORING AGENCY NAME(S) AND ADDRESS(ES)

EOARD
PSC 802 BOX 14
FPO 09499-0014

10. SPONSOR/MONITOR'S ACRONYM(S)

11. SPONSOR/MONITOR'S REPORT NUMBER(S)
CSP 03-5059

12. DISTRIBUTION/AVAILABILITY STATEMENT

Approved for public release; distribution is unlimited. (approval given by local Public Affairs Office)

13. SUPPLEMENTARY NOTES

14. ABSTRACT

The Final Proceedings for 12th International Symposium Advanced Display Technologies, 25 August 2003 - 27 August 2003

This is a multidisciplinary conference centered on development of display capabilities. Topics to be presented include Field Emission Displays, Liquid Crystal Displays, Organic Luminescent Displays, W = V + V = Vacuum Fluorescent Displays + Volume Vision, Electroluminescent & Electrochromic Displays & Ergonomics,Ray-Tubes, Selected Developments (PDP, Projection Devices, Civilian and Military Applications etc.)

15. SUBJECT TERMS

EOARD, Displays, Human Factors, Operator-Machine Interface

16. SECURITY CLASSIFICATION OF:			17. LIMITATION OF ABSTRACT	18. NUMBER OF PAGES	19a. NAME OF RESPONSIBLE PERSON
a. REPORT	b. ABSTRACT	c. THIS PAGE			VALERIE E. MARTINDALE, Lt Col, USAF
UNCLAS	UNCLAS	UNCLAS	UL	246	19b. TELEPHONE NUMBER *(include area code)* +44 (0)20 7514 4437

12th INTERNATIONAL SYMPOSIUM

Advanced Display Technologies: Basic Studies of Problems in Information Display (FLOWERS'2003)

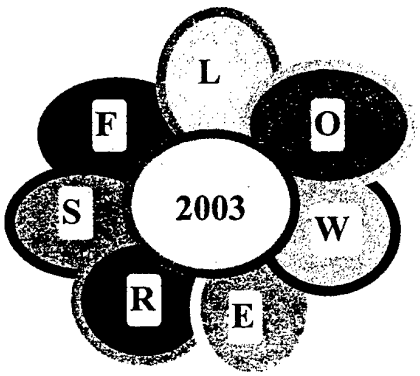

SYMPOSIUM PROCEEDINGS

August 25 –28, 2003

Korolev, Moscow Region, Russia

Moscow

SID Russia Chapter

2003

We wish to thank the following for their contribution to the success of this conference:

SID – The International Society for Information Display,
Ministry of Industry, Science and Technology of the Russian Federation,
European Office of Aerospace Research and Development of the USAF,
SPIE – The International Society for Optical Engineering,
SID Texas Chapter,
LG Technology Center of Moscow

We are grateful for the information support to magazines:

Information Displays (SID, USA)
Electronic Components (Russia)
Electronics: Science, Technology Business (Russia)
Inventor (Russia)
Quantum Electronics (Russia)
Telecommunications and Radio Engineering (Russia)

ORGANIZING COMMITTEE

Oleg Krokhin (Russia), Chair

Igor Litvak(Russia), Co-Chair

Alexander Smirnov(Belarus), Co-Chair

Victor Sorokin(Ukraine), Co-Chair

Allan Kmetz(USA), SID President

Aris Silzars(USA), SID Past-President

Jean-Pierre Budin (France), SID Regional Vice-President, Europe

Myung Hwan Oh (Korea), SID Regional Vice-President, Asia

Munisamy Anandan (USA), SID Regional Vice-President, Americas

Jenny Needham (USA), SID Administrator

Victor Belyaev (Russia), International Committee Chair

Igor Kompanets (Russia), Program Committee Chair

Vladimir Samsonov (Russia), Local Committee Chair

Edward Goushchin (Russia), Exhibition Committee Chair

Zvi Yaniv (USA), Invention Committee Chair

Irina Revokatova (Russia), SID Russia Chapter Treasurer & Secretary

Edmund Akopov (Russia), SPIE Russia Chapter

Boris Gorfinkel (Russia)

Alexei Ivlyushkin (Russia)

Maxim Tomilin (Russia)

Sofiya Torgova (Russia), Liquid Crystal Society SODRUZHESTVO

Yuri Tzirkunov (Ukraine)

Ken Werner (USA)

PROGRAM COMMITTEE

Igor Kompanets (Russia), Chair

Vladimir Brezhnev (Russia) – LCD

Vladimir Feofanov (Russia) – applications

Wolfgang Haase (Germany) - materials

Rauzah Hashim (Malaysia) – materials

Boris Kogan (Russia) – PDP

Vladimir Kustov (Russia) – OLED

Igor Litvak (Russia) – ergonomics, standards

Anatoly Mikhalchenkov (Russia) – CRT, LCD

Elena Novikova (Russia) - projection displays

Lee Soon Park (Korea) - LCD

Alexander Rakhimov (Russia) – FED, CNT

Alexander Sadchikhin (Russia) - projection displays

Vladislav Samorodov (Russia) - PDP

Kent Skarp (Sweden) –production displays

Evgueny Terukov (Russia) – TFT LCD

Harm Tolner (Netherlands) - PDP

Sofia Torgova (Russia) – LCD, OLED

Sun Yiaowei (Singapore) - LCD

Nickolai Zhukov (Russia) – LCD, VFD, FED

Victor Zyryanov (Russia) – LCD

INTERNATIONAL COMMITTEE

Allan Kmetz (SID Chair), Honorary Chair

Victor Belyaev (Russia), Chair

Sergey Bukesov (Korea, KAIST)

Vladimir Chigrinov (China, Hong-Kong, SID Russia Chapter)

Min-Koo Han (Korea, SID Korea Chapter)

Darrel Hopper (USA, USAF)

Stanislaw Klosowicz (Poland)

Shigeo Mikoshiba (Japan, SID President-Elect)

Shohei Naemura (Japan, SID Japan Chapter)

Vasily Nazarenko (Ukraine, SID Ukraine Chapter)

John Raines (UK, SID UK/Ireland Chapter)

Han-Ping Shieh (Taiwan, SID Taiwan Chapter)

Nickolai Zhukov (Russia)

Sergey Yakovenko (USA, SID Belorussia Chapter)

LOCAL COMMITTEE

Vladimir Samsonov (Russia), Chair

Yuri Troitsky (Mashpribor, Korolev), Vice-Chair

Alexander Morozenko (Head of Korolev Adminisrtation)

Irina Revokatova (SID Russia Chapter Treasurer & Secretary)

INVENTION COMPETITION COMMITTEE

Zvi Yaniv (USA, SID Texas Chapter), Chair

Victor Belyaev (Russia, SID Russia Chapter), Vice-Chair

Valery Fedorkov (Russia, RF Ministry of Industry, Science and Technology)

Valentina Kovalenko (Russia, Patent Attorney)

Oleg Serdyukov (Russia, Izobretatel' (Inventor Magazine)

THE PROGRAM OF THE CONFERENCE "BASIC STUDIES OF PROBLEMS FOR INFORMATION DISPLAYING" (FLOWERS'03)

Sunday, August 24

9-00...20-00. Registration of participants.
19-00...22-00. Reception.

Monday, August 25

8-00...10-00. **Registration of participants.**

10-00...10-15. **Opening Ceremony.**
Oleg Krokhin, Symposium Chair
Igor Kompanets, Program Committee Chair (organization remarks)

10-15...12-00. **Plenar Session.**
Chairmen: *Ken Werner and Igor Kompanets.*

10-15 (PS-1). *Darrel Hopper* (Wright-Patterson Air Force Research Laboratory, USA). Displays of Year 3000.
10-50 (PS-2). *Victor Belyaev* (Cometa Central R&D Institute, Russia). Russian displays: market & products.
11-25 (PS-3). *Vladimir Samsonov* (Mission Control Center, Russia). Information displaying in the Mission Control Center, Korolev.

12-00...12-20. **Coffee-break.**

12-20...14-00. **Session "Emissive Displays".**
Chairmen: *Victor Sorokin and Jerzy Zieliński.*

12-00 (ED-1). *Harm Tolner* (Philips Components BV, The Netherlands). Optimization of Plasma Display Panels.
12-20 (ED-2). *Alexey Ivlyushkin, V.Samorodov* ("Plasma" Co., Russia). The state and tendencies of the development of plasma display panels.
12-40 (ED-3). *Boris Gorfinkel, N.Z hukov* (R&D Institute "Volga", Russia). Modern vacuum fluorescent displays.
13-00 (ED-4). *V.I. Kozlovsky, Yu.V. Korostelin, A.B. Krysa, Ya.K. Skasyrsky, Yu.M. Popov* (Lebedev Physical Institute, Russia), *P.I. Kuznetsov* (Institute of Radioengineering and Electronics, Russia). Laser CRT: last results concerning an improvement of parameters.
13-15 (ED-5). *V.I. Konov, V.D. Frolov, A.V. Karabutov, E.D. Obraztsova, S.M. Pimenov, A.S. Pozharov, S.V. Terekhov* (General Physics Institute of RAS, Russia), *B.I. Gorfinkel, N.P. Abanshin, N.D.Zhukov* (R&D Institute "Volga", Russia). Development of cold cathode displays on single-wall carbon nanotubes.
13-30 (ED-6). *A.N. Lachinov, V.M. Kornilov, Yu.M. Yumaguzin, E.E. Tchurlina* (Institute of Molecule and Crystal Physics, Russia). Photon and electron emission from polymer films under electric field influence.
13-45 (ED-7). *Yu. Trofimov, V. Posedko, S. Lishik, V. Kalenkov, I. Mironenko, V. Sivenkov* (Institute of Electronics of NASB, Belarus). Ultra bright LED light sources for display applications and illumination.

14-00...15-00. **Lunch.**

15-00...16-30. **Exhibition of display devices and materials.**

15-00...16-30. **Poster Session "Emissive Displays"**
Chairmen: *Boris Gorfinkel and Alexander Smirnov.*

(ED-P1). *A. Vitukhnovsky, T. Limonova, K. Anikin* (Lebedev Physical Institute, Russia). Organic light emitting diode studies by near-field scanning optical microscopy.

(ED-P2). *A.S.Nasibov* (Lebedev Physical Institute, Russia). Semiconductor Laser Sources for LCD and DMD Projectors.

(ED-P3). *Vance Lin* (Toppoly Optoelectronics Corp., Taiwan). A 2.2-inch QCIF AMOLED with high quality ITO.

(ED-P4). *O.M.Makienko* (R&D Institute "Platan", Russia). 4-th generation laser kinescope.

(ED-P5). *M.K. Samokhvalov, R.R. Davidov* (Ulyanovsk State Technical University, Russia). Determination of phosphor activator parameters for using the voltage-brightness characteristics of thin-film electroluminescent structures.

(ED-P6). *E.I. Terukov, M.S. Bresler, O.B. Gusev, Yu.A. Nikolaev* (Ioffe Physical-Technical Institute, Russia). Efficient optical converter of visible to infrared light at 1.54 micrometers.

(ED-P7). *M.S. Bresler, O.B. Gusev, E.I. Terukov, Yu.A. Nikolaev* (Ioffe Physico-Technical Institute, Russia), *A. Froitzheim, W. Fuks* (Hahn-Meitner-Institut, Germany). Electroluminescence in amorphous-crystalline silicon heterostructures.

(ED-P8). *A.O. Dmitrienko, T.A. Akmaeva, V.V. Martynov* (Saratov State University, Russia), *B.I. Gorfinkel* (R&D Institute "Volga", Russia). Service life of cathodoluminescence screens with Y_2O_2S:Eu phosphor and processes of screen degradation.

(ED-P9). *A.O. Dmitrienko, B.I. Gorfinkel, V.V. Mikhailova, V.P. Dmitrienko, O.I. Zhbanov, T.A. Gerasimova* (R&D Institute "Volga", Russia). Phosphors for low voltage vacuum fluorescent displays and full color field emission displays.

(ED-P10). *I.V. Shein, S. L. Shmakov, A. O. Dmitrienko* (Saratov State University, Russia), *A.A. Hazanov* (RDI "Volga", Russia). Structure, Conductivity and Cathodoluminescent Properties of Electroforetically Deposited Luminescent Compositions Exited by Low Energy Electrons: for VFD Application.

(ED-P11). *Yu. Trofimov, V. Posedko, L. Survilo, A. Posedko, I. Mironenko, V. Sivenkov* (Institute of Electronics of NASB, Belarus). RGB LED backlights and LED panel mount indicators.

(ED-P12). *Yoon-Kwan Lee, Song Jun Weon, Woo-Hyun Jo, Byung-Joon Rhee, Jung-Won Kang, Eun-Ho Yoo* (LG Electronics Inc., Korea). A Study on Various Factors for Jitter Reduction in PDP device.

(ED-P13). *N.Sostchin* (R&D Institute "Platan", Russia), *A.Vishniakov* (Mendeleyev University of Chemical Technology, Russia). Nine key problems of PDP phosphors technology.

(ED-P14). *M.I. Kalinin, Yu.N. Kosyakov, A.A. Lyabin, Yu.V. Petrushenko* (R&D Institute "Platan", Russia). Super-bright projection electron-beam devices for aircraft collimator equipment.

(ED-P15). *M.M. Sychov* (St. Petersburg Institute of Technology, Russia), *Y. Nakanishi, H.Kominami* (Shizuoka University, Hamamatsu, Japan), *Y. Hatanaka* (Aichi University of Technology, Japan). Influence of Zn Doping and Laser Annealing on Y_2O_3Eu Thin Film Phosphor Properties.

(ED-P16). *A.G. Rodionov, L.L. Ejenkova* (Plastpolymer J.S.Co., Russia), *M.M. Sychov, A.A. Alexeev, V.G. Korsakov* (St. Petersburg State Institute of Technology, Russia). Binder for high brightness electroluminescent panels.

(ED-P17). *V.F. Ivanov, A.A. Nekrasov, O.L. Gribkova, A.V. Vannikov* (Frumkin Institute of Electrochemistry of RAS, Russia). Electroluminescent Phenomenon in Polyaniline Films Doped with CdS Nanoparticles.

(ED-P18). E.I. Maltsev, D.A. Lypenko, S.V. Kirillov, B.I. Shapiro, A.V. Vannikov (Frumkin Institute of Electrochemistry of RAS, Russia), V.D. Rumyantseva, A.F. Mironov (Moscow State Academy of Fine Chemical Technology, Russia), Yu.L. Slominsky, A..I. Tolmachev (Institute of Organic Chemistry of NASU, Ukraine), *H.F.M. Schoo* (TNO Institute of

Industrial Technology, The Netherlands). New Electroluminescent Polymer Materials Based on Cyanine and Porphyrin Nanocrystals.

(ED-P19). *N.A. Vlasenko, Z.L. Denisova, Ya.F. Kononets, L.I. Veligura, and Yu.A. Tsyrkunov* (Institute of Semiconductor Physics of NASU, Ukraine). Near-Infrared Electroluminescence of ZnS:Er and ZnS(Se):Cr TFEL Devices.

(ED-P20). *M.G. Tomilin, A.E. Puisha* (Vavilov State Optical Institute, Russia), *A.I. Chuvashov* (Institute of Fine Mechanics and Optics, Russia), Abramov V.S. (Corvet Co., Russia). LED modules containing Frenel lenses.

16-30...19-00. **Excursion (Mission Control Center, Korolev).**

Tuesday, August 26

8-00...10-00. **Registration of participants.**

9-00...11-00. **Session "Non-Emissive Displays –1".**
Chairmen: *Vladimir Agabekov and Darrel Hopper.*

9-00 (NED-1). *Vladimir Chigrinov* (Hong Kong University of Science and Technology, China). Liquid crystal displays: modern state and prospects of applications.

9-25 (NED-2). *Alexander Smirnov* (Belorussian State University of Informatics and Radioelectronics, Belarus). LCOS and LED microdisplays: main principles of design, fabrication and application.

9-50 (NED-3). *Victor Sorokin* (Institute of semiconductor physics of NASU, Ukraine). Cholesteric reflective LCDs characterization.

10-15 (NED-4). *Eugene Pozhidaev* (Lebedev Physical Institute, Russia). Ferroelectric liquid crystal displays: basic physics and prospects of applications.

10-40...11-00. **Coffee-break.**

11-00...13-00. **Session "Non-Emissive Displays – 2".**
Chairmen: *Vladimir Chigrinov and Jyrkki Kimmel.*

11-00 (NED-5). *S. J. Klosowicz* (Institute of Applied Physics, Poland). Polymer-dispersed liquid crystals for information displays.

11-20 (NED-6). *M.D.Efremov, I.G.Neizvestnii, V.A.Volodin, A.V.Vishnyakov* (Institute of Semiconductor Physics SB RAS), *G.M.Zharkova* (Institute of Theoretical and Applied Mechanics SB RAS), *V.Ya.Zyryanov* (Institute of Physics SB RAS), *V.F.Shabanov* (SKTB «Nauka» SB RAS), *V.N.Ulasyuk* (ELTAN Ltd, Russia). Liquid crystal composite films: perspectives in new AM TFT displays.

11-40 (NED-7). *M.G. Tomilin* (Vavilov State Optical Institute, Russia). Bistable LCDs with improved performance characteristics.

12-00 (NED-8). *G.M. Zharkova, I. V. Samsonova, S. A. Strel'tzov, V. M. Khachaturjan, A. P. Petrov* (Institute of Theoretical and Applied Mechanics of SB RAS, Russia). Liquid crystal composites with a spatially periodic structure.

12-15 (NED-9). *A. Morozov, G. Nevskaya, A. Shevchenko* (Novosibirsk State Technical University, Russia). The method of manufacture of LC cells with several areas of homogeneous nematic.

12-30 (NED-10). *G. King, P. Lazarev, A. Manko, V. Nazarov, S. Remizov* (OPTIVA, Inc., USA). LCD applications of thin crystal film polarizers.

12-45 (NED-11). *Yu.P. Guscho* (Moscow State University of Radioengineering and Electronics, Russia). Advances in viscoelastic displays.

13-00...14-00. **Lunch.**

14-00...16-00. **Exhibition of display materials and devices.**

14-00...16-00. **Poster Session "Non-Emissive Displays".**
Chairs: *Galina Nevskaya and Janucz Parka.*

(NED-P1). *A.I. Krivoshey, L.A. Kutulya, N.S. Pivnenko, V.V. Vashchenko* (Institute for Single Crystals of NASU, Ukraine), *G.G. Rode, A.S.Tolochko, V.I.Kulishov* (Institute of Physics of NASU, Ukraine). Inversion of spontaneous polarization sign in smectic-C* phase for some chiral 2,6-*bis*-arylidene-3*R*-methyl-cyclohexanones.

(NED-P2). *L.A. Kutulya, N.I. Shkolnikova, A.I. Krivoshey, L.V.Chepeleva, M.N. Pivnenko* (Institute for Single Crystals of NASU, Ukraine), *A.O.Doroshenko* (Kharkov Karazin National University, Ukraine). Photoinducted inversion of helix in a system nematic - chiral dopant.

(NED-P3). *A.Andreev, T.Fedosenkova, E.Pozhidaev, Yu.Bobylev, V.Shoshin, I.Kompanets* (Lebedev Physics Institute of RAS, Russia), *L.Kutulya* (Institute for Single Crystals of NASU, Ukraine). Electrically controlled birefringence and light phase modulation in helix free FLC.

(NED-P4). *V.I. Maschenko, S.A. Udra, L.A. Kazarin, V.I. Gerasimov* (Lomonosov Moscow State University), *V.V. Belyaev* (Cometa Central R&D Institute, Russia). Polymer nanogel use for liquid crystal orientation.

(NED-P5). *V.V. Belyaev* (Cometa Central R&D Institute, Russia), *A.Y. Kalashnikov* (Moscow Technical University for Radio Engineering, Electronics & Automation, IT Laboratory of Gosstandart Russia), *M.F. Grebyonkin* (MAMI Moscow State Technical University, Russia). Dynamics of electrooptic response in twist cells with double frequency addressing.

(NED-P6). *V.V. Belyaev, A.B. Kuznetsov* (Cometa Central R&D Institute, Russia), *M.F. Grebyonkin* (MAMI Moscow State Technical University, Russia), *A.Y. Kalashnikov* (Moscow Technical University for Radio Engineering, Electronics & Automation, IT Laboratory of Gosstandart Russia). Figure of merit of liquid crystal substances and mixtures for displays with homogeneous planar and vertical alignment.

(NED-P7). *V.A. Loiko, D.A. Yastrebov, V.A.Loiko* (Stepanov Institute of physics of NASB, Belarus). Spectral reflectance and transmittance of holographic polymer dispersed liquid crystal films.

(NED-P8). *V.V. Berdnik, V.A. Loiko* (Stepanov Institute of Physics of NASB, Belarus). Polymer-dispersed liquid crystal films: multiple scattering regime consideration.

(NED-P9). *A.V. Barannik, V.Ya. Zyryanov, V.F. Shabanov* (Kirensky Institute of Physics of SB RAS, Russia), *V.A. Loiko* (Stepanov Institute of Physics of NASB, Belarus). Interference oscillations in dynamics of electrooptical response of nematic PDLC films.

(NED-P10). *O.O. Prischepa* (SKTB "Nauka" of SB RAS), *V.Ya. Zyryanov* (Kirensky Institute of Physics of SB RAS, Russia). Texture and optical properties of stretched composite films doped by lecithin.

(NED-P11). *V.Ya. Zyryanov* (Kirensky Institute of Physics of SB RAS, Russia). Uniaxially oriented films of polymer dispersed liquid crystals: preparation, physical properties and display applications.

(NED-P12). *V.Ya. Zyryanov, A.V. Barannik, R.D. Ilvutikov, V.F. Shabanov* (Kirensky Institute of Physics of SB RAS, Russia), *E.P. Pozhidaev* (Lebedev Physics Institute of RAS, Russia). Structure and electrooptical properties of unoriented films of polymer dispersed ferroelectric liquid crystals.

(NED-P13). *P. Shum, Q. Wang and X.W. Sun* (School of Electrical and Electronic Engineering, Singapore). High azimuthal index doughnut beam generated by liquid crystal spiral phase plates.

(NED-P14). *X.W. Sun, B. J. Chen, P. Shum* (School of Electrical and Electronic Engineering, Singapore). Fabrication of ITO thin films by filtered cathodic vacuum arc deposition.

(NED-P15). *Marek Olifierczuk, Jerzy Zielinski* (Institute of Applied Physics, Poland). Two-parameters optimization procedure of TN display.

NED-P16. *Jerzy Zieliński and Marek Olifierczuk* (Institute of Applied Physics, Poland). Multi-parameters optimization procedure of the contrast ratio in TN two-polarizer reflective display

(NED-P17). *Yu.Kolomzarov, P.Oleksenko, V.Sorokin, P.Titarenko, R.Zelinskyy* (Institute of Semiconductor Physics of NASU, Ukraine). Oblique reactive cathode sputtering as a method for creation of orienting liquid crystal microrelief.

(NED-P18). *A.Rybalochka, V.Sorokin, S.Valyukh* (Institute of Semiconductor Physics of NASU, Ukraine), Two-row addressing method for cholesteric LCD.

(NED-P19). *S. Valyukh, A. Rybalochka, V. Sorokin, P. Tytarenko* (Institute of Semiconductor Physics of NASU, Ukraine), *K. Skarp* (Dalarna University, Sweden). A method for measurement of reflective twist nematic liquid crystal cell properties.

(NED-P20). *I.Valyukh, A. Slobodyanyuk* (National Taras Shevchenko University, Ukraine), *R. Lymarenko* (Institut of Applied Optics, Ukraine), *K. Skarp* (Dalarna University, Sweden). Numerical Study of Reflectivity of Monochrom Double-Layer Cholesteric Liquid-Crystal Displays.

(NED-P21). *S. Shahab, V. Agabekov, N. Ariko, N. Ivanova* (Institute of Chemistry of New Materials of NASB, Belarus). Thermo-optical properties of polyvinyl alcohol films modified by dichroic dyes.

(NED-P22). *N. Ivanova, V. Agabekov, V. Verbitski* (Institute of Chemistry of New Materials of NASB, Belarus), *A. Tsaruk, V. Hreben, V. Dlugunovich* (Stepanov Institute of Physics of NASB, Belarus). Reflectance of aluminum reflectors for LCD.

(NED-P23). *A. Shevchenko, G. Nevskaya, A. Morozov* (Novosibirsk State Technical University, Russia). Research of effect pretilt of molecules on reorientation and optical properties of the plane-oriented nematic in LC-mikrolenses.

(NED-P24). *G.E.Nevskaya, A. Gvozdarev* (Novosibirsk State Technical University, Russia). The comparison of electrooptical properties of LC-microlenses with different nematic alignment.

(NED-P25). *S.A. Studentsov, V.A. Brezhnev, B.I. Gorfinkel, N.D. Zhukov* (R&D Institute "Volga", Russia), *I.S. Bezludnaya, G.V. Simonenko* (Satatov State University, Russia), *V.A. Ezhov* (Institute of General Physics of RAS, Russia). Memomi-screen: a high contrast passive matrix LC display with TV fast response.

NED-P26. Boris A. Umanskii, Sofia I. Torgova, Nikolai V. Novoseletskii, Galina N. Dorozhkina (State Research Center "NIOPIK", Russia and OOM-Lab, Italy), Alfredo Strigazzi (Politecnico di Torino and OOM-Lab, Italy). Liquid Crystal Photo-Alignment Induced by Azodyes.

NED-P27. *Pavel Lazarev, Victor Nazarov, Natalia Ovchinnikova and Sergey Remizov* (Optiva, Inc., USA). Printed Optical Components for Liquid Crystal Displays.

16-00...19-00. **Excursion (Korolev Museum in "Energiya" Corp., Korolev).**

19-00...22-00. **Banquet.**

Wednesday, August 27

8-00...10-00. **Registration of participants.**

9-00...11-00. **Session "Display Ergonomics and Applications - 1".**
Chairmen: *Vladimir Feofanov and Stanislav Klosowicz.*

9-00 (DEA-1). *Jyrki Kimmel* (Nokia Research Center, Finland). Display Technologies for the Mobile Information Society.

9-25 (DEA-2). *Darrel Hopper* ((Wright-Patterson Air Force Research Laboratory, USA). Aviation Display Devices and Market.

9-50 (DEA-3). *Igor Kompanets* (Lebedev Physical Institute of RAS, Russia). 3-D displays: advances, problems and prospects.

10-15 (DEA-4). *Konstantin Bogachov, Igor Litvak* (Moscow State Technical University of Electronics & Mathematics, Russia). The comparative analysis of information perception quality on screens of CRT and TFT LC displays.

10-40...11-00. **Coffee-break.**

11-00...13-00. **Session " Display Ergonomics and Applications - 2".**
Chairmen: *Vladimir Samsonov and Xiaowei Sun.*

11-00 (DEA-5). *Vladimir Feofanov* (R&D Institute "Electroautomatika", Russia). Aviation Display Devices in Russia.

11-20 (DEA-6). *G. G. Demirchogljan, V.I. Verhoturov, S.N. Verhoturov, V.B. Filippov, V.A. Kundik* (Russian Physical Culture Scientific Research Institute). Skin electrical display for blind.

11-40 (DEA-7). *A.V. Sadchikhin, A.G.Morozov, S.B.Sozinov* ("AR Technologies" Corp., Russia). Information display large screen projection systems.

12-00 (DEA-8). *Yu. Trofimov, V. Posedko, V. Sivenkov, I. Mironenko, S. Lishik* (Institute of Electronics of NASB, Belarus). A New Approach to the Design of Highly Efficient Large Size LED Displays With Improved Ergonomics.

12-15 (DEA-9). *Phil Surman, Ian Sexton, Richard Bates, Kam Chaun Yow, Wing Kai Lee, Michael Craven* (De Montfort University, UK). Beyond 3D television: the multi-modal, multi-viewer TV system of the future.

12-30 (DEA-10). *A. Putilin, I. Gustomiasov, A. Chernopiatov* (Lebedev Physics Institute of RAS, Russia). Application of waveguide holograms in displays and planar illuminators.

12-45 (DEA-11). *A.V. Shabanov, V.F. Shabanov, V.Ya. Zyryanov* (Kirensky Institute of Physics of SB RAS, Russia), *S.Ya. Vetrov* (Krasnoyarsk State Technical University, Russia). Tunable spectral filters based on photonic crystals with liquid crystal defect layers.

13-00...14.00. **Lunch.**

14-00...15-30. **Exhibition of display materials and devices.**

14-00...15-30. **Poster Session " Display Ergonomics and Applications".**
Chairmen: *Eugene Terukov and Yury Trofimov.*

(DEA-P1). *K.A. Bogachov* (Moscow State Technical University of Electronics & Mathematics, Russia). Investigation of the methods of estimating a visual fatigue when working with displays.

(DEA-P2). *D. V. Fel'dman* (Moscow State Technical University of Electronics & Mathematics, Russia). The estimation of self-descriptiveness of symbols' elements of synthesized alphabets and the possibility of it's application.

(DEA-P3). *A. U. Terent'ev* (Moscow State Technical University of Electronics & Mathematics, Russia). Research of Type and Choice Parameters' Optimization Possibility Means of Information Display.

(DEA-P4). *I.Yu. Morozov* (Moscow State Technical University of Electronics & Mathematics, Russia). Research of adaptive opportunities of the multimedia equipment.

(DEA-P5). *E.A. Naumov* (Moscow State Technical University of Electronics & Mathematics, Russia). Calculation and designing of the reflecting and transmission displays for achieving the maximal contrast.

(DEA-P6). *V. Goltraf, T. Goncharova, V. Kobzev, A. Nefedovitch* ("Avrora" Corp., Russia). Assessment of ergonomic characteristics of the operator's work with the display instruments of ship's control systems.

(DEA-P7). *M.N. Burdaev, A.K. Aylamazyan, G.S. Osipov, V.M. Khachumov* (Yu. Gagarin Center for Astronaut Training). Graphic Forms of Operating Monitoring and Prediction of Orbital Structures of Satellite Systems.

(DEA-P8). *A.M. Ilyanok* (Atomic & Molecular Engineering Laboratory, Belarus). The dynamic architectural display.

(DEA-P9). *N.S.Severinovsky, K.G. Simforov* (JSC «Kiev Factory of Relay and Automatic Machinery», Ukraine). Perspectives of applications of illuminated indicator boards for visual information displaying.

(DEA-P10). *A. N. Shesterkin, O.V. Kuznetzov* (Ryazan, Russia). The screen for symbol data representation.

(DEA-P11). *J. Parka* (Institute of Applied Physics, Poland). Liquid Crystal 3D Displays.

(DEA-P12). *S.V. Smagin* (Moscow Technical University for Radio Engineering, Electronics & Automation, Russia), *V.V. Belyaev* (Cometa Central R&D Institute, Russia), *A.V. Sadchikhin, S.N. Sozinov* (AR Technology Co., Russia). Model of Lens Integrator of Projection Systems.

DEA-P13. *A.I.Afanas'ev, V.I.Krichevsky* (GNPP "TSIKLON-TEST", Russia). Research of an electromagnetic susceptibility of computer displays to magnetic fields of industrial frequency of 50 Hz.

15-30...19-00. **Excursion (Yuri Gagarin Center for Astronaut Training, City of Zvezdny gorodok).**

Thursday, August 28

9-00...13-00. **Poster Session " Display Invention Competition".**
Chairmen: *Victor Belyaev and Valery Fedorkov.*

13-00...13-45. **Discussion of results of the Conference, Exhibition and Invention Competition.**

13-45...14-00. **Announcement of results of the Invention Competition.**

14-00...15.00. **Lunch.**

15-00...19-00. **Moscow sightseeing (bus or boat trip).**

SYMPOSIUM

PAPERS

PLENAR SESSION

Chairmen: *Ken Werner and Igor Kompanets*

PS-1. **Displays of Year 3000**

Darrel Hopper
Air Force Research Laboratory
AFRL/HECV Bldg 248 Rm 300
2255 H Street
Wright-Patterson AFB OH 45433-7022
< darrel.hopper@wpafb.af.mil>

Paper is not available

RUSSIAN DISPLAYS MARKET & PRODUCTS

Victor V. BELYAEV
SID RUSSIA CHAPTER
Cometa Central R&D Institute

OUTLINE

- PC Monitors
- TV Sets
- Display products with moderate resolution
- Displays development in Russia
- Displays application

PC MONITORS

Ministry for Communications:

Russian IT market growth – 18% /year

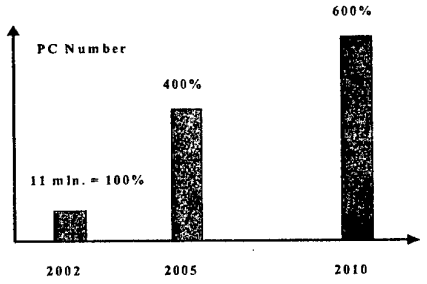

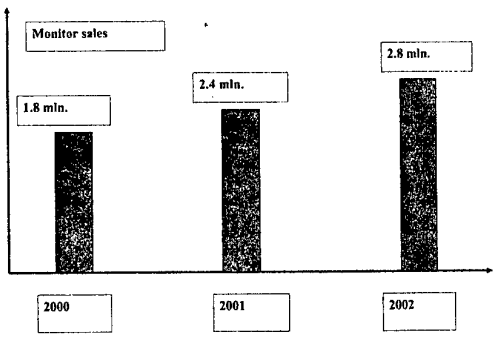

SALES IN RUSSIA

LCD MONITORS

2000 – 30,000

2001 – 120,000

****

NOTEBOOKS

69,000 – 76,000 PER YEAR

Rolsen Factory in Fryazino, Moscow

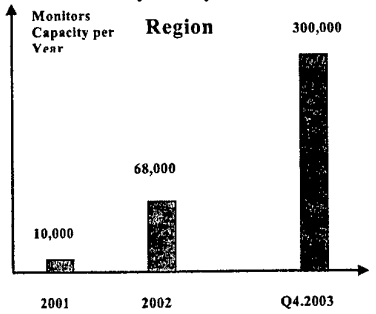

C708 flat CRT - 17" (43 cm) – Share 60%

2003

ROLSEN – 10% of Russian Market

Oversea companies - 90%

LG, Samsung, Sony, Apple,

PowerCyber et al.

Network of distribution companies

Evaluation of the Russian market of monitors

To-date prices ~$170 for a CRT monitor, ~$200 for a LCD monitor

Year	2002	2010 (Forecast)
Market capacity	$0.8 bln.	$4.8 bln. (the same prices)
		$2.4 bln. (the prices are twice reduced)
Money saved in Russia (logistics, custom, distribution, income tax)	$0.16 bln.	$0.96 bln. Or $0.48 bln.
Number of employees	1000-1500	

RUSSIAN MARKET OF THE TV SETS

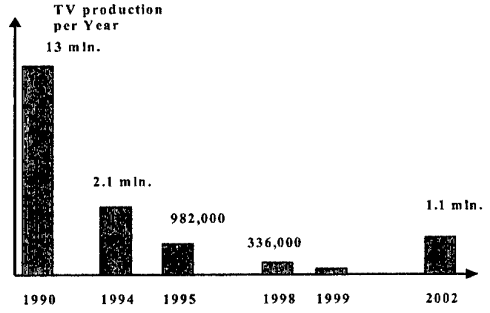

TOTAL MARKET IN 2002
4.4 mln. units

Growth 25%/year

Main technology CRT

(LCD TV ~25,000<1%)

Main share – 17"-23" (43-61 cm)

Company	Sales in Russia, mln. units	Share in Russian market, %
Samsung	1,2	30
LG	1,0	25
Daewoo	0,2	5
Thompson	0,15	3,75

Other - Philips, Sony, Matsushita (Panasonic) et al.

LCD TV in Russian Market

LG-Philips (Korea-The Netherlands),

Sharp (Japan), Loewe (Germany),

Nakamichi (Japan), Karat (Russia)

AUTOMOTIVE LCD TV

2.5-3″ Sanyo, Casio since 1995

5-7″ JVC since 1999

Production of Russian TV sets in 2002

Trade mark	2002 production, thousands units	Share in production of domestic TV sets, %
Rubin	550	50
SOKOL	230	21
Rolsen	200	18
Others	120	11
Total	1100	100

DYNAMICS OF THE RUSSIAN TV MARKET IN 2001-2002

TV Sets Production in Russia

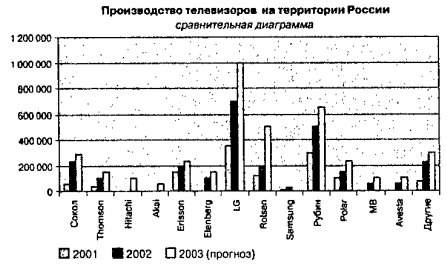

PROSPECTS:

DIGITAL TV

- Production of digital joysticks for analog TV sets in Rateus Factory, Zelenograd, Moscow Region
- Production of hybrid TV sets with both analog and digital receivers in Kozitsky Factory, Saint-Petersburg
- A prototype of a passive addressed LCD for a TV in Volga R & D Institute, Saratov

Russian market of displays with moderate resolution (60-240 lines)

Cellular phones, PDA, palms etc.

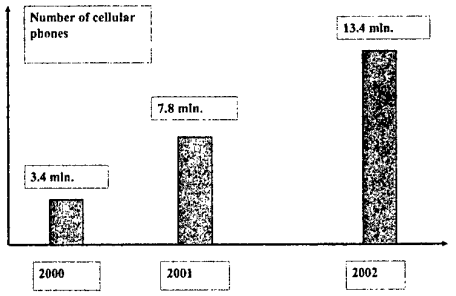

Opportunity of production of this kind of displays in Volga, Saratov and Platan, Fryazino (LCD, entire cycle of production), MELT, Display (using of LCD imported modules), NIIME-Micron, Zelenograd (OLED)

DIGITAL PHOTOCAMERAS MARKET IN 2002

	World	Russia
Sales, units	26,500,000	85,000
Growth	59.3%	136%
Average price	-	652 euro
Growth	-	-23%

RUSSIAN DISPLAY PRODUCTS

VACUUM FLUORESCENT DEVICES (TFT VFD)

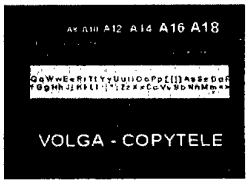

VOLGA R&D Institute, Saratov

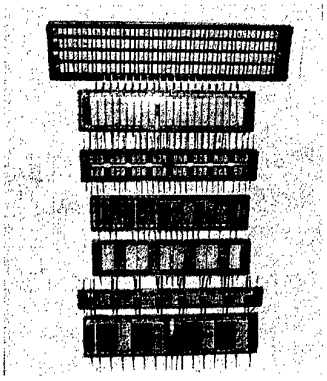

A Fragment of a Big Screen with Brightness up to 5000 cd m^{-2}

PDP Tiled Big Screens

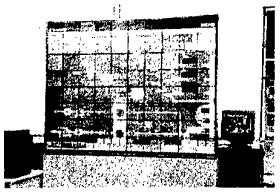

INCOTEX, Moscow ELARA, Cheboksary

AC PDP 19 cm Modules from PLASMA, Ryazan

PDP TILED SCREEN

19cm x19cm & 41x41 cm moduli		Any resolution standard	
	Pixel size : 3mm 6 mm 12 mm	AC & DC PDP	Screen thickness 10 cm
Pick luminance 700 cd m^{-2} (3 mm pixel)	Pick luminance 1000 cd m^{-2} (12mm pixel)		Correction optics to eliminate edges

PROJECTION DLP AND LCD SYSTEMS

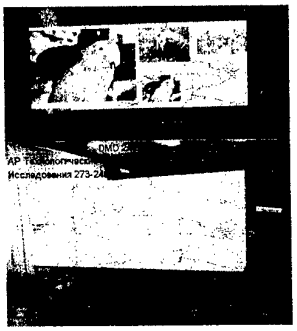

AR Technology, Moscow

50", 67", 100" videocubes

****

Small gap (~0.1 mm) technology

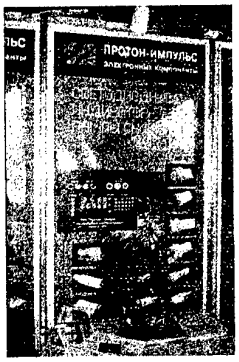

Bright LED

Proton-Impulse, Oryol Institute of Electronics, Minsk, Belorussia

LED RoadInformer

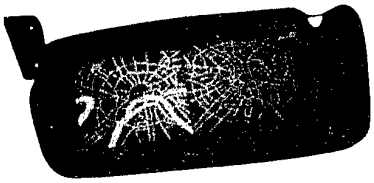

Production in Zelenograd, Moscow Region

LASER CRT - QUANTOSCOPE

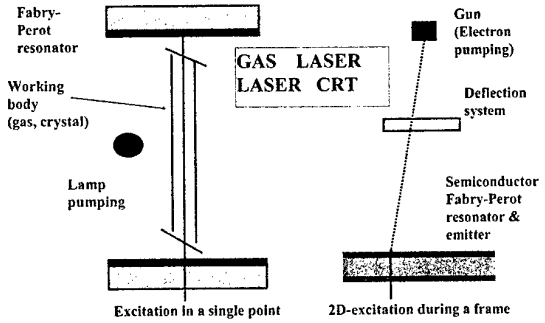

LASER CRT PARAMETERS

Emission power – 4-12 W

Colors - Red, Green, Blue

Light flux of white – 5000 – 12000 lm

Resolution – 1000 – 3000 TV lines

Tube length – 92 cm (1995), 35 cm (2000)

Power consumption – 1-4 kW

Platan, Physical Lebedev In-te, AR Technology

A compact laser CRT for home theatre Platan, Fryazino

LCD TECHNOLOGIES

Type of LC	Technology	Main advantage	Companies
Any	Method of LC photoalignment by polymeric cinnamate films	Fabrication of displays with multidomain pixels for better viewing angles	NIOPIK, Dolgoprudnyi, Moscow Region Institute of Physics, Kiev, Ukraine
Cholesteric	"100%" polarizers for reflection-mode projection devices	2 times improvement of light efficiency	NIOPIK – LG AR Technology
Ferroelectric and antiferroelectric LC	Modes for volume and surface-volume bistability and grey scale LCD	Significant simplification of technology	Physical Lebedev Institute, Moscow Institute of Single Crystals, Kharkov, Ukraine

STN - Improvement of driving circuitry for passive LCDs

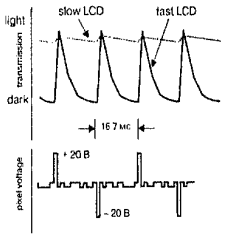

Operation with TV Frame Rate

Pulsar, Moscow + Volga, Saratov

DISPLAYS FOR AIRCRAFTS, HELICOPTERS, SPACECRAFTS

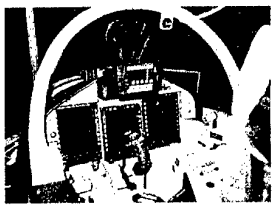

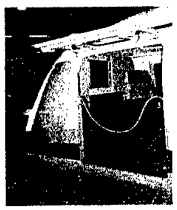

YaK-130 pilot cabin

3 Italian TFT LCD

Kazan Helicopter Factory

Domestic Rugged Displays

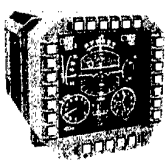

R&D Institute of Computer Engineering, Minsk, Belorussia

AVIAPRIBOR-Holding, Moscow & Ulianovsk

AVIAPRIBOR-HOLDING (Moscow & Ulyanovsk)

- **Indicators IM-7, IM-8 implement receiving, processing and displaying information of pilot and navigation complex, on-board systems and power units. IM-8 displays also information from the aircraft or helicopter radar. IM-12 displays character and graphic information on the spatial location and movement of the aircraft or helicopter.**
- **The AVIAPRIBOR indicators provide contrast ratio 60:1 (IM-7) or 250:1 (IM-8, IM-12) at normal incidence and 10 lx ambient luminance and 3:1 at viewing angles ±60° and 100 000 lx ambient luminance.**

R&D INSTITUTE OF COMPUTER ENGINEERING (NIICT), BELORUSSIA

- Liquid crystal color indicator ZhKI-Ts is to display graphic and TV information in a pilot's cabin. Its software is compatible with any display protocols owing to using the EEPROM.
- A color multi-functional indicator MFI-Ts and a cathode-ray indicator ELI-1 are used in MIG and SU aircrafts for displaying at high ambient luminance.

Collimating Displays

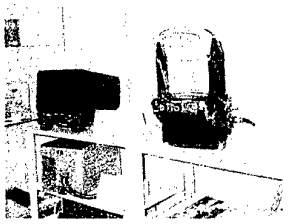

Fazotron-NIIR, Moscow
RPKB, Ramenskoye, Moscow Region
Elektroavtomatika, S-Petersburg

ELD – Piastr-PUI (EDIS, S-Petersburg) with a PLANAR (USA) Panel

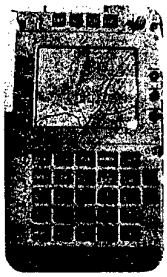

- An analog of UNS-1C (Universal Avionics, USA)
- Size 146x228x170 mm
- Display area 96x77 mm
- Mass 4.5 kg
- Pixels number 320x256
- View ability up to 75 000 lx
- International protocols MIL-STD 1553 and ARINC-429

Ship Displays
Display Design Bureau, Vitebsk, Belorussia
Avrora, S-Petersburg

R&K- Russian Notebook for Astronauts with 13.3" LCD

Other space displays – R&D Institute for Avionic Equipment, Zhukovsky, Moscow Region – 10.4" LCD

BIG SCREENS IN MISSION CONTROL CENTER, KOROLEV

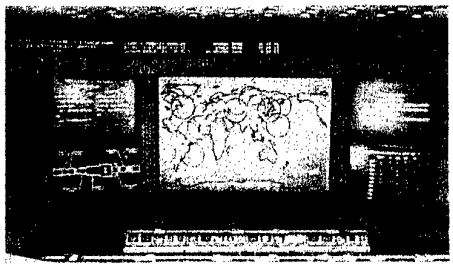

Information Display of International Space Station In Russian Mission Control Centre

Vladimir K. Samsonov

Russian Mission Control Centre Korolev, Moscow region, Russia

Abstract

Implantation of new information technology in displays for control of Russian Segment of International Space Station (ISS-RS) in Russian Mission Control Centre enhances the new level of control quality. It is shown, that the united network of workstations, terminals and TV-projectors for large screens enhances operational efficiency, coordination and reliability of control actions. The methods and any software of visualization of real space situation for large and small screens are described.

The flight control of the Russian segment of the International Space Station (ISS) is carried out from the Russian Mission Control Center (MCC) in the city of Korolev in the Moscow area. The Russian MCC is known all over the world since the joint Russian-American program "Sojuz-Appollo" (the first docking in space of the Russian and American space ships). Since then, the traditions of international cooperation in space gained a wide experience in the flight management, and the systems of display of information became conform to all the requirements of the staff and of the mass media. This was very important in order to popularize the space researches in Russia and abroad. The wide experience of work of the systems of display of the information was gained during 15 years of the flight management of the Russian space complex "MIR".

The flight management of the Russian segment of the ISS is carried out from a separate building in MCC. This building has three control rooms (before the Main control room was used to manage the flight of the Russian super heavy space rocket system "Energia-Buran").

Now in the Main control room work operators managing the Russian segment in whole. (Fig. 1)

One little control room is used to manage the flight of the space cargos "Sojuz" (with crew) and "Progress" (with cargo for the ISS) (Sojuz/Progress Control Room).

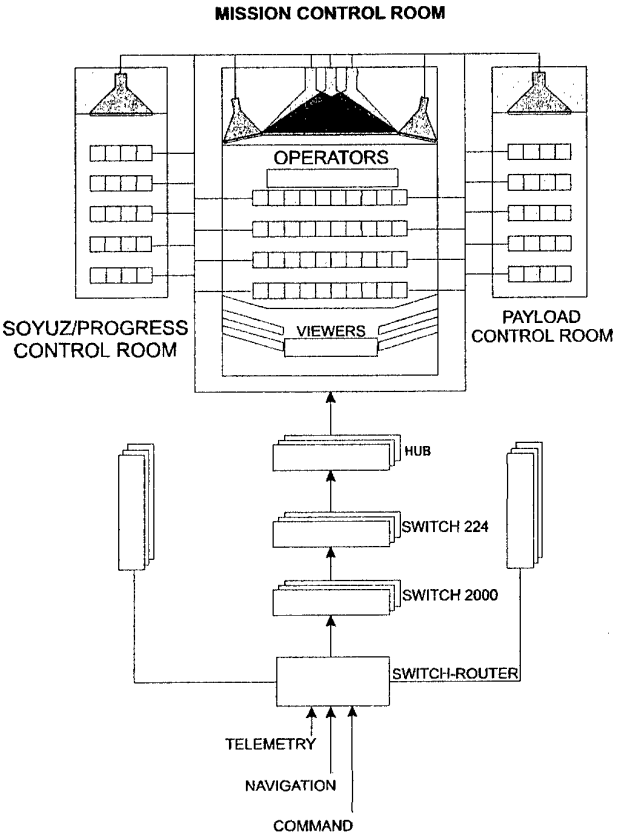

Figure 1

Another little control room is the Payload Control Room. The support groups are situated in all the premises of the Center.

The means of display of the information are represented by big screens and indicator panels (the Main and little control rooms) and by individual terminals at the operators' working places.

The means of display of the information with big screens were designed on the base of the next principles:

- creation of the "effect of presence" in order to facilitate the process of decision taking in the given interval of time according to the information displayed in real time,
- display only the essential information in this period of time without any excess,
- each piece of information must be displayed in his own place on the screen,

- any information received in the Center can be viewed on any indicator panel at the operators working places and on the big screens

The big screens are the rear-projection screens that create the comfort working conditions to the operators and observers at the balcony of the second floor in the Main Control Room.

The image is created by TV projectors (Barco etc.), slide projectors and graph plotters.

The MCC was modernized on the base of inculcation of new information technologies based on the use of fiberglass nets that form the branches of ballistic, telemetric and command and program information. The working stations placed at the operators working places, the separate terminals, the TV projectors and big screens are the users of these nets.

The information is distributed via fiberglass nets and cables by ordinary 2-levels scheme 100 MB "router-server", and then it is divided by switches and routed to the terminals (PC, work stations, X-terminals, TV projectors).

It must be said, that the system of TV switching, which exists in the Center since 1970, is very much in use nowadays in the process of the flight control, displaying telemetric information from the workstations and terminals with the TV output. It appeared to be efficient and economical to use it in order to distribute the command and program information for small quantities of operators in remote premises. It appeared to be essential the using of the systems of TV switching. The users of this system were provided with cables and necessary equipment in every building of the MCC. The system is necessary in the time of alterations in the efficient structure of flight control due to the moving of the staff. The qualitatively new principle of displaying information was inculcated in the MCC in 1998-1999. It uses the computer graphics according to the concept of imitational modeling of the conditions of the space ship progressing in real time mode and in the mode of analyses and planning of the flight.

The inculcation of the new informational technologies in the processes of display of the information at operators working places uses all the possibilities of the equipment Hewlett-Packard that is in use in the MCC.

The solution of "classical" problems of display of the informational model of the flight on the big screens and panels intended for big quantities of specialists and observers who don't take part in the process of the flight management (administrators, press, guests) demanded special efforts that resulted in original researches in the processes of display of the start, the exit into an orbit, and the trajectory of flight of the space ships with the map of the world in the background.

The program complex (PC) for displaying on the big screen of the processes of the start of the space ship and its exit into an orbit is also interesting. To do this, the imitational model of the start trajectory was written in the language C. This model is displayed in the co-ordinates H km (altitude) and L km (distance) and with a site of terrestrial surface in the background. The general image is accompanied by a graph of overload in the co-ordinates Nx, g, and t sec. [1]

The special features of the complex are the following:

- synchronization of the imitational model with the real time,
- combination of the graphics of different complexity with the speed of images updating.

The complex uses the "client-server" technology, when the server manages the processes of display of the information and synchronizes them, transmits to the clients graphical images and initial data. The client makes the direct forming of images.

The imitational model of the processes of the launching is written in the language C++ in C++ Builder environment. The display of information is realized using the system timer and the operator can adjust the process. A symbol of the space ship is made beforehand with graphic editor. Its movements are memorized in the form of a sequence of sprites binded in time. The operational complex permits to display different types of space ships (rockets with 2 or 3 stages, automatical stations, etc.). The fluency of movement is represented in a sequence of complex sprites. The data structure describing a complex sprite looks like a "tree", where the leafs are the structures describing simple sprites.

The program complex created in the MCC in order to display the trajectories includes the following computer technologies:

- "client-server" technology;
- synthesis of the images of objects of complex spatial forms with elements of virtual reality by method of return trace of beams;
- object oriented approach in solving the problems of imitational modeling of complex systems;
- "Distributed Component Object Model" technology;
- other technologies used in the modeling of the conditions of movement of space objects following the ICC program.

The complex uses the following program products (fig. 2):

- Service Control Manager – special process controlling the remote start of the servers building the image;
- Borland Database Engine (BDE) – the library, which represents the nucleus of the processor of databases, based on the IDAPI (Integrated Database Application Program Interface) technology;

- Borland SQLinks – the drivers of access to the SQL server of databases;
- COM (Component Object Model) – server of access to the data [2].

The complex permits to form the graphical images of several objects at the same time (for example, the image of the MIR station and the image of "Sojuz" approaching it for a junction) in the real time mode and in the mode of analysis and planning of flight operations.

It is very important that the MCC has the possibility to transmit the displayed information to remote users (stations of tracking, foreign centers of management, design offices, managing bodies).

The complex is developed by the way of widening the graphical possibilities with the purpose to use them in difficult situations (for example, junction of the objects in space in the conditions of tracking by the real information received from the co-ordinates determined by the operator).

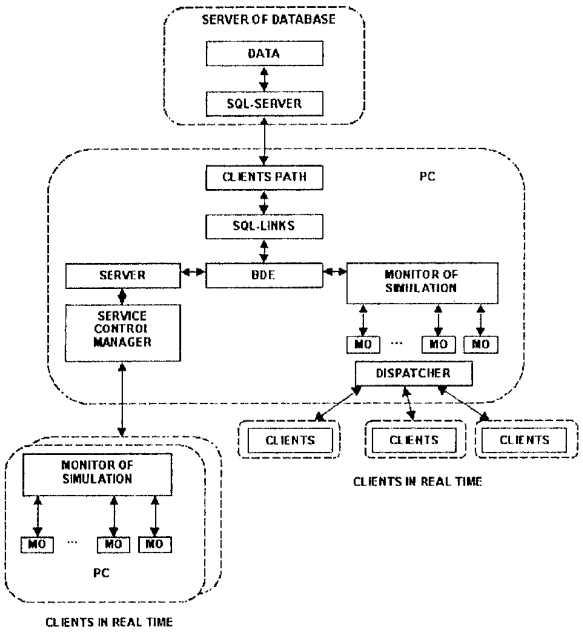

Figure 2

References:

1. The Procedure of Visualizing the Spacecraft In-Orbit Injection Applying the Virtual Presence System. T.Yu. Vorobieva, etc. - Cosmonautic and Rocket Building. 2000.
2. The Complex of Simulating and Visualizing Spacecreaft Motion Conditions under the Program of Mission Control of the International Space Station Functional-Cargo Module. V.F. Afanasiev etc. Cosmonautic and Rocket Building. 2000.

EMISSIVE DISPLAYS

ED-1. **Optimization of Plasma Display Panels**

Harm Tolner
Philips Components BV, The Netherlands
<harm.tolner@philips.com>

Paper is not available

ED-2. **The state and tendencies of the development of plasma display panels**

A.N. Ivlyushkin, V.G Samorodov

"Plasma" Co., Ryazan
<plazma@niigrp.ryazan.ru>

Main efforts of JSC "Plazma" in PDP developments are focused on the enhancement of light emission, of optical contrast under external illumination as well as on increasing the information capacity and resolution ability.

Last years the brightness of collective use screens in a new PDP generation was increased as a factor 4-5. The light emission was increased as a factor 5-6, while the lifetime was increased as a factor 1.5.

Due to new technology advances one expect increasing the active square of PDP screens up to 4 times, brightness – up to 1000 cd/ m^2, light emission – up to 5 lm/W as well as decreasing a pixel size down to 2 mm.

MODERN VACUUM FLUORESCENT DISPLAYS (VFD)

B.I. Gorfinkel, V.V. Zhidkikh, N.D. Zhukov, A.P. Loginov, E.V. Rusina, V.L. Frolov
R&D Institute VOLGA: 101, 50 let Oktyabrya, Saratov 410052, Russia;
E-mail: gorfinkl@san.ru

ABSTRACT: The paper evaluates modern status of development of low voltage cathodofluorescent displays. It is noted that currently the most important science & engineering and economic achievements could be expected from carrying out developments of cathodofluorescent displays using active matrix substrates (AMVFD).

Vacuum fluorescent displays, VFD's, are widely and for a long time known as self-luminous (emissive) means of information display. The recognized features of VFD's are:

- High luminance of information display – up to 3500 cd/m^2 ;
- Multicolor with using light filters, practically the whole optical range;
- High viewing angle - ±160°;
- Wide temperature range – from –60 to +70°C;
- Life time – up to 50000 hr
- High resistance to radiation, climatic and mechanic exposure, etc.

The listed above features defined the fields of VFD application from clocks and calculators to car and air borne equipment.

VFD's use effect of low voltage (10...100 V) or middle voltage (100-500) cathodofluorescence at which cathodophosphors emit light under exposure to low energy electrons. The efficiency level of some cathodophosphors achieved in recent years is 10...12 lm/W, and in special conditions it is –17 lm/W.

Several foreign companies are involved in development of VFD (mainly Japanese Futaba, Noritake Itron). In Russia the principle VFD developer is R&D Institute VOLGA.

VFD produced by foreign companies are mainly designed for displaying alpha-numerical, illustrating and graphic information without gray scale and color formation. Their active area do not exceed 200 cm^2 [(GP1063A01A made by Futaba features an active area (256x64) mm^2].[1]

We believe the main reason of the fact that Japanese creators of VFD did not master the next dimension range was competition with LCD. However, today it is clear that VFD compete successfully with LCD especially in severe operation conditions. Currently Japanese companies began production of modules using VFD for direct replacement of "some popular LCD modules" (a series of LCD emulators produced by Futaba)[1].

At the same time R&DI VOLGA did not terminate development of VFD with large scale active area including VFD screens. Monochrome VFD screen with 768x576 pixels and a pitch 0.22 mm was built as well as prototypes of 7, 10, 12 and even 14 inch displays – screens with full color image format up to SVGA (600x800). But problems of life time of color middle voltage sulfide phosphors and high cost of driver IC's for operation with voltage 200...300 V essentially hamper further work in this direction. (Cost of high voltage drivers used for control of experimental full color VGA VFD-screens was $20, and decrease of cost up to 2...3 dollars is expected only at demands of them up to hundreds thousand pcs per year).

On of the prospective trends in development of VFD technology is building of an active matrix VFD (AMVFD).

Active matrix displays – is a well-known technology. The main problem, which is solved using active substrates, is ensuring of optimum, most frequently static mode of pixel excitation (LCD, VFD, OLED etc.). Used for this effect dynamic addressing of instructions for pixel excitation for instance in two coordinates, X and Y, as it is known, solves the problem of reduction of the number of outside leads (M*N)/(M+N) times, where M is number of pixels in X coordinate, and N is a number of pixels in Y coordinate. Thus elements for pixel control should perform a function of addressing an instruction signal for excitation of memory and switch of voltage (current) corresponding to static mode of pixel excitation.

AMLCD uses as a rule a matrix of thin film single-transistor cells of pixel control, which perform a function of addressing and switch of control voltages, and a memory function is performed by inter-electrode capacitances of LC cells. Thin film transistors, due to low mobility of electrons and holes (charge carriers), even for a single-transistor cell of pixel control, occupy up to 15% of the area of the AMLCD substrate. Ensuring of allowable defect density requires extremely high uniformity of thin film structures (α- or poly-Si) across the whole display area. The latter defines the cost of AMLCD and the level of investments for their production. So the cost of the plant for AMLCD production in the volume 150 pcs per year is estimated as $500 mln.

At the same time the low mobility of charge carriers in thin film transistors, their low operation voltages and fast response restrict possibility of placing active matrix indicators of row and column addressing circuits on the substrates. Thus (N+M) outside leads are positioned on periphery of active matrix displays,

which does not only hamper testing of displays in their production but complicates the structure and increases the cost of the finished display device.

An alternative to thin film structures for using as a substrate in AMVFD is a substrate of mono-silicon chip.

We spoke out an idea of using a mono-silicon chip plate as an anode substrate as long ago as in 1976.[2] In early 80-s the Japanese company Ise Electronics Corporation reported on creation of AMVFD prototype on a Si substrate (23x23) mm^2 which displayed a TV picture.[3]

However, later Noritake Co. Began production of AMVFD as monochrome dot-matrix indicators (MW – initial letters in their name), anode plates of which are assembled of several tens (up to 32) Si chips. Each of these chips accommodates 256 pixels, and for each of them control switches and elements of static memory, loaded with data from 256 digits receiving shift register, are made. Maximum size of an active area, for instance of MW25632EB, is (256x32), a pixel pitch is 0.3 mm, number of outside leads – 47, luminance – 3500cd/m^2 for anode voltage 15 V and specific consumption power as low as 0.8 W/10 cm^2. [4]

In the most common case a cell controlling one pixel in AMVFD comprises two MOS transistors: one of them is addressing and the other is switching anode voltage. Memory function in this case is performed by capacitance, formed between a gate and a source of the switching transistor.

Calculations carried out in R&DI VOLGA showed that in this case the total area occupied by transistors is only about 1% of VFD display area. (Compare with 15% of the substrate of thin film single-transistor cells).

Probability of occurrence of defects in such system is minimum. Using of mono-silicon substrate allows also to accommodate, on its periphery drivers for row and column addressing for essential reduction of the number of outside leads.

R&DI VOLGA has developed the fist series of AMVFD on substrates of a mono-silicon chip with number of pixels (160x80) and (320x256). These displays use only one Si substrate with double-transistor cells for control of each pixel. Figures 1 and 2 present pictures of images shown by AMVFD (320x256) using a mono Si substrate.

The most important factors, defining using of that or another technology (or its elements) is the level of its maturity and availability. Technologies meeting these requirements allow not only creating displays with optimum characteristics but also providing effective division of labor and co-operation in their production. It means that AMVFD on silicon substrates may become competitive in their class of displays with minimum investments for preparing them for production.

In Russia and Byelorussia semiconductor production using 200 mm diameter silicon plates was mastered. In other countries – even using plates with 300 mm diameter. In case of using such plates in a whole format or making of them fragments, for instance ¼ of the information area, then it is not difficult to imagine AMVFD with a diagonal 6...12 and, may be, even 14 inches.

One of the essential challenging problems of VFD is non-productive power lost for cathode heating.

In 90-s some companies (Candensent, Pixtech etc.) were working on development of matrix displays with so called Spindt tip cathodes, but the displays built by them were not widely used. One of the reasons was, as we think, very complicated and expensive technology of micro tip cathode formation.

R&D Institute Volga also is working on development of field emitters which are based on original technological decisions. In 2000 the Institute found and patented the design and technology of formation of the planar edge emitters using thin film diamond carbon with application of the equipment designed for planar cycle of micro electronics.[5,6]

SUMMARY

We have developed and produce monochrome low voltage cathodofluorescent screens operating in a multiplex mode with a number of pixels up to 768x576. We have made prototype displays with diagonal 7...14 inches with a format of full color display of 600x800 pixels. We made a first series of high luminance active matrix cathodofluorescent displays (AMVFD) operating in a quasi static mode on the substrates manufactured of mono Si chips with 160x80 and 320x256 pixels. It was shown that in a number of applications low voltage cathodofluorescent screens may successfully compete with LCD's. The production technology of the cathodofluorescent displays, including AMVFD made using mono Si chips, allows to organize their production, in particular in Russia, with minimum investments.

REFERENCES

1. www.futaba.com
2. Patent of RF #645460 of 03.09.1976
3. T. Nikamura, K. Kiyozumi: Vacuum Fluorescent Display, Advances in image pickup and display, volume 5, 1982
4. www.noritake-itron.com
5. Patent of RF #2152662 of 10.07.2000
6. Patent of RF #2196372 of 10.01.2000.

Fig 1. Displaying the graphic information on an AMVFD screen

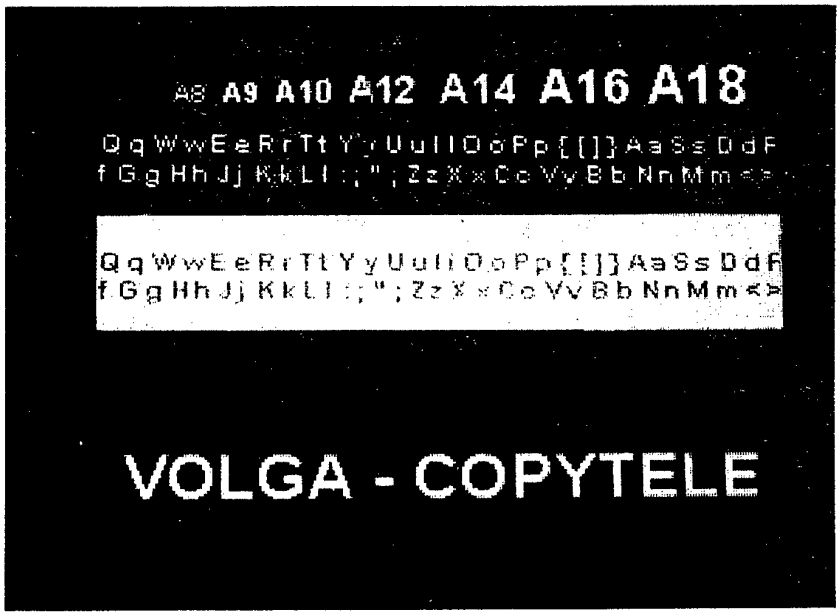

Fig 2. Displaying the text information on an AMVFD screen

Laser CRT: Last Results Concerning An Improvement Its Parameters.

V.I. Kozlovsky, Yu.V. Korostelin, P.I. Kuznetsov[1)], A.B.Krysa, Ya.K. Skasyrsky, Yu.M. Popov

P.N. Lebedev Physical Institute of RAS, 53 Leninsky pr., 119991 Moscow, Russia

[1)]Institute of Radioengineering and Electronics of RAS, 1 Vvedenskogo, 141120 Fryazino, Russia

Abstract. The main room temperature characteristics of laser screens made of bulk II-VI compound crystals are presented. To date output power of 4 W with e-beam-light efficiency 4-5 % has been achieved for blue (455 nm), green (525 nm) and red (620 nm) spectral ranges. A problem of blue emission has been solved in main by using high-quality ZnSSe single crystals obtained by improved vapor phase growth technology. Last results obtained on basis of multi quantum well (MQW) epitaxial structures are reviewed also. Although lasing has been achieved on a set of MQW structures such as ZnCdSe/ZnSe, CdSSe/CdS at room temperature their characteristics are still worse than the characteristics of bulk laser screens. Using of a periodic-gain InGaP/AlInGaP MQW structure has allowed decreasing the laser threshold of "red" laser screen about ten times less. Output power and efficiency of such a MQW laser have been increased also.

Keywords: laser, CRT, II-VI compound, III-V compound, MQW heterostructure, wafer bonding

1. Introduction

A laser cathode-ray tube (LCRT) was one or the most promising inventions in the field of electron-beam-pumped semiconductor lasers [1]. However, thirty years have already elapsed after the first reports on the experimental implementation of LCRTs [2,3] but this invention has not found so far wide applications in the economy because of the absence of laser screens (LSs) that could efficiently work at room and higher temperatures. Problem with outgassing of the LS that is important for preparation sealed LCRT, is not solved also. In this paper, we present last results obtained with LSs made of both II-VI compound single crystals and multi quantum well structures. These results allow hoping on near future commercialization of the LCRT technology.

2. Laser screens on bulk II-VI compounds for room temperature operation

Until now active elements of the LCRT named below as laser screens (LSs) were produced from single crystals of II-VI compounds for visual spectral range. Technology of making of LSs is relatively easy. Moreover the threshold of such LSs is low enough at temperature range T < 200 K. Therefore some demonstration set-ups were developed with cryogenic cooling machines [4-5].

Early it was demonstrated that LSs may work at room temperature also [6]. However the semiconductor layer thickness should be as small as a rectifiable electron path length. It corresponds to 10-15 microns at electron energy 45-50 keV. For sealed devices it was difficulty to do such small thickness along large-area LSs because single crystals used before had some pours. High-energy electrons passed through these pours in the semiconductor layer to glue layer stimulating its gassing. As a result, life time of the sealed LCRT was limited by worsening internal vacuum. Increasing the semiconductor thickness leads to increasing the threshold and decreasing the laser efficiency.

This problem was solved in P.N. Lebedev Physical Institute in collaboration with Research Institute of Materials Science and Technology (Zelenograd) by means of additional cleaning of starting materials in vapor growth technology. It allows a decrease of pour concentration in single crystals. For real blue LCRT working at RT was developed a vapor phase growth technology for large-area ZnSSe single crystals [7].

Based on these advanced materials several series of LSs with thin semiconductor layer were made in Platan company (Fryazino). Fig. 1 shows the main characteristics of these LSs obtained on experimental set-up. Measurements were carried out at scanning

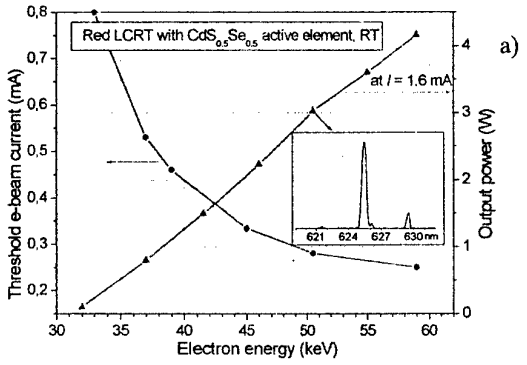

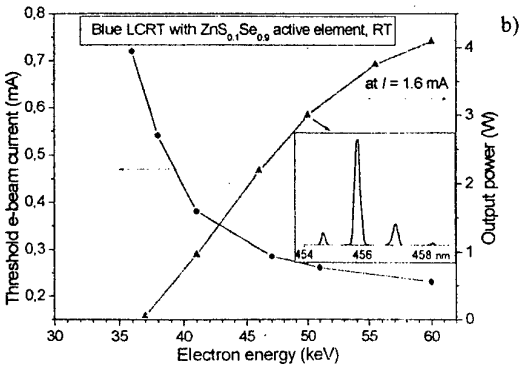

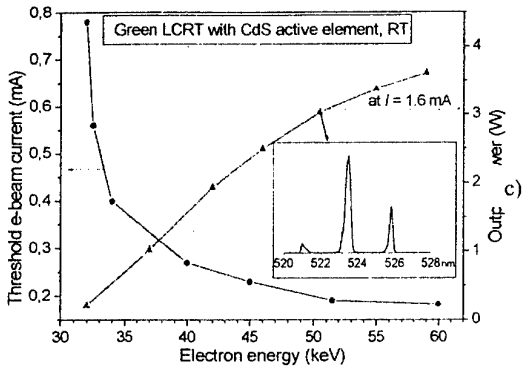

Fig. 1. Dependence of the threshold current and the output power on the electron energy for different bulk LSs emitting in red (a), blue (b) and green (c) spectral regions. Inserts show lasing spectra.

mode of electron beam pumping. Scan velocity was higher $4 \cdot 10^5$ cm/s. Repetition rate was 50 Hz. Electron beam spot on the LS was 15-25 μm at small current, increasing with increasing the current and decreasing the electron energy up to 50 μm. LSs emitting in red, green and blue spectral ranges were made of $CdS_{0.5}Se_{0.5}$, CdS and $ZnS_{0.08}Se_{0.92}$, respectively.

One can see that for all LSs the output power at E_e = 50 keV and I_e = 1.6 mA may be as high as 3 W. Decrease of the output and increase of the threshold current with decreasing the electron energy are due to decreasing the real excess of the threshold in current density mainly. The threshold current density is estimated as 50-60 A/cm^2. To work with such a threshold the special CRT with high e-beam intensity is required. Fig. 2 shows the sealed tube developed by

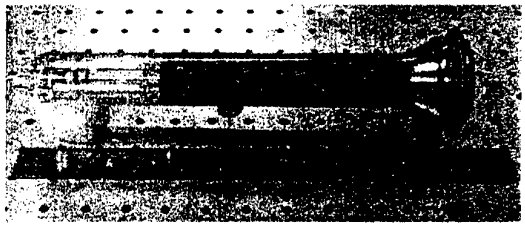

Fig. 2. Sealed LCRT. Distance between holes of the table is 1 inch.

Pricipia LightWorks Inc. in collaboration with P.N. Lebedev Physical Institute. The fist image with bad optical superposition of colors is presented in Fig. 3.

3. Laser screen on MQW structures

Theoretical estimation shows that the threshold obtained experimentally is close to its limit for bulk LS [8]. Further essential improvement of LCRT characteristics is possible only at using multi layer heterostructures, in particular multi quantum well (MQW) structures. Fist laser was released on the 150 ZnCdSe/ZnSe QW structure grown by molecular beam epitaxy on GaAs substrate [9]. Lasing at λ = 485 nm

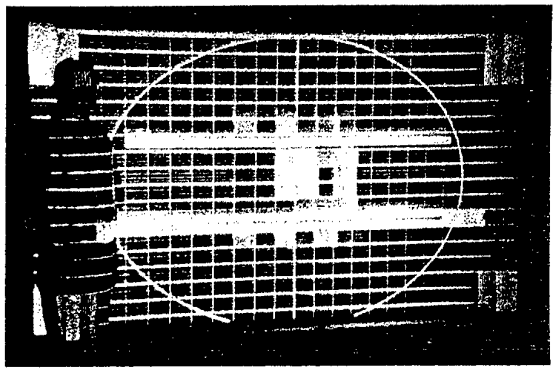

Fig. 3. First image obtained by laser projector with three LSs working at room temperature and E_e = 45 keV.

with power of 1.6 W and efficiency of 1.5 % was achieved at E_e = 50 keV. The threshold was estimated as j_{th} = 50 A/cm^2 at E_e = 40 keV. Later the power was increased to 2.7 W [10]. However the threshold was only a little smaller than the threshold of the bulk LS. Other disadvantage of the structure used was small total thickness. High-energy electron passed through the structure and destroyed the glue layer bonding the structure to a sapphire support. (The total thickness of the structure after removing a growth GaAs substrate was only 2-4 μm). It led to destroy the LS as a whole. To decrease the threshold and to increase the total semiconductor layer in LS, new structure design was tested. The 15 ZnCdSe/ZnSe QW structure was grown on a ZnSe substrate and cavity was formed by such a way that a part of the ZnSe substrate remained inside the cavity [11]. However all these efforts did not give better results on a whole in comparison with results achieved on the bulk LSs.

Really good results were obtained only in this year. First we have realized a laser with very small threshold at room temperature [12]. The GaInP/AlGaInP MQW structure was grown by MOVPE on GaAs substrate misoriented by 10^0 from (001) to (111)A surface. The structure contained the 1 μm thick GaAs buffer layer, the 6 nm thick GaInP layer, 17 pairs of the 286.5 nm thick AlGaInP barrier and the 8 nm thick GaInP QW, the 4.38 μm thick AlGaInP passive layer and the top 6 nm GaInP layer. It was intended that the QWs would be at wave antinode of lasing cavity mode and the barrier thickness was smaller than double carrier diffusion length. The first and top GaInP layers were used to prevent the AlGaInP layers from oxidation during making the cavity. The AlGaInP and GaInP layers were matched to the GaAs substrate. The Al content was 0.3.

The top surface of the grown structure had small enough microroughness. The RMS was smaller 1 nm. The cathodoluminescence (CL) spectrum at room temperature is shown in Fig. 4. The maximum of the CL spectrum was close to 630 nm. Fig. 4 shows also the photoreflection (PR) spectrum that has a feature near 620 nm in wavelength. The feature is due to interference on the structure period.

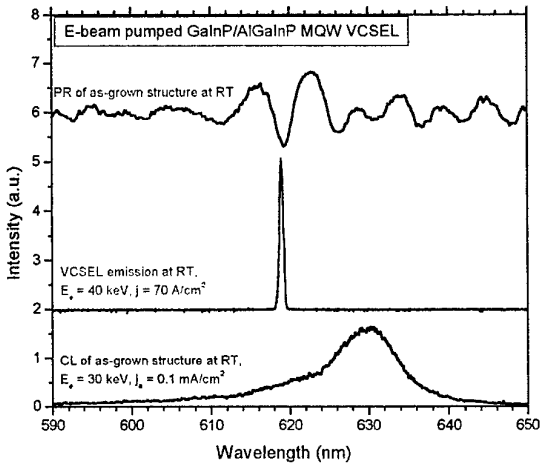

Fig.4. CL at E_e = 30 keV, j_e = 0.1 mA/cm^2 (lower curve) and PR (upper curve) spectra of as-grown structure, and lasing spectrum of VCSEL emission at E_e = 40 keV, j_e = 70 A/cm^2 (middle curve).

The six pairs of alternative quarter wave SiO_2 and TiO_2 layers were coated on the structure to form first mirror of the cavity. The structure with the first mirror was glued by epoxy to sapphire holder, the GaAs substrate and buffer were removed by polishing followed etching in KOH-H_2O_2-H_2O solution, and the second 7 pair mirror of the same design was coated. The formed cavity was pumped by scanning electron beam with electron energy of 25-60 keV, current of 0-1.7 mA, e-beam diameter of about 20-50 μm depending on the electron energy and current, and scan velocity of about $4 \cdot 10^5$ cm/s.

Lasing was achieved at electron energy from 25 to 60 keV, T = 80 and 300 K (RT). At RT the threshold current was as small as 25 μA at 40 keV. It corresponds to about 8 A/cm^2. That is 7 times smaller than typical threshold of LS made of bulk CdSSe (620 nm) at the same electron energy. The output power of the VCSEL was 0.7 W at RT, 40 keV and 1.7 mA. It is about three times smaller than the output of the bulk laser. Total divergence angle did not exceed 15^0 at maximum e-beam current used. Spectrum of the laser emission is present on Fig. 4 (middle curve) at 1.7 mA in the e-beam current. At all excesses of the threshold the lasing spectrum contains only one longitudinal cavity mode at 619 nm. The spectral mode position coincides practically with minimum in PR spectrum due to MQW period and is on the short wave side of QW emission line. It means that the MQW period is mismatched with maximum gain. Theoretical analyze of observed results has shown that low threshold lasing requires the position of the QWs to coincide with the antinodes of the cavity mode, at the maximum of the gain spectrum due to the QW ground state [12].

Using these results we grew more optimal structure to increase the output power at low threshold. New structure contained 25 QW of the same composition and thickness and MQW period was matched better with spontaneous emission maximum. Total thickness of the structure was practically the same as for previous structure. More transparent mirror containing 5 pairs of SiO_2/TiO_2 layers was used as the first mirror of the cavity while the 7.5 pair SiO_2/TiO_2 stack followed 0.1 μm thick Al layer were used as the e-beam bombarded mirror.

In this case, lasing was achieved on two modes of λ = 632 and 636 nm. At E_e = 42 keV, the threshold current was not exceed 0.03 mA along the 2 cm^2 area sample and output power at 1.6 mA was as high as 6 W with efficiency higher 8 %. Dependence of the threshold current and output power on electron energy are presented in Fig. 5. These measurements were

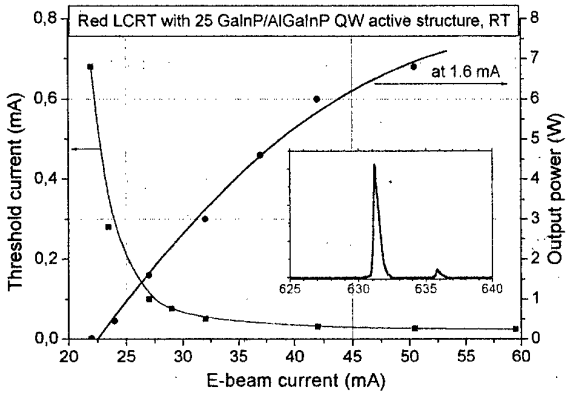

Fig. 5. Dependence of the threshold current and the output power on the electron energy for LS made of GaInP/AlGaInP MQW structure. Insert shows lasing spectra.

carried out at the same conditions as ones presented on Fig.1. Comparison of Fig. 5 with Fig. 1a shows strong improvement of the main characteristics for the LCRT emitting in red spectral range.

Other very promising result obtained also in this year is an achievement of lasing on MOVPE-grown multi-layer CdSSe/CdS structures [13]. Peculiarity of these structures is that they have hexagonal crystal lattice. Such a lattice is expected to be more stable to a formation of defects than cubic one. So the life time problem should be solved more easily.

The main characteristics of the LS made of a CdSSe/CdS structure grown on CdS substrate and contained 40 2-nm thick CdSSe layers are presented in Fig. 6. Lasing was observed at λ = 548 nm, being at short wave side of the spontaneous emission maximum (λ = 573 nm) as well as in the case of Fig. 4. However here the short wave shift is due to a peculiarity of the type-II band alignment of the CdSSe/CdS structure used. We hope that lower threshold and higher efficiency will be obtained by using the CdSSe/ZnCdS structures with the band alignment of the type I.

For blue range, well-known ZnSSe/ZnMgSSe MQW structures may be used at making the LSs. The best results were achieved by using MBE technology mainly [9-11]. Unfortunately fist positive results obtained by MOVPE technology in [14] was not

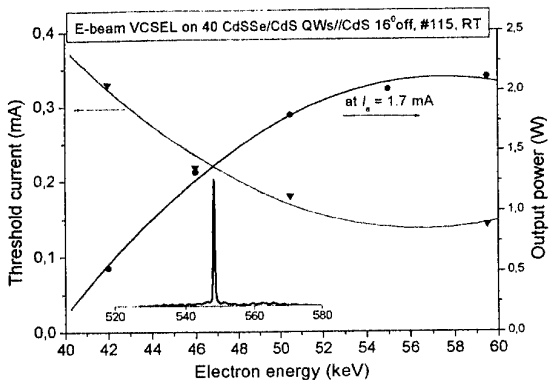

Fig. 6. Dependence of the threshold current and the output power on the electron energy for LS made of CdSSe/CdS MQW structure. Insert shows lasing spectra.

developed later because the interest in ZnSe-based injection lasers was dropped in that time. The MOVPE is more promising technology for the LS production because its growth rate is higher that at MBE. That is important to grow thick structures required for e-beam pumping.

4. Conclusion

Last time a noticeable progress is observed in the LCRT technology. A substantial improvement of the LCRT characteristics at room temperature for main three colors was achieved due to the improvement of the technology of LS manufacturing from single crystals. By this way a full color television projector with high resolution and the radiation flux of 2000-4000 lm may be realized in near future.

On other hand the theoretical advance of the epitaxy technology was firstly confirmed experimentally at using the GaInP/AlGaInP MQW structure emitting in red region. Now it is clear that soon the same promising results will be obtained in blue and green regions also. Only problem that remains a serious obstacle of commercialization of the LCRT technology, is the problem of bonding the active structure to the sapphire or other dielectric support being a tube window simultaneously.

This work was supported in part by Russian Foundation for Basic Research, Grants 01-02-16409, Russian Academy of Sciences Programs "Low-dimension quantum structures", Semiconductor lasers" and "New materials and structures", Russian Federation Program "Physics of solid-state nanostructures" and Principia LightWorks Inc., CA.

References

[1] N.G. Basov, O.V. Bogdankevich, A.S. Nasibov. Cathode-Ray Tube. US Patent 3558956, 1971.

[2] Parkard I.R., Tait W.C., Dierssen G.H. Appl. Phys. Lett., **19**, 338 (1971).

[3] N.G. Basov, O.V. Bogdankevich, A.S. Nasibov, A.N. Pechenov, V.I. Kozlovsky, P.V. Shapkin, V.M. Kamenev, V.M. Pochernyaev, V.P. Papusha. Dokl. Akad. Nauk SSSR, **205**, 72 (1972).

[4] A.S. Nasibov, V.I. Kozlovsky, P.V. Reznikov, Ya.K. Skasyrsky, Yu.M. Popov, J. Crystal Growth **117**, 1040 (1992).

[5] V.N. Ulasyuk. Kvantoscopy. Radio i Svyaz', Moscow, 1988.

[6] V.I. Kozlovsky, A.S. Nasibov, A.N. Pechenov, Yu.M. Popov, P.V. Reznikov. Sov. J. Qauntum Electronics, **7**, 1283 (1977).

[7] Yu.V. Korostelin, V.I. Kozlovsky. phys. stat. sol. (b) **229**, 5 (2002).

[8] V.I. Kozlovsky, Yu.M. Popov. Quantum Electronics **33**, 48 (2003).

[9] N.G. Basov, E.M. Dianov, V.I. Kozlovsky, A.B. Krysa, A.S. Nasibov, Yu.M. Popov, A.M. Prokhorov, P.A. Trubenko, E.A. Shcherbakov, Quantum Electronics **25**, 726 (1995).

[10] V.I. Kozlovsky, E.A. Shcherbakov, E.M. Dianov, A.B. Krysa, A.S. Nasibov, P.A. Trubenko. J. Crystal Growth **159**, 609 (1996).

[11] V.I. Kozlovsky, Yu.V. Korostelin, Yu.M. Popov, Ya.K. Skasyrsky, Yu.G. Sadofyev. phys. stat. sol. (b) **229**, 1033 (2002).

[12] V.Yu. Bondarev, V.I. Kozlovsky, A.B. Krysa, J.S. Roberts, Ya.K. Skasyrsky. E-beam pumped GaInP/AlGaInP MQW VCSEL. Proc. of 15-th International Conference on Indium Phosphide and Related Materials, May 12-16, 2003, Santa Barbara, CA, USA.

[13] V.I. Kozlovsky, V.Yu. Bondarev, D.A. Sannikov, P.I. Kuznetsov, V.A. Jitov, G.G. Yakushcheva, L.Yu. Zakharov, K.P. O'Donnell, C. Trager-Cowan. E-beam longitudinal pumped laser on MOVPE-grown hexagonal CdSSe/CdS MQW structure. Proc. of 10th European Workshop on Metalorganic Vapour Phase Epitaxy, Lesse, Italia, June 8-11, 2003.

[14] V.I. Kozlovsky, A.B. Krysa, Yu.V. Korostelin, P.V. Shapkin, H. Kalisch, M. Luenenbuerger, M. Heuken. J. Crystal Growth, **184/185**, 124 (1998).

ED-5. **Development of cold cathode displays on single-wall carbon nanotubes**

V.I. Konov, V.D. Frolov, A.V. Karabutov, E.D. Obraztsova, S.M. Pimenov, A.S. Pozharov, S.V. Terekhov

General Physics Institute of RAS, Russia
<vik@nsc.gpi.ru>

B.I. Gorfinkel, N.P. Abanshin, N.D.Zhukov

R&D Institute "Volga", Russia

Paper is not available

PHOTON AND ELECTRON EMISSION FROM POLYMER FILMS UNDER ELECTRIC FIELD INFLUENCE

A.N.Lachinov, V.M.Kornilov, Yu.M.Yumaguzin, E.E.Tchurlina

Institute of Physics of Molecules and Crystals,
Ufa Research Center RAS
<lachinov@anrb.ru>

The paper presents the results of investigation of two excellent phenomena peculiar to some polymers. These are electroluminescence (EL) and electron field emission. EL was found to be of threshold origin, the threshold being 3 V. The voltage varied within a range of 0 V to 100 V. The quantum efficiency was 10 %. The results obtained led to a conclusion that EL is due to the recombination processes developing in the polymer proper, for light-emitting accompanying the sample failure belongs to a quite different spectrum area. EL arises when the polymer is in a dielectric state. There is no EL when the polymer is in a conducting state.

The paper shows that the deposition of an electroactive organic polymer film on the graphite or metal surfaces leads to the decrease in the effective work function. As a result we obtained a system that possesses the emission efficiency comparable to that of the diamond-like films. The electric field emission was studied with the use of a scanning emission microscope (SEM). The paper presents the analysis of the surface morphology and surface distribution of emission centers (EC).

ED-7. ULTRA BRIGHT LED LIGHT SOURCES FOR DISPLAY APPLICATIONS AND ILLUMINATION

Yu. Trofimov, V. Posedko, S. Lishik, V. Kalenkov, I. Mironenko, V. Sivenkov

Institute of Electronics NASB, Logoiskii trakt 22, 220090 Minsk, Belarus
<senso@inel.bas-net.by>

The modern level and prospects of development ultra bright LED light sources is considered, the basic problems of their creation, ways of the decision and possible areas of application are analyzed.

The own development in the field of creation one-color and RGB energetically effective LED light sources with consumed electrical power up to 30 W and with the light characteristics superior traditional light sources of the appropriate electrical power are described.

ED-P1. Optimization of Organic Light-Emitting Diodes (OLED) Using Scanning Near-Field Optical Microscope (NSOM)

Tatiana Limonova[1)], Oksana Kotova[2)], Elena Perevedentseva[1)], Oleg Mirzov[1)], Raida Baigeldieva[1)], Natalia Kuzmina[2)], Aleksei Vitukhnovsky[1)] and Leonid Lepnev[1)]

[1)] P.N. Lebedev Physical Institute RAS, Leninsky prospect, 53, Moscow, 119991, Russia

[2)] Faculty of chemistry, M.V.Lomonosov Moscow State University, Vorobjovy Gory, Moscow, 119899, Russia

Abstract: Structure optimization for multi-layer electroluminescent (EL) devices with rare-ion as a source of emission have been done. EL devices ITO/PEDOT/PVK/$TbL_3(TPPO)_2$/Al (HL = HSal, HPA) were produced and their electrical and optical characteristics were studied. Dependence of surface quality for EL device on solvent nature was established by means of NSOM using. Tetrahydrofurane was found to be more suitable solvent for these devices.

Keywords: Organic light-emitting diodes, scanning near-field optical microscope, surface quality.

INTRODUCTION

At present OLED are of great interest for electronic industry. These devices are used for manufacture of color screens with flat panels. They have low working voltage (4-5 V). Their color can be easily managed (for multi-color OLED). They can be produced on flexible substrates. Technology of their manufacture is rather simple and consequently cheap what is important for commercial applications.

Application of rare-earth elements (REE) complexes with organic ligands as EL materials is an important step toward improvement of manufacture technology for EL devices since such complexes are more stable with respect to oxidation. They also possess thermostability and have narrow luminescence band as compared with organic and polymer materials [1].

However the problem of EL materials production characterized by high light monochromaticism as well as by high quantum yield and stability of work characteristics is not now solved.

Efficiency of OLED's work is determined by many factors among which in addition to active layer emission efficiency as well as to chage carriers life time and others covering quality keeps the important place. For stable performance of such devices homogeneous amorphous films of active layer substance are necessary. The presence of breakages in films results in short circuit of electrodes and thickness inhomogeneity or small crystals inclusions lead to inhomogeneity of current density and to non-uniform brightness as well as to local processes of substance destruction and to electrodes detachment.

Taking into account importance of the problem and lack of detaled investigations surface quality for active layers based on REE complexes the purpose of this work was establishment of dependence for surface quality of such layers produced by spin-coating method on solvent nature during optimization of OLED by means of NSOM.

EXPERIMENT

In the framework of this problem carboxylates with composition TbL_3 and $TbL_3 \cdot nH_2O$, where HL – ortho-substituted benzoic acids: salicylic acid (HSal) and phenylanthranyl acid (HPA), were synthesized and characterized by elemental, IR spectroscopic and thermal analysis. Terbium complexes of salicylic and phenylanthranyl acids were selected from the set of complexes under consideration for OLED production as have a large quantum yield of photoluminescence and at the same time possessing good solubility in standard organic solvents like ethanol, toluene, chloroform and tetrahydrofurane. Influence of mixed-ligand complex creation of $TbL_3 \cdot nQ$ –type on spectrum character, intensity and relative quantum yield of photoluminescence was studied. O-donor ligand triphenylphosphine oxide (TPPO) was selected as neutral additional ligand Q (Fig.1).

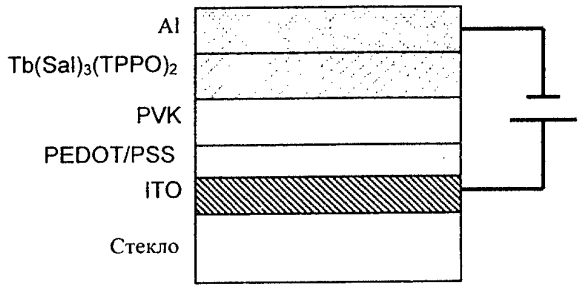

Fig. 1a. Structure of OLED based on terbium complex.

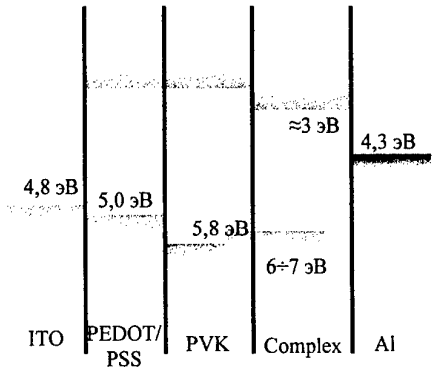

Fig. 1b. Energy diagram of OLED

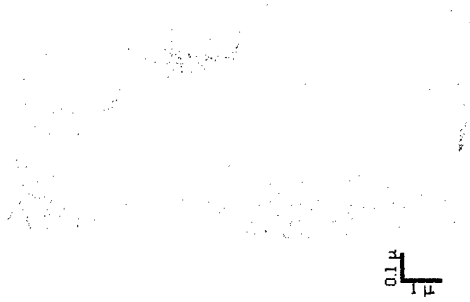

Fig. 2a. Surface topography of the film $Tb(Sal)_3 \cdot H_2O$. Mean-square roughness 66 nm.

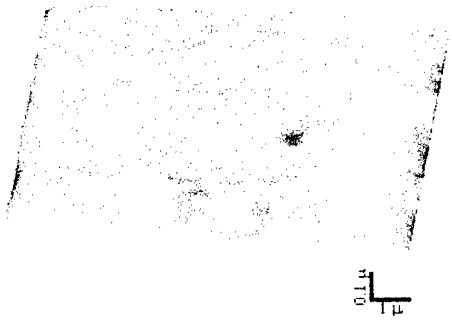

Fig. 2b. Surface topography of the film $Tb(Sal)_3 \cdot (TPPO)_2$. Mean-square roughness 9 nm.

Firstly addition of TPPO leads to increase of quantum yield for these complexes. Secondly its addition was expected to improve film-creation properties of the substance due to presence of phenyl rings. Actually, atomic force microscopy results confirmed this assumption [2] (Fig.2).

As a result it was found that conversion $Tb(Sal)_3$ and $Tb(PA)_3$ to mixed-ligand complexes with TPPO is accompanied by solubility and thermal stability increase as well as by improvement of film creation properties.

Initially single-layer OLED based on $Tb(Sal)_3(TPPO)_2$ was prepared. This device produced EL with extremely low efficiency (emission well seen by eye was obtained at voltage of 11 V and very high current density ≈200 mA/cm^2), and low stability (half-degradation time about several minutes). Such high current density is evidence of misbalance of hole and electron currents in the film of material.

Next tested structure was double-layer OLED using standard polymer mixture PEDOT/PSS as a hole transporting layer. This device displayed brightness equal to brightness of previous one under two orders smaller current densities. Since PEDOT/PSS mixture is known to be the material with good hole and bad electron conductivity one may suppose such layer manufactured from this mixture to be a layer blocking electrons from their direct penetration from work substance into ITO. Thus two orders current decrease with retaining of brightness in the second device is evidence of the fact that electron current is predominantly flows through the layer $Tb(Sal)_3(TPPO)_2$. This may be mainly caused by two reasons such as better conditions for electrons injection as compared with hole one as well as by better electron mobility in $Tb(Sal)_3(TPPO)_2$ film. Therefore layers which block through electron passing and improve hole injection in the work medium must be included for OLED optimization. As the deep HOMO levels location is characteristic of REE complexes [3, 4], high barier (right up to 2 eV) exists for hole injection from ITO (and even from PEDOT/PSS) layer into $Tb(Sal)_3(TPPO)_2$ one. Consecuently addition of one more hole conducting layer with HOMO, intermediate between HOMO/PEDOT PSS and HOMO $Tb(Sal)_3(TPPO)_2$, into the OLED structure can result in improvement of the current balance. Polyvinylcarbazole (or PVC, see Fig. 1) is a good candidate for this purpose.

In order to investigate the dependence of the active layer surface quality on the nature of the solvent, the intermediate p-type conductivity PVC (poly(9-vinylcarbazole)) layer has been spin-casted from chloroform on the ITO surface and the EL $Tb(Sal)_3(TPPO)_2$ complex layer has been spin-casted from ethyl alcohol or tetrahydrofuran (THF). Quality of the surface of each layer has been investigated using the near field scanning optical microscope (NSOM). It turned out, that the ITO surface is generally regular, but contains individual irregularities with the size about 100 nm (fig. 3).

Deposition of the intermediate PVC layer increases the size of surface irregularities to about 300 nm. The use of THF for deposition of the $Tb(Sal)_3(TPPO)_2$ complex layer allows to obtain smoother surface (irregularities about 200 nm, see fig. 4) than the use of ethyl alcohol (irregularities about 300–400 nm, see fig. 5).

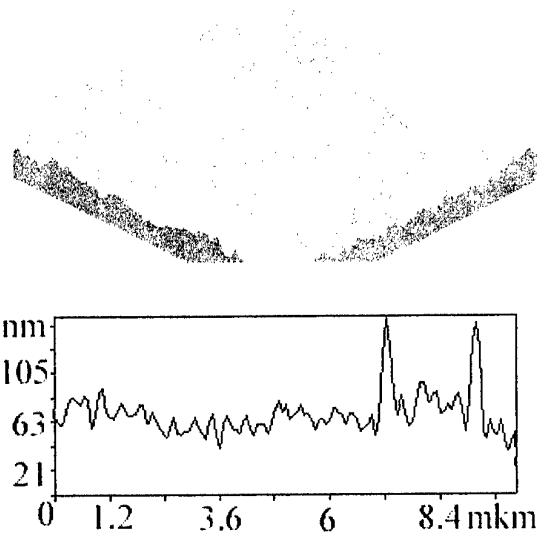

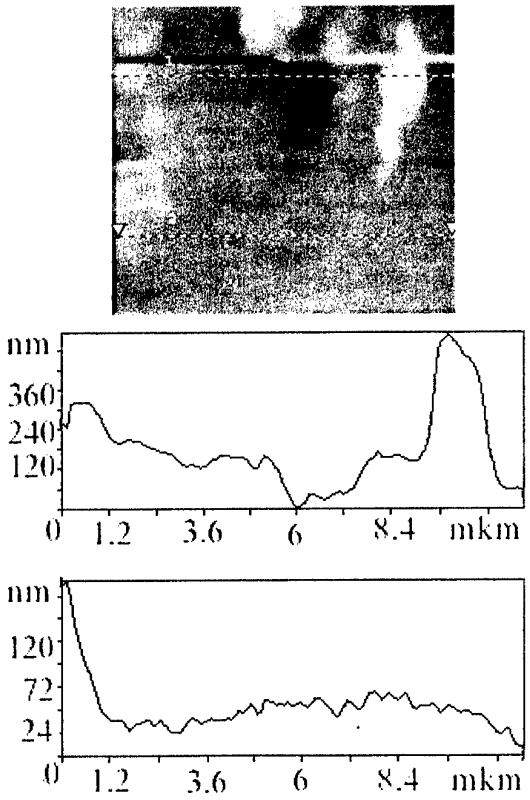

Fig. 4. Surface of the ITO/PVC-$CHCl_3$/$Tb(Sal)_3(TPPO)2$–EtOH EL layer

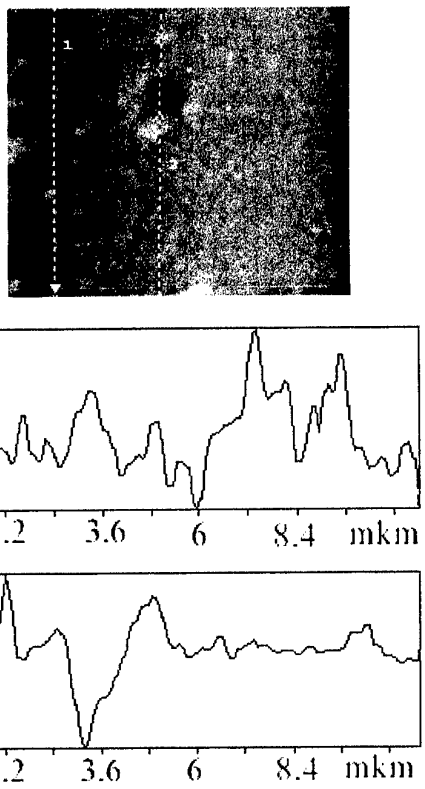

Fig. 5. Surface of the ITO/PVC-$CHCl_3$/$Tb(Sal)_3(TPPO)2$–THF EL layer

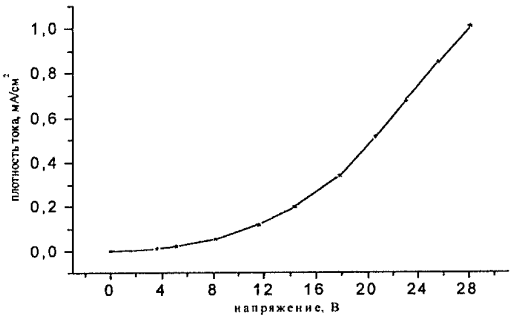

Fig. 7. V–I Diagram of ITO/PEDOT:PSS/$Tb(Sal)_3(TPPO)_2$/Al.

The multilayer EL devices with the ITO/PEDOT/PVC/$TbL_3(TPPO)_2$/Al (HL = HSal, HPA) structure have been manufactured and their electric properties have been studied. The emission layers of multiligand $Tb(Sal)_3(TPPO)_2$ and $Tb(PA)_3(TPPO)_2$ complexes have been spin-casted from THF. Presence of the bands corresponding to the terbium energy level transitions in the photo- and electroluminescence spectra indicates that the rare earth ion is the source of

radiation (fig. 6). Slight difference between the photo- and electroluminescence spectra can be interpreted by different methods of excitation of Tb (III).

The voltage-current (V–I) characteristic of the manufactured light-emitting device has been measured (fig. 7).

Two parts, low-voltage nonlinear and linear, can be distinguished on the V-I diagram. At low voltages the current is limited by carrier injection, while at high voltages the principle role is played by the carrier mobility limitation in the layers (electric resistance). Similar characteristics have been obtained for the ITO/PEDOT/PVC/$Tb(PA)_3(TPPO)_2$/Al light-emitting device.

The final composition of the device is: ITO/PEDOT-PSS/PVK/$Tb(Sal)_3(TPPO)_2$/Al.
Composition and prospective energy diagram are shown in fig. 1. The obtained device demonstrated considerable increase of operation time (30 minutes an more) over the single layer OLED.

CONCLUSIONS

1. The intermediate PVC and PBD layers on the ITO surface have been obtained by spin-coating from chloroform; the EL $Tb(Sal)_3(TPPO)_2$ и $Tb(PA)_3(TPPO)_2$ have been deposited on them by spin-coating from ethyl alcohol and THF.
2. The surface of each layer has been investigated by near field scanning optical microscopy.
3. The complex layer moderates irregularities of the polymer surface. The most smooth surfaces of the deposited $Tb(Sal)_3(TPPO)_2$ films have been obtained using tetrahydrofuran as a solvent.
4. Experimental ITO/PEDOT/PVC/$Tb(Sal)_3(TPPO)_2$/A and TO/PEDOT/PVC/$Tb(PA)_3(TPPO)_2$/Al light emitting devices have been manufactured by spin coating.

ACKNOWLEDGEMENTS

This work has been supported by the RFBR grants 02-03-33204, 03-02-16734, 03-02-16817 and SS-345.2003.2.

REFERENCES

[1] Crosby G.A., Whan R.E., Freeman I.I., "Spectroscopic studies of rare earth chelates", J. Chem. Phys. v.66, p.2493, 1962.

[2] S. Eliseeva, O. Kotova, N. Kuzmina, O. Mirzov, K. Anikin, L. Lepnev, E. Perevedentseva, A. Vitukhnovsky, "Electroluminescent properties of the mixed ligand complex of terbium salicylate with triphenylphosphine oxide", Synthetic Metals, 2003, in press.

[3] S. Capecchi, O. Renault, D.-G. Moon, M. Halim, M. Etchells, P.J. Dobson, O. V. Salata, V. Christou, "High-Efficiency Organic Electroluminescent Devices Using an Organoterbium Emitter" Adv. Mater. v.12, No.21, p.1591-1594, 2000.

[4] S. W. Pyo, S. P. Lee, H. S. Lee, O. K. Kwon, H. S. Hoe, S. H. Lee, Y.-K. Ha, Y. K. Kim, J. S. Kim, "White-light-emitting organic electroluminescent devices using new chelate metal complexes", Thin Solid Films v.363, No.1/2, p.232, 2000.

ED-P2. **Semiconductor Laser Sources for LCD and DMD Projectors**

A.S.Nasibov
P.N.Lebedev Physical Institute, RAS,
E-mail: nasibov@mail1.lebedev.ru

The principal deficiency of the light sources for LSD and DMD projectors are:
low brightness, weak color transmission, and weak richness. It is possible to improve this situation by using e-beam pumped semiconductor lasers as the sources. However, such light sources have some drawbacks:

- the threshold goes up with temperature;
- a great number of the technological operations;
- destruction of the semiconductor films under the action of radiation and an electron beam;
- X-ray radiation at the electron energy 45-50 keV.

This problem may be solved by means of manufacture of SLS as a transparency sapphire substrate on which the $A_2 B_6$ or $A_3 B_5$ microcrystals are grown. These microcrystals form a massive of the semiconductor microresonators [1]. This technology provides a good heat conductivity and a resource increasing. The natural crystal facet provides decreasing of surface losses. The microscopic size of the optical resonators ensures their good quality and high efficiency. Such type of a SLS may be pumped by scanning and pulse e-beam. Depending on the semiconductor compounds the SLS may radiate blue, green, and red monochromatic light. Different variants of the scanning and pulse SLS are considered.

1. Rus. Pat. #21914553. 14.11. 2000. Bul .# 29, 20.10.2002

ED-P3. A 2.2-inch QCIF AMOLED with High Quality ITO

Yen-Chung Lin, Hsiu-Chun Hsieh, Wei-Chieh Hsueh, An Shih, Shih-Chang Chang, Yaw-Ming Tsai
Chiu-Fen Tseng, and Kuang-Jun Chen

Advanced Technology Research Center, Toppoly Optoelectronics Corp., Chu –Nan, Taiwan, R.O.C.

Abstract

The characteristics of ITO film on different under-layers including Si-containing insulators and organic materials were investigated. It was found that the visible light transmittance of ITO film on different under-layer is maintained, however, the surface morphology of ITO film depends strongly on different under-layers. Also observed is the strong dependence of surface roughness on luminance efficiency. Base on these results, a new pixel structure with insulating material is proposed for AM-OLED applications. By means of low temperature poly-silicon (LTPS) technology, we developed a multi-color 2.2-inch QCIF AMOLED with good properties of ITO film. These technologies will open up the OLED applications to high efficiency and long lifetime AMOLED displays.

1. Introduction

Organic light emitting display (OLED) is one of the most attractive display technologies due to its self light-emitting, thin size, wide viewing angle, and fast response characteristics [1-2]. Low temperature poly-Si thin film transistors (LTPS TFTs) have been widely applied not only in active liquid crystal displays but also in active matrix organic light emitting display (AMOLED). Recently, the OLED displays driven by LTPS-TFTs have become the best candidate in order to achieve high resolution, less driving voltage and low power consumption [2-3].

As the OLED technology is continuous improved, two major issues need to be improved, the first issue is OLED materials and its process improvement, and the second issue is the variation of TFT characteristics, such as Vth, and mobility. The non-uniform TFT characteristics can cause display image uniformity problem and circuit failure. The operation of pixel is less dependent on TFT characteristics with the current driving design. However, the requirements of smooth surface morphology of ITO film as anode material in OLED is to improve the image quality and lifetime. And, the film properties including conductivity, transmittance, surface morphology and work function of ITO film dominate the device characteristics of Active Matrix OLED. The surface morphology of ITO film must be smooth enough, or the device would produce large leakage current or point discharge and thus cause a defect pixel.

In this study, we investigated the characteristics of ITO film on different under-layers. It was found that the different under-layers resulted in significantly different surface morphology of ITO film; the surface roughness of ITO film on the organic material is larger than it on Si-containing insulator materials, witch is comparable to commercially available ITO film for passive OLED. Based on these results, a new pixel structure of TFT in AMOLED is proposed. In this new structure, planarization layer is formed after data bus patterned, however, in the display area, the planarization layer is removed, thus the pixel ITO is contacted with Si-containing insulator material and performed low surface roughness for AM-OLED application.

2. High Quality ITO - Experiments

The ITO films were deposited by using DC magnetron sputtering on commercial glass substrate. The different under-layers including SiOx or SiNx were deposited by PECVD method, and the organic materials were deposited by coating method. Surface morphology of these films was investigated using SEM and AFM. OLEDs were fabricated on the ITO film with or without under-layers. The basic device structure is ITO/ HIL/ HTL/ EML/ ETL/ LiF/ Al. C545T doped Alq3 is used for the green EML. The luminescence was measured by PR650.

3. High Quality ITO - Results

3.1 Morphological Effects

Figures 1 (a) to (e) shows the AFM image of the ITO film on different under-layers. The surface image for ITO film on SiNx or SiOx film is similar to ITO film without under-layers. On the other hand, the image of ITO film on organic material shows rougher surface. The smooth ITO film surface will avoid the large leakage current and the defect pixel due to the point discharge effect of ITO film [5].

The AFM measurement data was summarized in Table 1. The surface morphology of ITO film using different under-layers was further verified by SEM analysis as shown in Figures 2 (a) to (e). From Figure 2, a highly smooth surface of ITO film on SiNx and SiOx layer can be seen, and a rougher surface of ITO film on organic material.

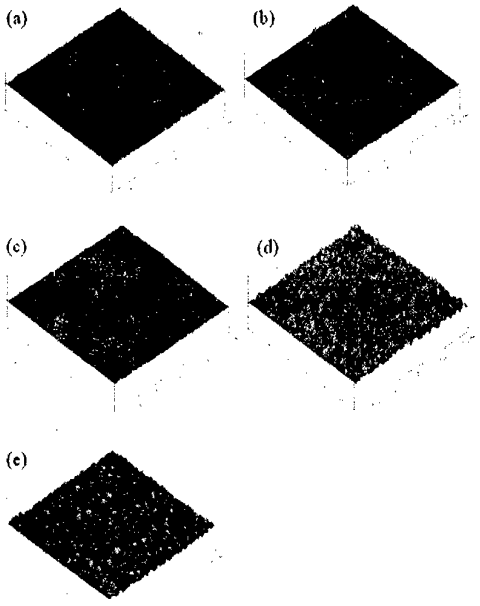

Figure 1. The AFM image of (a) ITO(750Å) without under-layer (b) SiNx(3000Å) / ITO(750Å) (c) SiOx(3000Å) / ITO(750Å) (d) organic material A / ITO(750Å) (e) organic material B / ITO(750Å).

Table 1. The surface roughness of ITO film (750Å) on the different under-layer

Under layer category	Ra (nm)
Without under-layer	0.99
SiOx	0.86
SiNx	0.61
Organic material A	3.08
Organic material B	3.67

Furthermore, the transmittances of ITO film on different under-layers are almost the same comparing with ITO film without any under-layer (i.e. ITO deposited directly on top of glass substrate). That results shows in table 2. The transmittance of ITO film is not strongly dependent on the different under-layer.

3.2 PM-OLED

Using these ITO films, we further fabricated PM-OLED samples. The 750Å, 1000Å and 1500Å ITO film properties and device characteristics of PM-OLED are shown in Table 3. The average roughness of 1000Å and 1500Å ITO film is larger than 750Å ITO film on the same under layer. And using 750Å ITO film with SiOx under-layer resulted in higher efficiency than that using 1000Å and 1500Å ITO film. The results indicate the OLED device characteristics are dominated by the surface morphology of ITO film.

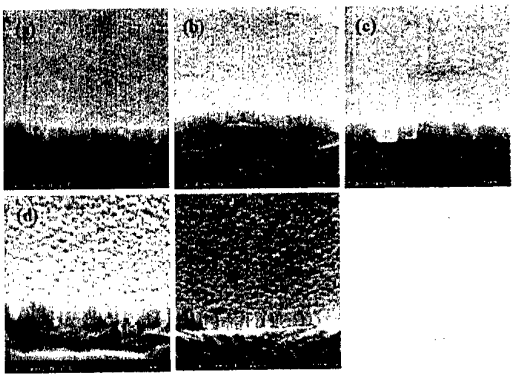

Figure 2. The SEM image of (a) ITO(750Å) without under-layer (b) SiNx(3000Å) / ITO(750Å) (c) SiOx(3000Å) / ITO(750Å) (d) organic material A / ITO(750Å) (e) organic material B / ITO(750Å).

Table 2. The transmittance of ITO film (750Å) on the different under-layer

Under layer category	Transmittance (%)
Without under-layer	90
SiOx	88
SiNx	90
Organic material A	91
Organic material B	91

Table 3. The ITO film properties and device characteristics of PM-OLED with the same under-layer

Film Stack	Ra (nm)	Efficiency (cd/A)
SiOx / ITO (750 Å)	0.86	17.12
SiOx / ITO (1000 Å)	1.11	11.79
SiOx / ITO (1500 Å)	1.47	11.62
Commercial ITO for PMOLED	0.78	17.85

3.3 New Pixel Structure for AMOLED

According to the discussed results, a new pixel structure of AMOLED was proposed. As show in Figure 3, we deposited a passivation layer under ITO layer instead of organic planarization layer to obtain smooth ITO surface. Another insulation material was also deposited on ITO to cover the edge of pixel electrode. This insulating material defines the light emitting area as well as prevents leakage of short between cathode and anode at the pixel edge, where the organic light emitting material has poor step coverage.

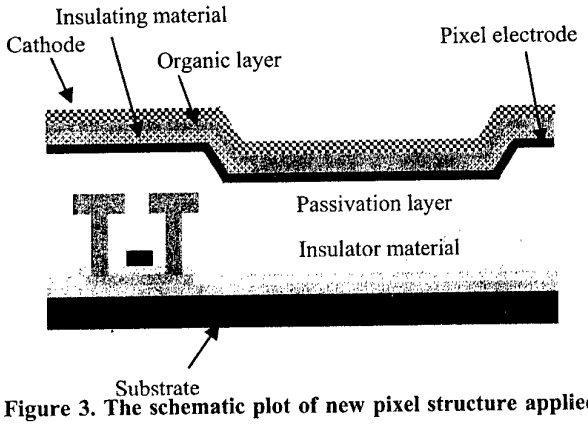

Figure 3. The schematic plot of new pixel structure applied in AM-OLED.

4. 2.2-inch QCIF AMOLED

4.1 Pixel and Driver Design

According to some investigation, the multi-transistors pixel circuit combined with current driving method can promote the image uniformity regardless of device characteristic variation. Nevertheless, the TFT characteristics variation due to manufacturing process can be reduced in Toppoly, the basic pixel circuit with 2 TFT structure is sufficient to attain the good image quality in small size panel such as 2.2", as shown in Figure 4. Moreover, the simple 2 TFT structure is much easier to achieve the high aperture ratio due to the less layout area than multi-transistors structure, and is beneficial to enhance the brightness of display. The leakage current is the major issue in LTPS technology that can affect the accuracy of gray level and contrast ratio, thus the dual gate structure is applied on both switching TFT and driving TFT to improve the performance of AMOLED.

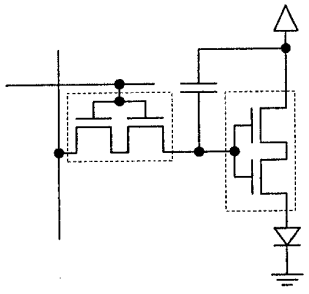

Figure 4. The 2-TFT pixel circuit

Figure 5 is a block diagram of integral driver in this LTPS-TFT 6-bit AMOLED. It is composed of horizontal and vertical shift-registers, data switches. The gateline is controlled by the

scanning signals from output of vertical shift-registers. During the turn-on period of one gateline, the horizontal shift-registers control the switch, therefore, the input 6-bit data signal for each color will be sent from the outside drvier to the pixel respectively.

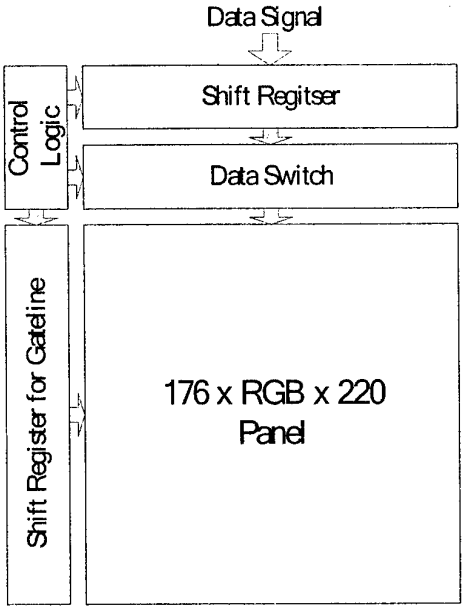

Figure 5. Integral driver block diagram

4.2 OLED Material

Because of the high aperture ratio of pixel layout, the conventional bottom emission type OLED which emitting the light through the aperture and glass substrate shows good competence in our design. The device structure of OLED used for 2.2-inch AMOLED is described as follows. The TFT combined with high quality ITO as new pixel structure on glass was used as the starting substrate. This device consists of ITO/CuPc/NPB/Alq3:C545T/Alq3/LiF/Al. The copper phthalocyanine (CuPc) and Naphthyl-Substituted Benzidine Derivative (NPB) are used as anode buffer layer and hole transporting layer respectively. The tris-(8-hydroxyquinoline) aluminum (Alq3) doped with C545T forms the electron transporting and emitting layer. The top metal electrode is evaporated with aluminum and lithium fluoride (LiF). The R, G, B pixels are produced by means of different dopant material doped in Alq3. Photometric characteristics of OLED were measured using a Photo Research Spectra model PR-650 photo-spectrometer, as shown in Figure 6.

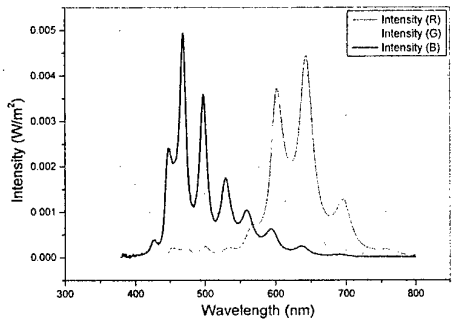

Figure 6. Spectrum of R, G, B, three original OLED material

4.3 Performance of 2.2-inch AMOLED

The specifications of the 2.2-inch AMOLED are summarized in table. 4. This display has 176x220 pixels, each of which has individual R, G, and B emitters. Low temperature poly-silicon technology has been used to fabricate the TFT and integral driver circuit. On the other hand, the conventional shadow mask method is applied to deposit the OLED material on to TFT array. Figure 7 shows a high gray-level image on the Toppoly AMOLED display.

Table 4. Specifications of AMOLED display

Display size	2.2 inch diagonal
Pixel number	176 x RGB x 220
Dot pitch	66 x 198um
Color depth	6 bits for each color
Color coordinates	R (0.59, 0.36) G (0.41, 0.54) B (0.20, 0.27)
Peak luminance	250 cd/m^2
Contrast ratio	> 2000 (in dark) > 200 (in 500 Lx)
Power consumption	1.92 W

5. Conclusion

We investigated the surface roughness of ITO film depends strongly on different under-layer. The surface roughness of ITO film on the organic materials is 3 times larger than that on Si-containing insulating materials. And the OLED characteristics depend on the surface morphology of ITO film. The less rough ITO surface, the better OLED efficiency is obtained. A 2.2-inch QCIF AMOLED with new pixel structure has been realized. The developed display has such attractive progress such as good image uniformity, high contrast ratio and it has potential for high performance display applications.

Figure 7. Image on the fabricated display

6. References

[1] K. Utsumi, Monthly DISPLAY '02, p. 58-61 (2002).

[2] Y. H. Yeh, et al., EURODISPLAY '02, p. 29-32 (2002).

[3] I. W. Wu, journal of the SID '94, p. 01-14 (1994).

[4] K. Inukai, et al., SID '00, p. 924 (2000).

[5] J. R. Gu, Industrial Materials, p. 169 (2001).

ED-P4. **4-th Generation Laser Kinescope**

O.M.Makienko
R&D Institute PLATAN
Fryazino, Moscow Region, 141 120 Russia

First a new device - 4-th generation laser kinescope is demonstrated. It's main feature in comparison with former devices of such a class is the lack of active cooling a laser target. This advantage is due to a new target construction. Besides, some other former disadvantages are restricted also.

The first compact device was produced for the Russia Navy. It's laser target consists of three radiation zones of red, green and yellow colors. The laser radiation power in each zone is not less than 1.0 W.

Evidently this device after its modification can be used in many Air Force, Army and civil applications where a laser scanner is required. More, since 4-th generation laser kinescope possesses the exploitation parameters of usual projection luminescent cathode tubes, it is able to change them in modern equipment.

ED-P5. Determination of the Phosphor Activator Parameters for Using Voltage-Brightness Characteristics of Thin-Film Electroluminescent Structures

M. K. Samokhvalov, R. R. Davidov
Ulyanovsk State Technical University, Ulyanovsk, Russia

A method for determining the concentration and electron-impact excitation cross section of the activated emission centers in the phosphor layer of a thin-film electroluminescent capacitor structures, based on the measurements of brightness as a function of the applied alternating voltage amplitude and frequency, is analyzed. The error of determination of the parameters of electroluminescence excited by alternating-sign ramp voltage is evaluated. The parameters of electroluminescent structures based on the ZnS:Mn and ZnS:TbF_3 films are presented.

At present, electroluminescent (EL) thin film structures are considered as promising elements for the creation of flat active displays. The development of effective and reliable device elements on this basis requires the investigating the properties of EL structures and establishing relationships between the parameters of emitting centers, structural and technological factors and special features of the EL excitation regimes in thin film structures. The study of physical processes in thin EL films is also of interest from the standpoint of elucidating of charge carrier production and acceleration in strong electric fields and the interaction of carriers with the activated emission centers. In this context we have developed the method for determining the main parameters of emission centers in phosphor films using the measurements of the voltage-brightness characteristics of EL structures.

The main equation of electroluminescence derived within the framework of the model of direct impact excitation of emission centers in a phosphor describes the kinetics of the variation of the concentration N^* of excited emission centers [1]:

$$\frac{dN^*}{dt} = \frac{\sigma}{e} j(N - N^*) - \frac{N^*}{\tau} \qquad (1)$$

where σ is the impact excitation emission center cross-section of, e is the electron charge, j is the current density in the luminescent film, N is the concentration of the emission centers, τ is the emission decay time constant. Using this equation in a stationary regime, whereby the emission centers pass into the excited state, produce emission and return to the initial state the within a period of the excitation voltage variation to ensure that: $\int_0^T \frac{dN^*}{dt} dt = 0$, and taking into account Talbot's law we derive the relationship between the average brightness of thin film EL structures and the applied voltage parameters. This relationship, obtained within the framework of the model of direct impact excitation of emission centers in a phosphor, is as follows:

$$B_1 = \frac{\eta_0 B_0 f\, k(V - V_{th})}{B_0 + \eta_0 f\, k(V - V_{th})}, \qquad (2)$$

where V and t are the amplitude and frequency of the applied voltage, V_{th} is the threshold voltage, B_0 is the maximum brightness corresponding to the average brightness in the case, when all activator centers pass from the excited to the ground state within the voltage variation period; and η_0 is the maximum light efficiency {yield} (a physical meaning of this quantity is the light yield under conditions that the active current passing through the film excites all activated emission centers and that the accelerated electrons don't interact with excited centers). The coefficient $k = 4 V_n C C_D C_L^{-1}$ is determined from an expression for the average power dissipated in the phosphor layer $P = kf(V - V_{th})$. Here C is the capacitance of the whole EL structure, C_d and C_l are capacitances of the dielectric and phosphor layers, respectively [2, 3].

The brightness and light efficiency are essential parameters of the light sources. However, in the case of thin film EL emitters their values are strongly depend on the measurement conditions. This circumstance complicates a comparison of these characteristics for various thin film EL structures. The proposed effective parameters B_0 and η_0 depend on the properties of the materials employed and the structural factors while being independent of the excitation conditions. These quantities determine the maximum brightness and light efficiency of a phosphor film. We suggest using these characteristics for the comparison of various display elements and for calculation of regimes and device controlling the operation of such displays.

Using simple transformation Eq. 2 can be written in the form:

$$\frac{1}{B_1} = \frac{1}{B_0} + \frac{1}{\eta_0 f\, k(V - V_{th})} \,. \qquad (3)$$

According to this relationship, determination of the maximum brightness and light efficiency can be based on the measurements of the voltage-brightness characteristics of the EL structures for various frequencies of the excitation voltage. By plotting the experimental data in the *1/B* versus *1/f* (or *1/B* versus $1/(V-V_{th})$ we can determine the B_0 and η_0 values by measuring the slopes of these linear plots and by extrapolating these plots to intersect with the ordinate axis.

The maximum brightness of an EL structure is determined by the phosphor properties and by parameters of the emitting element design: $B_0 = \eta_c d_L N \tau^{-1}$, where η_c is the effective light output is determined by the optical constants of the material employed, d_L is a thickness of the phosphor layer.

The maximum light efficiency also depends on the phosphor properties:

$\eta_0 = (\pi \eta_c \sigma N)(eE_{Lth})^{-1}$, where E_{Lth} is a threshold value of the electric field strength in a phosphor. Thus, once the maximum brightness and light efficiency of a phosphor are determined we can calculate the principal parameters of emission centers in the EL layer – the concentration of activators and their impact excitation cross section. The proposed method of analysis of voltage-brightness characteristics is especially convenient for determining the impact excitation cross section of emission centers, since other methods require either a complicated instrumentation for the kinetic investigations or additional measurements of the dissipated power [4, 5].

We have experimentally studied the properties of thin film EL capacitors using multiplayer metal-dielectric-phosphor-dielectric-transparent electrode systems prepared by the vacuum deposition onto glass substrates. The phosphor layer represented a film of manganese (0.5 at. %) and terbium fluoride-doped (5%) zinc sulfide with a thickness of 1 - 1.5 μm. The dielectric layers were obtained by depositing solid solutions of zirconium and yttrium oxides with a thickness of 0,2-0,3 μm. The sample structures were characterized by measuring their voltage-brightness characteristics and the frequency dependencies of integral brightness for the EL excited by a alternating voltage.

Fig. 1 and fig.2 are plotted for Mn-doped and TbF_3–doped ZnS-based luminescent structures using show typical experimental plots of the brightness versus amplitude and frequency of the excitation voltage plotted in the *1/B* versus *1/f* and *1/B* versus $1/(V-V_{th})$ coordinates, respectively. As seen from these data, the experimental plots are well approximated by straight lines intersecting at the origin. This indicates that the experimental results are consistent with the theoretical relationship derived within the model of direct impact excitation of the emission centers in a phosphor film.

Using the proposed method and based on the measurements of the voltage-brightness characteristics and the frequency dependencies of integral brightness we determined the maximum brightness $B_0 = (1.02 \pm 0.13) \times 10^4$ cd/m^2 and maximum light efficiency $\eta_0 = 7.6 \pm 0.5$ lm/W. These values agree with the data obtained by other methods and with the known characteristics. We have also estimated the parameters of manganese activated emission centers in a ZnS-based phosphor: the activator concentration was found to be $N=(3.3 \pm 0.2) \times 10^{18}$ cm^{-3} and impact excitation cross-section, $\sigma = (1.4 \pm 0.2) \times 10^{-16}$ cm^2.

Moreover, the EL structures with ZnS-based TbF_3-doped phosphors were investigated. We have also determined the parameters of emission centers of these materials, such as the concentration $N=(5.6 \pm 0.7) \cdot 10^{17}$ cm^{-3} and impact excitation cross-section, $\sigma=(1.0 \pm 0.3) \times 10^{-16}$ cm^2. The maximum brightness for TbF_3 was found to be $B_0=(6,7 \pm 0,6) \times 10^3$ cd/m^2 and maximum light efficiency $\eta_0=1.4 \pm 0.2$ lm/W.

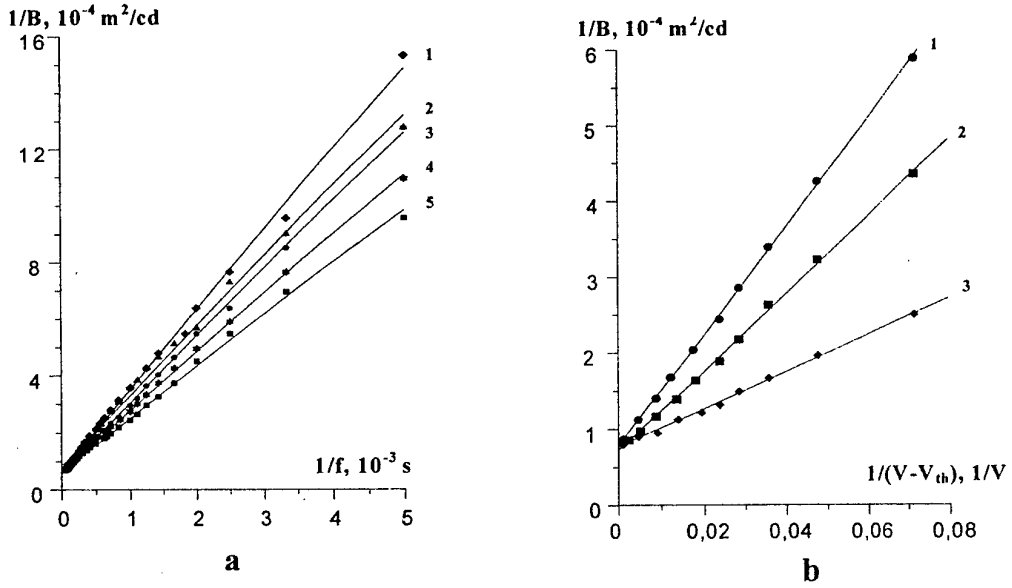

Fig.1. The plots for ZnS-based Mn-doped EL structure. (a) - inverse brightness *1/B* versus inverse frequency *1/f* for excitation voltage amplitudes *V=200 (1), V=207B (2), V=214B (3), V=221B (4), V=228B (5)*; (b) - inverse brightness *1/B* versus inverse voltage amplitude $1/(V-V_{th})$ for excitation voltage frequencies: *f=0.8 kHz (1), f=1kHz (2), f=1.6kHz (3).*

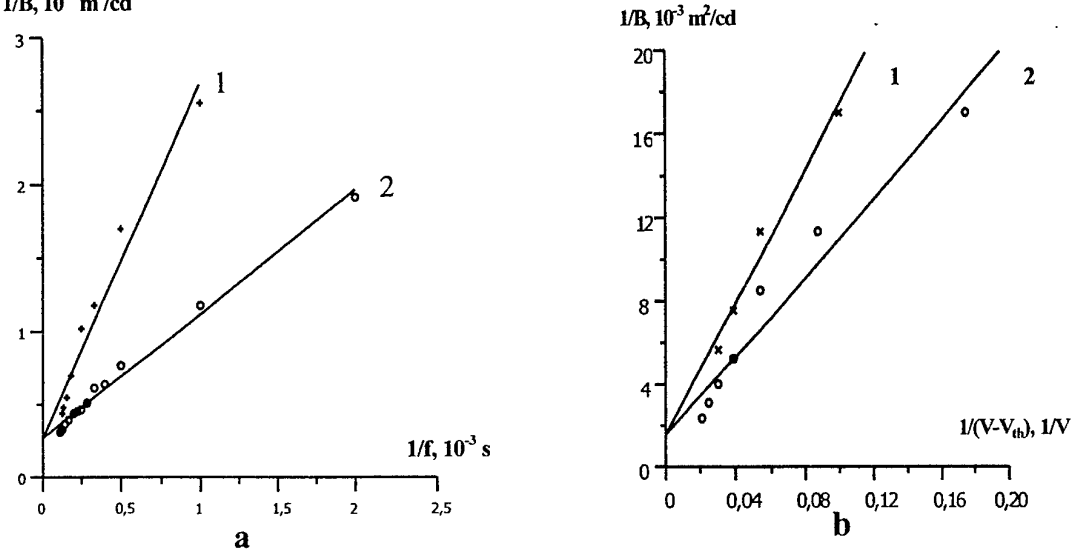

Fig.2. The plots for ZnS-based TbF_3-doped EL structure: (a) - inverse brightness *1/B* versus inverse frequency *1/f* for excitation voltage amplitudes *V=175B (1), V=180B (2)*; (b) - inverse brightness *1/B* versus inverse voltage amplitude $1/(V-V_{th})$ for excitation voltage frequencies *f=2 kHz (1), f=3 kHz (3).*

REFERENCES

1. R. Mach and G. O. Muller, Phys. Status Solidi **81** (2), 609 (1984).
2. M. K. Samokhvalov, Zh. Tekh. Fiz. **66** (10), 139 (1996). [Tech. Phys. **41**, 1045 (1996)]
3. M. K. Samokhvalov, Thin-Film Electroluminescent Radiation Sources (UlGTU, Ul'yanovsk, 1999).
4. M. K. Samokhvalov, Zh. Prikl. Spektrosk. **62** (3), 182 (1995).
5. M. K. Samokhvalov, Pis'ma Zh.Tekh. Fiz. **21** (15), 78 (1995) [Tech. Phys. Lett. **21**, 621 (1995)].

ED-P6. **Efficient Optical Converter of Visible to Infrared Light at 1.54 micrometers**

E.I. Terukov, M.S. Bresler, O.B. Gusev, Yu.A. Nikolaev

Ioffe Physico-Technical Institute, Polytekhnicheskaya 26,

194021 St.Petersburg, Russia

E-mail: eug.terukov@mail.ioffe.ru

We have previously reported on the observation of efficient room temperature photoluminescence at 1.54 μm in erbium-doped amorphous silicon films. We believe that in contrast to erbium-doped crystalline silicon in these films a different mechanism of excitation of erbium ions operates which determines higher efficiency of emission at 1.54 μm. Further optimization of material parameters resulted in an external quantum efficiency amounting up to 0.1% due to both an increase of absolute value of PL intensity and suppression of temperature quenching of PL.

In our previous experiments excitation of erbium luminescence was done by pumping with lasers with photon energies exceeding the bandgap of amorphous silicon (E_g= 1.8 eV). The radiation was passed through grating monochromator and detected with nitrogen-cooled germanium detector. In this work we used conventional halogen lamp KGM 100 as an excitation source.

Erbium-doped films of a-SiO_x:H with a thickness of 1 μm were sputter deposited on 300 μm crystalline silicon substrate by MASD method. Concentrations of erbium and oxygen determined by Rutherford backscattering technique were 1.5×10^{19} cm^{-3} and 4.3×10^{21} cm^{-3}, respectively.

The spectrum of erbium PL is recorded at room temperature from silicon substrate by excitation with white light of sputtered films. It should be noted that we are observed the intensive PL at 1.54 μm. An erbium line is clearly seen with a broadening characteristic of erbium ions in an amorphous matrix.

This effect can be used for optical conversion of visible to infrared light at 1.54 μm.

ED-P7. **Electroluminescence in amorphous-crystalline silicon heterostructures**

M.S. Bresler, O.B. Gusev, E.I. Terukov, Yu.A. Nikolaev, A.Froitzheim[1], W. Fuhs[1]

Ioffe Physico-Technical Institute, Polytekhnicheskaya 26, 194021 St.Petersburg, Russia
E-mail: eug.terukov@mail.ioffe.ru
[1] Hahn-Meitner-Institut, Abt. Silizium-Photovoltaik, Kekuléstr. 5, D-12489 Berlin, Germany

Heterojunctions of amorphous and crystalline silicon are very promising candidates for high efficient solar cells. The low temperature processing is of particular interest in the framework of future reduction of c-Si substrate thickness. Efficiencies above 20% have been reported for such structures [1].

We here show that heterostructure solar cells fabricated from amorphous and crystalline silicon exhibit strong electroluminescence (EL) at room temperature while operating as a p-n junction biased in the forward direction.

The EL was observed when square shape current pulses up to 100 mA with a 1:1 duty cycle were applied to the structure. The figure below shows an example of EL spectra measured at room temperature (1) and at liquid nitrogen temperature (2). The temperature dependence and intensity of the EL were found to depend on the a-Si:H/c-Si interface treatment. Interesting features are also revealed from capacitance spectroscopy and I-V cures measured at different temperatures under illumination. Results will be discussed in the framework of defect interaction and recombination process.

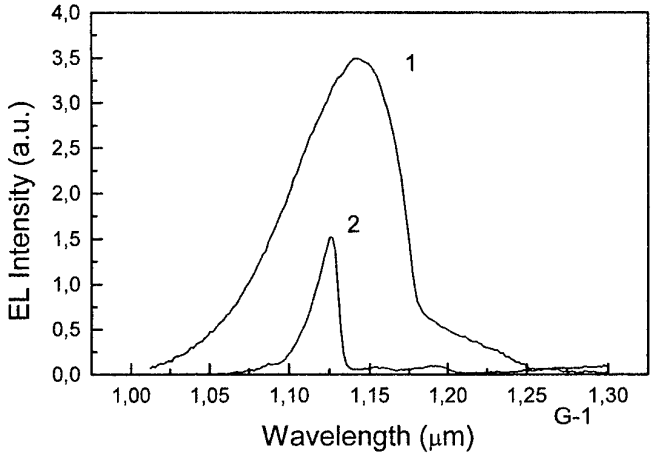

[1] M. Taguchi et al, "HIT Cells-High Efficiency crystalline Si cells with Novel Structure", Prog. Photovolt: Res. Appl. 2000; **8**; 503-513

ED-P8. Service Life of Cathodoluminescence Screens with Y_2O_2S:Eu Phosphor and Processes of Screen Degradation

A.O. Dmitrienko,* B.I. Gorfinkel**, T.A. Akmaeva*, V.V. Martynov*
*Saratov State University, Saratov, Russia
**Research Institute "Volga", Saratov, Russia

Abstract

Phosphors based on Y_2O_2S:Eu are very promising phosphors for vacuum fluorescent displays (VFD) and field emission displays (FED). One of most important characteristics of phosphor compositions is their resistance to electron bombardment. Our report includes data about brightness degradation resistance of Y_2O_2S:Eu phosphors at high current densities of excitation.

Researched influence of phosphor surface modification on brightness and efficiency of cathodoluminescence. We found that surface modification also alters phosphor conductivity. This fact is very important for Y_2O_2S:Eu phosphors which must be mixed with conductive powder of ZnO or In_2O_3 to provide charge dissipation during electron bombardment of VFD and FED screen surfaces.

As modifiers we used Bi_2S_3, $Bi(NO_3)_3$, SnO_2:Sb, WO_3, MoO_3, V_2O_5, MgO.

We determined mechanism of phosphor surface modification influence on service life and stability of cathodoluminescence compositions and proposed mechanism of luminescent layer degradation.

Introduction

The compositions of Y_2O_2S:Eu with conductive additives In_2O_3 or ZnO will effectively convert the energy of slow (100 - 500 eV) electrons into visible radiation. At the present time this phosphor is actively used as red component of screens of vacuum florescent displays (VFD). The feature of these displays is that required brightness can be achieved only under high (more then 1 mA/cm^2) current densities. Therefore the phosphor for these devices must not only effectively convert the energy of excitation into visible radiation but also be stable to electronic bombardment. Phosphors based on oxides and oxosulfides of rare earths have an advantage before semiconductor phosphors based on ZnS - CdS system in terms of stability. It is known that Y_2O_2S:Eu serving at 8 mA/cm^2 and excitation voltage up to 500 V is stable after several thousand hours of service. Under same conditions of excitation (Zn,Cd)S based phosphors lose their brightness after several hundred hours. At higher current densities oxosulfidic phosphor also degrades. At present time detailed mechanism and chemical reactions during this process are not known.

Since the effect of medium voltage CL is sensitive to surface quality chemical modifying of phosphor grain surface can greatly increase brightness and efficiency of CL. Besides that chemical surface modification can greatly increase conductivity of phosphor. This particularly important for oxosulfidic phosphors which have up to 15% ZnO or In_2O_3 added as conductive additive to ensure the sewer of charge during electron bombardment in VFD and FED.

The interest to Y_2O_2S:Eu phosphor is increased in connection with possibility to use it in field emission displays.

The aim of our work is to clarify the influence of phosphor grain surface modification on CL stability and to determine degradation mechanism of red emitting Y_2O_2S:Eu.

Experimental

Y_2O_2S:Eu phosphor was obtained by precipitation of oxalates with the following thermal decomposition.

Yttrium and europium oxides were dissolved in HNO_3 (ρ=1,2 g/cm^3), solution cooled and saturated solution of oxalic acid was added to form oxalates. Precipitate was filtered, dried and mixed with sulfur, Na_2CO_3 and Na_3PO_4 (as flux). Mixture was loaded in quartz crucibles and heated temperature of 1000°C for 4 hours in reductive atmosphere. The samples then was cooled, grinded and washed consecutively 0,01M solution of HCl and distilled water. Dried phosphor then was a subject to modifying processing.

As modifiers we used following materials: Bi_2S_3, $Bi(NO_3)_3$, SnO_2:Sb, WO_3, MoO_3, V_2O_5.

Chemical modifying of phosphors was conducted in two ways. The first way is mechanical grinding of phosphor powder with calculated amount of solution of salts corresponding, then heated at 900°C for 2 hours in CO+CO_2 atmosphere in quartz rig. The second way is heating under pressure $5 \cdot 10^{-3}$ Torr the phosphor and modifier placed in different parts of two sectioned quartz ampoule with following cooling at room temperature. During modification with tin oxide the heating was performed in two stages: 30 min at 300°C on air, then 1 hour at 450°C in reductive atmosphere. Modifying with tungsten and molybdenum oxides was performed at the temperature 400–700°C for 1-3 hours. The amounts of modifying agents were: bismuth – 0,02–3,0 at.%, vanadium – 0,02–0,2 at.%, tin oxide – 1 at.%, molybdenum and tungsten - 0,01-0,5 at.%

For modification by MgO and Y_2O_3 the phosphor was treated by formiates of corresponding metals then treated by ultrasound for 45 seconds. Then the mixture was dried and heated at 450°C for 2 hours on air. After that the sample was cooled to the room temperature and then heated in CO + CO_2 atmosphere for 2 hours.

Discussion

The influence of grain surface layer (<10 nm) state for Y_2O_2S:Eu phosphor on its CL efficiency is great. Therefore chemical modification of grain surface of this phosphor has great effect on brightness and efficiency of its CL.

We found that brightness of CL at 100–250 V greatly depends both on type of modifying reagent and on its amount and on the way of modification. It must be noted that phosphor modification with bismuth by $Bi(NO_3)_3$ is not suitable since it cause 40 - 60% brightness decreasing. The best results are obtained with modification by bismuth through gaseous phase of bismuth sulfide during heating in two sectioned quartz ampoule (brightness increases by 30%). More positive influence on brightness of CL renders modification by vanadium during heating both in ampoule and under coal layer.. The greatest increase of brightness - 60% - exists at vanadium contents 0,1–0,5 mass.% and with modification by heating on air at 450 °C for 30 minutes and then in quartz ampoules at 400–500 °C during two hours.

Modification by tungsten increases the brightness of low and medium voltage CL by 40–60%. The best results were obtained with phosphor treating by 0,5 mass.% of tungsten oxides (VI) and heating in vacuum at 600°. It is possible to consider SnO_2:Sb as a good modifying agent since the brightness increases by 10%.

In all cases the deep influence on brightness increasing render the temperature and atmosphere of isothermic heating which forms modificator film.

Particularly interesting is the fact that in the number of cases the brightness of CL increases while intensity of photoluminescence (PL) decreases.

Question about modifying agents influence mechanism is very important since clarification of this mechanism allows to determine the CL efficiency limit and to select the most efficient modifiers correctly. It is possible to say that brightness increase is not conditioned by phosphor conductivity increase after modification since it is changed insignifically. We suppose that making the modifier film on phosphor grain surface creates the conditions favorable for migrating of carriers deeper into the grain where probability of radiative recombination is much higher than in surface layer. Such migration of electrons and holes can be connected with appearing of electric fields created by high concentration of positively charged oxygen vacancies or other reasons (the luminescent effect of field). This field mechanism can be proved by the fact that spectra of PL and CL are practically identical and are not changed by modifiers of different nature and amount.

The question about VFD and FED screens stability is principal and must be specially discussed. It is well known that CRT where Y_2O_2S:Eu и Y_2O_3:Eu phosphors are used the energy of electrons is more then 10^4 eV ant service life of CRT is more then 10^3 hours [1] because of low current density on the screen (1–5 $\mu A/cm^2$). At these conditions the probability of electron stimulated reactions is very low.

This effect is similar to photoeffect and photocatalysis and photodecomposition in semiconductor phosphors based on ZnO, ZnS and CdS [2, 3]. It is known that probability of photodecomposition caused by UV light with energy higher then E_g is determined not by radiation energy but by radiation intensity. In this case photochemical decomposition of phosphor doesn't occur when radiation intensity is below threshold and is independent of UV photons energy [4]. It is also known that the penetration depth of high energy electrons (> 1 keV) is comparable with transition length of generated photon and diffusion length of carriers is comparable with phosphor grain size (1 micron). These facts prove that mechanisms of degradation caused by high energy electrons and photons are similar.

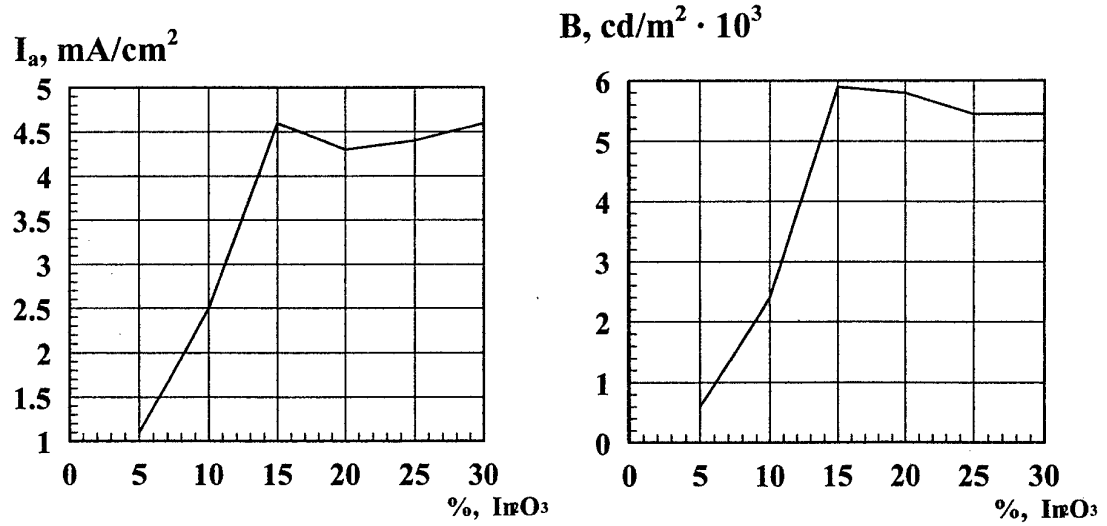

Fig. 1. Current and brightness dependance on In_2O_3 quantity in Y_2O_2S:Eu phosphor composition (Ua = 250 V).

There is completely different picture in VFD and FED. The current densities in FED and VFD 10^3–10^4 times higher then in CRT. It is clear that the probability of electron stimulated processes in surface layer of phosphor grain is very high even at low (10–500 eV) energy of excitation.

We noted above that Y_2O_2S:Eu phosphor is typical insulator with conductivity of 10^{-11}–10^{-13} $\Omega \cdot cm^{-1}$. Since the excitation energy in VFD and FED is very low and current density is high the conductive additive is added to phosphor to ensure the sewer of charge. As conductive additive is used In_2O_3 powder with mean grain size of 0,2–0,3 μm which cover phosphor grains with conductive layer and provides the sewer of electrons to anode.

The additive plays two roles. On the one hand, as it was noted, it increases the screen conductivity. On the other hand In_2O_3 as nonluminescent component of screen is a ballast that negatively influences on brightness and efficiency of CL. In this connection it was necessary to determine the optimum In_2O_3 concentration in its composition with phosphor.

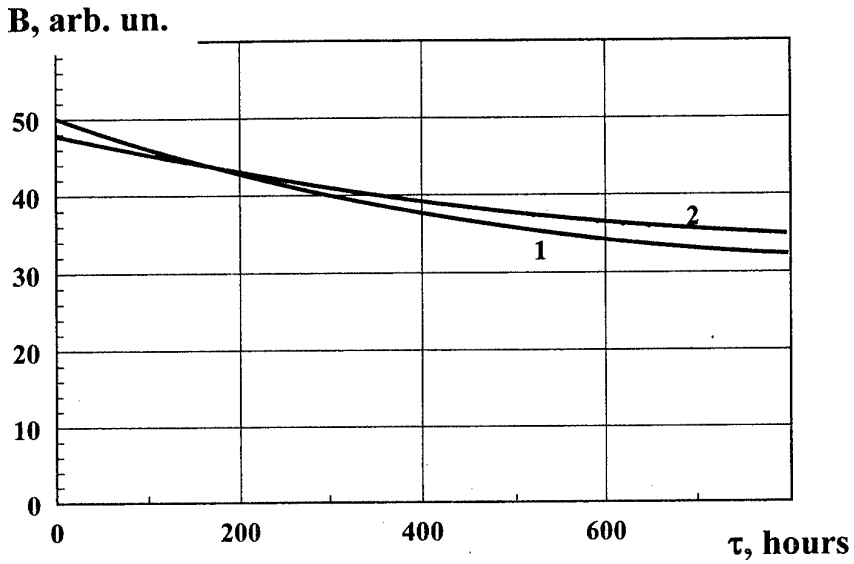

Fig. 2. Brightness change of modified (2) and nonmodified (1) phosphors during screen service (ja = 5 mA/cm^2, Ua = 300 V).

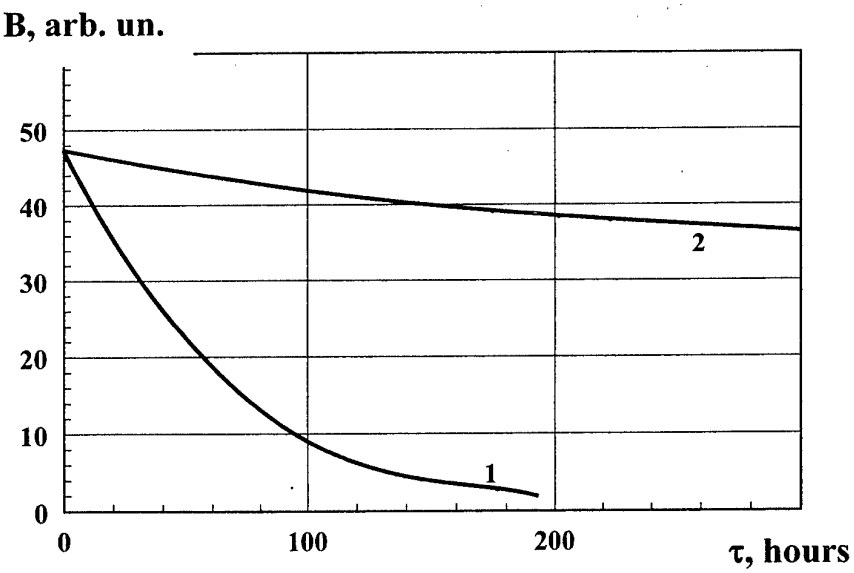

Fig. 3. Brightness decrease at different current densities. 1 – 10.7 mA/cm^2, 2 – 5 mA/cm^2. Ua = 300 V.

Fig. 1 shows that anode current and brightness of CL of the screen sharply increase when concentration of In_2O_3 increases from 5 to15 mass%. Further increasing of In_2O_3 concentration up to 30 mass% practically does not change the screen conductivity but brightness decreases by 10%. Therefore during the research of screens stability we used 15 mass% of In_2O_3.

Obtained dependences of current on screen and efficiency during the course of continuos exploitation show that least decline of anode current has Y_2O_2S:Eu (from initial 10 mA/cm^2 to 7 mA/cm^2 after 6000 hours); its efficiency practically remains on former level. These data show that matrix of Y_2O_2S:Eu phosphor is more stable to electron bombardment in contrast with semiconductor matrix ZnS. Efficiency of (Zn,Cd)S:Ag,In phosphors also stays high for the whole time of usage. However this phosphorus is not suitable for full color FED since its color coordinates do not match red TV standard.

We found that Y_2O_2S:Eu phosphor stability practically does not depend on chemical modification of grain surfaces by that modifiers which raise brightness and efficiency of CL. Fig. 2 shows curves of brightness change for modified and nonmodified phosphors after continuos usage in stationary mode for 800 hours.

We researched stability of phosphors under different current densities. Curves of brightness declination in conditions of stationary excitation are shown on Fig. 3. One can see that at current density less then 5 mA/cm^2 brightness practically does not change. Under higher current density (10 - 11 mA/cm^2) the sharp decline of brightness exists during first thousand hours. We found that at voltages 150–500 V and current density less then 5 mA/cm^2 the value of brightness declination practically does not depend on excitation voltage. Opposite this, under high current density (~10 mA/cm^2) observable brightness decreasing exists even at voltages above 100–150 V. These data indicate CL screen degradation is defined mainly not by value of electron energy but by the number of electrons bombarding unit of screen surface in unit of time.

Y_2O_2S:Eu phosphor is a typical insulator and does not possess highly denominated photoeffect. It also stable to photochemical decomposition under the action of UV radiation both in neutral and in oxidation atmosphere. We consider that resistance to photostimulated chemical processes on Y_2O_2S:Eu- phosphor grain surface is closely related to its higher stability to electron stimulated chemical processes in contrast with semiconductor phosphors.

For clarification of nature of reactions that occur under the action of electronic bombardment we researched the CL screen surface composition by method of AES.

The element composition of CL screen surface directly after fabrication of VFD is shown in Table 1. The composition of this VFD screen surface after continuos work of 1400 hours in stationary mode is shown in Table 2. The comparison of element composition in Tables 1 and 2 shows that contents of oxygen on phosphor grain surface significantly decreases. Also one can see that after display service the signal of indium is absent though contents of In_2O_3 in phosphor screen composition is more than 10 mass%. At the same time sulfur concentration on grain surface significantly increases. In some cases there is darkening of the screen of VFD after usage of 400 hours and more.

These data allow to expect that main reasons of CL screens degradation are electronic-stimulated decomposition of matrix yttrium oxosulfide with forming of surface phases of yttrium and sulfur and poisoning of conductive additive In_2O_3 by products of yttrium oxosulfide decomposition. Probably this is connected with reactions which occur on phosphor grain surface:

$$3Y_2O_2S = 2Y + 3S + 2Y_2O_3$$
$$Y_2O_2S = 2Y + SO_2$$
$$2Y + 3S = Y_2S_3$$
$$2\,In_2O_3 + 9S = 2In_2S_3 + 3SO_2$$

Table 1. Surface composition of Y_2O_2S:Eu phosphor screens before exploitation.

Screen Composition	Concentration of elements, at.%					
	Y	S	In	O	C	Cl
Y_2O_2S:Eu+ +10% In_2O_3	33,0	16,1	4,4	38,0	8,1	–
Y_2O_2S:Eu+ +15% In_2O_3	22,0	13,8	7,6	46,0	9,2	1,1

Table 2. Surface composition of Y_2O_2S:Eu phosphor screens after 1400 hours of working in VFD at different current densities (with 15 mass % of In_2O_3)

j, mA/cm^2	Concentration of elements, at.%						
	Y	S	In	O	C	Cl	Ba
1,2 - 1,6	12,8	38,0	14,3	11,8	16,0	0,8	4,6
7,8 - 8,4	22,0	67,0	1,0	4,3	4,8	–	0,4

Thus we found in spite of significantly higher stability of Y_2O_2S:Eu phosphor in contrast with semiconductor phosphors it is affected by decomposition under high current density with the result of poisoning not only conductive additive In_2O_3 but also oxidic cathode in VFD and autoemitting cathode in FED.

Conclusion

Our research shows that brightness saturation is caused not by low concentration of activator in matrix but by low rate of energy migration from surface layer to grain volume. It is shown also that under excitation voltages 200–300V observable saturation occurs at current density higher then at 1,5-2,0 mA/cm^2.

There are two ways to solve the problem of conservation of high efficiency of red emitting Y_2O_2S:Eu CL. The first way is to change the oxosulidic matrix to oxidic, the second way is to form on Y_2O_2S:Eu phosphor grain surface the thin films stable to electronic bombardment at high current density.

Screen stability to electron bombardment is practically independent of chemical modification of phosphor grain surface by modificators that increase brightness and efficiency of Y_2O_2S:Eu CL. Oxidic matrices such as Y_2O_3, Gd_2O_3 and La_2O_3 don't guarantee high efficiency of medium voltage CL. Therefore the first way is not perspective in near future. The forming of modificator films leads to sever decrease of CL efficiency since the part of excitation energy dissipates in this film. It is known that forming the SiO_2 film on the surface of ZnO:Zn phosphor leads to low voltage CL brightness and efficiency decreasing [5, 6]. But after 100 hours of exploitation brightness of ZnO:Zn phosphor greatly decreases and ZnO:Zn,SiO2 phosphor retains high brightness.

References

1. B.I. Gorfinkel, B.V. Abalduev, R.S. Medvedev, A.P. Loginov. Nizkovoltnye luminescentnye indikatory. Moscow, 1983, pp. 112.
2. F.F. Volkenstein. Electronnye processy na poverhnosti poluprovodnikov pri hemosorbtsii. Moscow, 1987, pp. 432.
3. V.F. Kiselev, O.V. Krylov. Elektronnye yavleniya v adsorbtsii i katalize na poluprovodnikah i dielektrikah. Moscow, 1979, pp. 235.
4. S. Itoh, T. Tonegawa, K. Morimoto, H. Kukimoto. Surface analysis of $Zn_{1-x}Cd_x$ phosphors exposed to UV light irradiation. J. Electrochem. Soc., 1987, V. 134, pp. 2628–2631.
5. B.V. Abalduev. Nizkovoltnaya katodoluminescentsiya. Moscow, 1977, pp. 32.
6. S.S. Galaktionov, Z.I. Guretskaya, A.N. Vorob'ev, A.V. Tkachev. Nizkovoltnye katodoluminofory i osobennosti ih issledovaniya. Trudy MHTI imeni Mendeleyeva, 1981, Vol. 120, pp. 64–83.

ED-P9. **Phosphors for Low Voltage Vacuum Fluorescent Displays and Full Color Field Emission Displays.**

Dmitrienko A.O.*, Gorfinkel B.I., Mikhailova V.V.**, Dmitrienko V.P.*, Zhbanov O.I.*, Gerasimova T.A.***

* Saratov State University

** SRI "Volga", Saratov

DmitrienkoAO@info.sgu.ru

Presented data about brightness, efficiency, spectral characteristics and stability of sulfides, oxides and oxosulfides based phosphors.

Special attantion was payed to studying of influence of composition and syntesis conditions on phosphor luminescent parameters in low voltage (25-50V) flat vacuum fluorescent displays (VFD) and in middle voltage (300-1500V) field emission displays (FED).

Also studied phosphor grain size influence on its cathodoluminescence in VFD and FED.

Shown comparison of characteristics of semiconductor (zinc – cadmium sulfides) and rare earth element (oxides and oxosulfides of yttrium–gadolinium–gallium) phosphors.

ED-P10. Structure, Conductivity and Cathodoluminescent Properties of Electroforetically Deposited Luminescent Compositions Exited by Low Energy Electrons: for VFD Application

I.V. Shein *, A. A. Hazanov **, S. L. Shmakov *, A. O. Dmitrienko *

* Saratov State University, Russia
** SRI "Volga", Saratov, Russia
410071 Saratov, Astrakhanskaya st., 83, chemical faculty
E-mail: DmitrienkoAO@info.sgu.ru

Abstract

The presence of submicron fractions in theY_2O_2S:Eu phosphor powder is shown to be undesirable.

We confirm that the best low-voltage electrophysical properties of luminescent composites based on ZnS:Ag,In; Y_2O_2S:Eu; ZnS:Cu,Al; (Zn,Cd)S:Ag,In; could be obtained if the fine fraction of these phosphors is removed and the average grain size of conducting additive (CA) is enlarged up to 0.8-1.0 μm. CdS powder was successfully used as CA for Y_2O_2S:Eu-based composites exited by low-energy electrons.

For comparison of luminescent composites conductivity could be used such behaviour function of testing triode as Ianode/Igate versus applied voltage with an impulse switching-up of testing triode.

To accurately compare luminescent composite conductivity values, high quality dynamic vacuum must be used to avoid poisoning of the cathode, which may increase the differences of the volt-ampere curves of the testing triodes under comparison.

Key words: phosphor, polydisperse, cathode, distribution, submicron , structure, conductivity, low voltage.

Introduction

There is a plenty of papers on elecrophoretic deposition of cathodoluminescent coatings, they speak that optimized working suspensions must contain a narrow fraction of a phosphor with a grain size of 2-3 μm plus 10-20 wt. % of a conducting additive (CA). The thickness of a luminescent coating should be 4 to 9 μm, depending on the electrical properties of the phosphor or phosphor-based composition.

Some other papers deal with the electrical properties of luminescent coatings, they note that the accelerating voltage of such a coating may significantly differ from the voltage applied to the display. This difference obviously should be minimized to raise the integral display efficiency. The integral efficiency of cathodoluminescence, defined as the luminance to excitation power ratio, depends not only on the properties of the phosphor alone but also on the composition and structure of the luminescent coating (subject to the formula and technology of sedimentation).

We carried out a number of experiments on electrophoretic deposition of various phosphor compositions based on ZnS:Ag,In; ZnS:Cu,Al; (Zn,Cd)S:Ag,In; ZnO:Zn; Y2O2S:Eu in order to relate the electrophysical characteristics of displays and coatings with the technology and structure of phosphor layers.

Fine particles are known to move faster at electrophoresis than coarse grains due to a lower viscous resistance of liquid for small particles moving. This results in a heterogeneity of the phosphor layer. As a rule, the lower layers of electrophoretically-deposited coatings are enriched with fine particles of both In_2O_3 (that is not good at its excess since the layer must be translucent) and phosphor, which seems to be the main cause of the poor reproducibility of traditional phosphor coatings.

Object and Deposition Experiments

Coatings based on a polydisperse phosphor Y_2O_2S:Eu were prepared and examined. The grain size distribution curve of luminescent powder of interest had a local maximum near 0.2-0.3 μm and a main maximum between 2-3 μm. This phosphor batch gave suspensions staying turbid for many hours while other ones sedimented completely during few minutes.

The cathodoluminescence of the coatings made of the polydisperse phosphor with 20 wt % of CA was rather dim and irregular, with a number of dark spots. More CA may probably be needed.

Suspensions with 20 to 35 wt % of CA were prepared and test indicators were manufactured. The anode current of all the devices was rather low and rose slightly at increasing the CA content. Dark spots shone under perpendicular UV illumination while slanting UV one gave a pattern with shades. The location of the dark spots at cathodo- and photoluminescence did not coincide.

An optical microscope allowed us to see that the coatings were drastically affected by washing and had a developed relief (Fig. 1). Moreover, the electrode was seen to be densely covered with so fine particles that they seemed a continuous cloudy layer with coarse (1-3 μm) grains at long distances from each other.

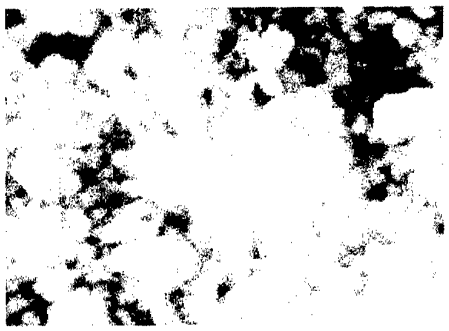

Fig. 1 SEM photo (magnification 2000) of standard Y_2O_2S:Eu cover drastically destroyed by washing.

We suggest that any electrode reaction is hindered on the areas densely covered with a mixture of fine dielectric (phosphor) and conducting (CA) particles, and the amount of the binder formed (hydroxides) is not enough to provide good adhesion of the layer being deposited.

To eliminate fine fractions and agglomerates with submicron particles by simple dissolution, we annealed the phosphor powder in air at 500°C and steeped the annealed sample in a 3% solution of formic acid. Such a treatment led to an increase of the brightness. Average parameters of the devices were obtained: the overall brightness at a level of 100 cd/m^2 (an anode voltage 250 V and pulse current densities 120 mA/cm^2 and σ=240). See a SEM photo of the luminescent coating in Fig. 2.

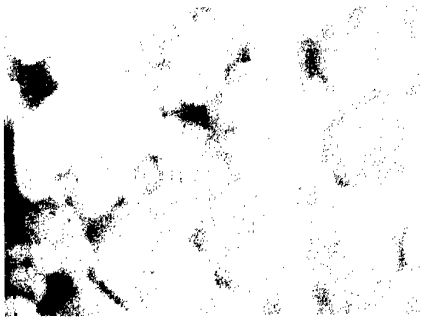

Fig. 2. SEM photo (magnification 3500) of Y_2O_2S:Eu cover (composite with CA) prepared after treatment of polydisperse powder.

Further, in order to separate the middle fraction, we used multiple sedimentation of the powder in a 3% solution of formic acid. The fine fraction was removed with the supernatant. Coatings without CA were made, their luminescence was bright at voltages above 300 V. The body of monodisperse covers is porous. We think that primary electrons could penetrate into the body of composite by multiplying deflection through the porous of the grain packing and cause secondary emission incident onto the electrode. If penetration is not so deep or the energy of primary electrons is not enough, it causes charging of the composite.

In another experiment we removed the superfine fraction only. A suspension with 15 wt % of CA (instead of usual 20 %) and 5 wt % of the polydisperse CdS powder (an average grain size 1.5 μm) was prepared. Another one contained 5 % of CA and 15 % of CdS. As the emptiness around coarse phosphor grains is concurrently occupied by either CA particles or fine dielectric particles of Y_2O_2S:Eu, it seems reasonable to introduce semiconducting CdS in order to multiply the number of contacts in the conducting particle network and to enhance the number of secondary emission circuits through the body of the luminescent composition.

Plates of 3-colour indicators were used for comparison of two types of composition namely, with sulphide and standard one.

The display electrode topology were sequentially covered with compositions with a sulphide additive and without it but with 20 wt % of In_2O_3 for comparison. At depositing the second coatings, we did not apply positive voltage to the already formed ones (as it is done at depositing different-colour phosphors) in order to avoid anodic oxidation of one of the coatings, which would cause changes in its electrical properties.

The coatings made from suspensions with sulphide additives possessed bright uniform luminescence.

Electrophysical Characteristics of Vacuum Test Systems

In order to simplify the physical pattern of cathodoluminescence, we used two types of testing lamp: a one-segment simple triode named IP and a simplest colour-synthesising display model. The second one differ from IP by fine topologies of the anodes. An IP has a rectangular bulb, 3 direct-heated oxide cathode threads stretched 3 mm from each other, a flat anode at 2 mm from the cathode plane, and a square-plaited grid (the area of a square being ~0.6 mm^2) placed on equal distances from the anode and cathode.

The present section treats the conductivity of polydisperse phosphor composites and its relation with the coating structure.

Experiment 1

The luminescence pattern resembled coarse tree bark, the dark areas amounted up to 50-60% of the total area at anode voltages below 100 V. Under a voltage of 90-100 V, these spots started to dimly shine. As a rule, the bright areas had distinct borders with the dark ones. The shape of the dim areas did not change with time. Above 150 V, the dark spots shrank or immediately disappeared but the non-uniformity remained up to 250 V. The red field current under this voltage was 30-40% lower than the usual one for this type of devices.

No dim spots were seen with a microscope at 300 V. When the grid and anode voltage did not exceed 250 V, dim and bright areas of the coating were well distinguished with a microscope.

The known method for estimating the voltage drop across the layer by means of comparison of volt-ampere curves in the presence and absence of the phosphor coating [2] seems to be incorrect. When a test triode is turned-on, positively-ionized gases start to quickly desorb from the luminescent coating. They bombard the cathode and poison it. As a result, the volt-ampere curves of the full triode lie significantly lower than those of the reference one, and the voltage drop seems noticeably overestimated.

In order to reduce the average power and the effect of desorbtion on the volt-ampere curves we used pulse excitation for exploring the electrophysical characteristics of our devices. The pulse current was found not to change in time under pulse excitation of low and moderate power about 0.1 W/cm^2.

The ratio of the pulse anode current to the pulse grid one was noticed to be constant and not depending on voltage at equal potentials on both electrodes. The linear dependence remained from 20 to 110 V, and this range was chosen to perform measurements. The behaviour function of Ia/Ig versus applied voltage looks like a horizontal line for lot of displays with ZnO:Zn; (Zn,Cd)S:Ag,In (through 50 to hundreds volts).

We reduced the grid voltage to $U_a/2$ in order to avoid possible problems concerned with secondary emission from the powder coating (in case of its high resistance) to the grid.

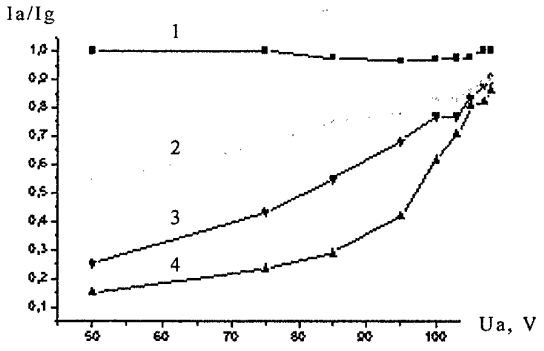

Fig. 3 Graph of Ia/Ig-impulse functions:

1— ZnO:Zn; (Zn,Cd)S:Ag,In+20 % CA
2 — (Zn,Cd)S:Ag,In without CA
3 — ZnS:Cu,Al+20% CA
4 — Y2O2S:Eu+20% CA

Electron trajectories are determined by the anode-to-grid voltage ratio provided that secondary emission effects are negligible; as a consequence, the anode-to-grid current ratio must be a function of the anode-to-grid voltage ratio only. The Ia/Ig ratio must be sensitive to any deviation of the mean potential of the luminescent coating surface from the external terminal potential.

Fig. 3 presents a number of normalized Ia/Ig curves. One can see that the current ratio of triodes with various coatings tends to a certain constant at increasing the excitation energy, this corresponds to the maximum conductivity (in some cases it may tend to zero electric resistance) of the powder composite.

The shape of such curves is rather diverse for measurements under various conditions (different suspension formulae, particle distribution, etc). We have optimized the compositions of binary and ternary polydisperse suspensions.

Experiment 2

This experiment demonstrates how the structure of the coating influences its electrical properties. Introduction of 5% of CdS into the polydisperse suspension has led to the volt-ampere curve (1) of such a coating going above that of the standard one (2) (Fig. 4). The other conditions were kept equal, and this enables us to state that this effect is due to the CdS addition only.

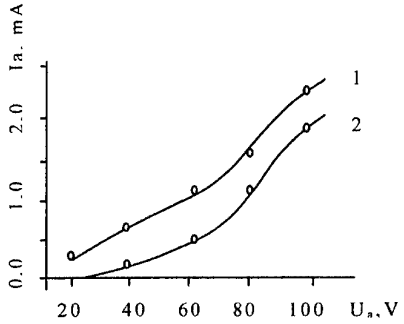

Fig. 4 Volt-ampere curves of display testing model there 1 electrode is covered by doped with 5 wt.% of CdS luminescent composite and standard one (2).

This dope is of special importance for the beginning of the low-voltage range, where the induced conductivity is very low and poor reproducible on polydisperse powders.

Experiment 3

The R, G, B electrode groups were sequentially connected to the anode circuit (the area of the connected electrodes increased by 2 to 3 times) in a pilot device with the display topology of the anodes, S of the screen being 0.6 cm^2.

The electrodes not connected to the anode circuit were connected to the cathode.

A set of grid characteristics were recorded at an anode voltage 40 V and a number of areas of the anodes. The integral anode current rose with the anode area. This test demonstrate that the mean (effective) potential of all display screen (or strip) is less than that applied to the terminals and that it affects the cathode current.

In this way, the presence of small areas of low potential caused by structure-induced high-voltage drop along with the effect of positive feedback between electron-stimulated conductivity and excitation power leads to generation of wide dark spots with distinct boundaries.

Summury

1. It is shown, fore comparison investigation of luminescent composites conductivity could be used a behaviour function of Ia/Ig versus applied voltage with an impulse switching-up of testing triode.
2. The presence of submicron fractions in theY_2O_2S:Eu phosphor powder is shown to be undesirable. We confirm that the best low-voltage electrophysical properties of luminescent composites based on ZnS:Ag,In; ZnS:Cu,Al; (Zn,Cd)S:Ag,In; Y_2O_2S:Eu could be obtained if the fine fraction of these phosphors is removed and the average grain size of conducting additive is enlarged up to 0.8-1.0 μm.
3. We suggest that the behaviour function of Ia/Ig of the Y_2O_2S:Eu-based composite is affected by secondary emission conductivity stimulated by the growing applied voltage.

References

[1] Y. W. Jin, J. E. Jang, W. K. Yi, J. E. Jung, N. S. Lee, J. M. Kim, D. Y. Jeon, J. P. Hong, Performance of electrophoretic deposited lov voltage phosphors for full color field emission display devices, J.Vac. Sci. Technol. B 17(2), p. 489, 1999

[2] S. A. Bukesov, B. I. Gorfinkel, N.V. Nikishin, A.O. Dmitrienko, Metody ozchenki elecrtoprovodnosti ekranov v realnom displee, Electronnaya Promyshlennost, 2, p. 8, 2000

ED-P11. **RGB LED BACKLIGHTS AND LED PANEL MOUNT INDICATORS**

Yu. Trofimov, V. Posedko, L. Survilo, A. Posedko, I. Mironenko, V. Sivenkov

Institute of Electronics of the National Academy of Sciences of Belarus,
Logoiskii trakt, 22, 220090 Minsk, Belarus

The possible variants of manufacturing as monochrome, and RGB LED backlight and LED panel mount indicators are considered, the received results and spheres of possible applications are analyzed.

Samples LED backlights for LCDs with brightness 200-800 cd/m^2 of various colours of a luminescence and a luminescence tolerance not more than 10 % at amount LEDs up to 100 pieces are developed and created.

The LED panel mount RGB indicators for easy front panel mounting with the size of a luminous surface 18x18 mm^2 with an opportunity of uniform mixture of colors in any combination and brightness of primary colors, accordingly, 480,820, 160 cd/m^2, provided by one LED on color are developed and created.

ED-P12. A Study on Various Factors for Jitter Reduction in PDP device

Yoon-Kwan Lee, Song Jun Weon,Woo-Hyun Jo
Byoung-Kuk Min, Byung-Joon Rhee, Eun-Ho Yoo
Digital Display Research Lab., LG Electronics Inc.
16 Woomyeon-Dong, Seocho-Gu, Seoul 137-724, Korea

Abstract

The various factors for jitter reduction in order to realize a speedy driving and prevent miswriting in the process of addressing in PDP device were systematically investigated. The study was carried out on 7.5-inch diagonal panel with a variation of experimental factors such as barrier rib height, kind of dielectric layer, electrode disposition and discharge gas and finally was evaluated on large area panel. Also the wide range of characterization such as optical properties, electrical properties and discharge properties were performed. From the technical and academic viewpoints in the present work, we could conclude that the major factor affecting the jitter property can be possibly confined to barrier rib height, electrode disposition and phosphor.

1. Introduction

The PDP has attracted much attention because of its extensive potential usage and unique features such as wide viewing angle, non-linearity, memory function, long life time, and simple panel structure which is suitable for fabrication of large scale panel compared to other display devices [1]. The structure of ac-PDP device is as shown in Fig.1. The color radiation is produced when the phosphors are excited with vacuum ultraviolet rays with a 147 nm wavelength emitted by a plasma discharge [2]. In recent years, many researches have been accomplished to improve picture quality, process yield, cost reduction etc. but still is required to attain a speedy driving and minimize a miswriting. And also, to overcome the limit of scan time and response time in driving, it is very important to reduce the jitter time in discharging process, especially in the process of addressing. In line with this technical issue, we have extensively studied the method for jitter reduction with various experimental factors, and consequently obtained very desirable results that are practical to a PDP device. From this results, the major factors governing a jitter time were the rib height, electrode disposition and phosphor, and the total jitter time we obtained was approximately 1.3 μs, which was highly favorable time for preventing a miswriting and realizing a single scan driving in PDP device.

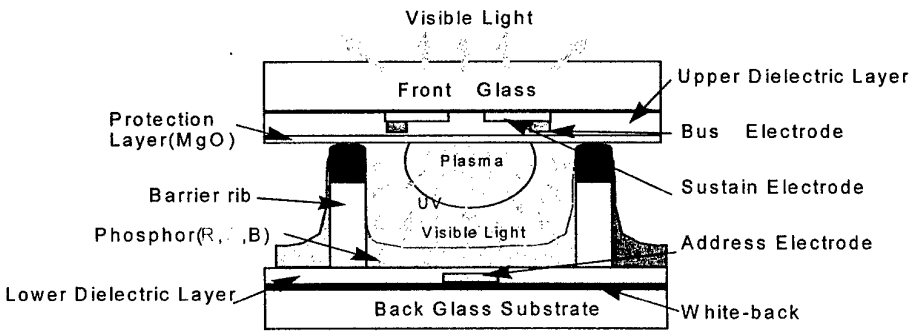

Fig. 1: Structural details of the full-color AC-PDP

2. Experimental procedures

The 7.5-inch diagonal panels fabricated by experimental factors were employed to test. The panel was ac-PDP type and the pressure of 500 torr was used for plasma discharging. The experimental factors include the rib height, dielectric layer, MgO protective layer, gas composition, phosphor, electrode disposition and all factors was systematically evaluated. The experimental factors varied in the range of 80 um to 130 um, 8%Xe to 14%Xe for discharging gas, 10 to 25 for dielectric constant of dielectric layer respectively. Also the electrode disposition, MgO protective layer and phosphor were selected based on theoretical foundation and analysis. The MgO protective layer was deposited by electron beam evaporation with a change of content of dopant. The barrier rib and dielectric layer were formed on a soda-lime glass substrate by several sequential processes: paste forming, screen-printing, exposure & development, patterning, sandblasting and sintering. The phosphor layer was formed on barrier rib by means of screen printing process and heat treatment. The IR spectrometer was utilized to measure jitter time during applying addressing pulse in the process of discharging because it has been the IR of 823 nm pulse is generated from Xe exited ions with the vacuum ultraviolet(VUV) of 173 nm, and the discharge characteristics can be indirectly analyzed from the IR waveforms[3].

3. Result & Discussion

Table.1 and Fig.2 show the variation of jitter time with experimental factors, rib height, thickness of lower dielectric layer (WB), dielectric constant of lower dielectric layer. The height of rib in reference sample was approximately 130 μm and the dielectric constant of lower dielectric layer is 12 to 20. The most effective factor governing the jitter time among the measured data was the rib height that the total jitter time was lowered by 41% from 3.68 μs to 2.18 μs whereas other factors such as thickness of dielectric layer and dielectric constant of layer slightly affect the jitter time. In particular, at a sample with rib height of 80 μm, the pure time of jitter than the formation time of jitter appreciably contributed to reducing the total jitter time. The reason for remarkable reduce of jitter time in rib with 80 μm height is thought to be a strong electric field and a stable accumulation of well-charge

formed between scan electrode and address electrode due to lower height of barrier rib than that of reference sample. However, as shown in Fig.3, the efficiency of sample with a rib height of 80 μm in contrast to other samples considerably dropped by about 13% at 210V. It is conjectured that this phenomenon can be attributable to the decrease of discharge volume because the distance between bus electrode and address electrode get closer.

Jitter Time	Reference	Rib= 80 μm	WB= 10 μm	WB= 15 μm	WB= 20 μm
T_{form}	0.55 μs	0.38 μs	0.63 μs	0.52 μs	0.59 μs
T_{furc}	3.13 μs	1.80 μs	3.27 μs	2.63 μs	2.93 μs
$T_{form} + T_{furc}$	3.68 μs	2.18 μs	3.90 μs	3.15 μs	3.52 μs

Table. 1: Variation of jitter time with experimental factors

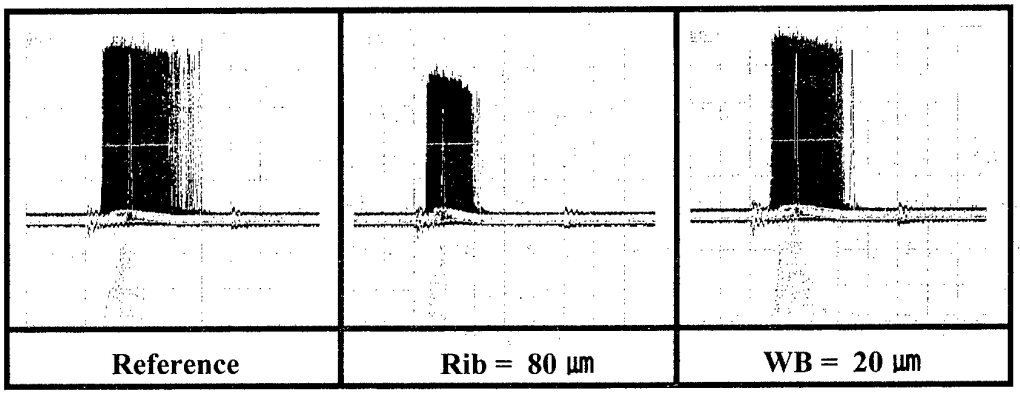

Fig. 2: IR Spectrum taken in addressing period by samples

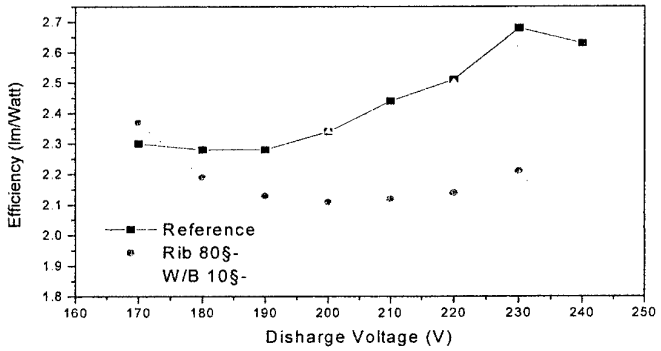

Fig.3: Change of efficiency by voltage increment

As shown in Fig4., the jitter time was observed differently by kinds of electrode disposition. The jitter time was measured at discharging voltage of 210 V with the composition of 14% Xe-Ne gas under

swiping condition of 5000 scan time at 768 line. The B type electrode having the structure of electrode positioned inside discharge space was improved by about 13% at a total jitter time when compared to the A type electrode which the electrodes are placed near by barrier rib. It is assumed that this phenomenon can be attributable to the increase of Xe excited ions due to the concentrated electric field formed around the B type electrode. However, the B type electrode structure has its drawback in terms of discharge efficiency and brightness since the electrodes disposed at inside plane of discharge space cut off the appreciable portion of visible light generated from phosphor.

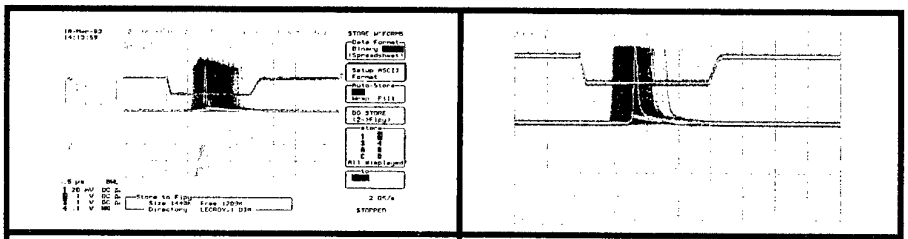

A Type Electrode	B Type Electrode

(A)	(B)
T total jitter = 1.6 μs	T total jitter = 1.4 μs
T formation = 0.6 μs	T formation = 0.5 μs
T pure = 1.0 μs	T pure = 0.9 μs

Fig.4: Comparison of jitter time by kinds of electrode disposition

Fig5.demonstrate that the particular treatment of phosphor plays a role in reducing the jitter time. The phosphor with charged surface by a special treatment resulted in a shortened jitter time, 1.18 μs down to 10% when compared to that of normal phosphor, 1.32 μs. It is presumed that this is due to the fact that the charged surface on phosphor prevents the excited ions from inflowing into phosphor by a counter-interaction, finally restraints a reduce of the ion density in discharging space.

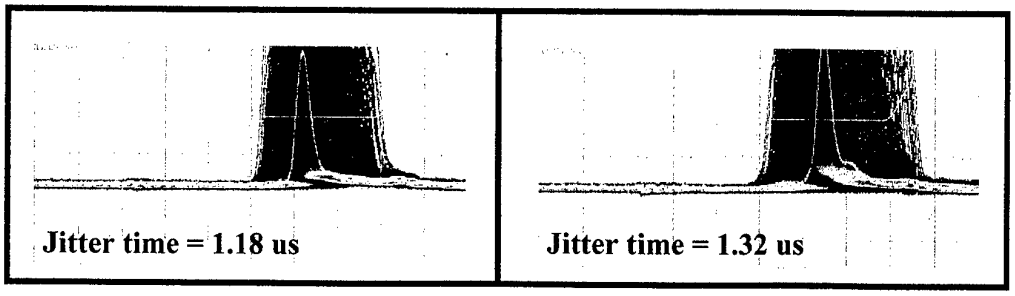

(A) charged surface (B) no charged surface

Fig.5: Variation of jitter time with and without surface treatment on phosphor

4. Conclusion

In this work, we analyzed the relationship between a jitter time and some various factors such as rib height, electrode disposition, and phosphor. By a combination of these factors, the required jitter time for a high speed driving and a correct writing was realized successfully. The dominant factor affecting the jitter time was mainly the rib height. Also the electrode disposition and phosphor gave an appreciable effect to reduce the jitter time. However, the additional study is necessary to achieve best picture quality in PDP by improving the discharge efficiency and brightness.

References

[1] H.Uchiike, Display Devices 95, pp. 34-37, 1995.

[2] H.Uchiike,H.Tsuchiya, N.Awaji, T.Shinoda and Y.Fukusima,Characteristics of Discharges Pattern in Surface-Discharge AC Plasma Display Panels, *IEEE Trans.Electron Devices* 7, pp. 943-950, 1984.

[3] N.Uemura, Y. Yajima, Y. Kawanami, K. Suzuki, N. Kouchi, and Y. Hatano, "Kinetic Model of the VUV Production in AC-PDPs as Studied by Time-resolved Emission Spectrocopy," IDW '00 Digest, pp.639-642,(2000).

ED-P13. Nine Key Problems of PDP-Phosphor Technology

Naum P. Sostchin (Research and development Institute "Platan", Friasino, Moscow Region, Russia, 141195, Zavodckoi av.2),
Anatoli V.Vishniakov (Mendeleyev's University of Chemical Technology of Russia, Moscow, Russia, 125047, Moscow, Miusskaya sq. 9)

The new procedure for estimation of ultimate effectiveness of blue, green and red PDP-phosphors was developed. It was shown that the effectiveness of PDP-panel in white color is determined by blue phosphor. The traditional PDP- phosphors with high brightness and very good color purity were prepared in the framework of modified solid state technology. Phase homogeneity; morphology and particle size, resistibility against device gas atmosphere, high secondary ion-electron emission coefficient, decay-time are designated as most important characteristics of PDP-phosphors. To prolong the useful life phosphors were covered by high transparent water-resistant coating layer with low secondary ion-ion emission coefficient. Coating layers were chosen from the group comprising inorganic materials or glass materials, and namely borates, phosphates, borosilicates, phosphosilicates, or silica.
Keywords: PDP-phosphors, ultimate effectiveness, coating layers

The estimation of PDP-technology perspectives has to take into account the values of effectiveness of PDP-phosphors that can be reached [1-3]. In this report we consider algorithm for calculation of ultimate effectiveness of PDP-phosphors based on the following characteristics:

- reflection coefficient for VUV radiation (R_{VUV});
- coefficient of spectral correspondence between the λ =147 nm radiation and the phosphor excitation spectrum (k);
- quantum yield for each PDP-phosphor (Φ);
- Stoks's loss at luminescence (W_S);
- lumen-equivalent calculated from luminescence spectrum and color coordinates Q_L.

The main characteristics mentioned above were found as:

1. The reflection coefficient was determined by Relay's equation from experimental data concerned to VUV reflection spectrum of oxide materials. The absorbed radiation (P) was found by :

$$P = P_0(1-R_\lambda)$$

2. The Stoks's loss was calculated by relation:

$$W_S = K\frac{Л_{exc.max}}{Л_{max.lum}}$$

where K – the ratio of half-width excitation and luminescence spectrums;.

3. The integral radiation lumen-equivalent (Q_L) of each PDP-phosphor was determined from the equation:

$$Q_L = = 683 \cdot \frac{\int_{400}^{780} S_Л V_Л dЛ}{\int_{400}^{780} S_Л dЛ}$$

where S_λ – relative wave length distribution in luminescence spectrum; V_λ – eye spectrum sensitivity curve; 683 (lm/W) – lumen-equivalent for monochromatic radiation of λ=555nm,

To simplify the integration procedure the half-width of luminescence spectrum for each phosphor was accepted to be equal to 60 or 80 nm. Color coordinates of PDP-phosphors were calculated by the well known integrals.

$$x = \int_{400}^{780} S(Л)\,\bar{x}\,(Л)\,dЛ \quad \text{and} \quad y = \int_{400}^{780} S(Л)\,\bar{y}\,(Л)\,dЛ$$

The initial data for PDP-phosphors and Q_L values calculated are collected in Table 1. The table 2 summarizes information concerned to all parameters calculated and ultimate effectiveness of blue, green, and red PDP phosphors . As one can see the effectiveness of PDP-phosphors differs rather strong. The green phosphor has the highest level and blue one possesses the lowest value. The relation for effectiveness is close to 1 (blue); 8-9 (green), and (3-4) for red. It comes to the conclusion that the effectiveness of PDP-panel in white color is determined by the blue phosphor.

Spectral and color characteristics of PDP-phosphors Table 1

Color/composition	λ_{max}, nm	$\Delta\lambda_{0,5}$, nm	Color Coordinates, x,y	Q_L, lm/Watt(light)
Blue:				
$BaMgAl_{10}O_{17}$	450	60	x=0,145; y=0,06	40
$BaMg_2Al_{14}O_{24}$	450	80	x=0,150, y=0,08	60
Green:				
Zn_2SiO_4Mn	520	60	x=0,21; y=0,71	400
$(ZnMg)_2SiO_4Mn$	535	80	x=0,25, y=0,68	500
Yellow-green:				
$(YGd)BO_3Tb$	545	15	x=0,33; y=0,63	540
Red:				
Y_2O_3Eu	605	10	x=0,628; y=0,365	260
$Y_2O_2BO_3Eu$	610	10	x=0,635; y=0,368	240
$(Y,Gd)EuBO_3$	625	10	x=0,642; y=0,352	205

Energy parameters of PDP-phosphors Table 2

Color of luminescence	VUV reflection coefficient, R_{VUV}, %	Spectrum correspondence coefficient (k)	Stoks's loss (W_S) %	Ultimate effectiveness ($F_i=P_0 \cdot R_{VUV} \cdot k \cdot W_S \cdot Q_L$), Lm/Watt(electr)
Blue	40	1.0	60-65	9-10
	50	0,9	60-65	7,5-8
Green:				
$\Delta\lambda_{0,5}$=60-80 nm	40	0,8	75	57
$\Delta\lambda_{0,5}$=15 nm	40	0,9	80	72
Red	30	0,8	85	27
	50	0,8	95	20

The contribution of blue (f_b), green (fg) and red (f_r) light fluxes of all panel pixels on total luminous efficiency can be calculated by equation:

$$f_b : f_g : f_r = y_b \begin{vmatrix} y_g - y_w & y_r - y_w \\ x_g - x_w & x_r - x_w \end{vmatrix} : y_g \begin{vmatrix} y_r - y_w & y_b - y_w \\ x_r - x_w & x_b - x_w \end{vmatrix} : y_r \begin{vmatrix} y_b - y_w & y_g - y_w \\ x_b - x_w & x_g - x_b \end{vmatrix}$$

where x_b, y_b, x_g, y_g, x_r, y_r, x_w and y_w are x and y color coordinatesfor blue, green, red PDP-phosphors (see table 1), respectively, and for the standard white light source D_{65} (x=0,31 and y=0,32).

As a result we have $f_b : f_g : f_r$ =0,07: 0,69 : 0,24.

Total luminous efficiency of PDP screen can be calculated by:

$$\frac{1}{F_w} = 2 \sum_{i=b,g,r} \frac{f_i}{F_i} = 2\left(\frac{0,07}{F_b} + \frac{0,69}{F_g} + \frac{0,24}{F_r}\right)$$

where (2) is coefficient considering the constructional features of PDP-panel. In result we have: $F_W \leq 15$ lm/W. Realistic values should be less because the working surface of PDP-panel constitutes about (65–75%) of the total panel surface. Thus F_W will be in the range of 10–11 lm/W.

The achievement of this level should be based:

- on optimization of gas discharge and panel technology in the field of physics and
- on improvement of PDP-phosphors characteristics in the solid state chemistry.

The list of requirements to the new generation of PDP phosphors includes the following characteristics having a great impact on brightness, effectiveness and stability phosphors:

1. High phase homogeneity;
2. Morphology and particle size (spheroids with diameter less then 2 microns)
3. Decay time less than 10 ms
4. Resistibility to device gas atmosphere
5. High secondary ion- electron emission coefficient

At the moment in the framework of modified solid state technology (heat treatment at 1200-1400°C in H_2 or CO/CO_2 atmosphere) we prepared the blue-[$BaMgAl_{10}O_{17}$ Eu (λ_{max}=450nm)], green [Zn_2SiO_4 Mn(λ_{max}=515nm), $(Y\text{-}Gd)BO_3$ Tb] and red [$(Y\text{-}Gd)BO_3$ Eu (λ_{max}=625,7 nm)] PDP-phosphors having very good brightness and color purity: 0,92; 0,98 and 0,987 respectively.

To detect phase homogeneity of a sample XRD analysis is used as a rule. But in the case of red borate phosphor it is enough to measure luminescence spectrum. The appearance of two picks in spectrum with λ=609 nm and λ=611 nm indicates at the presence of the oxide or oxoborate phases. Usually when a pick of λ_{max}=625,7 nm dominates in spectrum XRD analysis proves the only phase, namely phase of borate solid state solution.

After heat treatment the powder have a particle size greater than 3 microns. Adding of some chemicals into a mixture of raw materials can promote selective etching of face crystal taking place at high temperature annealing and results in the spheroids particle formation. For PDP-panel the optimal particle size is 1-2 microns. That is why powders should be grind in a high-speed planetary milling machine to decrease particle size. The grinding procedure improves the morphology of particle (the form-factor is increased up to 0,7) but unfortunately it leads to the brightness fall. Thus, it is very important to have a margin of brightness after phosphor synthesis. The level of this resource depends on particle size and type of phosphor.

The alternative technology based on co-precipitation or sol-gel process allows obtaining powders with smaller particle size and good phase homogeneity. These processes are appealing to green zinc silicate phosphor production. Nevertheless the conventional solid state process is more preferable for aluminate and borate compositions due to its simplicity.

It is possible to use for phosphor synthesis raw materials of very high dispersity (particle size $\leq$ 1 micron) also. But in this case there is a serious problem being caused by agglomeration of powder during mixing, drying and sintering at high temperatures.

A major advantage of PDP-panel in comparison with traditional CRT is their high stability and their long durability accordingly. A limiting factor for PDP screens may be stability of the phosphors used. Since the phosphors are not fully isolated from the surrounding atmosphere phosphors may be destroyed under the influence of high temperatures and surrounding gas atmosphere. To prolong the life time a phosphor should be covered by a high transparent water-resistant coating layer with low secondary ion-ion emission coefficient. Preferably, the coating is to be chosen from the group comprising inorganic materials or glass materials, and namely borates, phosphates, borosilicates, phosphosilicates, or silica.

To manufacture such a coating a colloidal solution of a borosilicate, a phosphosilicate, or an alkali silicate is added to an ammonium hydroxide solution. Starting compounds used for a coating with an orthophosphate are soluble metal salts of Al, Sc, Y, Lu, La, and Zn. Water is generally used as the solvent. Phosphoric acid, preferably 85% phosphoric acid and urea are added to this solution. After the resulting solution has been filtered the phosphor powder is added. The suspension is heated while stirring until the pH value of the suspension reaches 7. After cooling down to room temperature the phosphor with coating is filtered off, rinsed, and dried.

The very important parameters of PDP-phosphor are the time-period for rise of brightness up to steady state level and the decay-time for level of 1%. The values concerned to the phosphors prepared are shown in table 3.

Table 3

Dynamic characteristic of PDP-phosphor

Color of luminescence	Time-period for brightness rise from 10% up to 90%, s	Decay-time, s	
		Down to 10%	Down to 1%
Blue	$5\cdot10^{-4}$	$1{,}5\cdot10^{-3}$	$8\cdot10^{-3}$
Green	$1\cdot10^{-4}$	$2\cdot10^{-3}$	$1{,}2\cdot10^{-2}$
Red	$1\cdot10^{-7}$	$5\cdot10^{-7}$	$1\cdot10^{-6}$

The dynamic characteristics of PDP – phosphors are controlled by matrix composition and by impurities introduced into crystal matrix. The decay-time of luminescence can be regulated by increasing activator concentration or by doping of a crystal with 3d (Fe, Co) and 4f ($Pr^{3+,4+}$, $Sm^{2+,3+}$)– elements. That is why concentration of elements with variable oxidation state in raw materials should be less than 10-20 ppm.

References:

1. S Kubota, et. al., New blue emitted phosphors for PDP J.Electrochem.Soc., 149, H134 (2002)
2. R.P. Rao et.al.,Eu^{3+} activated red emitted PDP-phosphors. J.Luminescence, 87-89, 929 (2000)
3. Hong GY et.al., New three colors phosphors for PDP. Chin.J Lumin., 20 (4), 311-315,1999,

ED-P14. **Super-bright projection electron-beam devices for aircraft collimator equipment.**

M.I. Kalinin, Yu.N. Kosyakov, A.A. Lyabin, Yu.V. Petrushenko

R&D Institute "Platan", Russia

Paper is not available

ED-P15. Influence of Zn Doping and Laser Annealing on Y_2O_3Eu Thin Film Phosphor Properties

M.M. Sychov[1], Y. Nakanishi[2]
H. Kominami[2], Y. Hatanaka[3]

[1] St. Petersburg Institute of Technology, Russia
[2] Shizuoka University, Hamamatsu, Japan.
[3] Aichi University of Technology, Japan
msychov@yahoo.com

Abstract
In this paper we report effect of zinc doping on crystal and luminescent properties of electron-beam evaporated europium doped yttrium oxide thin film phosphor. It is shown that optimal doping allows to increase CL luminance about 10% and significantly improve color properties. Further improvement of luminance is achieved by the 307nm laser annealing as supposed due to elimination of surface defects. Films are transparent and show good linearity and stability of luminance thus being suitable for FED display application.

Key words: cathodoluminescence, FED, yttrium oxide

Introduction
Subject of this study are crystal, surface and luminescent properties of electron-beam evaporated Y_2O_3:Zn,Eu thin film cathodoluminescent phosphors. Utilisation of thin film phosphors is expanding and includes such application as flat panel displays, sensors and optoelectronics [1]. Recently films with cathodoluminescent properties were suggested for high resolution field emission displays (FED) [2]. Yttrium oxide based materials are degradation resistant under cathode rays and do not contaminate electron emitters in the FED [3,4]. Europium activated yttria phosphor has excellent color properties and is a member of oxo-anion phosphor triad [5]. The problem however is low luminance of film phosphors. In this paper the problem is addressed in two ways. Recently it was reported that introduction of Zn into Y_2O_3 powders improves their cathodoluminescence [6]. Here we attempted to use same approach for thin film phosphor. Another way to improve luminance is to eliminate killer centers associated with structural defect, especially surface ones, what was achieved by UV laser annealing.

Experiment
Pellets of the composition $Y_{1.96}Eu_{0.04}O_3$ with different ZnO content were cold-pressed and sintered at 1000 °C. Phosphor films were evaporated with the deposition rate ~1 A/s on fused quartz substrates at $2*10^{-5}$ Torr background pressure. XRD patterns were obtained with the use of Rigaku Geigerflex. Film morphology was investigated by Seiko Instrument SPA 400 atomic force microscope, DFM mode. To study film composition Auger Electron Spectroscopy apparatus ULVAC AQM808 was utilized. Luminescence properties of the films were characterized by PL measurements under the 325 nm excitation of He-Cd laser and CL measurements in reflection mode with current density 60 uA/cm^2. Brightness and color coordinates were controlled with Topcon BM-7 luminance colorimeter.

Film Structure
All films grew as cubic yttrium oxide and were oriented along (222) direction. While (222) peak FWHM and intensity were not significantly affected, however 20%Zn doping of the pellet provided improvement of the film crystallinity. Peak position for the films shifts with rise of zinc content in the pellet showing change of crystal structure – fig.1.

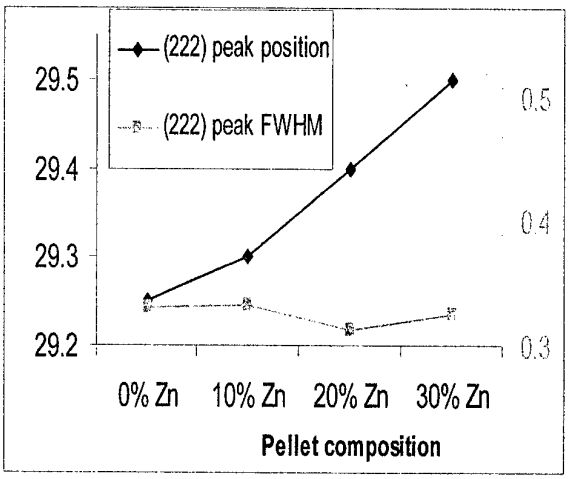

Fig. 1. Film crystal properties depending on Zn doping.

AFM study of the fabricated films showed that surface morphology and roughness did not change much with the doping except for the films fabricated from 30% Zn pellets. In the later case grain size significantly decreased which is quite unfavourable for the surface-sensitive low-voltage cathodoluminescence.

Cathodoluminescence
CL spectra show little change with the doping and no evidence of Zn-related emission was found. There is only 10% improvement of film CL luminance as a result of zinc doping – fig.2. For 30% Zn pellet luminance abruptly decreased due to change of film morphology and threshold voltage. According to Auger data, only 6% is Zn content in the film fabricated from pellet with 30% Zn. So it is supposed that re-evaporation of Zn from substrate takes place during deposition and that is the reason for lower achieved effect comparing to powders.
Most important positive effect of Zn doping in the improvement of color properties of the film. As one can see from the fig. 3, doping allows to obtain more saturated red color and thus improve color gamut of the display.

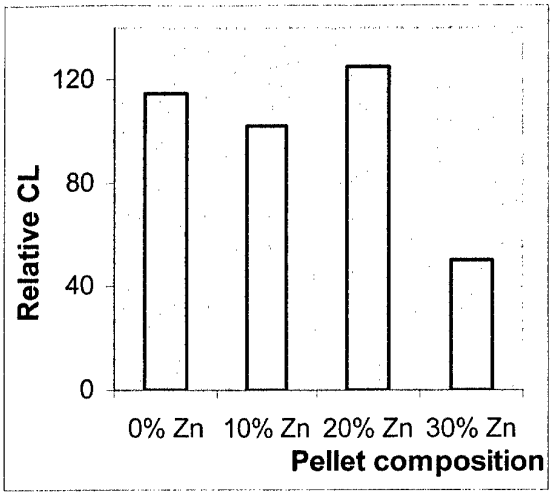

Fig.2. Zn doping effect on CL.

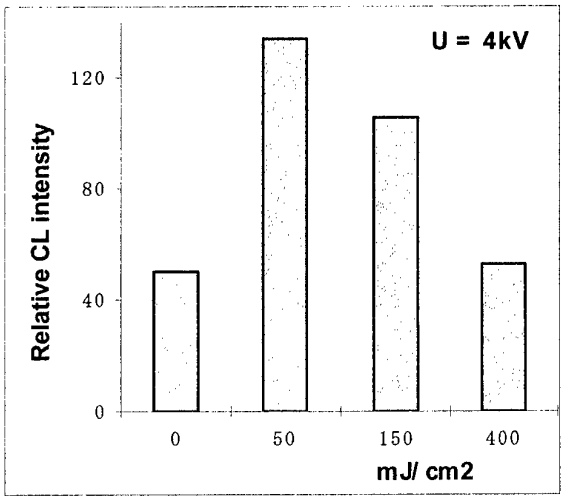

Fig.4. Laser annealing effect on CL.

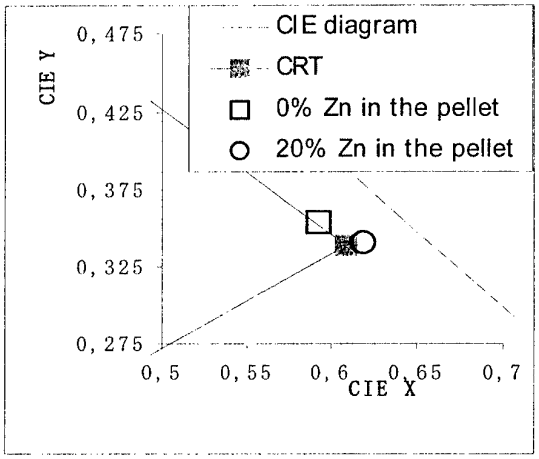

Fig. 3. Effect of Zn doping on CL color coordinates.

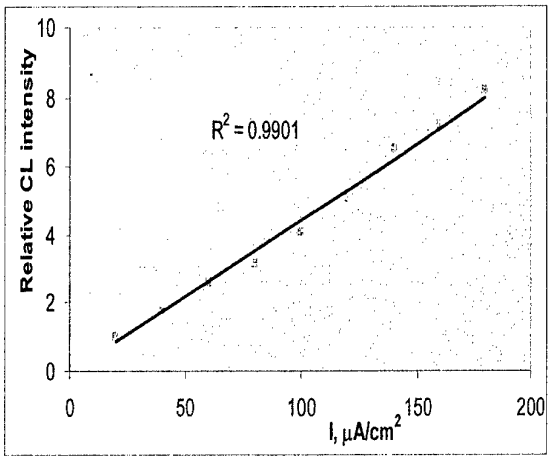

Fig. 5. Luminance-current dependance.

Laser Annealing Effect

Attempt to further improve CL luminance was undertaken with the help of laser irradiation. Laser annealing of as-deposited films was performed with the use of 307nm industrial scanning laser. One can see from the fig. 4, that CL luminance was improved more than two times for the optimal dose 50 mJ/cm^2.

It is supposed that moderate doses provide surface defect annealing effect due to absorption of energy on levels associated with structural defect, while higher doses cause ablation of the layer.

Phosphor's stability

Finally current dependence of luminance was measured and found to by perfectly linear in the studied range – fig.5.

Ageing behaviour of fabricated films was also studied. Luminance decreases abruptly during first minutes of ageing and then levels to about 70% of initial value and quite stable up to 30 Coulomb electron dose at 2 kV and 60 μA/cm^2 conditions.

Conclusions

To summarize we have developed cathodoluminescent film with good properties for field emission display applications. Zinc doping and laser annealing allowed to improve luminance and color properties of the film phosphor as well as ensure its good stability.

References

1. L. Lou, W. Zhang, A. Brioude, C.Le Luyer, J. Mugnier. Optical Materials 18 (2001) 331-336
2. S. Ito et al., Extended Abstracts of 3rd Int. Conf. on Sci.&Technol. of Display Phosphors, Huntington Beach, CA (1997) 275
3. H.C. Swart, J.S. Sebastian, T.A. Trottier, S.L. Jones, P.H. Holloway. J. Vac. Sci. Technol. A13, 1697 (1996)
4. G.A. Hirata, J. McKittrick, M. Avalos-Borja, J.M. Siqueros, D. Devlin. Appl. Surf. Science 113/114 (1997) 509
5. E.T. Goldburt, V.A. bolchouchine, B.N. Levontovitch, N.P. Sochtine. J. Vac. Sci. Technol. B17 (2), Mar/Apr 1999
6. M.Kottaisami, Y.Nakanishi et. al. Electronics Display Conference, Nagasaki, p.45 (2000)

ED-P16. **Binder for the High Brightness Electroluminescent Panels**

A.G. Rodionov, M.M.Sychov *, L.L Ejenkova., S.A. Alexeev *, V.G. Korsakov *

Plastpolymer J.S.Company, St. Petersburg, Russia
* St. Petersburg Inst. of Technology, Russia
msychov@yahoo.com

Abstract
Electroluminescent panel (ELP) is a light-weight reliable backlighting device for the LCD displays. Modern technology of high brightness flexible ELPs requires polymer binders with high dielectric constant, transparency, elasticity, adhesion and stability. Such a binder was developed on the base of modified cyan-ether of polyvinyl alcohol. Influence of precursors, synthesis conditions and polymer structure on its electrical and mechanical properties was studied with the usage of FTIR and ^{13}C-NMR-spectroscopy, gel-chromatography, dynamical mechanical analysis and electrical measurements. Electroluminescent samples were fabricated with the use of the binder by screen printing technology and showed good uniformity of luminescence, better adhesion and 40% increased brightness comparing to the commercial binder.

Key words: electroluminescence, backlighting, binder

Introduction
Polymers with special properties are widely used in the thick film electronics for the fabrication of functional layers and composites. Their usage allows to develop flexible technologies and decrease fabrication cost. In particular, polymers with high dielectric constant (high k polymers) are used in fabrication of capacitors and electroluminescent panels. Flexible flat electroluminescent panels (ELP) based on AC powder EL phosphors are light-weight low power consumption devices for LCD backlighting in personal digital assistants and cell phones.

ELP design includes transparent and rear electrodes which sandwich luminescent and protective layer – composites consisting of polymer matrix and phosphor and ferroelectric powders [1,2]. In ELP technology electrical properties of polymer is one of key factors defying device performance. Requirements to the polymer are the follows: high value of k, low tangent of electric losses, transparency, chemical and moisture resistance, good adhesion. In this paper we report development of the improved polymer for the ELP technology.

Polymer Binder Optimization
Plastpolymer J.S.Company and St. Petersburg State Institute of Technology jointly have developed advanced binder for the ELPs, based on the modified cyan-ether of polyvinyl alcohol binder (CEB).

Structure of the binder is presented on the fig.1. Values of indexes on the figure 1: x=(0,5÷12,0)%wt.; y=(0,5÷3,0)%wt.; z=(99,5 ÷ 85,0)%wt.; R – hydrocarbon radical.

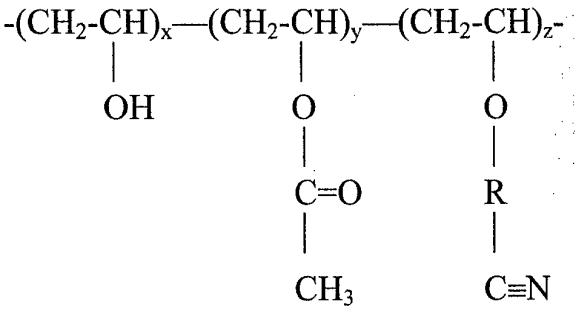

Fig. 1. Structure of cyan-ether binder.

The complex of investigations was fulfilled to study influence of key parameters of CEB molecular structure on its electrophysical and dynamical mechanical properties, and also on rheological characteristics of its solutions in some polar solvents. In particular, CEB structure was investigated and confirmed with the help of IR- and NMR^{13} spectroscopy. Realization of gel-chromatography of CEB solutions allowed to study molecular mass and compositional non-heterogeneity of the polymer. Compositional non-heterogeneity (non-heterogeneity of structure) of the polymer also was analyzed with the help of the data of dynamical mechanical analysis of CEB films.

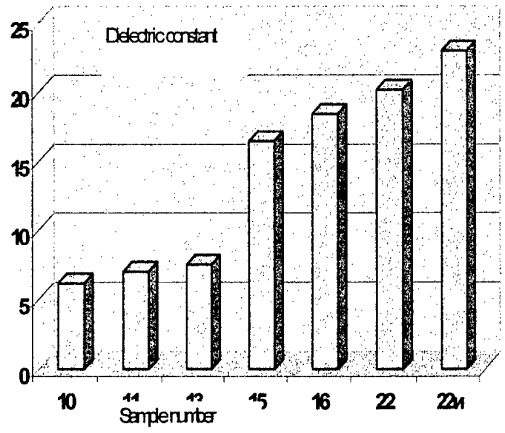

Fig. 2. Dielectric constant of synthesized polymer binders.

On the basis of the received data optimization of polymer structure and synthesis technology was performed. Figure 2 reflects the achieved increase of the value of dielectric constant of polymers as a result of optimization of precursors and process of synthesis.

Optical Properties
Fig.4 reflects the transmittance spectra of the starting

and photo-aged polymeric film. One can see that polymer has a high transparency in the visible range, however after photo-aging it has significantly worsened especially in the region of short wavelength.

During the ELP operation visible radiation of significant intensity is generated, and at use in products of external illumination and mobile electronics polymer also is subjected to the action of the visible and ultra-violet light. Decrease of light transmittance under the action of these factors results in decrease of the ELP brightness and efficiency. Therefore light resistance of polymer is the important characteristic and for its achievement CEB was modified with the appropriate additives. As a result – see fig.3 – stability of transmittance is achieved. Also it may be seen that the transmittance of developed polymer is much higher than that of the commercial analogue.

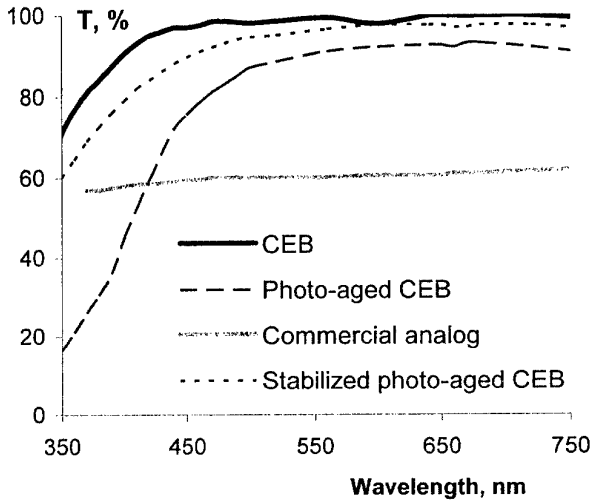

Fig.3. Transmittance spectra of the polymers.

Characteristics of the developed polymer are summarized in the table 1.

Table 1. CEB properties.

Parameter	*Value*
Dielectric constant	7 ÷ 22
tgδ	0.10 ÷ 0.15
Color	white
Light transmittance (550nm), %	~ 95
Viscosity of 25% solution, Pa*s	500...700

Thus, developed polymer binder have a wide range of values of dielectric constant that allows to use optimum polymer for concrete application, low dielectric losses, transparency and light resistance. Experimental samples of material were used for the fabrication of electroluminescent panels.

ELP optimization

Composition of the ELP's protective layer was optimized based on the dependence of k value of composite on the ferroelectric filler content. As it is shown on the fig.4, k value rises with the filler content increase from 23 for the plain polymer to above 100 for the composite with the 80%wt. of the barium titanate. Higher content of the filler leads to the non-uniformity of the functional layer and thus is not acceptable.

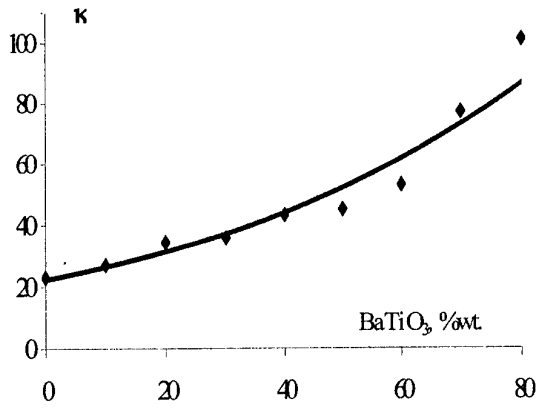

Fig. 4. Dependence of k on filler content.

Optimal thickness of ELP luminescent layer H was found from the dependence of electroluminescent brightness on H. As it is shown on the fig.5, there is an extremism on the dependence of ELP brightness on luminescent layer thickness. The reason for that is that there are two basic factors which are dependant on layer thickness.

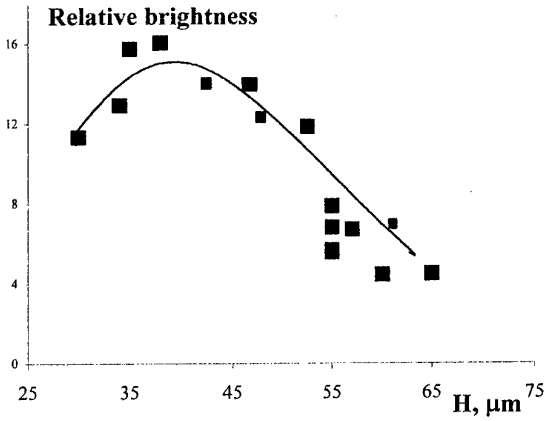

Fig. 5. Influence of luminescent layer thickness on ELP brightness.

T On the one hand increase of the layer thickness introduces additional number of the phosphor particles contributing into the luminescence, which positively influences brightness. On the other hand increase of the thickness decreases strength of the electrical field in the

luminescent layer (at constant voltage) and thus negatively influences brightness. Superposition of two factors gives resulting curve. As it follows from the fig.5, optimal luminescent layer thickness is about 40 μm.

Tests of the ELP samples based on developed polymer binder showed their good performance and stability [3]. Also polymer was tested in the structure of flexible electroluminescent panels in comparison with commercial binder. In particular, carried out by DooSong Tech company (Korea) tests have shown advantage of developed binder in comparison with commercially available samples – table 2 [4].

Table 2. ELP characteristics.

Binder	*Brightness, cd/m²*	*Color coord.*		*Adhesion*
		X	*Y*	
Commercial	56	0,184	0,403	Low
CEB	78	0,184	0,399	High

Developed binder provide significantly higher brightness of ELP samples as well as improved adhesion between its functional layers, hence reliability and durability.

High transparency of the polymer provides preservation of color characteristics of ELP luminescence dictated by the phosphor.

Conclusions

Results of tests show that the developed polymer has necessary transparency and stability and allows to fabricate high quality ELP functional layers with good adhesion and provides increase of brightness of electroluminscent light sources up to 40% in comparison with the available commercial analogue. The important advantage of the developed material also is much lower cost.

References

1. M.M. Sychov, Y. Nakanishi, V.V. Bakhmet'ev, V.G. Korsakov. Control of EL powder phosphor properties. SID International Symposium. Boston 2002. pp.400...403.
2. A.G. Rodionov, L.L. Ejenkova, M.M.Sychov, S.A. Alexeev, V.G. Korsakov. CEB – binder for the electroluminescent panels. In the book: News in the Ecology and Materials Science. SPb. PGUPS 2003, p.45-48
3. S.A. Alexeev, M.V. Diakonov, M.M. Sychov. Optimization of the ELP functional layers. Ecology and Energy Preservation 2003. SPb. p.40
4. DooSong Tech technical report KAS-A-401-14 RE(0). 23.08.2002.

ED-P17. Electroluminescent Phenomenon in Polyaniline Films Doped with CdS Nanoparticles

V.F. Ivanov, A.A. Nekrasov, O.L. Gribkova, A.V. Vannikov

A.N. Frumkin Institute of Electrochemistry Russian Academy of Sciences, 119071, Leninskii pr.31, Russia, Moscow

Abstract

Electroluminescence of polyaniline (PAn) films doped with CdS nanoparticles depends strictly on the level of the acid doping of polyaniline. The unusual current fluctuations during the short voltage impulses applied to PAn(base)/CdS film do not noticeably effect the kinetics of the recombination processes causing the light emission. One may suppose that this occurs because of the association of the nanoparticles along the electric lines of force, which causes compensation of the external field. Random "coalescence" of such associates causes arising of the areas, where the direction of electric field is opposite to that of the external electric field applied, and its amplitude exceeds the amplitude of the latter. The bias voltage impulses increase markedly the operation time.

Keywords: electroluminescence, polyaniline, nanoparticles, cadmium chalcogenides

Instability of electroluminescent systems, which leads to a rapid loss of their operation characteristics, is one of the main problems, which arise during development and investigation. Due to this it is of interest to investigate hybrid electroluminescent systems based on cadmium chalcogenide nanoparticles, which have high luminescence yield and are characterized by n-type conductivity, and conducting polymers (in particular, polyaniline) [1-5]. For preparation of electroluminescent composition we have used a system containing polyaniline (PAn) (polymer matrix) - cadmium sulfide (CdS), which being a n-type semiconductor, is known to exhibit photoluminescent properties [6-8]. Average thickness of polymer layer of the compositions obtained ranges from some tens of microns to ~2 μm. After application of the polyaniline layer containing CdS nanoparticles onto ITO an aluminum film was vacuum evaporated onto the sample. The sandwich structure thus formed was used for electroluminescence measurements. In further experiments both deprotonated (PAnB), and protonated (PAnS) samples were used.

Fig. 1 shows kinetics of change of current and intensity of light emitted by the cell based on the protonated polyaniline (PAnS) and CdS nano-particles after exposing the sample to voltage pulse.

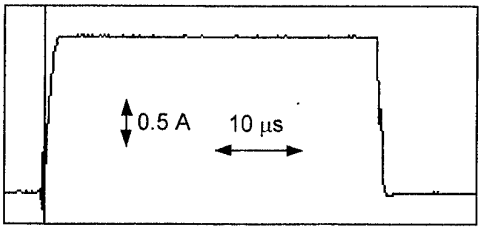

a)

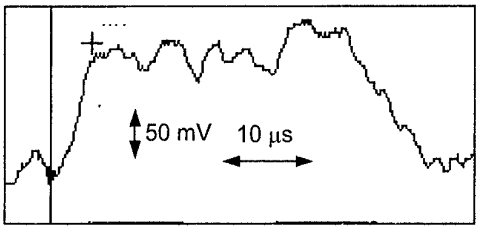

b)

Fig. 1. Kinetics of change of the current (a) and intensity of light (b) emitted by the electroluminescent cell based on PAnS-CdS during application of 15 V voltage pulse.

Fig. 2 shows the dependence of intensity of light emitted by the electroluminescent cell on the applied voltage.

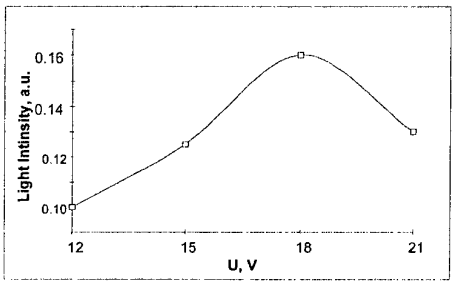

Fig. 2. Dependence of the emitted light intensity on the applied voltage for PAnS-CdS-based electroluminescent cell.

As distinct from the light, amplitude of current flowing through the cell linearly increases at increase of the applied voltage (Fig. 3).

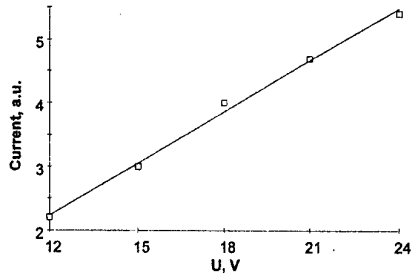

Fig. 3. Dependence of value of current flowing through the for PAnS-CdS-based electroluminescent cell on the applied voltage.

Due to this dependence of the ratio value of the emitted light intensity to the current passed through the cell decreases monotonically at increase of the applied voltage (Fig. 4).

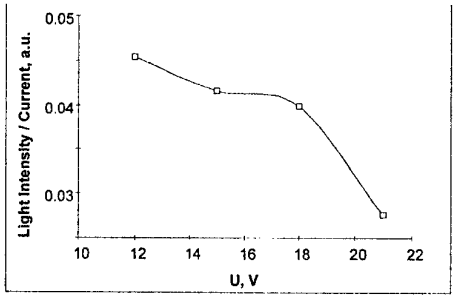

Fig. 4. Dependence of ratio of intensity of light emitted by the for PAnS-CdS-based electroluminescent cell to the current passing through it on the applied voltage.

Thus, effective quantum efficiency of the electroluminescence decreases at increase of the applied voltage.

For the electroluminescent cells on the base of deprotonated polyaniline (PAnB) and CdS nano-particles kinetics of current looks absolutely differently (Fig. 5a and 5b).

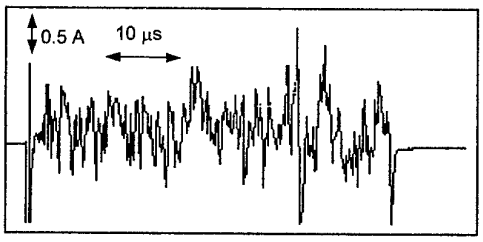

a)

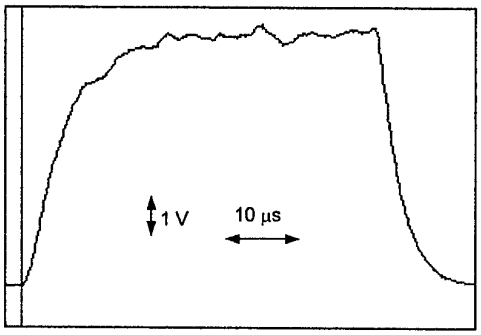

b)

Fig. 5. Kinetics of change of current (a) and intensity of light (b) emitted by the electroluminescent cell on the base of PAnB-CdS during application of a 16.8 V voltage pulse.

It should be noted that value of the stationary current in this case is lower than for the above described cell at the same value of the voltage pulse amplitude. On the other hand, the emitted light intensity is several tens of times higher. Thus, in this case quantum efficiency of the electroluminescence is approximately by 2 orders of magnitude higher than for the cell based on the protonated polyaniline (PAnS). Besides, unusual current fluctuations are observed, which are characterized by a high amplitude and existence of back current peaks while the direction of external electric field does not change.

Fig. 6 shows the dependence of intensity of light emitted by the PAnB-CdS electroluminescent cell on the applied voltage in a rather narrow voltage range. It is seen that it has a linear character, increase of the voltage by several percents leading to increase of the emission intensity by thousands of percents. Assessment of the emission intensity at ~ 17 V voltage gives the value about ~ 100 cd/m^2. However; at these conditions duration of permanent luminescence equals several seconds and is restored after approximately 20 hours of storage of the electroluminescent layer in an idle state.

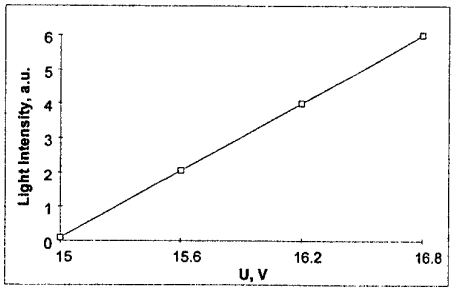

Fig. 6. Dependence of the emitted light intensity on the applied voltage for PAnB-CdS-based electroluminescent cell.

The observed phenomena may be explained on the base of notions about recombination of holes and electrons at the interface of CdS (n-type semiconductor) [9] and polyaniline with hole conductivity [10], which is accompanied by emission of a part of the energy released in this process. It is necessary to take into account that CdS nano-particles are distributed inside the polyaniline film and, therefore, the charge carriers transport comprises a hopping of the carriers between the nanoparticles. Thus, this process is essentially stochastic in its nature, which imposes significant limitations on the transport of n-type carriers. As distinct from a typical situation at an interface between phases with different type of conductivity, in this case is distributed along the whole bulk of the polyaniline film, which should lead to an increase of the light emission intensity. Lower (by approximately two orders of magnitude) emission intensity in case of use of highly conductive PAnS in comparison to the similar parameter for the cell based on poorly conductive PAnB, is evidently determined by mutual shunting of hole and electron conductivity channels, and a more efficient quenching of the excited states in polyaniline with quasi-metallic conductivity.

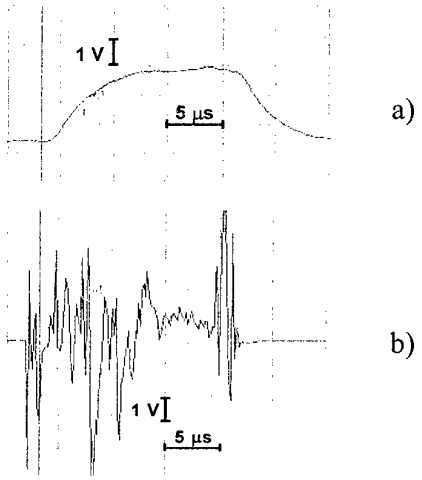

Fig. 7. Kinetics of the light emission (a) and the current transient response curve (b) during application to the EL cell of the first voltage pulse with the amplitude of 20 V and duration 20 μs.

An intensive luminescence was observed within the whole visible range of the spectrum after application to the samples of voltage pulses with the amplitude of 20 V and duration of 20 μs. Typical picture of the kinetics of emission intensity and the corresponding current transient response curve during the application of the first pulse are presented in Fig. 7. After passing 5 voltage pulses with at the interval of 10 s the emission response decreases significantly (Fig. 8a), and the current response at these conditions is presented in Fig. 8b.

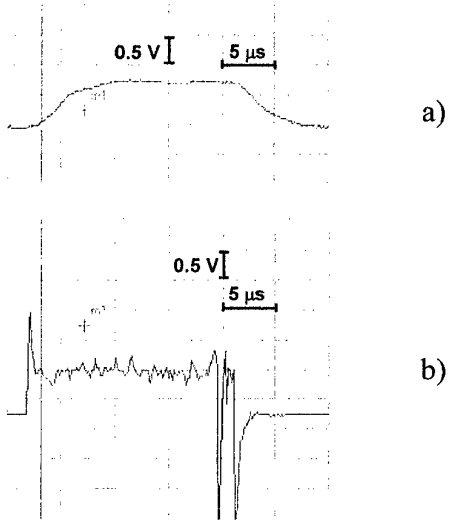

Fig. 8. Kinetics of the light emission (a) and the current transient response curve (b) during application to the EL cell of the 5th voltage pulse with the amplitude of 20 V and duration 20 μs.

In order to restore initial intensity of the signal, it is necessary to apply a voltage pulse of approximately the same amplitude but the opposite polarity.

After application of the pulse of the opposite polarity the amplitude of emission response increases again (Fig. 9).

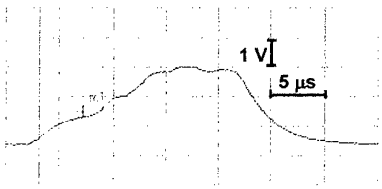

Fig. 9. Kinetics of the light emission during application to the EL cell of the voltage pulse of the direct polarity with the amplitude of 20 V and duration 20 μs after the "reanimation" of the sample by the pulse of the opposite polarity.

It is obvious from the above presented data that the phenomena have a complex nature. The fact that the intense fluctuations of the current during the electroluminescence do not noticeably effect the kinetics of the recombination processes causing the light emission deserves attention. Taking into account large area of PAN/CdS interface, one may suppose that the above phenomenon is due to charge/discharge processes of the corresponding capacitors at the polymer/semiconductor interface. The fact that, along with the charging of the

capacitors, their discharge occurs, at which the current direction changes to the opposite one (Fig. 7b) at the unchanged polarity of the applied external voltage, is a characteristic feature of these processes. One may suppose that this occurs because of the association of the nanoparticles along the electric lines of force, which causes compensation of the external field. Random "coalescence" of such associates causes arising of the areas, where the direction of electric field is opposite to that of the external electric field applied, and its amplitude exceeds the amplitude of the latter. The electric discharge occurring after the "coalescence" of the associates is responsible for the flowing of the opposite currents. In parallel with these processes the process also occurs, for which the formation of such random associates is the necessary condition of providing the transport of n-type charge carriers along the system of chains of CdS nanoparticles. The formation of the associates of the nanoparticles should proceed rather rapidly (during ~1 μs). Their high local concentration and low local viscosity of the PAN film may contribute to this. Verification of these suppositions will be performed later. Another interesting peculiarity of the observed phenomena is connected with the "reanimation" of the emission characteristics after passing the voltage pulse of opposite polarity. The observed "attenuation" of the light-emitting ability is evidently due to the corresponding decrease of the concentration of the main n-type carriers in CdS nanoparticles. This may be caused by the fact that transport of electrons along the chain of the nanoparticles in the direction from the metallic electrode occurs according to the hopping mechanism. Stochastic character of this process determines the decrease of the rate of restoration of the main carriers concentration as we are moving from the surface of the metallic electrode. In this case passing of the voltage pulse of the opposite polarity restores the initial concentration of the electrons.

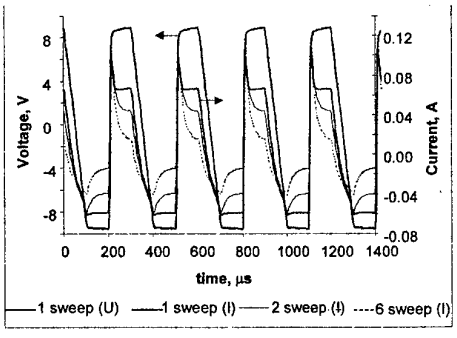

Fig. 10. Current transient curves during application to the electroluminescent cell based on PAn and CdS nanoparticles of several series of voltage pulses of alternate polarity and amplitude ±10 V. Duration of each series is 1 s.

The fact that the use of alternate voltage allowed to increase essentially operation life of the electroluminescent system based on polyaniline and CdS nanoparticles may serve as a proof of this point of view. Naturally, it is seen from Fig. 10 that current transient curves in this case have absolutely different shape and the decrease of the current amplitude occurs approximately 10^4 times slower.

Thus, the mechanism of electroluminescent processes in this system is rather complex. Gradual destruction of thin aluminum electrode on the surface of polyaniline film is, evidently, one of the main causes of the decrease of the current passing through the system. Unfortunately, due to technological reasons we failed to register spectrum of electroluminescence of the system based on polyaniline and CdS nanoparticles.

References:

1. M. Gao, B. Richter, and S. Kirstein, Adv. Mater., **9,** 802 (1997).
2. M. Gao, B. Richter, S. Kirstein and H.Mowald, J. Phys. Chem. B, **102,** 4096 (1998).
3. H. Mattoussi, I.H, Radżlowski, B. O. Dabbousi, E.L. Thomas, M.G. Bawendi and M.F. Rubner, J. Appl. Phys., **83,** 7965 (1998).
4. N.P. Gaponik, D. V. Talapin and A.L. Rogach, Phys. Chem. Chem. Phys., **1,** 1787 (1999).
5. A. Pron, P. Rannou, Progress in Polymer Science **27,** 135 (2002).
6. "Preobrazovanie Solnechnoi Energii" ("Solar Energy Conversion"), Ed: B. Serafin, Moscow, Energoizdat, 1982 (in Russian).
7. V.L. Bonch-Bruevich, S.G. Kalashnikov, «Fizika Poluprovodnikov» ("Semiconductor Physics"), Moscow, Nauka, 1990 (in Russian).
8. S.L. Spanhel, M. Haase, H. Weller, A.Henglein. J.Am.Chem.Soc. **109,** 5649 (1987).
9. 9. R. Bube, "Photoconductivity of solids", Moscow, "Inostrannaya literatura", 1962.
10. J.L. Bredas, K. Cornill, F. Meyers, and D. Beljonne, in: Handbook of Conducting Polymers, Second Edition, Ed. T.J. Skotheim, R.L. Elsenbaumer, J.R. Reynolds, Marcel Dekker, N.-Y.-Basel,-Hong Kong, 1 (1998).

ED-P18. New Electroluminescent Polymer Materials Based on Cyanine and Porphyrin Nanocrystals

E.I. Maltsev[1], D.A. Lypenko[1], S.V. Kirillov[1], B.I. Shapiro[1], V.D. Rumyantseva[2], A.F. Mironov[2], Yu.L. Slominsky[3], A..I. Tolmachev[3], H.F.M. Schoo[4] and A.V. Vannikov[1]

[1]Frumkin Institute of Electrochemistry of the Russian Academy of Sciences,
117071 Leninsky Prospekt 31, Moscow, Russia.
[2]Moscow State Academy of Fine Chemical Technology,
Moscow, Russia
[3] Institute of Organic Chemistry, National Academy of Sciences of Ukraine,
Kiev, Ukraine
[4]TNO Institute of Industrial Technology,
Eindhoven. The Netherlands

Electroluminescent polymer composites based on electron-hole conducting aromatic polyimides and nanosized cyanine and porphyrin crystals were developed for application in the polymer light-emitting diodes (PLEDs) with emission bands in the long-wave spectral region. Light-emitting diodes containing polymer nanocomposite emission layers exhibited very narrow electroluminescence bands not only in the visible range but also in the near infrared.

Keywords: nanocomposites, J-aggregate electrolumines- cence, polymer LEDs.

Introduction

Recently [1-4], it was demonstrated that certain electroactive polymers, doped with organic molecular nanocrystals, known as J-aggregates, exhibited efficient electroluminescence when used as emitting layers in polymer light-emitting diodes. Single-layer PLEDS based on polymer/J-aggregate composites had average power efficiency over 0.5 lm/W for the emission in the visible range. Organic molecular nanocrystals or J-aggregates are nanocrystalline compounds intermediate in molecular scale between structurally ordered crystalline materials and individual molecules. These nanosized molecular assemblies with a rigid crystalline structure have coherently coupled transition dipole moments which give rise to high second and third order susceptibility. In the case of cyanine dye J-aggregates, photoluminescence may be tuned from the yellow to red region depending on the molecular structure of the dye used. Some porphyrins also give J-aggregates but before the protonation of their molecules in the presence of organic acids. Certain types of J-aggregates possess high thermal stability that depends on the chemical structure of dye molecules. Polymer/J-aggregate nanocomposites combine the optical characteristics typical for organic crystals with the electronic properties of semiconductor polymers. An efficient red [2] and green [3] J-aggregate electroluminescence (EL) was observed in single layer polymer light-emitting nanostructures. Here, we report the electroluminescent characteristics of the new polymer/J-aggregate nanocomposites emitting in the visible and near IR regions. This multifunctional polymer material may be of interest for application in display and various modern optical fiber communication systems.

Experimental

The thiadicarbocyanine dye used for the formation of the crystalline phase in polymers was the newly synthesized triethylammonium salt of 3,3'-di(γ-sulfopropyl)-4,5,4',5'-dibenzo-12-methyl-11,13-(β,β-dimethyltrimethylene)thiadicarbocyaninebetaine (TCC) with well-determined polarographic half wave redox potentials relative to a saturated calomel electrode: $E_{1/2}^{red}$ = - 1.24 V, $E_{1/2}^{ox}$ = +0.43 V. Aromatic polyimides (PI) [3] were used as electroactive binders. This thermally stable polymers have been used previously as an electron-hole conducting and light-emitting medium in PLEDs. Crystals of the dye (0.1 mg) and PI powder (1.0 mg) were dissolved in chloroform (150 μl) at 60^{0}C. Next the temperature of the solution was cycled between 12^{0}C and 60^{0}C until the majority of dye molecules became associated and formed the nanocrystalline phase of J-aggregates. The process was monitored spectrophotometrically. Thin films were then fabricated by conventional spin coating of the chloroform solution containing the PI and J-aggregates under ambient conditions. The PLEDs described here consisted of 60-100 nm thick polymer/J-aggregate composite layer sandwiched between transparent indium-tin oxide on a glass substrate and Ca electrodes. Quantum efficiency was measured by an Ocean Optics SF2000 spectrometer and Ga-Al-As light-emitting diode (Model AL108a) as a reference IR source. Measurements were carried out at room temperature in air.

Results and discussion

The absorption spectra of TCC in PI film has λ_{max} = 722 nm and the polymer/J-aggregate composites exhibited λ_{max} = 767 nm. The presence of a shoulder on the high-energy side of the J-aggregate absorption peak implies the presence of a low concentration of non-aggregated dye molecules, that remained free during the growth of the J-aggregates. Selective exposure of the PI film doped with TCC, to light of 650 nm, brought about the appearance of photoluminescence (PL) band with λ_{max} = 735 nm. One-layer PLEDs with pure PI exhibited green EL with peak position at 565 nm. In the presence of TCC, instead of the PI EL band, only red emission with λ_{max} = 748 nm was registered suggesting that the dye molecules act as efficient energy acceptors in these matrixes. Finally, for layers doped with J-aggregates, a very narrow EL band was observed in the near IR with λ_{max} = 815 nm, that belonged to the nanocrystalline phase (J-aggregates) in the composite. In the case of polymer/porphyrin composites, the emission band PLEDs was located at λ_{max} = 730 nm.

Polarographically determined oxidation potential for TCC (+ 0.43 V) corresponds virtually to the HOMO level of the dye. Earlier, it was revealed for a mixture of different dye molecules and J-aggregates absorbed on the surface of semiconductor that their oxidation potential levels ($E^{ox}_{1/2}$) are closely positioned. One may infer that the relative location of the levels for a polymer matrix containing TCC molecules and their J-aggregates would also be close. The energy gap ($\Delta E_g^{J\text{-}agg}$) between the HOMO and LUMO of the J-aggregates, determined from the low-energy edge of their absorption band in the composite layer, was found to be 1.5 eV, while ΔE_g^M for TCC molecules was determined 1.6 eV. It was experimentally revealed for a wide range of PI/cyanine dyes layers, that the energy level of the electron transporting centers (3.3 eV that is -1.34 V relative to a saturated calomel electrode) lies substantially below the bottom of the conduction band of PI (2.6 eV). In regard to the hole transporting sites, they are located within the polymer energy gap at the level ≅ 5.35 eV (+ 0.71 V), whereas the upper level of the valence band for PI is equal to ≅ 5.6 eV in this system. It was shown

for CD doped polyimide layers exhibiting EL in the visible range, that both electrons and holes are injected into transporting sites in the nanocomposite. One may assume that a similar electron-hole injection mechanism takes place in the PI/J-aggregate layers described here. No PI EL was observed in the presence of J-aggregates. Just a faint shoulder was detected on the high energy side of the J-aggregate EL band that may be accounted for by the efficient exciton energy absorption of the nanocrystalline species.

In conclusion, we have developed a new type of electroactive polymer materials based on electron-hole conducting polymers, doped with cyanine and porphyrin nanocrystals, emitting from the visible to the near IR. ingle layer devices exhibit very narrow IR EL emission spectra. It was shown that the energy characteristics of the J-aggregates make them effective exciton energy acceptors and electron/hole transporting centers. Work is in progress on the formation of multi-layer polymer/J-aggregate LEDs emitting in the blue region.

This work has been supported by the Russian Fund for Basic Research under Project 03-03-33067, Dutch-Russian NWO project № 047.009.019 and the International Science and Technical Center under Grant No 2207.

References

1. E.I.Mal'tsev, D.A.Lypenko, B.I.Shapiro, M.A.Brusentseva, V.I.Berendyaev, B.V.Kotov, and A.V.Vannikov, Appl. Phys. Lett. J-aggregate electroluminescence in dye doped polymer layers, **73**, 3641 (1998).
2. E.I.Mal'tsev, D.A.Lypenko, B.I.Shapiro, G.H.W. Milburn, J. Wright, A. Hendriksen, V.I.Berendyaev, B.V.Kotov, and A.V.Vannikov, Appl. Phys. Lett. Electroluminescence of polymer/J-aggregate composites, **75**, 1896 (1999).
3. E.I.Mal'tsev, D.A.Lypenko, B.I.Shapiro, and A.V.Vannikov, Sci. Appl. Photo., Electroluminescence of cyanine dye J-aggregates in polymers, **43**, 15 (2001).
4. Maltsev E.I., Lypenko D.A., Shapiro B.I., Bobinkin V.V., Tameev A.R., Kirillov S.V., Schoo H.F.M. and Vannikov A.V. Near-infrared electroluminescence in polymer composites based on organic nanocrystals // Appl. Phys. Lett. 16 (2002) 3088.

ED-P19. Near-Infrared Electroluminescence of ZnS:Er and ZnS(Se):Cr TFEL Devices

N.A. Vlasenko, Z.L. Denisova, Ya.F. Kononets, L.I. Veligura, and Yu.A. Tsyrkunov
Institute of Semiconductor Physics, NAS of Ukraine, prosp. Nayki 41, Kiev, 03028,Ukraine

Abstract. Electroluminescent near - infrared (NIR) emitters are of interest to create special displays for such applications as communications, chemical sensoring, friend and foe identification, alighment and check of systems detecting NIR radiation, etc. The emitters based on radiative transitions in unfilled d - or f - shells are especially interesting due to the temperature stability of the emission wavelength (λ). In this paper, the first results of a study of NIR emitting electron - beam evaporated ZnS:Er and ZnS(Se):Cr thin - film electroluminescent structures (TFELS) are presented. There are two narrow bands with $\lambda_{max} = 980$ and 1530 nm in the emission spectrum of ZnS:Er TFELS whereas a broad band with the peak at ~ 2.4 μm takes place in the ZnS(Se):Cr structures. The mechanism of electroluminescence in both TFELS is the direct impact excitation of Er^{3+} and Cr^{2+} ions. Some characteristics of TFELS as NIR emitters are given.
Keywords: electroluminescence, thin-film structures, ZnS:Er, ZnS(Se):Cr, near-infrared emitters

1. Introduction.

NIR emitters are of interest for a number of applications such as communications, friend and foe identification, night - vision illumination sources, spectroscopic analysis, chemical sensoring, sources for alignment and check of systems detecting NIR radiation. At present, the known NIR emitters are thermal sources, narrow - gap semiconductor diodes and lasers, other solid state lasers. It is interesting to supplement the known NIR emitters by TFEL emitters. Due to their advantages (a flat durable architecture, a low - cost fabrication technique, the stability under an ionizing radiation, a wide range of operating temperatures) NIR TFEL emitters are promising to create some special displays for the above mentioned applications. TFELS activated by NIR emitting rare - earthes or transition metals are of especial interest because of the temperature stability of λ in the case of intrashell transitions. In this paper, the first results of a study of NIR emitting ZnS:Er and ZnS(Se):Cr TFELS made by electron - beam evaporation are given.

2. Experimental procedures

ZnS:Er TFELS under study were of a usual MISIM type, where M is an electrode (ITO,Al), I is an insulator layer (e.g.,Al_2O_3 / Y_2O_3 films with the thickness of 250 - 300 nm), and S is an electroluminescent (EL) film. ZnS(Se):Cr TFELS were of the MISIM or MSIM types. S and I layers were deposited by electron - beam evaporation. Doping of EL films with ErF_3 or Cr was performed by the co - evaporation of ZnS (ZnSe) and the dopant from separate sources. After deposition of the EL film, the samples were annealed in vacuum.

The spectrum of TFELS was measured by the spectral complex KSVU - 23 with a photomultiplier as the detector in the range from 400 nm to 1000 nm and by a spectrometer based on a MDR - 12 monochromator and a PbS detector in the range of 0.9 - 3.0 μm.

Electroluminescence was excited by sine wave voltage of 1 - 20 kHz. The voltage dependence of the intensity of the emission in different bands in the EL spectrum was measured. The power of the emission in observed NIR bands was estimated by the comparison of the photoresponce of the PbS detector on the given NIR emission and on an etalon visible emission, e.g., of ZnS:Mn TFELS. The spectral dependence of the PbS photosencivity was taken into account. The power of the visible emission, the luminance of which has been measured, was determined by the usual method [1].

3. Results and discussion

The typical EL spectrum of ZnS:Er TFELS is given in Fig.1. In addition to well known emission bands in the visible region [2], there are three bands in NIR at ~ 810 nm, 980 nm, and 1530 nm. The intensity of the bands at 980 and 1530 nm, especially of the latter, significantly exceeds the intensity of the visible bands. These NIR bands are rather narrow. Their width (20 -25 nm) is significantly less than that of the identical bands in the EL spectrum of sputtered ZnS:Er TFELS [3]. The dependence of the intensity (I) of all emission bands on the applied voltage (V) is given in Fig.2. It is seen that the intensity of the NIR bands relative to I of the green band decreases with increasing V. This is typical of the impact excitation mechanism of EL.

The decay of EL measured in the different bands of ZnS:Er TFELS is shown in Fig.3. The decay is faster, the shorter wavelength of the band. One can single out in the decay of each band an initial section with the faster decrease of the intensity. The exponential section intrinsic for intrashell transitions is followed then. The lifetime (τ) in the excited states respective to the bands, that was determined from the slope of the exponential section, is listed in Table. The time (τ_e) of the e fold decrease of the intensity of each band is also given in the table. This time is largely due to the initial decay, which is significantly faster for the visible bands than for the NIR bands. In the case of intrashell transitions, the fast initial decay results from non - radiative transitions owing to the resonance energy transfer to some lattice defects or to the relaxation onto lower levers. Hence, the weak initial decay for the NIR bands indicates that the radiative transitions are predominant

from the respective excited states whereas non - radiative transitions strongly reduce the efficiency of the visible luminescence.

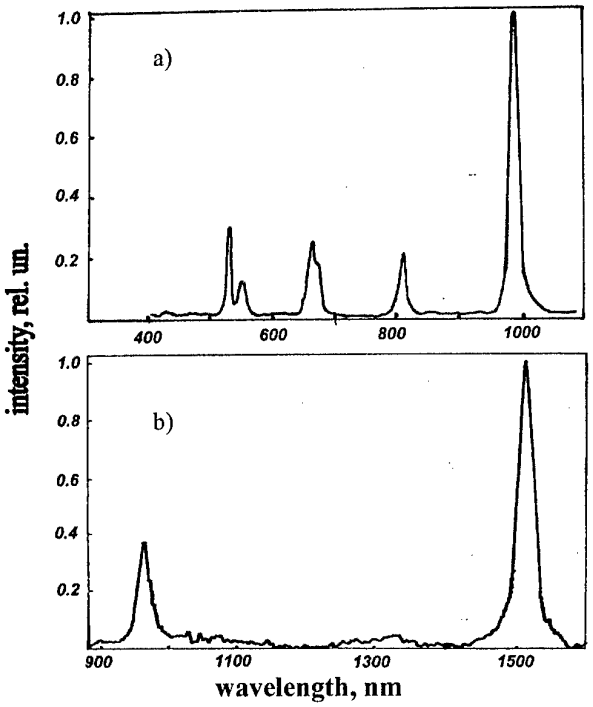

Fig.1. EL spectrum of ZnS:Er TFELS in ranges of 500 - 1000 nm (a) and 900 - 2000 nm (b).

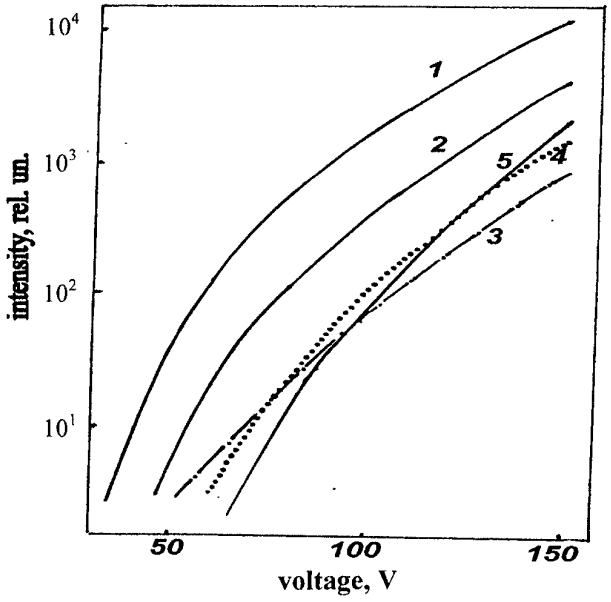

Fig.2. Voltage dependence of intensity of various bands in EL spectrum of ZnS:Er TFELS. λ_{max} of bands, nm: 1530 - 1; 980 - 2; 810 - 3; 665 - 4; 525, 547 - 5.

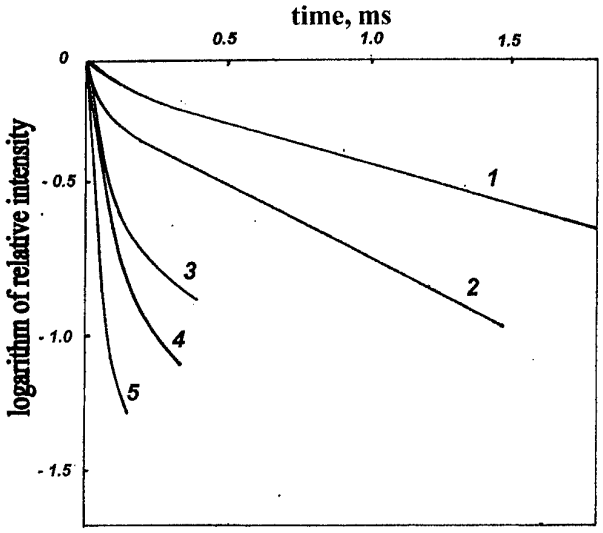

Fig.3. EL decay of ZnS:Er TFELS in various bands. Excitation by voltage pulses of 50 μs width and 40 Hz frequency. λ_{max} of bands, nm: 1530 - 1; 980 - 2; 810 - 3; 665 - 4; 525, 547 - 5.

Table. Lifetime and e fold - decay time for different excited states of Er^{3+} ion in ZnS:Er TFELS.

λ_{max}, nm	Excited state	τ, mc	τ_e, mc
1530	$^4I_{13/2}$	1,8	1,5
980	$^4I_{11/2}$	0,9	0,4
810	$^4I_{9/2}$	0,5	0,1
665	$^4F_{9/2}$	~ 0,3	0,05
525, 547	$^4S_{3/2}$, $^2H_{11/2}$	-	0,02

According to the first evaluation, the power of the NIR emission in the band of 1530 nm, which is the most suitable for optical fiber communications, is ~ 0.2 mWt/cm^2. The respective spectral density of the power is ~ 8 μWt / cm^2· nm.

The EL spectrum of ZnS:Cr and ZnSe:Cr TFELS is shown in Fig.4. The spectrum of photoluminescence of a ZnS:Cr crystal is also shown. The spectral region of the emission of both the crystal and the TFELS is the same and is due to the ^5E - $^5T_2$ transition in the 3d shell of Cr^{2+} ion. In the EL spectrum of the TFELS some extrema are seen, which have the interference origin. In addition to this NIR emission, there is a weak emission in the visible and NIR regions, intensifying with increasing λ. This emission is due to intraband transitions of hot free electrons. The existence of the weak visible emission will be useful for alignment of the NIR emitting ZnS(Se):Cr TFEL devices.

It has been found that the voltage dependence of the intensity of both the NIR emission and the emission of hot electrons has the similar shape like to an

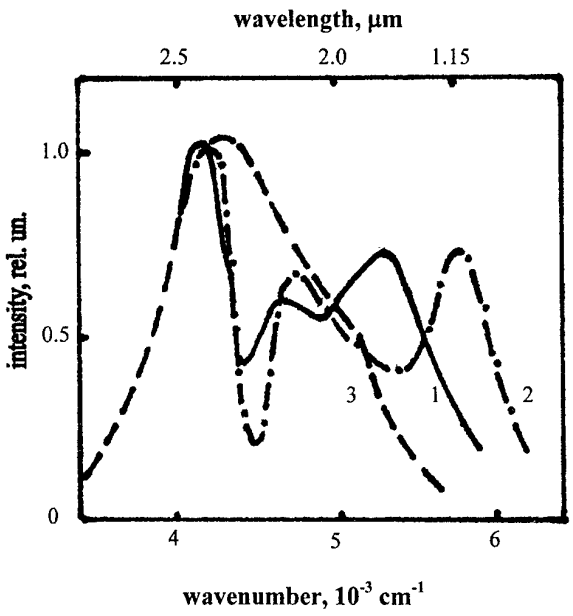

Fig. 4. EL spectra of ZnSe:Cr (1) and ZnS:Cr (2) TFELS. PL spectrum of ZnSc:Cr crystal (3).

exponential dependence (Fig.5). Such a dependence is typical of the impact excitation mechanism. The steepness of the I (V) dependence is rather high even in ZnS(Se):Cr TFELS of the MSIM type. Therefore, these NIR emitters are suitable for matrix EL devices. The evaluated power of the NIR emission of the first laboratory samples of ZnS(Se):Cr TFELS is equal to 0.2 - 0.4 mWt / cm^2.

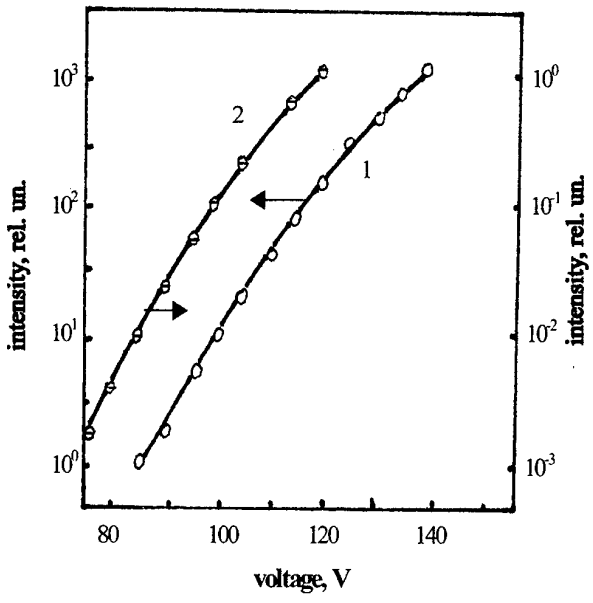

Fig. 5. Voltage dependence of intensity of NIR emission (1) and emission of hot electrons (2) of ZnS:Cr TFELS of MSIM type. f = 5 kHz.

4. Conclusions

It follows from the above characteristics that ZnS:Er TFELS are more effective emitters in the NIR region than in the visible one. The narrow band at 1530 nm, which is of interest as to optical fiber communications, is the most intensive in the EL spectrum of these TFELS. The radiative transition from the lowest excited level of Er^{3+} ion responsible for this band is accompanied by non-radiative transitions to a significantly lesser extent than the transitions in the visible region.

The broud - band emission in the range from 1.7 μm to 2.8 μm observed in the EL spectrum of ZnS(Se):Cr TFELS is the same as in photoluminescence of the number of wide - band 11 - V1 compounds (ZnS, ZnSe, CdSe etc.) doped with Cr. Last years, these materials are investigated largely as to development of NIR tunable optical lasers (see,e.g. [4]). The wavelengh of the emission of ZnS(Se):Cr TFELS can also be varied in the wide range by the change of the viewing angle or the layer thickness owing to the interference effect. Both studied TFELS are suitable for NIR devices with matrix addressing due to the steep voltage dependence of the emission intensity. As to the NIR emission power of the TFELS, it is expected that optimization of the dopant concentration and other technological factors will result in its increase.

References

1. A. Ono. Electroluminescent displays. World Scientific. Singapure. 1995. p. 170.
2. L.J. Meng, Ch. H. Li, G.Z. Zhong. The influence of the concentration of Er^{3+} ions on the characteristics of ac-electroluminescence in ZnS:ErF_3 thin films. J. Luminescence, **39**, 11, 1987.
3. A. Kale, W. Glass, M. Davidson, P.Holloway. Growth and Characterization of Near - Infrared Emitting Thin Film Electroluminescent Phosphors. Proc.11th Intern. Workshop on Inorganic and Organic Electroluminescence. Sept. 23 - 26, 2002, Ghent, Belgium, p. 57.
4. I.T. Sorokina, E. Sorokin. Broadly tunable compact continuous - wave Cr^{2+}:ZnS laser. Optics Letters, **27**, 1040, 2002.

ED-P20. **LED modules containing Frenel lenses**

M.G. Tomilin, A.E. Puisha
S.I. Vavilov State Optical Institute, Birzhevaya Liniya 12, St.-Petersburg, 199034, Russia
tomilin@soi.spb.ru, Tel. +812-114-0565, Fax + 812-328-3720
A.I. Chuvashov
Institute of Fine Mechanics and Optics, Russia, <Alexander@chuvashov.com>
Abramov V.S.
Corvet, Moscow, Russia

The last decade was characterized by great advance in LEDs development. LEDs applications are large size information screens and new type of bright light sources. Unfortunately not in all cases the radiation characteristics of LEDs are adapted to observer's field of view.

We developed new super bright LED modules containing Frenel lenses in the common body including RGB elements [1]. The red, blue and green crystals are placed in one LED raster conic pattern that allows forming any light energy distribution in the viewing angle [2]. Two types of LED modules with parallel (Fig.1) and perpendicular (Fig.2) orientation of cylindrical Frenel lenses relative LEDs were manufactured and examined. The results of indicatrix measurements for azimuthal angles from 0° up to 360° and polar angle 50° are shown on Fig. 1 and Fig. 2. Blue crystal is marked by the numeral 1, red - by numeral 2, green- by numeral 3. The particularities of indicatrix measurement results for full range of polar angles are discussed.

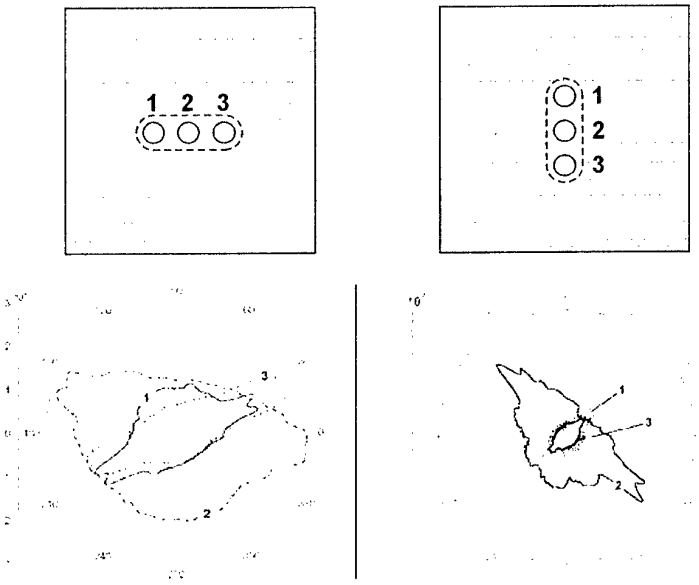

Fig. 1 Fig. 2

In order to achieve the uniform luminance intensity for large size displays it is necessary to obtain high repeatability of LED modules. The repeatability of luminance intensity distribution depends on the quality of Frenel lenses profile. The profile defects and inclusions may be the reason of poor luminance intensity repeatability. The nondestructive technique based on NLCs thin films was used to detect the quality of Frenel lenses profile. The results open the way for LEDs performance achievements.

The LED modules containing Frenel lenses gives also the possibilities to use super bright LEDs for backlighting in color LCDs, traffic signaling, contour lighting, and general illumination on direct sunlight and at nighttime with decreased current value.

References

1. Russian patent "Light emitting device", RU №2134000 C1.
2. M.G. Tomilin, V.S. Abramov, A.E. Puisha. Super Bright LED modules and their Application. EL'2002, Ghent, pp. 407-408.

NON-EMISSIVE DISPLAYS

NED-1. **Liquid Crystal Displays: future forecast and recent developments in HKUST**

Vladimir G. Chigrinov

Hong Kong University of Science and Technology, Clear Water Bay, Kowloon, Hong Kong,
Phone (852) 2358 8522, Fax: (852) 2358 1485, Email: eechigr@ust.hk

Liquid Crystal Displays (LCDs) still remain the most important part of Flat Panel Displays (FPDs). Starting from the first electronic calculator, produced by Sharp in 1973, LCDs finally become the winner of the large market of Electronic Imaging Devices. During the last two years LCDs aggressively come to the market of TV and desk-top PC monitors, replacing here common CRT devices. Recent Liquid Crystal on Silicon (LCOS) Philips projection TV models and the latest 54'' direct TFT- LCD, presented by Samsung clearly showed, that now popular Plasma Display Panels (PDPs) and Digital Light Projectors (DLPs) based on Micro-Electro-Mechanical (MEM) switchable mirrors will face a tough competition even in the direct view TV market. The amount of LCD sales exceeds even the optimistic forecast and nearly doubled in the last three years approaching USD 50 bln. While in 1997 the top ten LCD producers were mostly Japanese Companies, leading by Sharp, in 2002 Korean Companies Samsung and LG have replaced the leader, following by five Taiwanese and three Japanese Companies. The progress of TFT-LCD production is remarkable: the size of mother glass drastically increases (so called 6^{th} LCD generation), while the price go down due to the growth of the TFT-LCD yield. Besides TFT-LCD, which provides more than 80 % of total LCD sales, color and monochrome STN-LCD still cover the substantial part of LCD market, mostly mobile phone and small PC (PDA) sectors. However, the rapid decrease of TFT driving circuits cost and a growing demand to the higher resolution of LCD can soon result in TFT-LCD replacement of the common STN-LCD even in mobile phones. The other emerging LCD application is an electronic book (e-book), which requires a stable contrast image of the black symbols on the white background even without any supporting voltage, similar to the image of the usual book. Several technologies, such as cholesteric LCDs, Zenithal Bistable LCD (ZBD), $0 \Leftrightarrow \pi$ switchable LCDs, Bistable Twisted Nematic (BTN) LCDs and ferroelectric LCDs are competing for e-book applications.

Besides the present picture of LCD research and developments, we are going to consider the latest achievements in the LCD field in Hong Kong University of Science and Technology. We shall first describe the progress in photo-aligning materials and technology, such as azo-dye LC aligning layers and superthin polarizers. Secondly we shall present the new efficient LCD modeling and optimization software. In particular, we shall provide a new concept of high contrast transflective LCDs with patterned phase retarders and polarizers. Finally we shall comment on new LC passive elements for optical communication systems, such as LC switches, attenuators, controllable add-drop filters, equalizers, polarization controllers etc. In particular, a combination of LC with Photonic Crystals can be a start of a new generation of voltage controllable passive components for fiber optical communication systems.

NED-2. LCOS and LED Microdisplays: Design, Fabrication and Applications

A. Smirnov, V. Labunov, S. Lazarouk

Belarusian State University of Informatics and Radioelectronics, Minsk, Republic of Belarus

Abstract

Design, fabrication process and applications of LCOS and LED microdisplays are discussing in comparison. Special attention will be paid to a full inorganic electroluminescent microdislay based on aluminum / nanostructured porous silicon reverse biased light emitting Schottky diodes. Being of a solid state construction, this microdisplay is cost-effective, thin and also super high resolution, wide viewing angles, fast response time and wide operating temperature range. The advantages of full integration of a LED-array and driving circuitry onto a Si-chip will be also discussed.

Key words: microdisplay, liquid crystal on silicon (LCOS), light emitting diode (LED)light in weight due to very simple device architecture. Its benefits include

1. Introduction

A new very fast growing segment of electronic industry is the industry dealing with super miniature displays or microdisplays. They are finding the place in portable wireless communication devices, computing tools, digital still cameras, camcorders, advanced sell phones, and toys.

In principle, the simplest type of microdisplay is a light emitting device because it eliminates the need for an external light source and complicated optics, but their low luminance level limits their application to personal viewers. Most of the known light emissive technologies have been implemented as microdisplay technologies [1,2].

In this paper we are discussing in comparison LCOS-technology and an alternative cost-effective approach based on the usage of Al / nanostructured porous silicon (PS) reverse biased light emitting Schottky diodes fabricated onto a silicon chip together with addressing ICs. The main advantages of such an approach are:

1). The usage of a simple and cost-effective standard bipolar semiconductor manufacturing process which provides full integration of addressing ICs with an array of Al / PS light emitting diodes and helps to integrate a lot of functionality into the display's silicon backplane;

2). Very high resolution and nanosecond response time of a PS LED microdisplay;

3). Low cost and simplicity of PS LED microdisplay fabrication, especially, in the case of passive addressing.

2. State of the art

The first reversed biased PS LED was demonstrated by Richter et al. in 1991 [3]. A PS-layer was formed on a n-type silicon substrate following with the deposition of a semitransparent Au-electrode in order to form the Schottky structure. Light emission with the efficiency of 10^{-5}-10^{-6} was observed in the visible range with the peak of 650 nm [4]. The lifetime of such devices varied from 45 min. to 100 h, after which the emission attenuation took place [5].

In 1995, we made a significant improvement in the efficiency and stability [6] through the formation of an oxidized PS layer protected from atmospheric oxygen by the additional passivation. The oxidized PS layer was formed on a low resistivity n-Si substrate by anodozation in the transition regime [7], providing a continuous anodic oxide on the surface. Moreover, the additional passivation layer of a transparent anodic alumina Al_2O_3 was formed on the PS layer by a selective Al-anodization in an oxalic electrolyte during formation of an Al-Schottky electrode. It ensured the stability of continuous PS LED operation during 1000 h without visible degradation effects and increased quantum efficiency (10^{-3}-10^{-4}) [8].

In 1998, V. Kuznetsov et al. [9] improved a PS LED design in order to enhance the device efficiency till $5x10^{-3}$. In particular, they replaced the opaque electrode with a semitransparent silver electrode.

In 2000, the more efficient reverse biased PS LEDs have been reported by B. Gelloz et al. [10]. The quantum efficiency of about 10^{-2} has been obtained by using oxidized PS. Porous layer was formed on n+-silicon at 0°C. Then, the PS layer without drying was electrochemically oxidized by anodization in an aqueous solution of sulfuric acid. A Schottky barrier was formed by a transparent ITO deposition. The advancement of the anodization process by this way decreased the size of nonconfined silicon nanocrystals in PS. The enchanced quantum efficiency can be

explained by the reduction of leakage carrier flow through the nonconfined silicon nanocrystals. Recently, the highest quantum efficiency of about $1.2x10^{-2}$ has been obtained by pulsed exitation [11]. Pulse LED operation allows one to reach the highest current density through a LED structure, which corresponds to maximum efficiency values.

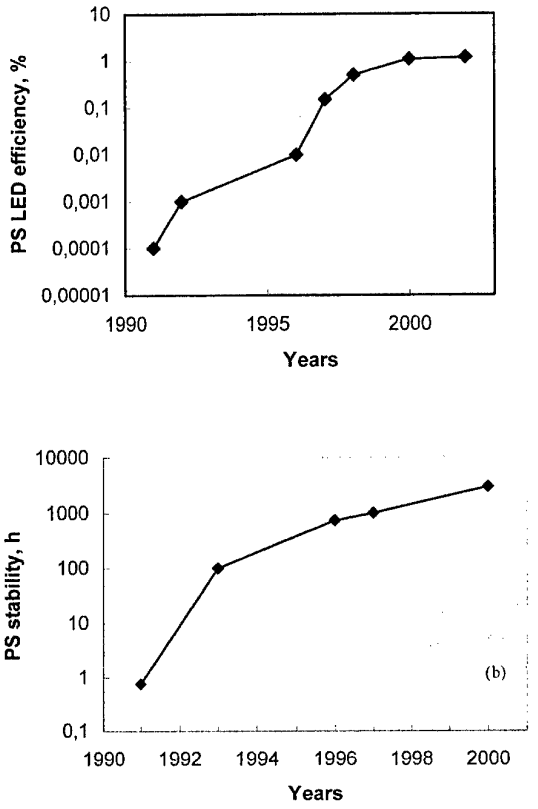

Fig.1. Efficiency (a) and stability (b) improvement of reverse biased PS LEDs.

Some common design ideas are present in all mentioned PS LEDs:
- all are formed on n-type silicon substrates due to the higher Schottky barrier compared to p-type material;
- in addition, n+-silicon substrates are preferable because of minimal series resistance of PS LEDs;
- PS must have homogeneous size distribution of nanocrystals over all the thickness and down to 1 μm. For this reason, oxidized PS was used in the device fabriccation and the temperature of the PS formation was chosen to be 0°C;
- reverse biased LEDs have a nonlinear EL-I characteristics with an efficiency increasing with a current;
- optimized LED geometry and pulsed bias provide maximum LED current with the highest efficiency value;
- reverse biased PS LEDs can be formed also onto polysilicon [12] or amorphous silicon [13] layers as well as onto a transparent sapphire [14] or glass [15] substrates.

3. PS LED array fabrication process

The fabrication process and a PS LED structure are shown in Fig.2. N-type single crystal silicon wafers with the resistivity of 4.5 Om·cm were used as substrates in our experiments. High doped n^+-silicon layer of about 100 nm thickness was formed on both sides of wafer by diffusion of phosphorous gas phase at a temperature of 950°C during 40 minutes (Fig. 2a). After doping treatment the surface resistivity of a sample was 10 Om/□ (10^{20} dopant atoms/ cm^3). Then wafers were etched in hydrofluoridric acid in order to remove the oxide formed during thermal treatment [16].

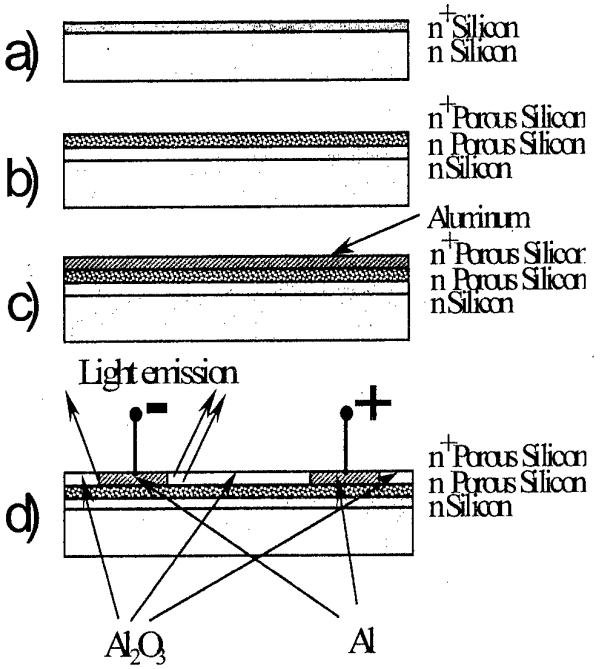

Fig.2. Schematic view of fabrication process and a PS LED structure: a) n-type silicon wafer with n^+-diffused layer; b) after anodization in transition regime, PS is formed both in n^+- film and in a substrate layer; c) aluminum layer is deposited by magnetron sputtering; d) the final structure after photolithography and subsequent aluminum anodization. Light emission at the edge of negative biased pad is evidenced.

The PS layer was formed by anodization in transition regime, in 1% HF aqueous solution at 2-5 mA/cm^2. The thickness of PS film was higher than the n^+-layer one, so that a thin layer of the n-substrate was also anodized (Fig. 2b).

To obtain metallic contact, 0.5 μm thick aluminum film was deposited by magnetron sputtering onto the porous layer (Fig. 2c). The Al electrodes (pads) were obtained by standard photolitography and subsequent electrochemical aluminum anodization process. Aluminum anodization produced the transparent insulating alumina (Al_2O_3) areas between the aluminum pads so that light could be revealed (Fig. 2d).
The electrical contact on the wafer back side (not shown in the picture) was provided by the n^+-diffused layer. Devices were biased connecting either two adjacent pads on the upper layer either one of the pads and the back side contact.

4. Experimental results

EL spectra were measured with the computer-aided spectrophotometer PEM-100, equipped with a cooled photomultiplier. PL spectra were measured under UV laser excitation at λ=337 nm.
Visible electroluminescence (EL) was recorded when DC or AC voltages larger than 4V were applied between the aluminium electrodes. The visible EL appears in the dark, at the edge of the electrodes at a reverse bias of 5-6 V. The intensity of emitted light increases with applied voltage. At applied bias higher than 7 V the emitted light was observable by the naked eye at normal daylight. Compared to forward biased solid state porous silicon devices, the structure has an increased stability (after 1000 hours of continuous operation under 7 V reverse bias, no appreciable modification was observed in emission intensity [17].
The dependence of light intensity via current density is shown in Fig. 3.
The EL brightness increases while increasing the applied voltage until thermal breakdown is reached. The thermal breakdown takes place when currents higher than 500 mA are measured through 0.02 mm^2 pad area (the current density referred to the pad area is more than 2500 A/cm^2). Referring to these pad areas, such currents are destructive. Limiting the current in the 200-250 mA range, bright and stable EL is visible even after 1000 hours of light emission. Moreover, current - voltage characteristics are reproducible at different time intervals, even after 1000 h of permanent applied voltage.
It is noticeable that EL intensity is higher when voltage is supplied between two adjacent electrodes than between an Al electrode and silicon substrate. This fact is reasonably related at the possibility to see or not the emission from the maximum electric field region that is under the Al layer when the substrate is the second electrode.

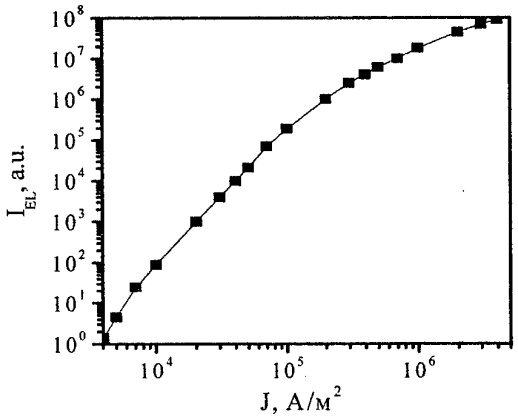

Fig.3. EL light intensity of Al/PS structures via current density.

The EL spectrum, measured in the 1.55 –3.105 eV energy range, for different currents through two adjacent electrodes are shown in Fig. 4.

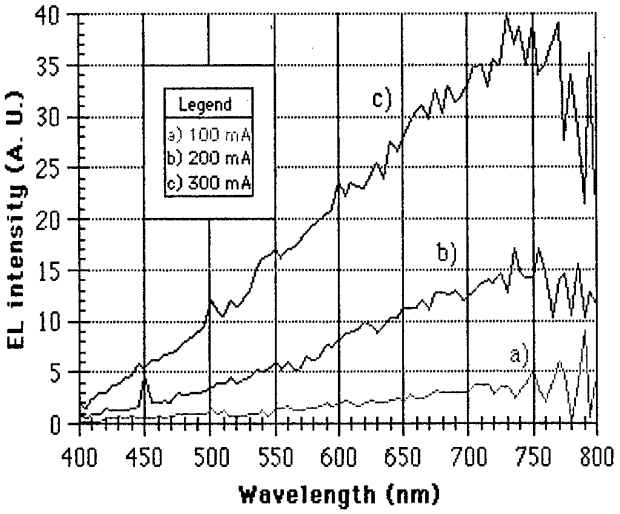

Fig. 4. EL spectrum for different currents through two adjacent electrodes at reverse bias.
Depending on PS anodizing regimes the emission peak can be both in the blue and in the red. But the emission spectra are very broad, with example which covers the whole visible range [18]. The other approaches are to be used for a color microdisplays to get a narrow light emission spectra, say, the integration of a PS LED with a PS microcavity [19].
If the current through the pads is related to the intensity of the emitted light a nearly quadratic dependence was found.
The special attention was paid to the response time of a PS LED. The transient electroluminescence waveform with the minimized response time is shown in

Fig.5. The delay time of 1.2 ns and the rise time of 1.5 ns can be evaluated from the curve presented in Fig.5 for the voltage pulses of 12 V.

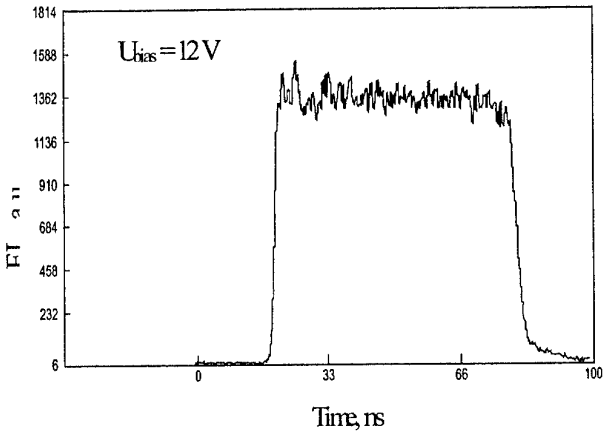

Fig.5. The rise and delay times for a PS LED.

The shortest response time was published for forward biased PS LEDs [20]. However, our devices are faster, because they have no diffusion capacitance. The main mechanism of minor carrier generation in reverse biased Al/ PS junctions is impact ionization at avalanche breakdown at high electric field. A regular columnar PS structure promotes the very fast avalanche breakdown due to non-uniform electric field distribution inside the PS layer [7]. The time of the avalanche response is estimated to be as less as 1 ps [21]. Thus, we have shown that our PS LEDs can operate in the nanosecond region. By further technology optimization, we hope to reach the sub-nanosecond range.

All fabricated samples demonstrated good reproducibility and stability even at high current densities. Their main parameters are listed in Table 1.

Table 1. Typical parameters of Al/PS LEDs

Parameter	Units	Value
Maximal quantum efficiency*	%	1.0
Optical power density	W/cm^2	0.1
Visual detection threshold	V	-4
Response time	ns	1.2
Frequency response	GHz	0.2
Minimal pixel size	μm	1x1
Estimated life time	h	>10000

* pulse operation

As can be seen from the Table 1 the PS LEDs are quite fast, so direct multiplex addressing can be applied. The resolution of Al/PS microdisplays can be as high as million pixels per 1 cm^2 that can not be achieved at present by other microdisplay technologies. In this case the pulse operating current for a pixel is varied from 1 to 10 μA, that corresponds to operating currents of silicon VLSI components.

The main disadvantage of PS LEDs is related to their low efficiency. Taken into account the reported quantum efficiency of about 1% (or power efficiency of about 0.3%), the estimated thermal load for a 100 Cd/m^2 PS LED is 0.3 W/cm^2. It is obvious that in this case the heat should be removed to prevent overheating effects. However, if the brightness is limited at the level of 20 Cd/m^2, the heat dissipation will not result in catastrophic overheating effects and a device can operate in continuous regime for more than 1000 h without any considerable degradation [22, 23].

5. LCOS microdisplay

We have designed and fabricated microdisplays of reflective type using Liquid-Crystal-on- Silicon (LCOS) technology for near-to-the-eye devices. Among the main advantages of LCOS-microdisplays are the following: a) small size and weight, low power consumption; b) low cost under mass production; c) established technologies and infrastructure, low starting investments [24].

A 14x11 mm silicon chip containing the array of 320x240 pMOS-transistors integrated with row and column drivers was assembled with the upper 0.7 mm ITO-coated glass and polarizer providing the cell gap of 1-1.5 μm filled with nematic LC. The size of Al reflective planarized pixel electrodes was 21.0 x 20.4 μm. The standard 1.2-μm three metal 5 V CMOS fabrication process with 16 photolithography steps which exhibits the low spread of important parameters (MOS threshold voltage, sheet resistances, transistor gain etc.) between wafer to wafer, across a wafer or across a chip was used. The proper selection of planarization technique as well as of LC-material and electro-optical mode have a tremendous impact on the LCOS microdisplay performance such as contrast, brightness, consumption, response time, driving voltage.

Untwisted- or twisted-nematic modes optimized for desired application were used. In untwisted modes, the LC forms a uniform birefringent layer. The optical performance is characterized by the retardation associated with the LC layer and by the angle ψ between the polarization axis of the input light and the axis of the extraordinary refractive index. For maximum efficiency of the birefringent layer, ψ should be 45°. NW modes typically operate

between $d\Delta n/\lambda$ =0.25 and 0, while NB modes operate between either $d\ \Delta n/\lambda$ =0.5 and 0.25 (ECB or HAN) or between $d\ \Delta n/\lambda$ =0 and 0.25 (VA). For twisted-nematic modes the alignment is easy and the manufacturing process is similar to traditional direct-view TN and STN displays. A good choice for NW applications could be self-compensated TN mode, while the reflective TN mode is well suited to NB applications. For all fabricated and tested LCOS microdisplays the contrast more than 100:1 and 16 gray levels provided by pulse width modulation technique were measured.

6. Conclusions

The analysis of reverse biased PS LED developments for the last ten years has shown considerable parameter improvement towards practical implementtations of these devices in microdisplay technology. Bright and stable light emission was observed in Al / PS reverse biased Schottky junction. The time stability of light emission was quite high thanks to reliable passivation of porous silicon surface in the presented device construction.

Developed LCOS- and light emitting microdisplays are totally compatible with modern silicon IC technology. Thus, LCOS and Al/PS light emitting structures fabricated onto a silicon chip containing driving circuitry can solve many miniaturization problems for microdisplay technologies.

7. References

[1]. Allen K. A big-picture view of microdisplays, Seminar Lecture Notes, Boston, USA, May 2002, pp. M12/1-74.

[2]. King C. History of TFEL technology at Planar System, Proc. Int. Conf. on Science and Technology of Emissive Displays and Lighting, Ghent, Belgium, September 2002, pp. 5-10.

[3].Richter A., Steiner P., Kozlowski F. and Lang W. Current-induced light emission from a porous silicon device, IEEE Electron Device Letters, 1991, No 12, pp. 691-693.

[4].Kozlowski F., Sauter M., Steiner P., Richter A., Sandmaier H., Lang W. Electroluminescent performance of porous silicon, Thin Solid Films, 1992, V. 222, pp. 196-199.

[5]. Kozlowski F., Steiner P., Lang W., Current-induced light emission from nanocrystalline silicon structures, Proc. NATO ARW Series E: Applied Sciences, 1993, V. 244, pp. 123-133.

[6]. Lazarouk S., Jaguiro P., Katsouba S., Masini, La Monica S., Maiello G., Ferrari A. Stable electroluminescence from reversed biased n - type porous silicon - aluminum Schottky junction device, Appl.Phys. Lett., 1996, V.68, pp. 2108-2110.

[7]. Bertoloti M., Lazarouk S., Ferrari A. et al. Porous silicon obtained by anodization in the transition regime, Thin Solid Films, 1995, V.255, pp. 152-154.

[8]. La Monica S., Lazarouk S. et al. Progress in the field of integrated optoelectronics based on porous silicon,Thin Solid Films, 1997, V. 297, pp. 261-264.

[9].Kuznetsov V., Andrienko I., Haneman D. High efficiency blue-green electroluminescence and scanning tunneling microscopy studies of porous silicon, Appl.Phys.Lett., 1998, V.72, pp. 3323-3325.

[10]. Gelloz B., Koshida N. Electroluminescence with high and stable quantum efficiency and low thre shold voltage from anodically oxidized thin porous silicon diode, J.Appl.Phys., 2000, V.88, pp. 4319-4322.

[11]. Lazarouk S., Smirnov A. Electroluminescent microdisplays based on Al / PS Schottky junctions. SPIE.- 2001.- June, V. 4511, pp. 68-71.

[12]. Lazarouk S., Bondarenko V., La Monica S et al., Electroluminescence from Al/PS reverse biased Schottky diodes formed on the base of highly doped n-type polisilicon. Thin Solid Films, 1996, V. 276, pp. 296-299.

[13]. Sercel P., Kwon D. et al., Visible electroluminescence from porous silicon/hydrogenated amorphous silicon pn - heterojunction devices, Appl. Phys. Lett., 1996, V.68, pp. 684-686.

[14]. Lazarouk S. Light emitting devices based on Al / PS Schottky junctions on sapphire substrates for display applications, Proc. 7 ADT Symp., 1998, pp. 293-196.

[15]. La Monica S., Lazarouk S. et al., Characterization of porous silicon light emitting diodes in high current density conditions, Solid State Phenomena, 1997, V. 54, pp. 21-26.

[16]. Lazarouk S., Smirnov A., Labunov V. Fabrication of a full inorganic EL microdisplay integrated with addressing circuitry onto a Si - chip, Proc. Int. Conf. IDMC - 2003, Taipei, Taiwan, February 2003, pp. P3-08 - P3-11.

[17]. Jaguiro P., Lazarouk S., Pavesi L., Smirnov A. Electroluminescence in porous silicon films of reverse biased Schottky junctions, Proc.ADT-2001, Minsk, Belarus, September 2001, pp. 112-115.

[18]. Lazarouk S., Jaguiro P. et. al. Porous silicon light emitting diode and photodetector integrated with a multilayer alumina waveguide. Physics, Chemistry and Application of nanostructures, World Scientific, Singapore, 1999, pp. 370-373.

[19]. Lazarouk S., Leshok A., Borisenko V.On the route towards Si-based optical interconnects, Microelectronic Eng., 2000, V.50, pp. 81-86.

[20]. Cox T.I., Simmons A.J. et. al., Modulation speed of an efficient porous silicon light emitting device, J. Appl.Phys., 1999, V.86, pp. 2764-2773.

[21]. Sze S. Semiconductor Devices: Physics and Technology, Bell Lab., A Wiley-Interscience publication, N.-Y., 1985.
[22]. Lazarouk S., Smirnov A., Labunov V. et al. Inorganic EL microdisplay based on Al / porous silicon light emitting Schottky junctions, Eurodisplay - 2002 Proc., Nice, France, October 2002, pp. 683-684.
[23]. Lazarouk S., Smirnov A., Labunov V. et al. Electroluminescent porous silicon microdisplay, EL-2002 Conference Proc., Ghent, Belgium, September 2002, pp. 391- 394.
[24]. A.Smirnov et al., Microdisplays: present status and future.- Electronic components, 2001, part 1.- No 2, pp. 6-14, part 2.- No 3, pp. 2-6 (in Russian).

NED-3. **Cholesteric reflective LCDs characterization.**

Victor Sorokin

Institute of Semiconductor Physics of NASU, Ukraine

Paper is not available

NED-4. Ferroelectric Liquid Crystal Devices: Basic Physics and Prospects of Applications

E. P. Pozhidaev

P. N. Lebedev Physical Institute of RAS, Leninsky pr. 53, Moscow 119991 Russia

The contribution will provide a brief review of basic properties of ferroelectric liquid crystals (FLC's), including their main electrooptical effects as a background for specific display devices. The most important topics of this item are:

- bistability and multiplex operation, origin of the physical gray scale generation for passively addressed SSFLC and DHF display cells,
- binary electrooptical response of τ-V_{min} mode displays,
- V-shape mode as a background of continuous gray scale of TFT FLC displays,
- actively addressed SSFLC and DHF micro displays with the LED matrix as the most promising kind of FLC display devices,
- non-display applications of FLC cells,
- analyses of already developed FLC displays, or why industrial manufacturing of FLC displays still doesn't exists?

Managing of display cells parameters both with a chemical structure of FLC's and boundary conditions will be analyzed also mainly as author's original approach. Problems of FLC display cells optimization are under discussion here, taking into account how to combine the basic parameters of FLC's and FLC cells:

- low temperature eutectic of a broad temperature range multicomponent FLC mixtures and their smallest electrooptical response time,
- high alignment quality and stability of operation in gray scale modes,
- relationship of FLC's bulk properties and the surface anchoring for optimization of electrooptical modes.

The main ideas for providing of high alignment quality of FLC display cells as well as the alignment steadiness will be considered in terms of:

- relationship between surface free emerges of aligning surfaces and FLC's,
- if there are principal advantages in photo-alignment of FLC's in comparison with traditional rubbed polyimides?
- chevron-free structures of smectic layers as a necessary condition of the long time alignment steadiness,
- mechanical stability of liquid crystal layers and the shock problem occurrence.

Specific features of the FLC displays image quality in comparison with the NLC displays one will be discussed also.

NED-5. **Polymer-dispersed liquid crystals for information displays**

S. J. Kłosowicz

Institute of Applied Physics, Military University of Technology, Kaliskiego 2, 00-908 Warsaw, Poland, e-mail sklosowicz@wat.edu.pl

The purposefulness of application of polymer-dispersed liquid crystals (PDLC) in information displays is presented. The special attention is paid to devices working in external light, e.g. outdoor systems. At first a short information regarding essential optical and electrooptical properties of PDLC is given. Then a brief information regarding methods of preparation of such systems and optimization of their morphology is presented. The advantages and disadvantages of PDLC based displays are discussed. In fact, each group of liquid crystals embedded in polymer binder, including ferro- and antiferroelectric smectics, can be adopted for information systems. However, the main attention is devoted to nematic and chiral nematic materials because unique properties of PDLC systems are the most pronounced for those materials.

NED-6. **Liquid crystal composite films: perspectives in new AM TFT displays.**

M.D.Efremov[1], I.G.Neizvestnii[1], G.M.Zharkova[2], V.Ya.Zyryanov[3], V.F.Shabanov[4], V.A.Volodin[1], A.V.Vishnyakov[1], V.N.Ulasyuk[5].

1- Institute of Semiconductor Physics SB RAS, Novosibirsk, Russia; 2- Institute of Theoretical and Applied Mechanics SB RAS, Novosibirsk, Russia; 3- Institute of Physics SB RAS, Krasnoyarsk, Russia; 4- SKTB «Nauka» SB RAS, Krasnoyarsk, Russia; 5- ELTAN Ltd, Fryazino, Russia.

The using of polymer films with liquid crystal capsules can greatly simplify the technology of LCD producing [1]. However, the main disadvantage of this approach is need of high electric voltage to rule the transmittance of a cell with appropriate contrast. The discussion of compatibility of such films with AM TFT technology is the main topic of present paper. The polymer films with liquid crystal capsules of various composition and structure were studied. It was shown, that the voltage drive could be decrease down to 20-30 V. The modeling of I-V characteristics of TFT of various types was carried out. The original approach for crystallization of amorphous films on not refractory substrates with low thermal budget was developed [2]. The polysilicon films on glass and polyimide substrate for AM TFT producing were obtained with the use of excimer laser treatments. The structural and electro-physical properties of the poly-Si films were studied. Testing poly-Si AM TFTs were produced and studied. The dynamical characteristics of the studied polymer films with liquid crystal capsules (turnon time 1 ms, turnoff time 5-7 ms) allow us to hope that this approach is applicable for AM TFT LCDs.

1. G.M.Zharkova, A.S.Sonin. Liqiud crystal composites. Novosibirsk: Nauka (in Russian), 1994. - 214 p.
2. M.D.Efremov, V.V.Bolotov, V.A.Volodin, L.I.Fedina, E.A.Lipatnikov. J.Phys.: Condens. Matter, **8**, 273 (1996).

NED-7. **Bistable LCDs with improved performance characteristics.**

M.G. Tomilin

Vavilov State Optical Institute, Russia

Several types of bistable LCDs with good performance characteristics and minima in the energy control have been developed by different groups in recent years.The characteristics of bistable LCDs utilizing nematic, cholesteric and ferroelectric liquid crystals are compared.

NED-8. Liquid Crystal Composites with Spatially Periodic Structure

G.M. Zharkova, I.V. Samsonova, S.A. Streltsov, V.M. Khachaturyan, A.P. Petrov
Institute of Theoretical and Applied Mechanics, SB RAS,
4/1, Institutskaya Str., Novosibirsk 630090, Russia

Using spatially non-uniform photo polymerization of starting mixtures and their phase separation into nematic liquid crystal and polymer, composites with spatially periodic structure have been obtained. The composites displayed the property of volume refractive-index modulation. Such composites are attractive for application as phase hologram-recording media with external electric field controlled diffraction efficiency.

Key words: optical grating, Bragg diffraction, holographically formed polymer-dispersed liquid crystals

Introduction

Presently, composite materials with liquid crystals (LCs) embedded into a photopolymer matrix have attracted considerable attention as media with holographically defined structure quite competitive in their properties with photopolymer materials based on other (than LCs) substances. Nowadays, owing to considerable birefringence of LCs and due to the possibility of controlling it with the help of an external electric field, phase gratings based on LC-based composites are generally regarded as optical media offering much promise in applications where diffraction efficiency of optical devices represents a critical parameter [1].

Various fabrication methods for such composites are known. One of such methods in the holographic one, in which composites with predefined spatially periodic structure are formed by exposing the initial material to interfering laser beams [1, 2].

The composites of interest exhibit good photosensitivity, high diffraction efficiency, light-scattering noise figure, and suitable electrooptical properties, determined, in large part, by the structure of the composite and by the characteristic sizes of light-scattering regions in it. These regions, enriched with the LC, are formed due to free-radical polymerization and phase separation processes. The characteristic dimensions of these regions depend on curing conditions (exposure dose and duration) and on the composition of the starting LC-pre-polymer mixture. In the present work, we studied properties of diffraction gratings formed on composites prepared from commercially available components. The present study was aimed at the structure and the optical properties investigations of the holographically formed material.

Experimental

Starting materials. The starting pre-polymer mixture comprised a nematic liquid crystal (NLC), an acrylate monomer (pre-polymer), and a photoinitiating system that included a dye component with maximum photosensitivity in the visible portion of the spectrum, and a co-initiator. The NLC was a cyanobiphenyl-oxyalcylcyanobiphenyl eutectic mixture. The monomer was pentaerythritol tetraacrylate (Aldrich). 1-vinyl- 2-pyrrolidinone (Aldrich) was used both as binding agent and a solvent for the dye and the co-initiator. Mixtures with a photoinitiating system were examined in which, as a dye and a co-initiator, respectively the methylene blue and triethanolamine were used. The NLC concentration in the initial pre-polymer mixture was 37 wt. %, and the dye concentration ranged from 0.1 to 0.4 wt. %. The components in the starting mixture possessed high room-temperature solubility. Such a multi-component system, due to the dye used, showed a maximal photosensitivity in the spectral region from 650 to 680 nm.

Gratings: fabrication procedure and characterization. The photopolymer mixture was prepared in the form of a homogeneous solution; this solution was subsequently pored onto the surface of a glass substrate covered with a thin layer of transparent conducting coating (ITO), and it was then capped with another such substrate. In this manner, an experimental cell was prepared, which consisted of a pair of ITO-coated surfaces with an LC-pre-polymer layer in between. The thickness of the cell, defined by lavsan layers, was 10 to 50 μm.

The laser curing treatment was performed through exposing the cell to laser radiation with periodically distributed light intensity at a wavelength to which the mixture was photosensitive. The optical system used to cure the samples is shown in Fig.1. The light source (1) was an ML120G laser diode (nominal power up to 30 mW) emitting light at a wavelength of 658 nm. The diode-emitted radiation, collected by collimator (2), was subsequently divided into two beams, A and B, by Fresnel mirrors (5). The angle between the mirrors was 270^0. Each beam passed one of two identical diaphragms (3) and, reflected from deflecting mirrors (4), entered the cell (6) with the pre-polymer mixture. The interference of the two coherent beams produces an amplitude grating formed on the glass surface of the substrate. The grating spacing was predefined by the wavelength of the incident light and by the convergence angle α of beams A and B. The convergence angle α could be varied by titling the mirrors (4) or by displacing the cell (6) into the intersection zone of the light beams. In the present experiments, the convergence angle of the beams ranged from 18° to 30°. To improve the contrast of the interference pattern, we took measures aimed at equalization of the intensities of the two beams. The

incident intensity was measured by means of IMO-2 power meter (7). In our experiments, the total power in beams A and B amounted to 45 mW/cm^2.

After the curing procedure, irrespective of the initial composition of the mixture, all cells we given the finish treatment (exposure to the light emitted by a «Photon» daylight lamp (44.5 mW/cm^2 illumination intensity at an exposure time of 40 seconds)) in order to accomplish the polymerization process.

To measure the angular dependences of light transmission (such dependences characterize the light scattering intensity in the cells), we used the procedure described in [3]. All measurements we performed for the case of normal incidence of He-Ne laser emission (λ=632.8 nm) onto the cell, without an analyzer in the light-detecting system (mean intensity); the measured signals were normalized by the incident intensity (I_0). From the measured dependences, we could estimate the grating spacing, the diffraction efficiency η_1 (the ratio between the first-order diffraction intensity and the incident intensity), and the refractive-index modulation amplitude Δn.

To measure the electrooptical characteristics of cells with recorded gratings, we used the standard LC–polymer composite cell characterization procedure [4,5].

Since the typical structural dimensions in formed materials fell into the submicrometer region, the morphology of these materials were studied by means of Scanning Electron Microscopy (SEM). Prior to performing the SEM investigations, the samples were soaked in hexane to remove the liquid crystal, then baked for several hours at 80°, and finally coated with 150 nm of gold.

Results and Discussion

Morphology and Diffraction Properties. For materials dealt with in the present study, the dimensions and shape of the NLC domains depend on the pore size of the photopolymer matrix. In turn, the dimensions and shape of matrix pores depend on initial composition of the starting mixture and on curing conditions (i.e., on parameters of the photopolymerization and phase separation processes). As is seen from the SEM micrograph of Fig.2, the grating spacing of the formed structure is about 1 μm, which value lies close to the one, 0.9 μm, estimated from the Bragg formula (with half of the angle between the interfering beams taken to equal 14°). Note that the obtained estimate of the grating spacing agrees well with the experimentally determined first-order diffraction angle - 28° (see Fig.3, curve 1). From SEM micrographs, it was also possible to estimate the pore sizes that determined the characteristic dimensions of NLC domains (0.2 to 0.5 μm). The estimated size of 0.5 μm corresponds to half the grating spacing (1 μm), probably, due to coalescence of NLC domains, which therefore can be considered as connected domains rather than isolated droplets. The mean pore sizes in the matrix were almost independent of the dye content (0.1-0.4 %) of the initial mixture for exposure durations longer than 20 seconds, which were sufficient for forming gratings with the maximum diffraction efficiency. Next, it should be noted that the fact that gratings with almost identical pore sizes in the polymer matrix were formed with exposure durations of 20-30 seconds and longer from initial mixtures with widely ranging dye contents cured with widely differing illumination intensities (6 - 45 mW/cm^2) is confirmed by close scattering-induced noise figures of all gratings obtained (see Fig.3, curves 1 and 2). However, gratings obtained in this study show rather high noise figures compared to those displayed by alternative (without LCs) photopolymer composites [3]. As is seen from Fig.4, the exposure duration of 20-30 seconds seems to represent an optimum (for the intensity 45 mW/cm^2) for forming gratings with the maximum diffraction efficiency η_1 at a fixed grating spacing and for those starting dye concentrations that were used in this study.

The performed experiments proved the very fact that volume phase gratings were formed. For these gratings, the refractive-index modulation amplitude Δn was estimated for the case of harmonically profiled volume transmission-type phase holograms [6]: $\eta_1=\sin^2(\nu)$, where η_1 is the first-order diffraction efficiency, $\nu=(\pi\cdot\Delta n\cdot d)/(\lambda\ \cos\Theta)$, d is the grating-cell thickness, λ is the reading wavelength (λ=632.8 nm), and Θ is the diffraction angle. For 10-μm thick gratings with η_1=0.24-0.3, we obtain $\Delta n\sim0.009\pm0.001$, and for 50-μm gratings with η_1=0.68, $\Delta n\sim0.0077$. Indeed, it is seen from Fig.5 that the maximum diffraction efficiency η_1 increases (at close values of Δn) with increasing cell thickness.

The obtained data agree well with previously reported data [7-9]. The diffraction efficiency of typical PDLC-gratings is rather high (25% and higher); unfortunately, because of spatial non-uniformity of the NLC rich regions, such gratings display high reading intensity losses for diffuse scattering.

Thus, the mean size of NLC domains for the composites under study represents a structural parameter that determines the grating period and scattering-induced noise figure. The scattering-induced noise can be reduced by decreasing characteristic pore sizes in the photopolymer matrix (and, hence, LC domains) down to values much smaller than the reading wavelength.

Electric Field Switching. As it was initially anticipated and subsequently confirmed by SEM studies, the gratings formed in the acrylate system of interest consist of alternating polymer-rich and NLC-rich regions. For this reason, such gratings can be expected to display electric field induced modulation of their diffraction efficiency. Preliminary results showed that the diffraction efficiency of such gratings indeed could be switched by applying an external electric field to samples. For example, on switching the applied voltage from 0 to 170 V (see Fig.6), our cell displayed a change in its maximum diffraction efficiency from 23 % to 7 %. This change was accompanied by equal but opposite change of the zero-order transmittance, clearly indicating that the refractive-

index modulation was indeed modified by the field. A high intensity of the electric field (~16 V/μm) required for switching the cells shows that the interaction between the NLC and the polymer is rather strong. This confirms that the NLC domains are small. On the other hand, typical response times of the gratings obtained in this study are 150 to 200 μsec, in line with previously reported data [10, 11]. Unlike typical relaxation times reported previously for PDLC-gratings, the relaxation times for the gratings under study are longer, amounting to 4 msec. This difference can be attributed to different structures of NLC domains formed in the matrix volume. In the present work, we used a cross-linkable monomer permitting obtaining matrices with different degree of the LC domain connectivity. According to the authors of [12], the connectivity of the LC cavity network may have a profound impact on switching times. In view of these, typical LC domains with sizes of 0.2 μm or greater in our gratings can be considered as an ensemble of connected domains, whose relaxation times are comparable with typical relaxation times of ordinary PDLC materials in which LC domains (or droplets) have micrometer-range sizes.

Conclusions

Spatially non-uniform photo polymerization and phase separation processes were used to obtain spatially periodic composite materials showing clear volume refractive-index modulation (up to $\Delta n \sim 0.01$). The material under study is characterized by photosensitivity equal 35 mJ/sm^2. The obtained data on the texture and scattering properties of gratings formed on these materials provides estimates of typical sizes of NLC domains formed by treating initial mixtures with He-Ne-laser energy of 230 to 2700 mJ/cm^2 (0.2 - 0.5 μm). The diffraction efficiency of such gratings may be as high as 32 % (for 10-μm cell thickness) or 70 % (for 50-μm cell thickness) and may be switched by applying an external electric field to the cell (16 V/μm) with the response time 150-200 μsec, and relaxation time 4 msec. The typical size of NLC domains in composites of this type represents a structural parameter that determines the grating spacing. For the system dealt with in the present study, the spatial-frequency limit is about 1100 mm^{-1}. In addition, the LC domain size determines the light-scattering properties of the composites. The latter circumstance is of utmost significance since it is light-scattering properties that determine the limit on storage density in media used for optical recording.

This work was supported by the Russian Foundation for Basic Research, grant N 02-03-33345, by the SB RAS Integration project N 18, and by the SB RAS young researcher project N 14.

References

[1] Paul S. Drzaic. Liquid Crystal Dispersions. World Scientific. 1995. 429p.

[2] R.L. Sutherland, L.V. Natarajan, V.P. Tondiglia, T.J. Bunning. Chem. Mater. Vol.5. P.1533-1538. 1993.

[3] T.N. Gerasimova, G.M. Zharkova, E.F. Pen, S.A. Streltsov, V.V. Shelkovnikov. Optical Journal. Vol. 69. P.49-52. 2002.

[4] G.M. Zharkova, S.A. Streltsov, V.M. Khachaturyan. Light Transmission by Polymer-Dispersed Liquid Crystals. Journal of Structural Chemistry. Vol. 34. N6. P.934-937.

[5] G.M. Zharkova, I.V. Samsonova, S.A. Streltsov, V.M. Khachaturyan. Effect of Polymer Concentration on the Structure of Cholesteric Liquid Crystal Composites and their Scattering Properties. Mol.Cryst.Liq.Cryst. Vol.331. P.533-540. 1999.

[6] R.J. Collier, Ch.B Burckhardt, L.H. Lin. Optical Holography. Academic Press. New York and London. 1971. 688p.

[7] F. Simoni, S. Di Bella, L. Lucchetti, G. Cipparrone, A. Mazzulla. Polymer Dispersed Liquid Crystals as Optical Storage Materials. Mat. Res. Soc. Sym. Proc. Vol.559. P.65-74. 1999.

[8] T. Yamamoto, S.Yoneyama, M. Hasegawa, A. Kanazawa, T. Shiono, T. Ikeda. Holographic Grating Formed by Photochemical Phase Transition of Polymer Azobenzene Liquid Crystal. Mat. Res. Soc. Sym. Proc. Vol.559. P.153-158. 1999.

[9] R. Caputo, A.V. Sukhov, C. Umeton, R. Ph. Uchakov. JETP. Vol.118. N6(12). P.1374-1383. 2000.

[10] L.V. Natarajan, R.L. Sutherland, V.P. Tondiglia, S. Siwecki, R. Pogue, et all. Electrically switchable reflection gratings in polymer dispersed liquid crystals. Mat. Res. Soc. Sym. Proc. Vol.559. P.109-116. 1999.

[11] V.P. Tondiglia, L.V. Natarajan, and R.L. Sutherland. Volume holographic image storage and electro-optical readout in a polymer-dispersed liquid-crystal film. Optics Letters. Vol.20. P.1325-1327. 1995.

[12] P Mach, P. Wiltzius, M. Magens, D.A. Weitz, Keng-hui Lin, T.C. Lubensky, and A.G. Yodh. Electro-optic response and switchable Bragg diffraction for liquid crystals in colloid-templated materials. Phys. Review E. Vol.65. 031720-3. 2002.

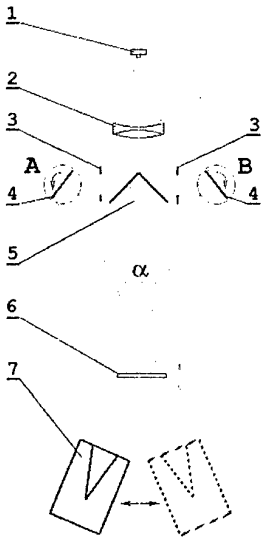

Fig.1. Holographic recording experimental setup.

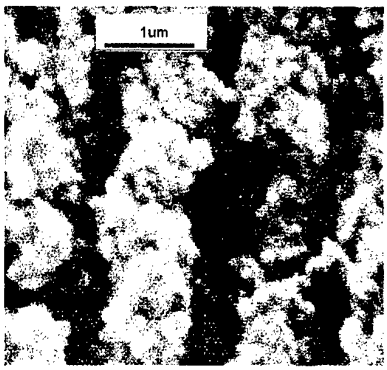

Fig.2. SEM micrograph of the surface of a transmission grating obtained in this work. In the photo, bright polymer-rich regions are clearly seen.

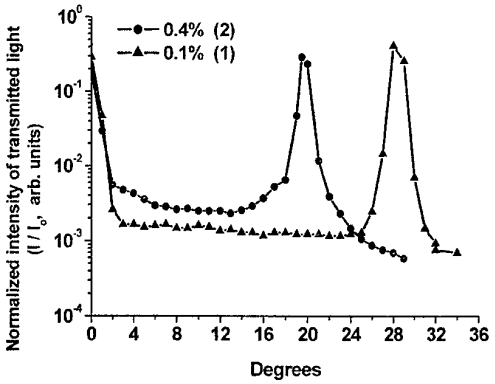

Fig.3. The angular dependences of light transmission. Reading wavelength is 632.8 nm. (1) – This gratin was written at the 658 nm an intensity of 45 mW/sm^2, with a 30-s exposure. The NLC loading was 37 % by weight and 0.1 % of dye. (2) – the intensity is 6.6 mW/ sm^2, and exposure time is 60 s. The NLC loading was 37 % by weight and 0.4 % of dye. The cell thickness is 10 μm.

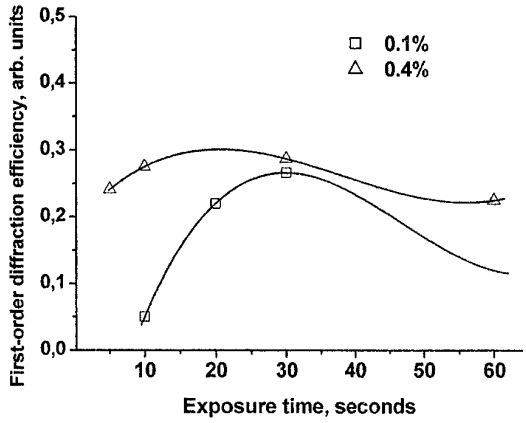

Fig.4. Diffraction efficiency as a function of exposure time. The recording conditions are the same as for (1) from Fig.3. The concentrations of the dye in initial compositions and exposure time are indicated on the picture.

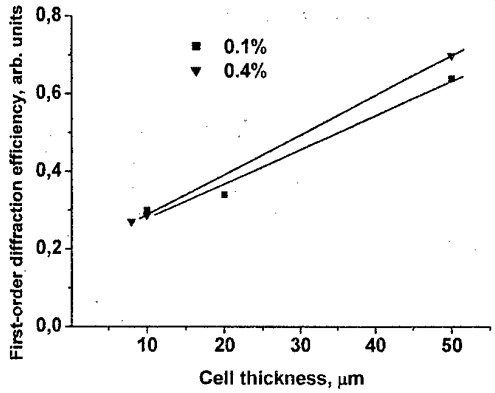

Fig.5. Diffraction efficiency as a function of cell thickness. The recording conditions are the same as for (1) from Fig.3. The concentrations of the dye in initial compositions are indicated on the picture.

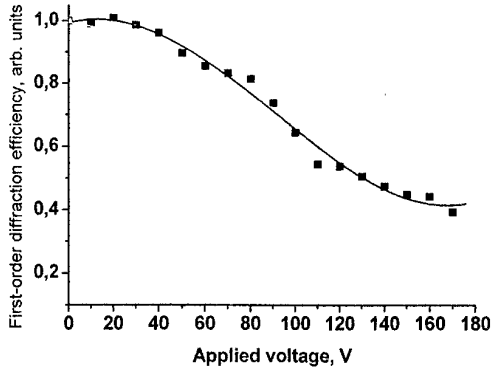

Fig.6. Diffraction efficiency as a function of switching voltage (field frequency is 125Hz). The diffraction efficiency $\eta_1(U)$ is normalized on that at zero electric field applied $\eta_1(0V)$=0.23. The same grating as in the case (2) from Fig.3.

NED-9. THE METHOD OF MANUFACTURE OF LC-CELLS WITH SEVERAL AREAS OF HOMOGENEOUS NEMATIC

A. Morozov, G. Nevskaya, A. Shevchenko

Novosibirsk State Technical University, K. Marx prosp. 20, Novosibirsk, 630092, Russia, e-mail: kof@ref.nstu.ru

Abstract.

The new method permitting to form on one surface of substrates of area with planar and gomeotropic orientation of molecules of LC is developed. These areas have clear boundary and are divided by disclination line. This method will allow to expand a sphere of application of liquid crystals, and also to improve the characteristics of different devices using LC.

Keywords: liquid crystal, orientation of molecules of LC

Introduction.

For generation image in display it is necessary to create clear boundary between areas with different orientation of molecules of LC. The operation of orientation and position of this boundary is realized with the help of an electrical field, which is formed by electrodes of different forms. Thus difficult image requires the complicated configuration of electrodes. This fact is essential limitation at development of optical devices and display on LC.

Recently methods permitting to create areas with different homogeneous orientation of molecules with the help of photopolymers have appeared [1]. The orientation of molecules of LC on surface of photopolymer depends on direction of polarization of ultra-violet radiation dropping on photopolymer. However, this method allows to receive on surface of substrate of area only with planar orientation.

We suppose the new method permitting to form on one surface of substrates of area with planar and gomeotropic orientation of molecules of LC. This method will allow to expand a sphere of application of liquid crystals, and also to improve the characteristics of different devices, using LC.

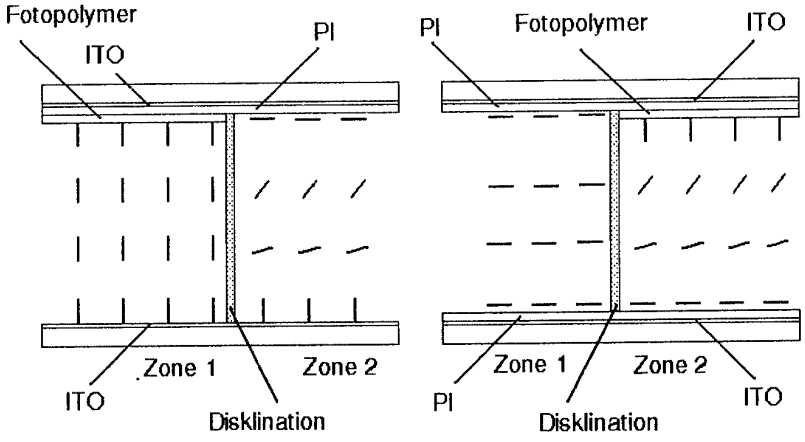

Fig. 1

Experiment.

It is created LC-cells, in which some areas gomogeneous nematic are realized. The structure of cells is shown on fig. 1. At manufacturing of a cell (fig. 1a) were used:

– Glass substrate with a layer ITO, on which the molecules of LC is oriented gomeotropically.

– Glass substrate with a layer ITO, covered by rubbing polyimide film. On this substrate molecules of LC is oriented planar.

– Photopolymer, which is put on polyimide film, and with the help of method photolitographic forms the image. On surface of photopolymer molecules of LC must be oriented gomeotropically. The photopolymer must be transparent and have energy of coupling with molecules of LC close to energy of coupling of LC with ITO. The rubbing of photopolymer with the help of caprone sweeper must not to add energy of coupling strongly.

– NLC positive dielectric anisotropy (5CB, LC-1289) with the component of licetin. The concentration of licetin was selected depending on LC, selected photopolymer and technology of manufacturing of a cell. As experiments have shown, the quality of orientation of molecules of LC strongly depends on concentration of licetin and selected technology of manufacturing of LC of a cell..

The selected materials have allowed to create in a zone 1 (fig. 1a) area gomeotropic orientation, and in a zone 2 - area hybrid orientation. It results to appearance disclination line on boundary of areas. Its width equal no more than 5-10 microns. In fig. 2 the photos of a cell (fig. 1a) are shown different controlling voltages.

The cell in the crossed polarizers is shown in fig. 2a. The controlling voltage is absent. The black area corresponds gomeotropic orientation, and colour corresponds hybrid orientation.

At giving of controlling sinusoidal voltage(frequency 3 kHz, amplitude-more 2V) reorientation of molecules is possible only in a zone 2 (Fig. 26). Width disclination) is decreased with increase of controlling voltage. The process of reorientation in a zone 2 does not differ from process of reorientation gomogeneous hybrid of a cell.

On fig. 1b the device of LC of a cell containing in zone 1 area with planar orientation, and in a zone 2 - area with hybrid by orientation is figured. At giving on a cell of controlling voltage the reorientation of LC is possible in both zones. Where the volts - phase characteristics will was essentially differ from each other.

Advantages of suggested method are:

– The method allows to create between controlling electrodes of area of LC, having different volts - phase characteristics. The possibility of forming of picture by a standard way is not excluded in suggested methodics.

– The areas with clear boundary are formed. With increase of controlling voltage the stability of boundaries only is going up.

– The method allows to use disclination line for protection against appearance of defects in inhomogeneous electrical fields.

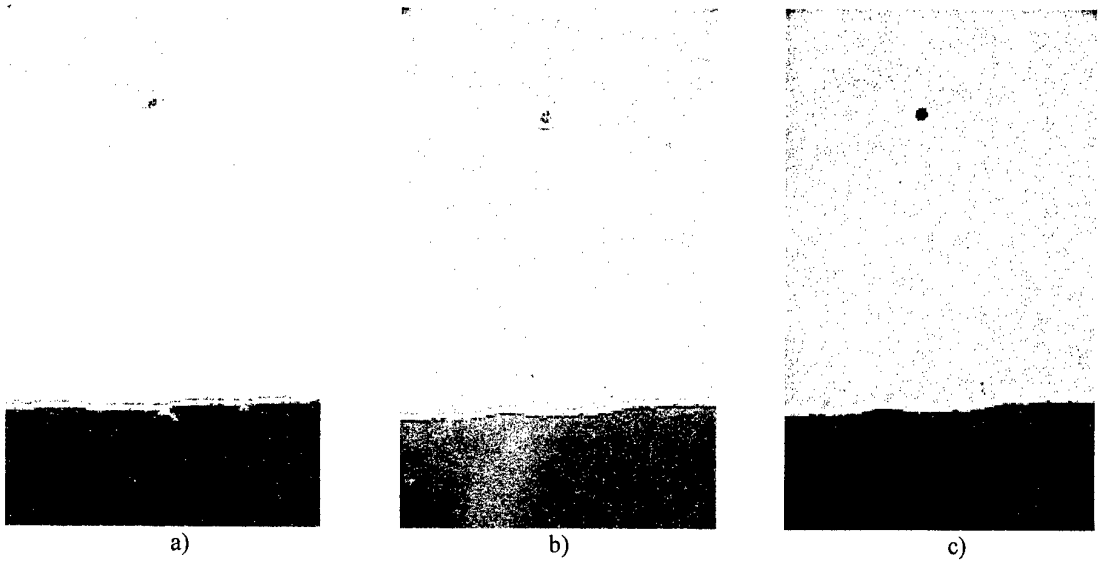

a) b) c)

Fig. 2

In a LC-cells it is possible to receive boundaries between the following pairs of gomogeneous areas of nematic: planer-gomeotropic, hybrid-hybrid, twist-gomeotropic (with using of operation of an superinposition) and gomeotropic-hybrid, planer-hybrid, hybrid-twist (without using of operation of an superinposition).

Application of method

Indicators. It is supposed to form the complicated image on address electrode through different areas of orientation of molecules of nematic. Thus producing of complicated configuration of electrodes (without necessary picture) is excluded.

Disclination structures, which represent as dispersions can be put on the image. It will allow to increase an angle of observation.

It is supposed to surround everyone pixel of a LC-matrix in disclination ring. It will reduce probability of appearance disclinations in a matrix and will increase an angle of observation (everyone pixel will be a microlens).

Controlled Fresnel phase plates. Using the suggested method, it is possible to create complicated figure of Fresnel zones without using of a complicated configuration of electrodes. Thus to the distortion of boundaries between zones is excluded .

It is supposed to create the proof-readers of phase front, controlled lenses of the large diameter adaptive elements of diffractional optics.

Microlenses. It is supposed to surround a microlens in disclination ring. It will reduce defects in microlenses and area of reorientation LC out of microlenses. So it is possible to exclude mutual influence of microlens in an array. It will allow to reduce limiting distance between microlens in an array.

References

[1] K. Shia, T. Kosa, P. Palffy-Muhoray, Y. S. Kim, Mol. Cryst. Liq. Cryst., 1997, Vol. 299, pp. 73-77

NED-10. **LCD applications of Thin Crystal Film Polarizers**

G. King, P. Lazarev, A. Manko, V. Nazarov, S. Remizov

Victor.Nazarov@optiva.ru, Sergey.Remizov@optiva.ru

OPTIVA, Inc., 377 Oyster Point Blvd. # 13, South San Francisco, CA 94080, USA

Optiva Inc. has developed new self-assembling nanomaterials and a manufacturing process of their Cascade Crystallization into Thin Crystal Film (TCF) exhibiting a high optical anisotropy and birefringence. This paper presents a wide range of liquid crystal display (LCD) applications and opportunities of TCF polarizers.

First, having fewer functional layers, TCF-on- plastic film product serves as a cheaper alternative to conventional iodine and dyestuff polarizers. Second, TCF sub-micron layer may be coated directly on top of SiO2 insulating film; this internal positioning of polarizers completely protects them from the harsh environmental effects. Third, Optiva polarizing film can be printed on glass and then covered by other functional layers (barrier, ITO, SiO2, PI). In this advanced layout, polarizer bears only optical function, while not affecting the LC driving.

A wide spectrum of passive TN and STN LCD designs is feasible with new thin film polarizers, including mobile and desk phones, welding masks, automotive devices, watches and calculators.

Transparent birefringent TCF can be used for manufacturing of other LCD optical components such as retarders and color correction films.

NED-11. **Advances in viscoelastic displays.**

Yu.P. Guscho

Moscow State University of Radioengineering and Electronics,
Russia

Paper is not available

NED- P1. Inversion of Spontaneous Polarization Sign in Smectic-C* Phase for Some Chiral 2,6-*bis*-Arylidene-3*R*-methyl-cyclohexanones

A.I. Krivoshey, L.A. Kutulya, N.S. Pivnenko, V.V. Vashchenko, G.G. Rode*, A.S. Tolochko*, V.I. Kulishov*

Institute for Single Crystals of National Academy of Sciences of Ukraine
60 Lenin Ave, Kharkov 61001, Ukraine, E-mail: kutulya@isc.kharkov.com
*) Institute of Physics of National Academy of Sciences of Ukraine
41 prospect Nauki, Kiev 03028, Ukraine, E-mail: kulishov@iop.kiev.ua

Abstract: Mesomorphic behavior has been studied in detail for 2,6-*bis*-arylidene-3*R*-methylcyclohexanones with ester groups linking benzene rings of both arylidene fragments and containing long terminal substitutes ($OC_{16}H_{33}$ and $C_{16}H_{33}$, compounds **1a** and **1b**, respectively). Wide-range SmC* phase was determined for these compounds by using polarizing microscopy, differential scanning calorimetry, small angle X-ray scattering and electrooptic measurements. The reversible temperature inversion of spontaneous polarization was revealed for compound **1a**. Origins of this effect were shown to be connected with conformational changes in exocyclic ester containing arylidene fragments leading to the variations of mutual orientations of carbonyl dipoles and, as a result, in the total molecular dipole and its projections on molecular axes. By the molecular simulation using semi-empirical PM3 method, close energies were found for conformers possessing essentially different directions and magnitudes of their dipoles in the case of isolated molecules. However, these energy differences become more significant on formation of molecular ensembles. A change in population of molecular ensembles having various dipole characteristics in the mesophase is considered as a main origin of the observed P_S inversion.

Keywords: Liquid crystal ferroelectric, spontaneous polarization, temperature sign inversion, 2,6-bis-arylidene-3*R*-methylcyclohexanone, molecular modelling

Introduction

Recently [1, 2] some series of 2,6-*bis*-arylidene-3*R*-methylcyclohexanones exhibiting wide-range liquid-crystalline phases were synthesized. Those of them which contain OCO ester groups linking benzene rings in both arylidene fragments and also long terminal substitutes R ($OC_{16}H_{33}$ and $C_{16}H_{33}$) (compounds **1a,b**) form SmC* phase according to the optical polarizing microscopy and electrooptical experiments [2].

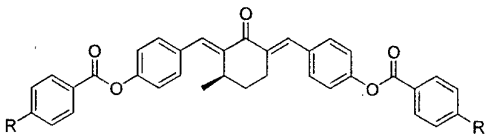

R = $OC_{16}H_{33}$ (**a**), $C_{16}H_{33}$ (**b**), H (**c**)

The reversible temperature inversion of the spontaneous polarisation (P_S) sign was revealed taken compound **1a** as an example [2]. Earlier, the similar effect was described in [3] for smectogenic-C* compounds **2** including, similarly to **1**, two ester groups.

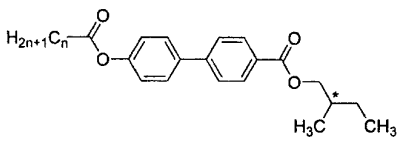

Suppositions about conformational origins of such an effect were made both in [2] and [3]. However, detailed investigations are necessary to establish the character of these conformational changes with the temperature.

For 1*R*,4*R*-2-arylidene-*p*-menthan-3-ones **3**, thermal *E–Z* isomerization has been proved unambiguously along with a relative photochemical process [4, 5] (Scheme 1) resulting in the photo-induced inversion of the P_S sign [6].

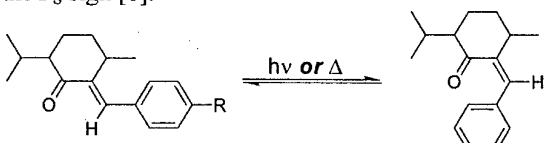

3*E* 3*Z*

Scheme 1

In this report, results of more detailed investigations of mesomorphic behavior for compound **1a** are presented using along with polarizing microscopy and electro-optical measurements also DSC and experiments on small angle X-ray scattering.

The reversible temperature inversion of the P_S sign revealed for **1a** is not connected with thermal *E–Z* isomerization as well as with a shift of the conformational equilibrium «*chair–twist*» for cyclohexanone ring, as it was shown for isolated molecules in [7]. Therefore we intend here to clarify opportunities of variations with temperature in populations of conformers forming as a result of internal rotation in exocyclic benzoate fragments. Such

conformers possess various magnitudes and orientations of the total molecular dipoles. Moreover, the energetics of potentially forming the mesophase molecular ensembles of the conformers of various types with strongly differing dipole moments is considered on the base of modelling results. The simulation of binary molecular ensembles as the simplest approximation accessible now was applied based on semi-empirical quantum-chemical method PM3. Modelling was carried out for **1c** as a model compound for smectogenic C* homologues **1a,b**.

Experimental

Synthesis of compounds **1a** – **1c** as well as microscopic, DSC and small angle X-ray scattering investigations were performed as described in [2].

The measurements of θ value temperature dependences were carried out by the extinction direction method. The rotation angles of the optic axis were evaluated by holding the sample between crossed polarizers and measuring the half-angle between the two extinction positions. The spontaneous polarization values were measured by the triangular wave method [8]. The LC compositions were placed in 5 μm "LINKAM" glass cells with transparent SnO_2 electrodes. The sign of P_S was determined by the field reversal method by optical observation of the director motion [9].

Semi-empirical quantum chemical method PM3 realised in MOPAC 6.0 software was used for molecular modelling.

Results and discussion

Compounds **1a,b** studied demonstrate typical for SmC* phase focal conic textures at the observation by polarising microscopy. Closely near to isotropic transition, marble textures of blue phases were seen for these compounds. The phase transitions from SmC* to blue phases are confirmed by DSC data (see Table 1).

Table 1. Mesomorphic characteristics of compounds **1**

	Cr		SmC*		BP		I
1a	•	107	•	180	•	185	•
1b	•	99	•	168	•	170	•

Compound **1a** give electrooptical response at almost overall mesomorphic range exhibiting the relatively low spontaneous polarization (the maximum $|Ps|$ value is 8 – 10 nC/cm^2). The smectic-C* tilt angle θ for this compound measured with electrooptical method is also small and remains almost invariable over the whole smectic mesomorphic range (the 2θ values are in the range of 9 ÷ 14 °) (see Fig. 1).

Experiments on small angle X-ray scattering (Fig. 2) show also an invariability of the layer spacing (42 Å) and, as consequence, of smectic-C* tilt angle θ over the whole temperature smectic range up to the transition to blue phase. The significant difference in the layer spacing for crystalline (30 Å) and smectic-C* (42 Å) phases according to data of the small-angle X-ray scattering is of essential interest. That can be connected with the different molecular organization in these phase and needs additional studying.

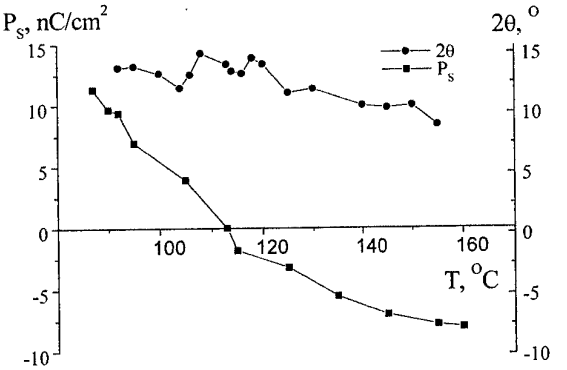

Fig.1 Spontaneous polarisation and tilt angle of compound **1a** in its SmC* phase [2].

The absence of any phase transitions in the range of the inversion of the Ps sign (around 114 °C) follows also from the DSC experiment.

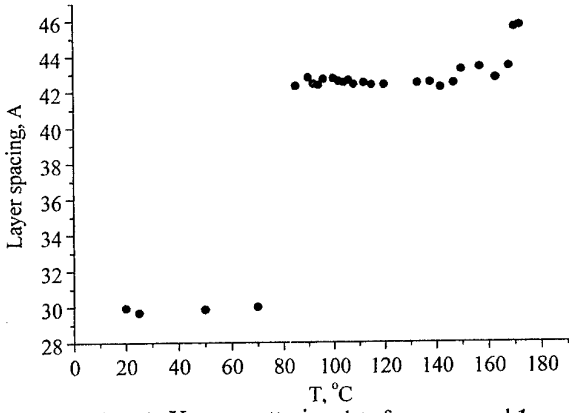

Fig.2 Small angle X-ray scattering data for compound **1a**.

The compounds **1** possess a great conformational diversity [7]. Those of conformational transformations, which result in the maximum change of the total molecular dipole moment and its projections on inertia axes, are of particular interest since they can be responsible the most extent for characteristics of the spontaneous polarization. The most important simulation results for isolated molecules are presented in Fig. 3 and Table 2. In Fig. 3 examples of conformers with various orientations and values of the total molecular dipole moment differing from each other with the opposite direction of the projections on one of inertia axes are presented. Variations in populations of such conformers with temperature would be responsible for the inversion of the P_S sign. However, for isolated molecules, any essential difference in energetics and populations between these conformers was not found (see Table 2). So, only slight preference

Table 2. Calculated energy characteristics (E) and some torsion angles (ϕ_i) for the conformers of model compound **1c** (PM3 method)

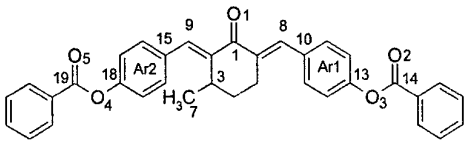

Conformer*	E, kcal/mol	Fraction		μ, D	Torsional angles**				
		30°	140°		$\phi_{Ar\text{-}1}$	$\phi_{Ar\text{-}2}$	φ_1	φ_2	φ_3
Ch-ax-1	–61.59	32.97	30.81	2.49	64.5	55.1	102.9	128.3	104.5
Ch-ax-2	–61.49	27.91	27.27	1.53	–60.3	54.7	124.3	128.6	104.6
Ch-ax-3	–61.36	22.47	23.26	5.69	62.2	55.3	59.7	5.0	64.4
Ch-ax-4	–61.18	16.65	18.66	6.48	–59.7	55.3	3.8	0.5	3.3

* Only preferential *chair*-like conformers of the cyclohexanone ring with the axial methyl group (*chair-ax*) are presented.

** $\phi_{Ar\text{-}1}$ – $C_6C_8C_{10}C_{orto'}$, $\phi_{Ar\text{-}2}$ – $C_2C_9C_{15}C_{orto'}$, φ_1 – angle between $C_1{=}O_1$ and $C_{14}{=}O_2$; φ_2 – angle between $C_1{=}O_1$ and $C_{19}{=}O_5$; φ_3 – angle between $C_{14}{=}O_2$ and $C_{19}{=}O_5$.

was given with simulation to conformers with low and intermediate magnitudes of molecular dipoles (with *chair*-like but *twist* cyclohexanone ring), though for the most high-energetic conformers with the maximal μ values the energy exceeds the one for conformers mentioned above only by 0.3 – 0.4 kcal/ mol. The similar results of simulation were obtained recently [10] by DFT simulation of some aromatic banana-shaped compounds with two ester groups.

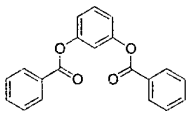

As a consequence, changes in conformer populations possessing so slight energy differences caused by temperature cannot be the origin of the effect on study.

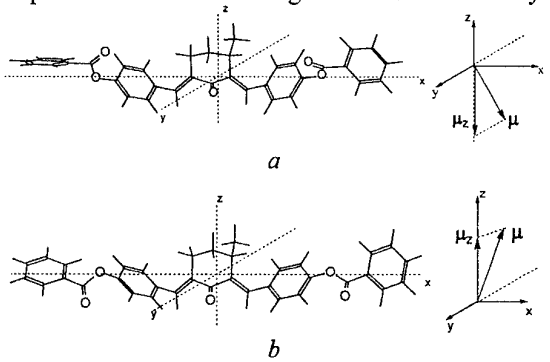

a

b

Fig. 3. Some conformers of model compound **1c** with various orientations of the total molecular dipole moment: *ch-ax-2* (*a*), *ch-ax-4* (*b*) (see Table 2).

However, it was quite well-grounded assuming that such a relative energetics of conformers possessing the various dipole moments can be essentially changed at formation of a mesophase owing to intermolecular interactions. Such a possibility can be considered to some approximation basing on results of the simulation for molecular pairs. Only the *chair*-conformers were considered here being more preferable than the *twist* ones [7]. Conformers with various mutual orientations of dipoles of carbonyl groups and, as consequence, different total molecular dipole moments, with various directions of turn for benzene rings *Ar1* and *Ar2* with respect to single bonds C_8—C_{10} and C_9—C_{15} were involved into modelled molecule pairs. Moreover, the different starting mutual arrangements of molecules in the pairs were taken to simulate their interactions.

Modelling accomplished has demonstrated a significant reduction in energies of conformer pairs in comparison with the total energy for single conformers (up to 5 – 10 kcal/mol, depending on conformational structures). The most reduction in energies is revealed for those binary ensembles, which consist of starting single conformers with the great polarity (e.g., ensembles of type *A* and *B*, Table 3). As a result, just such binary ensembles become the most preferable at room temperature.

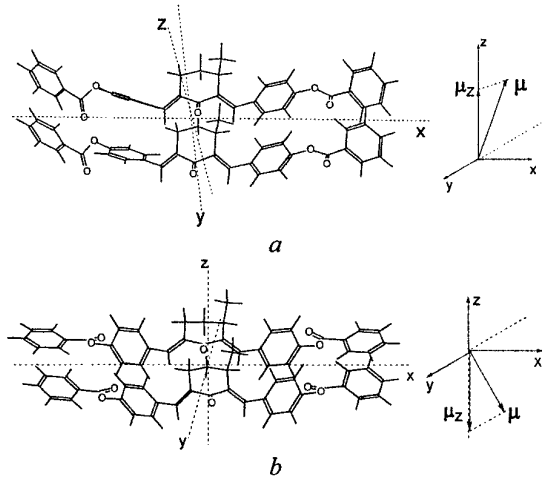

a

b

Fig. 4. Binary molecular ensembles of **1c** with different polarity and energetics: *A* (*a*) and *D* (*b*) (see Table 3)

Table 3. Some calculated characteristics binary ensembles of model compound **1c***.

Dimer	ΔE, Kcal/mol	ΔΔE, Kcal/mol	μ_{mol}	μ_{dim}	$\phi_{Ar\,1}$	$\phi_{Ar\,2}$	φ_1	φ_2	φ_3	*m*, 30°	*m*,140°
A	0	–10.41	5.69	10.94	79.8	64.5	53.3	3.9	52.8	96.78	65.44
			5.69		67.6	57.0	56.6	10.4	65.6		
B	0.97	–9.44	6.48	12.04	–65.6	54.3	4.3	12.7	15.8	2.92	19.98
			6.48		82.8	54.8	10.5	4.7	6.4		
C	1.79	–8.62	6.48	9.85	–63.8	54.1	5.0	8.9	12.7	0.15	7.33
			4.05		80.6	55.8	53.5	119.6	126.2		
D	1.80	–8.61	1.53	2.49	–60.0	59.8	131.2	127.9	101.0	0.15	7.24
			1.53		–60.4	53.2	122.2	125.5	110.0		

* Designations are the same as in Table 2; presented here some geometry parameters relate to single conformers included into binary ensembles; μ_{mol} and μ_{ens} are dipole moments of starting conformers and binary ensembles, correspondingly; *m* is molar fraction of the respective ensemble; ΔE is energy of the binary ensemble with respect to the one (*A*) with the minimal energy; ΔΔE is energy decrease on formation of binary ensemble

From results of the simulation follows also that the energy of the molecule interaction in binary ensembles under consideration depends to some extent on the character of twisting of arylidene fragments (torsion angles $\phi_{Ar\,1}$ and $\phi_{Ar\,2}$, Table 3, cf. data for ensembles *A* and *B* with C).

Such energetics of the binary ensembles leads to their distribution the qualitatively differing in comparison to isolated molecules. At 30 ^{O}C the most polar aggregates *A* and *B* are essentially preferential (Table 3). However, their population appreciably falls with temperature while the fraction of low polar ensembles rises. According to simulation results, directions of total dipole moment and its projections on inertia axes of binary ensembles are similar ones for isolated molecules (see fig. 4) of analogous polarity. Tendency of changes in populations of molecular ensembles with temperature showed by modelling can be considered as the most probable origin of the revealed effect.

Conclusion

Internal rotation in molecules of 2,6-*bis*-arylidene-3*R*-methylcyclohexanones with ester groups linking benzene rings of arylidene fragments results in the existence in forming SmC* mesophase of molecular ensembles with various magnitudes and directions of total dipole moment and its projections on inertia axes. The molecular simulation with semi-empirical method PM3 reveals a distinct tendency to the predominance of binary aggregates with the highest polarity (μ is 11–12 D) at room temperatures (20 – 30 °C) and to the reduction of their fraction with the increasing temperature. Simultaneous rise of fraction of low polar ensembles having opposite projection of dipole moment on the one of inertia axes is considered as the main possible origin of the inversion of spontaneous polarization sign.

References

1. A.I. Krivoshey, L.A. Kutulya, V.V. Vashchenko,"New chiral mesogens with non-conventional molecular shape derived from R-3-methylcyclohexanone" in *Proceedings of XV the International School-Seminar "Spectroscopy of Molecules and Crystals"*, Chernihiv, Ukraine, 2001, P. 76.
2. A.I. Krivoshey., L.A. Kutulya, V.V. Vashchenko et al., "New chiral mesogens 3(*R*)-methylcyclohexanone derivatives" , *Proc. of SPIE* (in press).
3. J.W. Goodby, E. Chin, J.M. Geary, et al., "The ferroelectric and liquid-crystalline properties of some chiral alkyl 4-n-alkanoyloxybiphenyl-4′-carboxylates", *J. Chem. Soc. Faraday Trans. I.*, **83**, 3429 – 3446, 1987.
4. S.N. Yarmolenko, L.A. Kutulya, V.V. Vashchenko, et al., "Photosensitive chiral dopants with high twisting power", *Liq. Cryst.*, **16**, 877 – 882, 1994.
5. L.V. Chepeleva, "*E,Z*-isomerization of chiral 2-arylidene-*p*-menthan-3-ones", Ph. D. (Chem) Thesis, Institute for Single Crystals, National Academy of Sciences of Ukraine, Kharkov; Kharkov State University, 1997, 91 pp. [in Russian].
6. L.A. Kutulya, V.V. Vashchenko, A.O. Doroshenko et al., "New Chiral *E*- and *Z*-isomers of the 1*R*,4*R*-2-Arylidene-*p*-menthane-3-ones in Induced Cholesteric and Ferroelectric Liquid Crystals", *Proc. SPIE*, **4418**, 89 – 98, 2001.
7. N.S. Pivnenko, A.I. Krivoshey, L.A. Kutulya et al., " Smectogenic C* 2,6-*bis*-arylidene derivatives of 3(*R*)-methylcyclohexanone exhibiting inversion of spontaneous polarization sign", *Proc. SPIE.* (in press).
8. K. Skarp, "Rotational Viscosities in Ferroelectric Smectic Liquid Crystals", *Ferroelectrics*, **84**, 119 – 142, 1988.
9. K. Terashima, M. Ichihashi, M. Kikuch, K. et al., "Some Observations on the Sense and Magnitude of Spontaneous Polarisation and Twisting Power of a Number of Ferroelectric Liquid Crystal Tapes", *Mol. Cryst. Liq. Cryst.*, **141**, 237-249, 1986.
10. T. Imase, S. Kawauchi, J. Watanabe, "Conformational analysis of 1,3-benzenediol dibenzoate as a model of banana-shaped molecules forming chiral smectic phases", *J. Mol. Structure.*, **560**, 275 – 281, 2001.

NED-P2. **Photoinducted inversion of helix in a system nematic - chiral dopant.**

L.A. Kutulya, N.I. Shkolnikova, A.I. Krivoshey, L.V.Chepeleva, M.N. Pivnenko

Institute for Single Crystals of NASU, 60 Lenin Ave, Kharkov 61001, Ukraine

E-mail: kutulya@isc.kharkov.com

A.O.Doroshenko

Kharkov Karazin National University, Ukraine

Paper is not available

NED-P3. ELECTRICALLY CONTROLLED BIREFRINGENCE AND LIGHT PHASE MODULATION IN HELIX FREE FLC

A.Andreev, T. Fedosenkova, E. Pozhidaev, Yu. Bobylev, V. Shoshin, I. Kompanets, L. Kutulya*

P.N. Lebedev Physical Institute, 53 Leninsky pr., Moscow 119991 Russia
*Institute for Single Crystals, Lenin Ave. 60, Kharkov, 310001, Ukraine.

Abstracts. The helix free FLC in which helix compensation is reached the addition two ore more chiral dopandes with contrast signs of optical activity are perspective materials due to the absence helix bend of the director that essential improves optical characteristics. The electrically controlled birefringence one can observe in some such FLC. Moreover helix free FLC with high spontaneous polarization (P_s>100 nC/cm^2) one can possess bistability and multistability.

Keywords: helix free FLC, electrically controlled birefringence change, light modulation.

The reorientation time τ_R of the director strongly depends on electric field frequency f for some helix free FLC with high spontaneous polarization. If the electric field interacted with P_s changes director's azimuthal angle φ only then FLC behaves like a liquid with viscosity γ_φ, and time $\tau_R \sim \gamma_\varphi / P_s E$ does not depend on f.

For considered FLC time τ_R sharply increases when the polarization reversal current becomes double one with frequency rising (Fig. 1). In absence of helix and shevron-defects one can suppose that dissipation energy channel appears which is caused with unbending the deformed smectic layers. There are elastic and ferroelectric domains in such FLC when the electric field is absent. Superposition of this type domains results in bending form of dislocation walls separating the domains [1]. Time τ_R increases due to simultaneous existence of two modes associated with both director reorientations along the azimuthal angle φ and smectic layers unbending.

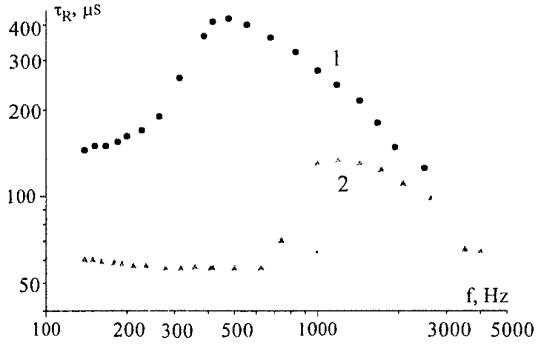

Fig. 1. Frequency dependencies of reorientation time for ZhKS-370. d=4 μm, E=3 V/μm (curve 1), E=5 V/μm (curve 2).

When frequency increases more the mode associated with smectic layers unbending predominates, time τ_R decreases (Fig. 1) and optical transmittance increases (Fig. 2, curve 1). Frequency increased one can decrease time τ_R in 2-3 times.

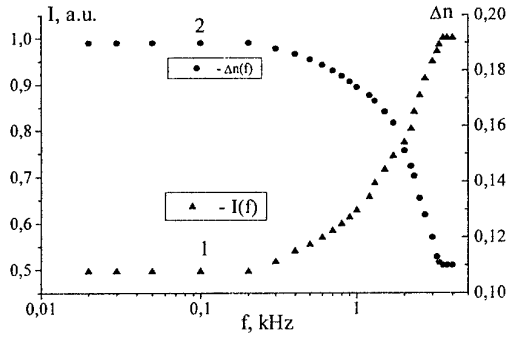

Fig. 2. Frequency dependencies of optical transmittance (curve 1) and birefringence (curve 2) for ZhKS-370. d=4 μm, E=3 V/μm.

The reason of birefringence change is periodical smectic layers deformations. Because of this ones the molecules tilted on angle θ (relative to the normal to smectic layers) deflect additionally on angle ψ relative to the rubbing direction. Then the projection of FLC's director onto the plane, which is orthogonal to substrates, is changed. Smectic layers unbend under electric field E for characteristic time $\tau_c \sim \gamma_\psi / ((P_c E \cos\varphi_0 - M)\theta^2)$, where γ_ψ - shift viscosity, M - energy of smectic layer bending [2]. Effective birefringence Δn for considered FLC changes when amplitude or frequency of control voltage changes (Fig. 2, curve 2). Frequency increase leads to changing the tilt angle ψ in every point of smectic layer. This is result in changing the birefringence ellipsoid orientation along smectic layer that is the cause of Δn change. Maximal Δn modulation is observed when the mode associated with changing the director's orientation due to smectic layers unbending (changing angle ψ) predominates. The thicker

electrooptical cell the wider Δn change interval. Electrically controlled birefringence change in helix free FLC allows change Δn in 1.5-2 times.

Predominance of the mode associated with smectic layers unbending leads to weakening the temperature dependence of time τ_R in wide interval - about 30°C (Fig. 3). Double polarization reversal current corresponding to static part means that two director reorientation processes exist: director reorientation along the azimuthal angle φ and smectic layers unbending. The correlation between polarisation reversal current picks changes with temperature rising, but reversal current duration is almost constant. Hence the reorientation time not depend on temperature. More, the higher voltage and frequency the wider temperature interval where τ_R is almost constant (Fig. 3, curve 3).

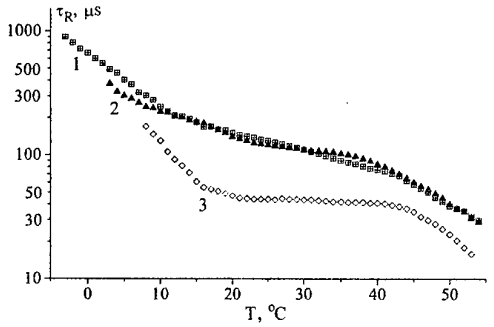

Fig. 3. Temperature dependencies of reorientation time ZhKS-370. f=140 Hz (1), 500 Hz (2) and E=3 V/μm; f=4 kHz (4) and E=5 V/μm. d=1,5 μm.

The helix free FLC possess multystability, that is different azimuthal angle φ conditions (partial switching), and hence optical transmittance, remain after electrical field switch off. There is a minimum impulse duration enough to transfer the structure from maximum to minimum optical transmittance and vice versa for any voltage to enough the azimuthal angle φ changes on 180°. If the impulse duration smaller, the structure transits to intermediate (partial switching) condition which remains after electrical field switch off. If some more the birefringence changes conditions with different birefringence and optical transmittance remain after electrical field switch off (Fig.4).

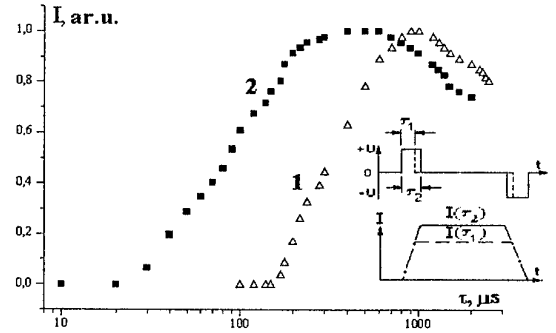

Fig. 4. ZhKS-370 optical transmittance dependencies from control voltage impulse duration; d=3,85 μm. 1 - E=1 V/μm, 2 - E=3 V/μm.

The cause of the birefringence change in absence of FLC helix can be bend or twist of the director in FLC volume – flexoelectrical effect. Electrically controlled birefringence Δn is observed in the tilt smectic phase existing between solid and smectic C* phases of the binary mixture consisting of nonmesogenic chiral dopant 2-arylidene derivative of 1R,4R-p-mentan-3 one (60PhBM) and nonchiral matrix 4-hexyloxysalicylidene-4-hexylaniline (O6SA6). This intermediate tilt phase (X-phase) exists in pure nonchiral matrix O6SA6 also [3]. Though spontaneous polarization is absent the linear electrooptical effect is observed due to flexoelectrical polarization arise. The change of the electric field sign switches FLC structure for the time shorter 200 μs (Fig. 5, curve 2). The threshold of flexoelectrical structure arising for planar oriented layers of O6SA6 is about 2 V/μm (Fig. 5).

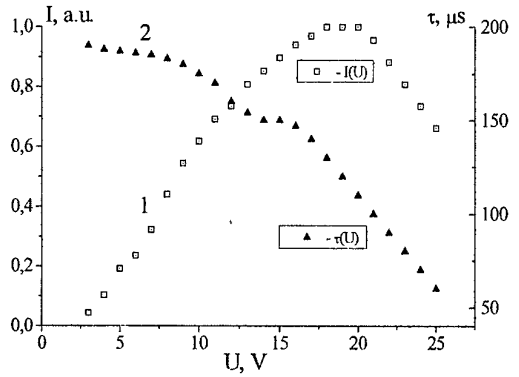

Fig. 5. Voltage dependencies of optical transmittance (curve 1) and switching time (curve 2) for O6SA6. f=300 Hz, d=1.7 μm, T=56°C.

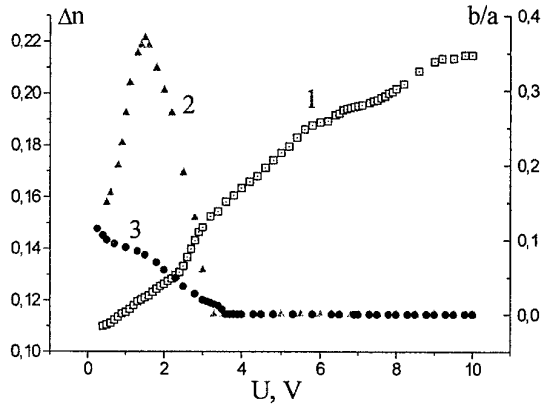

Fig. 6. Voltage dependencies of Δn (curve 1) and ellipticity (curve 2, 3) for orthogonal polarized incident light. ZhKSM-2.5.

The addition of chiral dopant 60PhBM into nonchiral matrix O6SA6 up to molar concentration 2.5% (ZhKSM-2.5) decreases the threshold of electrooptical response to 0.5 V/μm and increases optical transmittance considerably. When the flexoelectrical effect threshold does not exceed 2 V/μm the summary change of Δn is defined by small changes of the birefringence ellipsoid orientation in every

smectic layer (incomplete switching). As the result Δn rises linearly with electrical field voltage increase (Fig. 6, curve 1). In this case linearly polarized light becomes elliptically polarized one at the electrooptical cell output (Fig. 6, curves 2, 3).

Above flexoelectrical threshold (E≥2 V/μm) the cause of Δn changing are small director deflections on additional polar angle relative to rubbing direction. This is follow from smectic layer deformations that leads to changing the birefringence ellipsoid orientation in every smectic layer. In this case linearly polarized light remains linear polarized one at the electrooptical cell output (Fig. 6, curves 2, 3). That is the flexoelectrical deformations arising in electric field are the reasons of the birefringence change and light phase modulation in helix free FLC.

1. L. Beresnev, E. Schumacher et.al., Jpn. J. Appl. Phys., v. 34, № 5A, 1995, pp. 2404-2410.
2. T. Fedosenkova, A. Andreev et.al. Bull. P.N. Lebedev Phys. Inst., № 3, 2002, pp. 45-52.
3. 3. Narkevich J., Rabinovich A. et.al., Ferroelectrics, v. 114, 1991, pp. 385-399.

NED-P4. USE OF POLYMERIC NANOGELS FOR ORIENTATION OF LIQUID CRYSTALS

V.I. Mashchenko*, S.A. Udra*, L.A. Kasarin*, V.V. Belaev, V.I. Gerasimov***

* Lomonosov Moscow State University, Chemistry Department

** Cometa central R & D Institute

One of important and not solved up to the end problem of the tehnology of liquid crystal displays (LC-displays) is to set required orientation of liquid crystal (LC) molecules. On the other hand recently various nanocomposite materials are heavily used. Such materials by their own high specific surface can initiate orientation of LC molecules. Due to the last optical and electrooptical characteristics of light shutter and displays can be improved.

Therefore the aims of this work are development of a method for creation of composite nanomaterials based on fibergenerating polymer and low molecular mass nematic LC and investigation of their properties. Polyacrylonitrile`s gels with average radius of pores 15 nm were prepared and filled by LC - N-(4-Methoxybenzylidene)-4-butylaniline (MBBA) by an original technique. The content of LC is 90 mas. %. Further samples of nanocomposites were subjected to deformation by a method of zone stretching. The maximal linear elongation is 2000%. It is shown by methods of X-ray diffraction and IR-spectroscopy in the polarized radiation, that the orientation of the material of a matrix and LC molecules occurs in a direction of an axis stretching, order parameter of MBBA molecules growing with increase multiplicity of stretching.

Thus, it is possible to use the developed approach for orientation of LC molecules in the tehnology of displays based on polymeric composite materials.

This work was supported by the Russian Foundation for Basic Research (projects 02-03-33140, 03-03-06325, 03-03-06326), Program "Universities of Russia" (project No. УР.06.03.002).

NED-P5. Dynamics Of Electrooptic Response In Twist Cells With Double Frequency Addressing

V.V. Belyaev[a,b], M.F. Grebyonkin[c], A.Y. Kalashnikov[b,d]

[a]Cometa Central R&D Institute, 5, Velozavodskaya str., Moscow, 115280 Russia
[b]Moscow Technical University for Radio Engineering, Electronics & Automation,
78, Vernadsky prospect, 117454, Moscow, Russia
[c]Moscow State Technical University MAMI,
38, B. Semyonovskaya str., Moscow GSP, 195839, Russia
[d]Tests Laboratory of Information Technologies at FGUP IMI of GOSSTANDART of Russia,
Of.279, 5, Universitetsky prospect, Moscow, 117296, Russia

Abstract. Displays with the twist structure of the LC layer hold a leading position in TN and TFT LCDs. With low frequency inversion of the dielectric anisotropy sign, the use of double frequency driving in cells filled with LC material allows both switch-on and switch-off times of the electro-optic mode to be reduced. In our paper oscillograms of electrooptic response *vs.* high frequency (HF) voltage are presented for such LC cells. The bounce, which is induced by the back flow in strongly deformed twist cells, gradually decreases in magnitude with increasing HF voltage. It is suggested that the HF voltage suppresses the back flow in the vicinity of the cell's substrate surface. At the HF voltage that follows the disappearance of the bounce, the short response mode arises.

Keywords: twist-cell, double frequency addressing, relaxation mode.

1. Introduction

It is known that when switching on the voltage $U>U_{th}$ (U_{th} is the threshold voltage of the effect), the transmission of a twist-cell with a nematic LC without optically active addition , for example a cholesteric LC, increases monotonically at any U. The relationship for switch-on times $T_{on}\sim L^2(U^2/U^2_{th}-1)^{-1}$ (L is the cell thickness) is fulfilled qualitatively. When switching off a rather small voltage $U\leq 3\div 4U_{th}$, the relaxation of the transmission of the twist-cell likewise occurs monotonically. Yet, when switching on the voltage $U>4U_{th}$, in oscillograms of transmission of the cell, there appears a bounce that follows an initial decrease in the intensity of transmitted light [1]. For the first time, the assumption that the appearance of the bounce is associated with the back flow (it is induced by NLC reorientation) inside the twist-cell was made in [2]. The flow that realigns the director in the NLC reorientation under the action of the electric field arises from a greater density of the LC elastic energy in the near-wall layers of cell.

In [2--4], equations that describe the relaxation of the director and the flow velocity in the twist-cell were obtained analytically. In these works, the distributions of polar (θ) and azimuthal (φ) angles of the NLC director and the transmission of cell at different time instants after switching off voltage were calculated numerically as well.

The expression for the above angle θ obtained in [2] involves the possibility of existing several relaxing modes with the L/n period that is multiple of nth mode. The probability of their appearance reduces exponentially with increasing the order number of mode with the result that they have not been studied experimentally. Besides, it was suggested in [3] that upon relaxation of the LC director after switching off the voltage, the LC layer is twisted by 270°, 450°, and 90° ($2m$ - 1), where m is the integer.

The goal of this work was to investigate the possibilities of observing relaxing higher-order modes with twist angle >90° of the LC director in the twist-cell.

2. Experimental

For this purpose, the 36 μm thick twist-cell was assembled. Note that the optical path difference between ordinary and extraordinary rays propagating in the twist-cell and the relaxation time of damping modes increase with increasing the thickness. The above two circumstances improve the conditions for their observation.

In our experiment, the W1 mixture (E.Merck, Germany), which has a low frequency ($f_0\sim$10 kHz) of the sign inversion of the dielectric anisotropy at room temperature, was employed as an LC material. This made it possible to influence the relaxation process of the LC director after switching off a low-frequency voltage ($U\sim$30 V, $f\sim$1 kHz) that causes a significant deformation of this director (the angle of its inclination at the center of cell is $\theta_0\sim$80°). Since at the frequency $f>f_0$ $\Delta\varepsilon<0$, the action of electric field reduces angle of the inclination, such mixtures are used for decreasing relaxation time of the electrooptic response of LC cells [5, 6].

Figure 1 displays schematic of an experimental setup.

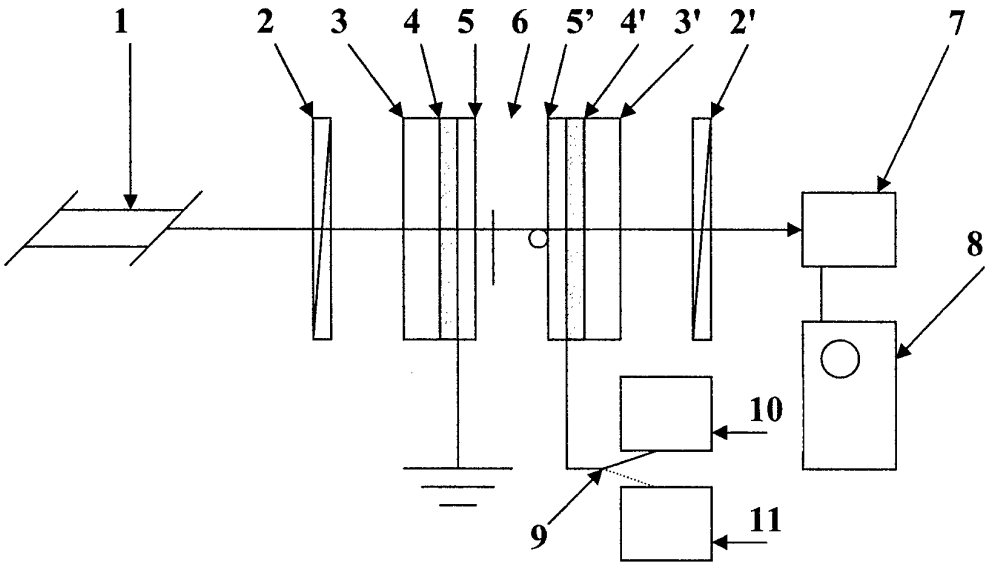

Fig. 1. Schematic of an experimental setup. 1. He-Ne laser; 2 and 2'. polarizer and analyzer with parallel axes; 3 and 3'. glass substrates; 4 and 4'. transparent electrodes; 5 and 5'. aligning coatings; 6. LC layer; 7. an FD-7K photodetector; 8. an S8-12 storage oscillograph; 9. switch synchronized with triggering oscillogram; 10. a G3-111 low-frequency (LF) generator (f = 1 kHz); 11. a G3-56/1 high-frequency (HF) generator (f = 50 kHz)

3. Results

Oscillograms of the relaxation of twist-cell 36 μm thick after switching off a low-frequency voltage are presented in Figs. 2 and 3. Hereafter, the terms "low frequency" and "high frequency" (1 kHz and 50 kHz, respectively) are used only with respect to the frequency of the sign inversion of the dielectric anisotropy. Note that at U_{HF}=0 two intermediate maxima are seen in oscillogram (Fig. 2).

Of special interest is the order of changing the types of oscillograms observed when the amplitude of high-frequency voltage U_{HF} is increased gradually (see Fig. 3). As U_{HF} increases from 0 to 6 V, the positions of extrema of transmission remain unaltered. In doing so, the height of a first maximum increases to the initial value of transmission, i.e., at this time instant light is polarized linearly and the direction of polarization is parallel to the axis of the analyser; while the intensity of light in a second minimum decreases and at 6 V reaches zero, i.e., light is polarized linearly and the direction of polarization is perpendicular to the axis of the analyser. The height of a second maximum remains practically unchanged.

With slightly increasing U_{HF} from 6 to 8 V, however, the second maximum disappears. Upon subsequent increase in U_{HF} the positions of both extrema change weakly and once again the intensity of the minimum reduces to zero (at U_{HF} = 0 V the original value of intensity of the first bounce is about 0.8 of the initial value at t=0). As in the case of second maximum, the intensity of the first maximum increases sharply at a certain value of U_{HF} equal to 15 V and then drops virtually to zero. At U_{HF}>12 V, a reduction in the front of oscillogram occurs with increasing control voltage, which is usual for any electrooptic effect in LC.

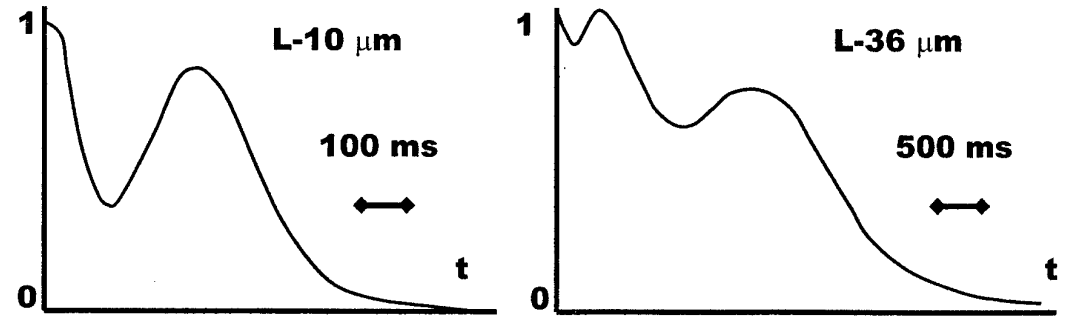

Fig.2. Transmission of twist cells 10 μm and 36 μm thick after switching-off the bias voltage $U>>U_{th}$. LC mixture W1 (E.Merck), U=30 V, U_{th}=3 V.

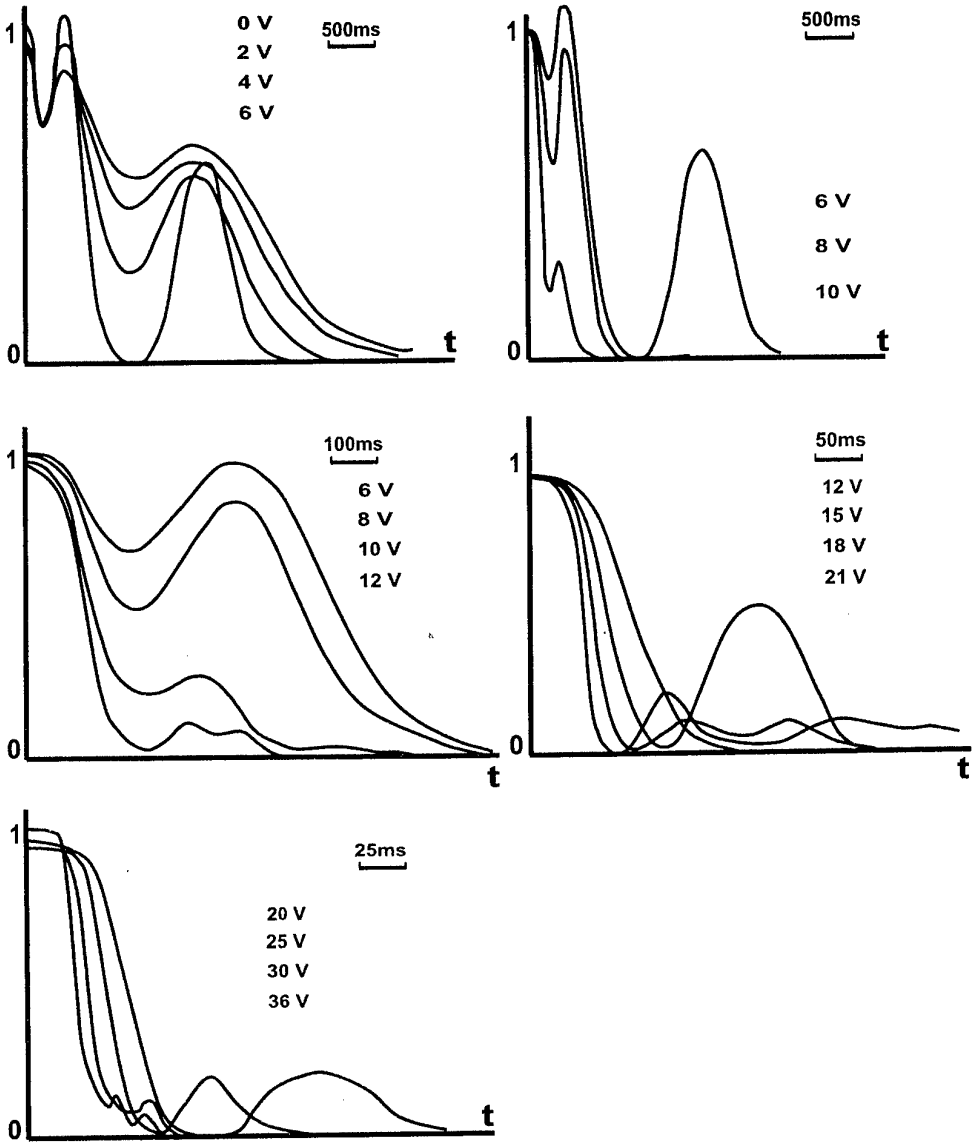

Fig.3. Transmission of the twist cell 36 μm thick at different values of the HF voltage (vertical columns).

4. Discussion

In order to interpret the observed oscillograms, let us consider, in the presence of one, two, or three relaxing modes, a likely structure of the LC director that is determined by the back flow in the LC cell and the interaction between the LC director and the high-frequency voltage.

Figure 4 shows distributions of the LC alignment across the thickness of the twist-cell at the initial instant of relaxation time and when the back flow is formed.

After switching off a low-frequency voltage the azimuthal angle in the cell changes from 0 to 90°. In this case, as a consequence of the existence of an extended zone with a high value of the polar angle of deformation, no rotation of polarization is observed and the twist-cell exhibits a maximum transmission when the axes of polarizer and analyzer are parallel to each other. The back flow gives rise to the angular twist 270° due to the inclination of the LC director whose direction is opposite to the direction of the realignment under the action of the low-frequency electric field (θ~100-110°) (Figs. 4a and 4b). A high-frequency electric field applied to the cell should lead to an increase in the angle of the inverse inclination. At small amplitude of U_{HF}, the elastic forces in the near-wall layers of the cell would resturn the relaxation process of the polar angle θ in the ordinary direction. This corresponds to the oscillograms at U_{HF} = 2 and 4 V. It is obvious that at U_{HF}=6V the action of the high-frequency field brings about the increase in the angle of the inverse inclination from 0 to 180° and the appearance of the extended structure with the angular twist -90° at the center of the cell. In this case, the zones with a high value of the

elastic energy of twisting which tend to restore the original value of the twist angle should arise in the near-wall layers. In the oscillograms this is manifested in the appearance of the high bounce at U_{HF}= 6 V.

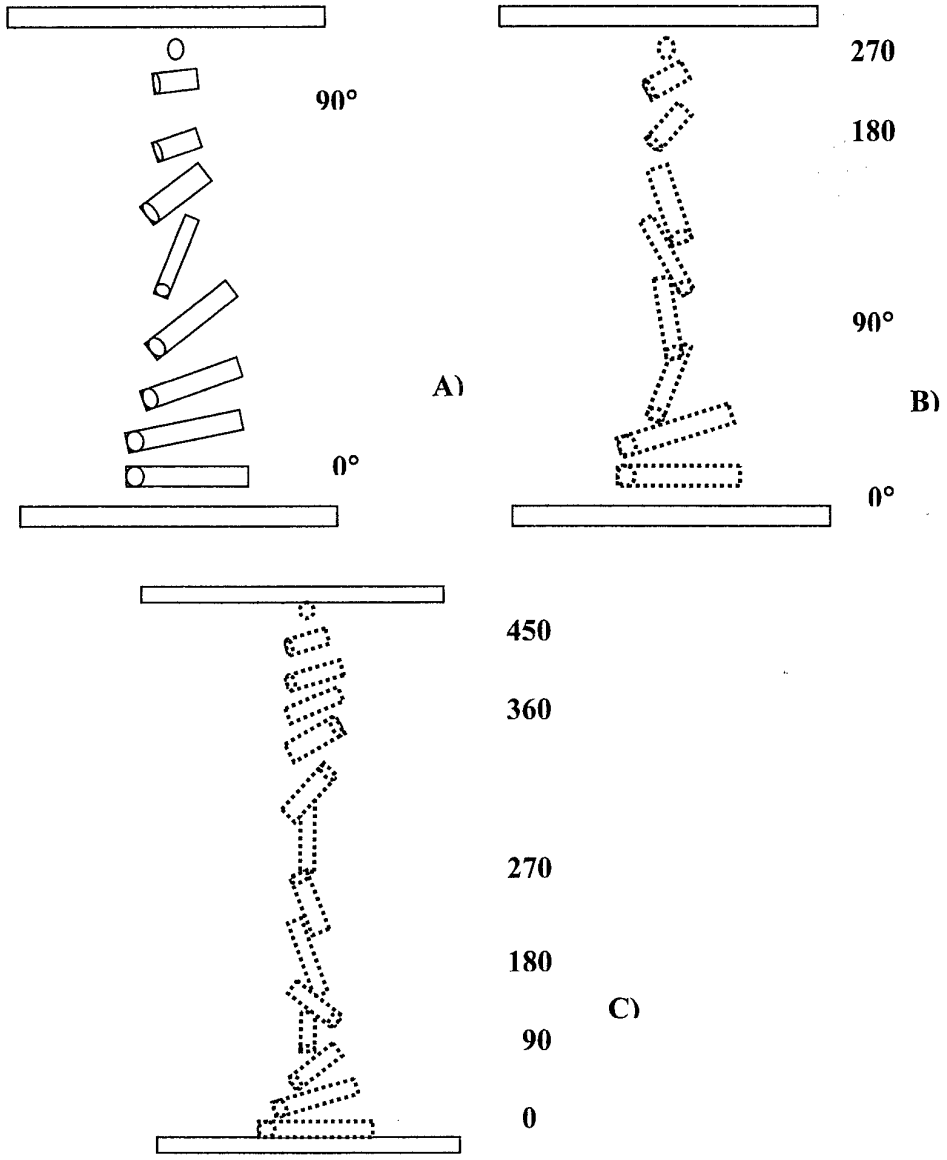

Fig. 4. Distribution of the alignment of the LC director across the thickness of the twist-cell. A, at the initial instant of relaxation after switching off a low-frequency voltage; B, the appearance of the inverse inclination and twist angle 270° due to the back flow of the LC; and C, a likely structure of the twist-cell with the twist angle 450° induced by the interaction of processes of the NLC realignment, the back flow, and the action of the high-frequency electric field.

After switching off a low-frequency voltage the azimuthal angle in the cell changes from 0 to 90°. In this case, as a consequence of the existence of an extended zone with a high value of the polar angle of deformation, no rotation of polarization is observed and the twist-cell exhibits a maximum transmission when the axes of polarizer and analyzer are parallel to each other. The back flow gives rise to the angular twist 270° due to the inclination of the LC director whose direction is opposite to the direction of the realignment under the action of the low-frequency electric field (θ~100-110°) (Figs. 4a and 4b). A high-frequency electric field applied to the cell should lead to an increase in the angle of the inverse inclination. At small amplitude of U_{HF}, the elastic forces in the near-wall layers of the cell would resturn the relaxation process of the polar angle θ in the ordinary direction. This corresponds to the oscillograms at U_{HF} = 2 and 4 V. It is obvious that at U_{HF}=6V the action of the high-frequency field brings about the increase in the angle of the inverse inclination from 0 to 180° and the appearance of the extended structure with the angular twist -90° at the center of the cell. In this case, the zones with a high value of the elastic energy of twisting which tend to restore the

original value of the twist angle should arise in the near-wall layers. In the oscillograms this is manifested in the appearance of the high bounce at U_{HF}= 6 V.

Upon subsequent increase in U_{HF} the energy of the electric field is sufficient to retain the major volume of the twist-cell with the angle of the inverse twist -90°, but the original twist angle +90° is still retained in the near-wall layers. Increasing voltage U_{HF} from 8 to 12 V brings about a decrease in the thickness of the above layers and in the amplitude of bounce. It is obvious that at U_{HF}>15 V these near-wall layers collapse and then under the action of the high-frequency field the whole cell is realigned as a unit.

5. Conclusion

Thus, after switching off a low-frequency voltage in twist-cells, the zones with twist angles 270° and 450° arise spontaneously therein, which is seen from the appearance of the two bounces in the oscillograms of transmission. The interaction of the high-frequency electric field with the elastic forces of the twist deformation leads to the inverse twist of the LC director and to the intricate type of oscillograms that is characterized by spike bounces.

The results of our investigation make it possible to clarify reasons for the appearance of beats of intensity when the regime of two-frequency modulation for displays and electrooptic gates is used.

REFERENCES

1. C.J. Gerritsma, C.Z. Van Doorn, P. Van Zanten, Phys. Lett. V.48A, P.263 (1974).
2. C.Z. Van Doorn, J. Phys. Colloq. (France). V.36, P.C1-261 (1975).
3. C.Z. Van Doorn, J. Appl. Phys. V.46, P.3738 (1975).
4. D.W. Berreman, V.46, P.3746 (1975).
5. V.V. Belyaev, V.G. Chigrinov, Sov. Phys. Crystallography V.23, P.811 (1978).
6. V.V. Belyaev, N.A. Vasiliev, I.N. Kompanets et al. Pis'ma v ZhTF (Letters to Soviet Applied Physics Journal) V.6, P.845 (1980).
7. V.V. Belyaev, Y.V. Devyatkin, V.G. Nazarenko, G.B. Nosov, A.S. Sonin, Proc. Vth International Symposium on Information Displays MINSK'96. Rakov, Belarus. 4-7 September 1996. P.176.

NED-P6. Figure Of Merit Of Liquid Crystal Substances And Mixtures For Displays With Homogeneous Planar And Vertical Alignment

V.V. Belyaev[a,b], M.F. Grebyonkin[c], A.Y. Kalashnikov[b,d]

[a]Cometa Central R&D Institute, 5, Velozavodskaya str., Moscow, 115280 Russia
[b]Moscow Technical University for Radio Engineering, Electronics & Automation,
78, Vernadsky prospect, 117454, Moscow, Russia
[c]Moscow State Technical University MAMI,
38, B. Semyonovskaya str., Moscow GSP, 195839, Russia
[d]Tests Laboratory of Information Technologies at FGUP IMI of GOSSTANDART of Russia,
Of.279, 5, Universitetsky prospect, Moscow, 117296, Russia

Abstract. Figure of merit for LC materials with both positive and negative dielectric anisotropy is considered as an information parameter of LC electro-optic shutters. Influence of chemical structure of different LC substances as well as concentration of components with different polarity on the magnitude of the figure of merit is investigated. Properties of new LC materials developed on the base of the approach considered are demonstrated.
Keywords: planar and vertical alignment of LC, physical properties, information data capacity, figure of merit.

1. Introduction

Displays with homogeneous vertical alignment of the LC material occupy now big share (>20%) of the LCD market. Besides of that homogeneous planar alignment of the LC is used in many systems of information processing like optically addressed spatial light modulators. It was shown in [1,2] that electrooptic response of such LC cells is described by a figure of merit M

$$M = \frac{\lambda L}{\tau_\pi}\frac{U_{th}}{\Delta U_\pi}$$

where λ - wavelength, L – cell's thickness, τ_π - switch time of the cell in the regime of change of the phase retardation by 1 π, U_{th} – threshold voltage of the electro-optic mode, ΔU_π – difference of bias voltage which corresponds to the change of the phase retardation by 1 π. While bias voltage $U \to U_{th}$ the figure of merit M transforms into combinations of LC physical parameters:

$$M_S = \frac{K_{11}}{\gamma_1}\Delta n\left(\frac{K_{33}}{K_{11}}+\frac{\Delta\varepsilon}{\varepsilon_\perp}\right)^{-1} \qquad M_B = \frac{K_{33}}{\eta_b}\Delta n\left(\frac{K_{11}}{K_{33}}-\frac{\Delta\varepsilon}{\varepsilon_{//}}\right)^{-1}$$

for both planar and vertical alignment of the LC (K_{11}, K_{33} – Frank elasticity coefficients, γ_1, η_b - viscosity coefficients, Δn – birefringence, $\Delta\varepsilon=\varepsilon_{||}-\varepsilon_\perp$- dielectric anisotropy.

The goal of the paper is to consider figure of merit M_S variation while changing structure of the molecular core, alkyl and alkoxy substituents and content of a nematic mixture of polar and weak polar substances, and to elaborate requirements to LC materials for displays with LC planar and vertical alignment.

2. Calculations of the figure of merit

2.1. Information data capacity of a LC shutter

According to the theory of data communication in the holographic systems [3], there was introduced a concept of the information data capacity for an LC shutter (a pixel of the display or a spatial light modulator (SLM))

$$P = -\tau_{fr}^{-1}\log_2(I_2/I_1) = \tau_\pi^{-1}\log_2\sin^2(\delta\Phi/2)$$

where the minimum possible time of the data communication τ_{fr} is taken to be equal to τ_π when $U=U_{th}+\Delta U_\pi$, I_1 and I_2 are the minimum and maximum intensities of the output signal of the display or the STLM (these intensities determine the dynamic range of the optical system), and $\delta\Phi$ is the difference in the phase delay $\Delta\Phi$ between selected and non-selected elements.

The values of M_S and P were calculated for different substances. The $P(M_S)$ dependence plotted at the logarithmic scale is described by the relationship $P \sim M_S^{2.2}$ with a good accuracy (Fig. 1). This means that the figures of merit M, M_S, and M_B under study are the information parameters of the electrooptic shutter or the display pixel.

2.2. Figure of merit of LC substances

The values of the physical parameters of the NLCs relating to different chemical classes and the values of the figures of merit M_S and M_B are listed in Table 1. For all of the substances when calculating the figure of merit M_B, the following assumptions were made. The value of the dielectric anisotropy is $\Delta\varepsilon/\varepsilon_\perp = -0.7$, which corresponds to the value of this parameter for the majority of the mixtures for the vertical alignment of the NLCs [4]. For the lack of data on the viscosity η_b, its value is taken as one fourth of the rotational viscosity γ_1 [5].

Among the polar compounds, the highest value of M_S is characteristic of the derivatives of biphenyl, pyridine, and phenyl-cyclohexane; and among weakly polar compounds, this value is characteristic of the derivatives of tolane and azoxy-compounds. The substances with greater birefringence are more preferable for the application mentioned.

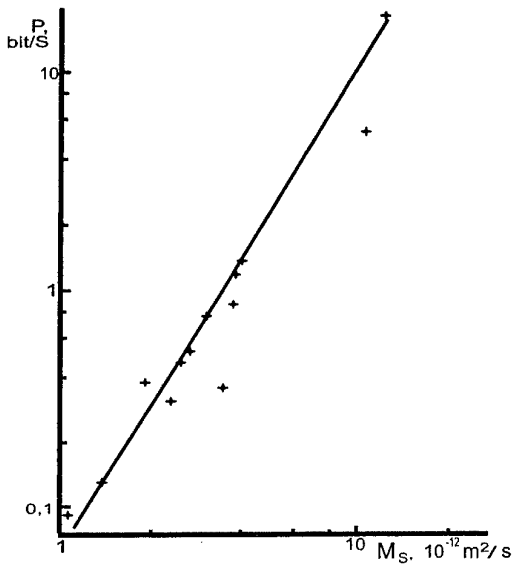

Fig.1. Information data capacity P of an LC shutter *vs* figure of merit M_S of an LC material for substances listed in Table 1

Because of lower viscosity and, as a rule, a greater value of the elasticity coefficient K_{33} as well as because of using the ratio K_{11}/K_{33} in the expression for M_B, which decreases the denominator of the fraction rather than the ratio K_{33}/K_{11} as in the expression for M_S, the figure of merit M_B exceeds M_S by a factor 4-20. Owing to this, the displays with the vertical alignment of the LCs have advantages over conventional LCDs based on the twist-effect. The highest value of M_B is characteristic of the derivatives of phenyl-cyclohexane, biphenyl, and tolane.

The physical properties of tolane derivatives have been studied in [6-10]. The values of M_S for this class of substances were calculated from the values of their physical parameters (Fig. 2). In the homologous series of these NLCs, the substances whose molecules have the most elongated shape, i.e., the directions of the C-C end bonds are parallel to the long axis of a molecule, exhibit an optimum figure of merit. This is the situation for the molecules that have odd number of carbon atoms in the alkyl chain and even number in the alkoxy-substituent. Note that all the ethoxy-derivatives of tolane have high values of M_S.

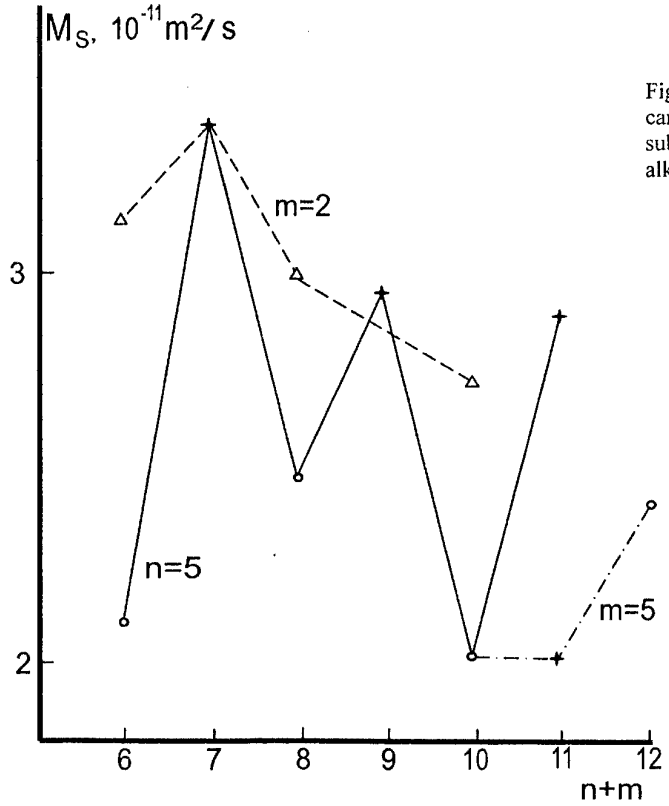

Fig.2. Figure of merit M_S *vs* total number of carbon atom in both alkyl (n) and alkoxy (m) substituents in a molecule of 4-alkyl-4'-alkoxytolane.

2.3. Figure of merit of LC mixtures

Figure 3 shows the dependences of the figures of merit M and M_S, and the half-wave voltage ΔU_π on the concentration of 4-heptyl-(4'-cyanophenyl)cyclohexane (PCH-7) in mixtures with a weakly polar material ZhK-440 composed of two azoxy-compounds. In the mixtures of PCH-7 and ZhK-440, the maximum of M_S and the minimum of ΔU_π are observed at the concentration of the polar component in an amount of 20 wt %, which, upon growth of the PCH-7 concentration, is related to a faster decrease in the birefringence as compared to analogous dependences of γ_1 and the ratio K_{33}/K_{11}. In similar materials, the concentration of the polar component in an amount of 40 wt %, at which the above ratio and the activation energy for the rotational viscosity are minimum, is optimum for twist-effect [11].

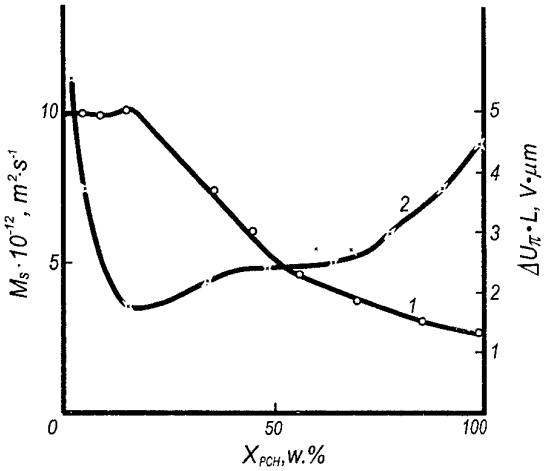

Fig.3. Dependence of the values of M_S and $\Delta U_\pi L$ on concentration x_{PCH} of the polar component in mixtures of ZhK-440 and PCH-7.

3. Conclusion

Thus, it is shown in this work that the figures of merit characterize the information data capacity of the pixels of the LCDs with the LC planar and vertical alignment. Also, the effect of molecular structure of NLCs and concentration of components of the LC material on the magnitude of these figures is estimated. This makes it possible to choose the content of the LC material that is optimum for obtaining maximum contrast and speed of response of the electrooptic device.

A set of LC materials for the electrically controllable birefringence (ECB) and twist modes was developed in cooperation with Vilnius University, Lithuania and R&D Institute for Applied Physical Problems, Minsk, Belorussia [12, 13]. Their parameters are listed in Table 2. They have advantages of low voltage, high birefringence and higher steepness of the voltage-transmission performance for the ECB-mode.

Table 1. Physical parameters and figures of merit of different nematic substances

Chemical formula	γ_1, Pa s	K_{11}, 10^{-12} N	K_{33}/K_{11}	$\Delta\varepsilon/\varepsilon_\perp$	Δn	T_{ni}, C	M_S, 10^{-12} m^2 s^{-1}	M_B, 10^{-12} m^2 s^{-1}
C_nH_{2n+1}-Ph-Ph-CN	0.11	7.65	1.38	1.95	0.183	39	3.82	49.3
C_nH_{2n+1}-O-Ph-Ph-CN	0.33	10.4	1.40	1.65	0.19	72	1.96	23.7
C_nH_{2n+1}-Cy-Ph-CN	0.1	11.5	1.78	1.8	0.11	56.4	3.53	71.4
C_nH_{2n+1}-BCO-Ph-CN	0.36	11.2	2.10	1.75	0.13	96.5	1.05	28.9
C_nH_{2n+1}-Pm-Ph-CN	0.19	10.2	1.10	2.95	0.18	51.2	2.39	26.4
C_nH_{2n+1}-Pr(5)-Ph-CN	0.184	7.50	1.28	1.55	0.178	44.2	2.56	25.1
C_nH_{2n+1}-Ph-Pr(5)-CN	0.220	8.25	1.40	1.08	0.18	49.2	2.72	26.7
C_nH_{2n+1}-Cy-Pr(5)-CN	0.178	7.45	1.75	1.35	0.105	58	1.42	24.2
C_nH_{2n+1}-Ph-Pr(4)-CN	0.350	14.0	1.50	0.95	0.190	62.7	1.44	33.4
C_nH_{2n+1}-Cy-Pr(4)-CN	0.140	8.80	1.57	0.47	0.13	57.3	4.01	38.4
CH_2=CH-C_2H_4-Cy-Ph-NCS	0.051	9.5	-	-	0.183	41.1	-	
C_4H_9-Ph-N=N(O)-Ph-CH_3	0.158	9.74	1.66	-0.06	0.28	74.7	10.79	88.0
C_nH_{2n+1}-Ph-COO-Ph-OC_2H_5	0.220	9.7	1.1	0.5	0.14	51.6	3.86	16.9
C_nH_{2n+1}-Cy-COO-Ph-OC_2H_5	0.134	12.7	1.3	0.2	0.10	73.6	6.32	33.5
C_5H_{11}-Ph-C≡C-Ph-CH_3	0.140	11.4	1.74	0.1	0.27	57.3	12.64	120.0

Designations of fragments are the following:
Ph, phenyl C_6H_4; Cy, cyclohexane C_6H_{10}; BCO, bicycle[2.2.2]octane C_8H_{14}; Pm, pyrimidine $C_4H_2N_2$; Pr(5), pyridine C_5H_3N, nitrogen being in the *orto*-position; and Pr(4), pyridine C_5H_3N, nitrogen being in the *meta*-position.

Table 2 Parameters of tolane-based LC materials for ECB- and twist-modes..

Mixture	Melting point, °C	Clearing point, °C	Δn, 546 nm	$\Delta U_\pi/U_{th}$	U_{th}, V (twist)	U_{sat}, V (twist)	$(U_{sat}-U_{th})/U_{th}$	$\Delta\varepsilon$
VK-7	4	62.5	0.212	0.101	1.07	1.21	0.24	13.0
VK-10	12	65.5	0.232	0.09	1.15	1.31	0.22	6.5

ACKNOWLEDGEMENT
The work was partially supported by the Russian Foundation for Basic Researches (grant #03-03-81305).

REFERENCES

1. V.V. Belyaev, V.G. Chigrinov, Applied Optics, V.32, P.141 (1993).
2. V.V. Belyaev, V.G. Chigrinov, A.B. Kuznetsov, N.F. Kovtonyuk, Rus. J. Tech. Phys. V.61, P.105 (1991).
3. S.B. Gurevich, V.B. Konstantinov, V.K. Sokolov, D.F. Chernykh "Data transfer and processing by holographic methods". Sobetskoye Radio Publishers, Moscow. 1978.
4. E.Merck Liquid Crystal Materials, A Prospect (2001).
5. V.V. Belyaev "Viscosity of nematic liquid crystals". Fizmatlit Editorial House, Moscow, 2002.
6. V.V. Belyaev, S.A. Ivanov, Sovyet Physics Crystallography. V.37, P.123 (1992).
7. V.V. Belyaev, Molecular Crystals and Liquid Crystals, V.265, P.675 (1995).
8. V.V. Belyaev, A.B. Kuznetsov, Sov. Journal of Optical Technology. V.60, P.420 (1993).
9. .V. Belyaev, Rus. J. Phys. Chem. V.75, P.855 (2001).
10. .V. Belyaev, Rus. J. Phys. Chem. V.75, C.981 (2001).
11. V.V. Belyaev, M.F. Grebenkin, G.A. Beresnev, Molecular Crystals and Liquid Crystals, V.103, P.1 (1985).
12. P. Adomenas, V.V. Belyaev, R. Bernotas et al. USSR Invention Application No.4,821,614. MCI C09K19/32. Filed 03.05.1990. Positive decision of the USSR State Committee on Inventions 30.07.1991.
13. P. Adomenas, V.S. Bezborodov, V.V. Belyaev et al. USSR Invention Application No.4,821,615. MCI C09K19/32. Filed 03.05.1990. Positive decision of the USSR State Committee on Inventions 30.07.1991.

NED-P7. Spectral Reflectance and Transmittance of Holographic Polymer Dispersed Liquid Crystal Films

V.A. Loiko, D.A. Yastrebov

B.I. Stepanov Institute of Physics, the National academy of Sciences of Belarus
F.Skaryna ave., 68, Minsk, 220072, Belarus.
E-mail: yastreb@dragon.bas-net.by

Abstract

The problem of the description of the light scattered by holographic Bragg gratings written in polymer dispersed liquid crystal composite system is considered. The effect of film and droplets parameters on diffraction switching is investigated.

Keywords: H-PDLC gratings, flat-panel displays, image capture.

Introduction

We made theoretical treatment of coherent reflection and transmission of light by H-PDLC films [1]. At first we consider monodisperse system of monolayers of fine spherical LC droplets. We are based on the following assumptions:

-quasi-crystalline approximation of the theory of the multiple scattering of waves for coherent component of the transmitted and reflected light calculations.

-Rayleigh-Gans approximation for definition of the amplitude scattering function of the separate droplet.

We worked out the method for calculation of coherent transmittance and reflectance for a film consisting from a set of monolayers of fine droplets. We investigated spectral behavior of reflection and transmission coefficients, diffraction efficiency on the optical characteristics of droplets, their concentration and amount of monolayers in the film.

Basic Relations

We used the Rayleigh-Gans approximation for finding the scattering amplitude of single droplet and the quasi-crystalline approximation [2] for calculation of coherent component of scattered light.

The Rayleigh-Gans approximation is applicable in the case

$$\left|\frac{n_{LC}}{n_m}-1\right|<<1, \qquad (1.1)$$

$$2kR\left|\frac{n_{LC}}{n_m}-1\right|<<1, \qquad (1.2)$$

where n_{LC} is ordinary or extraordinary refractive indexes of liquid crystal, n_m is refractive index of polymer matrix, $k=\frac{2\pi n_m}{\lambda}$ (λ is the wavelength of incident wave in vacuum), R is the radius of droplet.

The scattering amplitude in the Rayleigh-Gans approximation [3]

$$\bar{f}(\bar{k},\bar{k}')=-\frac{1}{4\pi}\int_V \bar{k}\times\bar{k}'\times\left\{\underline{\varepsilon}_r(\bar{r}_n)-\underline{I}\right\}\bar{E}(\bar{k},\bar{r}_n)\Big\}e^{-ik'r_n}dV \quad (2)$$

The scattered field:

$$\bar{E}_s=\bar{f}(\bar{k},\bar{k}')\frac{e^{ikr}}{r}, \qquad (3)$$

We used the theory of multiple scattering of waves to describe the scattering of light on the ensemble of scatterrers [4]. The equations of the theory of multiple scattering of waves are:

$$u_s=u_0+\eta\sum_i t^i u_i, \qquad (4.1)$$

$$u_i=u_0+\eta\sum_{\substack{j\\ j\neq i}} t_i^j u_j, \qquad (4.2)$$

here u_s is scattered field, u_0 is an incident wave, u_i is the field where i-th droplet is situated, η is the filling factor of droplets, t^i is the scattering operator of i-th droplet.

We can obtain the expression for u_s iterating Eq. (4.1) by Eq. (4.2):

$$u_s=u_0+\sum_i t^i u_i^0+\sum_i\sum_{\substack{j\\ j\neq i}} t^i t_i^j u_j^0+\sum_i\sum_{j\neq i}\sum_{k\neq j} t^i t_i^j t_j^k u_k^0+\ldots \qquad (5)$$

The first term in Eq. (5) is the incident wave in the point of observation. The second term includes N contributions of single scattering. The next sum describes $N(N\text{-}1)$ contributions by double scattering and so on.

Let us average Eqs. (4.1) and (4.2) on different configurations of scatterrers by the radial distribution function $g(R)$:

$$\langle u_s \rangle = u_0 + \eta \int t^i \langle u_i \rangle dr_i \,, \tag{6.1}$$

$$\langle u_i \rangle = u_0 + \eta \int g(|\overline{r_j} - \overline{r_i}|) t_i^j u_j dr_j \,. \tag{6.2}$$

In the case of random distribution of droplets we can separate scattered field on the average (coherent) $\langle u \rangle$ and fluctuation v fields:

$$u = \langle u \rangle + v \,. \tag{7}$$

After averaging total intensity can be written:

$$\langle |u|^2 \rangle = |\langle u \rangle|^2 + \langle |v|^2 \rangle \,. \tag{8}$$

We considered the scalar case of the theory of multiple scattering of waves. Let us convert the results for the vector case.

For droplets situated in parallel planes Eqs. (6.1) and (6.2) can be written in the form:

$$\langle \overline{E}(\overline{r}) \rangle = \overline{E_0}(\overline{r}) + \eta \sum_{m=1}^{M} \int_0^{2\pi} \int_0^{\infty} \overline{f}(\overline{R}, \overline{r}, \langle \overline{E}(\overline{R}) \rangle) \frac{e^{ik|\overline{r}-\overline{R}|}}{|\overline{r}-\overline{R}|} \rho d\rho d\varphi \tag{9.1}$$

$$\langle \overline{E}(\overline{R}) \rangle = \overline{E_0}(\overline{R}) + \eta \left\{ \int_0^{2\pi} \int_0^{\infty} \overline{f}(\overline{R}', \overline{R}, \langle \overline{E}(\overline{R}') \rangle) \frac{e^{ik|\overline{R}-\overline{R}'|}}{|\overline{R}-\overline{R}'|} * \right.$$
$$* \left[g(|\overline{R}-\overline{R}'|) - 1 \right] \rho' d\rho' d\varphi' +$$
$$\left. + \sum_{m=1}^{M} \int_0^{2\pi} \int_0^{\infty} \overline{f}(\overline{R}', \overline{R}, \langle \overline{E}(\overline{R}') \rangle) \frac{e^{ik|\overline{R}-\overline{R}'|}}{|\overline{R}-\overline{R}'|} \rho' d\rho' d\varphi' \right\} \tag{9.2}$$

Here $\overline{R}$ is the radius vector of droplet, $\overline{r}$ is the radius vector of the observation point, $\overline{E_0}$ is the incident intensity, $\overline{f}$ is scattering amplitude, M is the number of layers, ρ and φ are the polar coordinates in plane of layers.

Results

Using Eqs. (9.1) and (9.2) we can calculate spectral characteristics of transmitted and reflected light by holographic polymer dispersed liquid crystal films. The calculations were carried out at M=7; distance between layers is 300 *nm*; R=110 *nm*; η=0,56. Relative refractive index in the case of isotropic scatterrers is 1,098 (Fig. 1), relative ordinary refractive index n_o=0.981, and relative extraordinary refractive index n_e=1,097 (Fig. 4) in the case of anisotropic scatterrers.

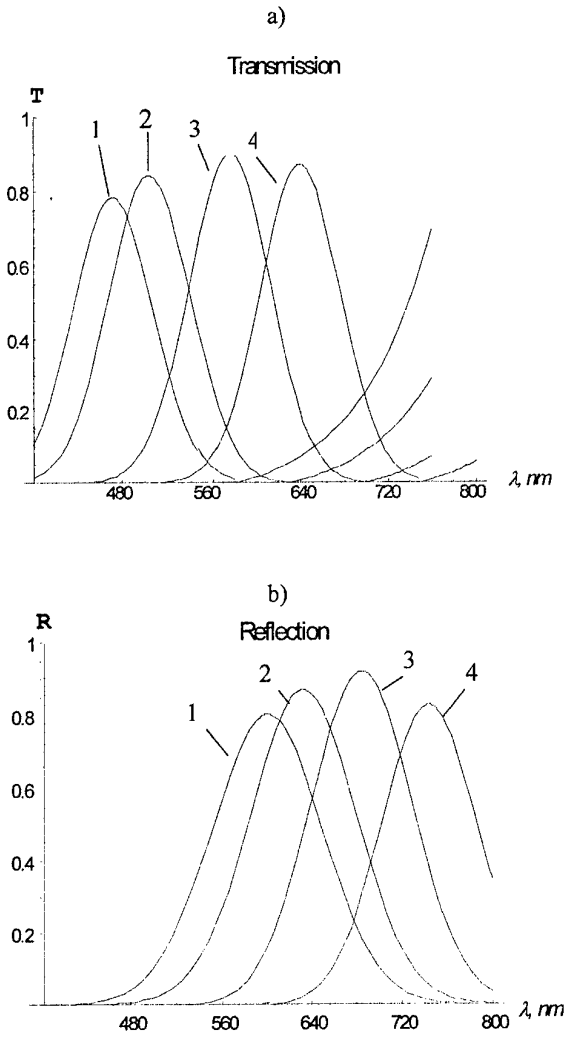

Fig.1. Spectral characteristics of reflection (a) and transmission (b) of light by multiplayer system of isotropic droplets at different incident angles: θ=0° (curve 1); 30° (2); 60° (3); 80° (4).

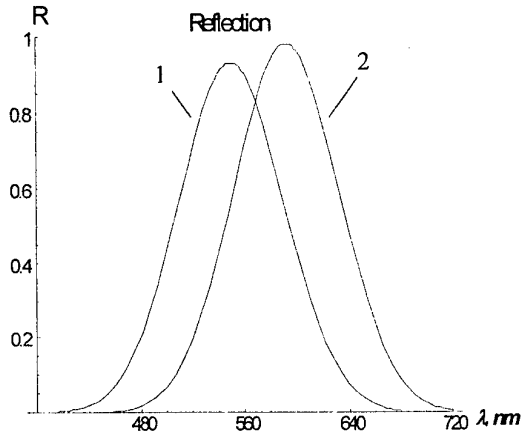

b)

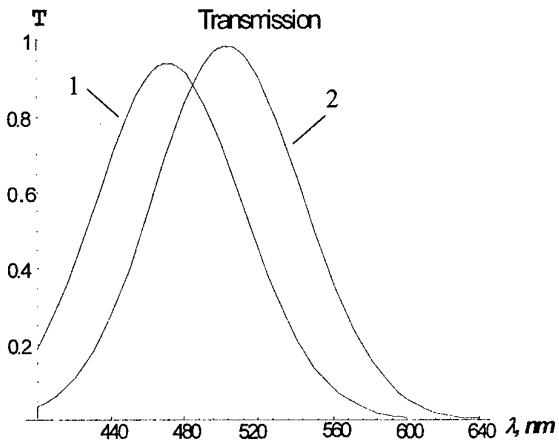

Fig.2. Spectral characteristics of transmission (a) and reflection (b) of light by multiplayer system of liquid crystal droplets at normal illumination.
1. Droplet directors are perpendicular to the film surface;
2. Droplet directors are parallel to the film surface.

Conclusion

We have proposed the model for calculation of coherent transmittance and reflectance for a film consisting from a set of monolayers of fine droplets. We investigated spectral behavior of reflection and transmission coefficients, diffraction efficiency on the optical characteristics of droplets, their concentration and number of monolayers in the film.

References

[1]. M. Jazbinsek, I. Drevensek Olenik, M. Zgonik, A.K Fontecchio, G. P. Crawford, "Characterization of holographic polymer dispersed liquid crystal transmission gratings", J. Appl. Phys., v.90, p.3831-3837(2001).

[2]. V.A. Loiko, V.I. Molochko, "Coherent Transmission and Reflection by a monolayer of Discrete scatterers", Part. Part. Syst. Charact., v.13, p. 227-233(1996).

[3]. S. Zumer, J.W. Doane, "Light Scattering from a small nematic droplet", *Phys. Rev.*, v.34, p.3373-3386, (1986).

[4]. A. Ishimaru, "Wave Propagation and Scattering in Random Media", Academic Press, New York, 1978.

NED-P8. Polymer-Dispersed Liquid Crystal Films: Multiple Scattering Regime Consideration

Valery A. Loiko, Vladimir V. Berdnik

Institute of Physics of the NASB, F.Scaryna ave. 68, 220072, Minsk, Belarus

Abstract

The model for calculation of radiative transfer in the PDLC films with regard to anisotropy of nematic liquid crystal droplets, the polydispersity of droplets, multiple scattering, and reflection on the boundaries of the layers has been developed. It can be used in wide range of optical thicknesses from small, when we can restrict ourselves by the single scattering approximation, to the large one, when we have to take into account multiple scattering of light. The results of calculations of angular structure of transmitted light at film illumination by the unpolarized light are presented.

Keywords: PDLC films, multiple scattering, contrast ratio, viewing angle.

Introduction

There are a lot of investigations on the problem of single scattering in PDLC films, but the investigations of multiple scattering in such films are only at the beginning. In this work a method for calculation of angular light distribution in PDLC films with spherical droplets is developed for oblique illumination by unpolarized light. The dependence of the unit volume parameters on the illumination direction, droplet polydispersity, and Fresnel reflection at the film interfaces are taking into account.

The method is applied for optically thin films, when multiple scattering is small, and optically thick films, when the contribution of multiple scattering is significant. It allows one to consider a gray scale for such films.

Radiative transfer equation

To describe light intensity in a PDLC film, the radiative transfer theory is used [1, 2]. In the isotropic case the scattering characteristics of a medium in the radiative transfer equation (RTE) are: scattering σ, absorption α, and extinction. $\varepsilon = \sigma + \alpha$ coefficients. These coefficients are connected with the scattering Σ_s, absorption Σ_α, and extinction Σ_e cross-sections by the relations: $\sigma = N\Sigma_s$; $\alpha = N\Sigma_\alpha$; $\varepsilon = N\Sigma_e$, N is the number of droplets per unit volume. One has to know too the phase function $X(\cos\gamma)$, which described the angular distribution of light scattered by the unit volume of the medium; γ is the scattering angle (the angle between the direction of the incident and scattered light);

$$\cos\gamma = \mu\mu' + \sqrt{1-\mu^2}\sqrt{1-\mu'^2}\cos(\varphi-\varphi'),$$

where $\mu = \cos\theta$ and $\mu' = \cos\theta'$ are the cosines of the axial angles of light scattered and incident on the unit volume; φ and φ' are the azimuthal angles of light scattered and incident on the unit volume, respectively. In the OFF state, when the droplets directors are oriented randomly, these characteristics do not depend on light propagation direction. In the applied field the elementary volume characteristics depend on light propagation direction, and the distribution of light in the layer has some peculiarities.

We consider bipolar droplets, assuming that the director configuration can be modeled as homogeneous. Some results on the opportunity to make this assumption were presented in [3, 4]. The more the difference between the ordinary refractive indices of a liquid crystal and a binder, the better is this assumption. The film is illuminated at angle θ_{0e} (Figure 1) from below by an azimuthally symmetrical light beam with intensity I_0. The light is scattered and absorbed by the droplets. A portion of the scattered light passes through the film and leaves it through the upper interface, the rest of the scattered light leaves the film through the lower interface. In the case of applied field, the PDLC film is an anisotropic, axial-symmetric system. The RTE for an anisotropic layer illuminated by a wide azimuthally symmetrical unpolarized light beam can be derived from the general equation [1] by integration on azimuth and taking into account directed light propagating upward and downward in the film [2, 5]:

$$\begin{aligned}\mu\frac{\partial I(z,\mu)}{\partial z} + \varepsilon(\mu)I(z,\mu) &= \\ = \int_{-1}^{1} X(\mu,\mu')\sigma(\mu')I(z,\mu')d\mu' &+ \\ + X(\mu,\mu_0)\sigma(\mu_0)I_0^{\uparrow}e^{-\frac{\varepsilon(\mu_0)z}{\mu_0}} &+ \\ + X(-\mu,\mu_0)\sigma(\mu_0)I_0^{\downarrow}e^{-\frac{\varepsilon(\mu_0)(z_0-z)}{\mu_0}} &,\end{aligned} \qquad (1)$$

Here $\mu_0 = \cos\theta_0$ is the cosine of the angle at which a parallel light beam propagates in the film; z is the film depth; z_0 is the film thickness; $I(z,\mu)$ is the azimuth-averaged intensity of light propagating at depth z at angle $\arccos\mu$; $\varepsilon(\mu)$ and $\sigma(\mu)$ are the extinction and scattering coefficients depending on the impinging light; $X(\mu,\mu') = \frac{1}{2\pi}\int_0^{2\pi} X(\mu,\mu',\varphi-\varphi')d\varphi)$. $I_0^{\uparrow}$ and $I_0^{\downarrow}$ are the intensities of collimated light beams, propagating upward and downward at the lower and upper interfaces inside the film.

Normally, the refractive indices of the polymer matrix and glass plates bounded the matrixare close in value. Therefore, we assume that no reflection occurs at the matrix-glass interface and restrict ourselves to the account of the Fresnel reflection at the air-glass (or plastic) interfaces.

We consider the scattering characteristics of the film in ON and OFF states.

The scattering and absorbing properties of the medium in the OFF state are determined by the phase function $X^-(\cos\gamma)$, the scattering coefficient σ^-, and the absorption coefficient α. These quantities are related to the scattering characteristics of separate droplets in the following way

$$\sigma^- = w\sigma_0^- = w\frac{\overline{\Sigma}_s}{v}, \qquad (2)$$

$$\alpha = (1-w)\alpha_0, \qquad (3)$$

$$X^-(\theta) = \frac{1}{\overline{\Sigma}_s}\frac{d\overline{\Sigma}_s}{d\Omega}(\theta), \qquad (4)$$

where v is the mean volume of liquid crystal droplets; w is the volume concentration of droplets; $\overline{\Sigma}_s$ is the scattering cross section averaged over the sizes and directions of droplet directors; $\sigma_0^- = \frac{\overline{\Sigma}_s}{v}$ is the scattering coefficient of liquid crystal droplets in the OFF state at unit volume concentration; $\frac{d\overline{\Sigma}_s}{d\Omega}(\theta)$ is the differential cross section of droplets averaged over the sizes and directions of droplet directors; α_0 is the absorption coefficient of the polymer.

In the ON state, the medium is characterized by the azimuth-averaged phase function $X^+(\mu,\mu')$, the scattering coefficient σ^+, and the absorption coefficient α.

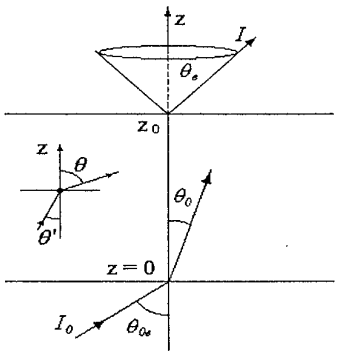

Figure 1. Schematic representation of scattering geometry in a film of thickness z_0 (section in the yz plane). Notations are in the text.

Optical parameters

To determine the unit volume parameters [6], we used the anomalous diffraction approach (ADA) [7]. We choose the log-normal size-distribution of droplets [8].

When the droplet directors are oriented perpendicular to the interface, the scattering coefficient can have a characteristic minimum whose position depends on the ratio between the refractive indices of the liquid crystal and the refractive index of the matrix [8]. In the OFF state, the value of the scattering coefficient does not depend on light propagation direction.

Contrast ratio

Contrast ratio (*CR*) depends on film properties, illumination and observation conditions. Initially we consider *CR* of a film illuminated by an azimuthally symmetrical conical wide light beam with vertex angle $\theta_e = \theta_{0e}$ of the cone (see Figure 1). A receiver collects transmitted light under the angle θ_{0e}.

Figures 2 and 3 show calculated dependencies of the contrast ratio. The account for scattered light leads to a decrease in the CR. The qualitative estimation of the scattered light influence for thin and thick films as well as the collection angle influence can be made for any practical situation using the above equations.

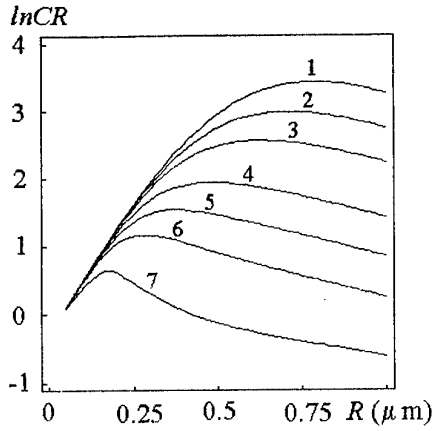

Figure 2. Dependence of $\ln CR$ on droplet radius at normal illumination by parallel beam for collection angle θ_c=1° (curve 1); 2° (2); 3° (3); 5° (4); 7° (5); 10° (6); 20° (7). n_e=1.7, $n_0 = n_m$=1.55, wz_0=10.

At normal illumination the dependence of contrast ratio *CR* on the radius at constant volume of droplets in the film is shown in Figure 4. It illustrates the situation when the receiver fully collects directly transmitted light and a part of scattered light. The latter is determined by the collection angle θ_c. With the increasing collection angle, the position R_m of the maximum on the dependence *CR-R* shifts to the smaller values. The shift of R_m to the smaller size values is due to an increasing contribution of multiply scattered light with the increasing collection angle.

At diffuse illumination CR values are smaller then at parallel beam illumination (Fig.3).

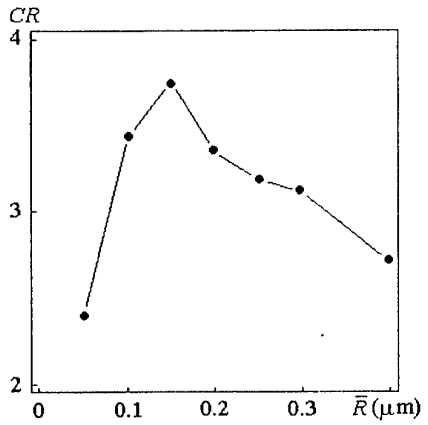

Figure 3. Dependence *CR* on mean droplet radius at diffuse illumination. C_v=0.2, n_e=1.7, $n_0 = n_m$=1.52, λ_0=0.5μm; $w \cdot z_0 = \dfrac{N \cdot v}{S} = 30\mu m$.

Conclusion

The proposed model allows to analyze the angular characteristics of reflected and transmitted light, contrast ratio as a function of illumination conditions, collection angles, spectral range of incident light, size and concentration of droplets, applied field, and director field configuration in the droplet. Some of the results can be used for the consideration of another types of composite LC films, where the multiple light scattering regime is achieved [9].

Acknowledgment

The research described in this publication was made possible in part by European Commission in the frame of INCO-Copernicus program (contract No. ERB IC15-CT98-0806).

References

1. Liou K.N. An introduction to atmospheric radiation (Academic Press, New York, 1980).
2. Loiko V.A., Berdnik V.V. "Multiple scattering in polymer dispersed liquid crystal films". Liquid Crystals. Vol. 29, pp. 921-928 (2002).
3. Loiko V.A. and Molochko V.I. "Polymer dispersed liquid crystal droplets: methods of calculation of optical characteristics". Liquid Crystals. Vol. 25, pp. 603-612 (1998).
4. Loiko V.A. and Molochko V.I. "The influence of the director field structure on extinction and scattering by a nematic liquid crystal droplet". Applied Optics. Vol. 38, pp. 2857-2861 (1999).
5. Loiko V.A., Berdnik V.V. "Radiative transfer in a layer with oriented spheroidal particles". J. Quantitative Spectroscopy & Radiative Transfer. Vol. 63, pp. 369-382 (1999).
6. Chandrasekhar S. Radiative transfer (Dover, New York, 1960).
7. Zumer S. "Light scattering from nematic droplets: Anomalous diffraction approuch". Phys.Rev. Vol. 37, pp. 4006-4015 (1988).
8. Drzaic P.S. Liquid crystal dispersions (World Scientific, New York, 1995).
9. Crawford G.P., Zumer S. (editors) Liquid crystals in complex geometries formed by polymer and porous networks (Taylor & Francis, London, 1995).

NED-P9. Interference Oscillations in Dynamics of Electrooptical Response of Nematic PDLC Films

A.V. Barannik, V.Ya. Zyryanov, V.F. Shabanov, V.A. Loiko*
L.V. Kirensky Institute of Physics, Akademgorodok, Krasnoyarsk 660036, Russia
*Institute of Physics, F. Scaryna Avenue 68, Minsk 220072, Belarus

Abstract

The dynamics of optical response of the films based on polymer dispersed nematic liquid crystal (PDNLC) under the action of rectangular electrical pulses is investigated. The oscillations of the curve of light transmission in composite films with large size nematic droplets are detected. The comparative analysis with the data of independent studies, where the volt-contrast curves were measured in a static mode, proves interference nature of the detected oscillations.

Introduction

Oscillations of transmittance curves depending on applied voltage which were measured in a static mode for monolayer PDNLC films have been earlier found and investigated in [1-6]. The effect is caused by the interference of light waves passed through LC droplets and through the polymer matrix between the droplets in a forward direction. Reorientation of a director inside nematic droplets under the action of an electric field applied to the composite film results in a change of phase retardation between two above-mentioned light waves causing the oscillatory behavior of volt-contrast curves. The number of maximums and minimums on the oscillatory curves is proportional to lateral size of nematic droplets.

The static mode is characterized by long time (10 s and more) of an increase of applied voltage contrasting with a typical value of reorientation time of nematic droplets (1 ÷10 ms). In optoelectronic devices, for example, in flat displays, the discrete addressing with high-frequency electric pulses influencing on separate elements of a screen is used. For this case, the study of the influence of interference effects on the optical response of PDNLC films controlled in a dynamic mode, when the duration of an electrical pulse is close to the characteristic time of reorientation of the nematic droplets is of great interest.

First report on study of interference oscillations in dynamic response in monolayer PDNLC films have appeared in [7], but the data was obtained for the sample with chaotic orientation of bipolar axes of nematic droplets inside the film. It has hindered to make thorough measurements and so the interference effects have been observed only for the descending part of optical response pulse. In this report we present the results of the study of uniaxially oriented PDNLC films.

Experimental

Films were made by a well-known PIPS-method [8] with use of photocured optical adhesive NOA-65 (Norland Products, Inc) as a polymer matrix and a nematic mixture of derivatives of alcylcyanobiphenyls similar to E7 (Merck) in weight ratio 1:1. The prepared homogeneous solution of initial components was placed between glass substrates coated ITO and divided by spacers with a thickness 10 micrometers. For the cure of photopolymer matrix, the mercury lamp was used. By means of a variation of technological parameters (temperature and an intensity of ultraviolet light) it is possible to control an average size of LC droplets inside the film. Before completion of curing of polymer matrix, when its plasticity still remains, the substrates were sheared relatively to each other to form the uniaxially oriented ensemble of elongated nematic droplets having monolayer arrangement inside polymer film (see an insert in Figure 1).

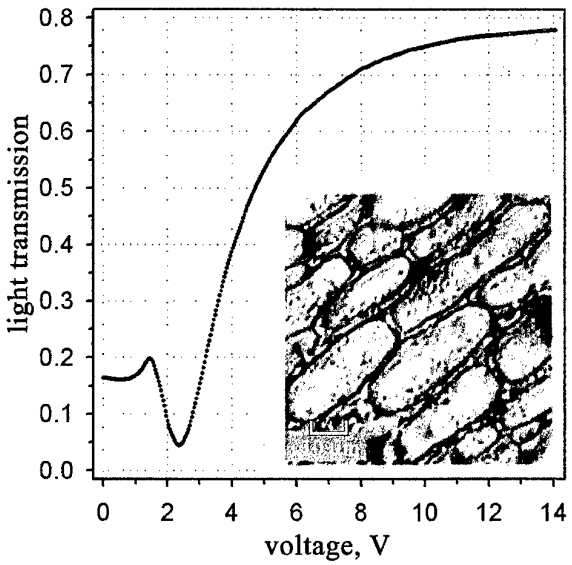

Figure 1. The dependence of the transmittance of sheared PDNLC film on applied electrical field and a microphoto of its fragment.

The measurement of electrooptical characteristics was carried out for a monochromatic radiation of He-Ne laser with wave-length 0.633 μm. Behind a sample the diaphragm was installed to cut off scattered light for detection only a direct transmitted light. Light transmission depending on applied voltage was measured for the alternating rectangular signal (500 Hz) with slowly increasing amplitude (1 V/s). The dynamics of optical response of PDNLC films was examined

depending on amplitude of the single rectangular electrical pulses by duration 3 ms.

Results and discussion

A microphoto of a fragment of the film sample and volt-contrast characteristics measured in a static mode corresponding to it is shown on figure 1. Polarization of a laser beam here coincides with a preferred orientation in film plane of the long axes of nematic droplets. Essential difference of a form of the curve (similar to the one measured in [7]) from typical S-shaped is observed. As was predicted in [7], the same oscillations should be revealed in transmittance curves of the dynamic response. The data obtained here confirm it.

Figure 2 shows the oscillograms of optical response for a series of square pulses with the amplitude from 3 to 15 volt. It should be noted that the oscillations are observed not only for relaxation curves (as in [7]) but for the rise-up portion of optical response too. The positions on a time axis of minimums and maximums of transmittance curves and their amplitudes have complicated dependence on the value of a control signal. In particular, in an operate time of a pulse the first maximum is observed only on three curves corresponding to voltage 3, 4.5, and 6 V. Both in static and in dynamic case the light transmission of a composite film in a minimum point has smaller value, than in an initial state before an action of the electrical pulse. It shows the possible way to increase the modulation depth.

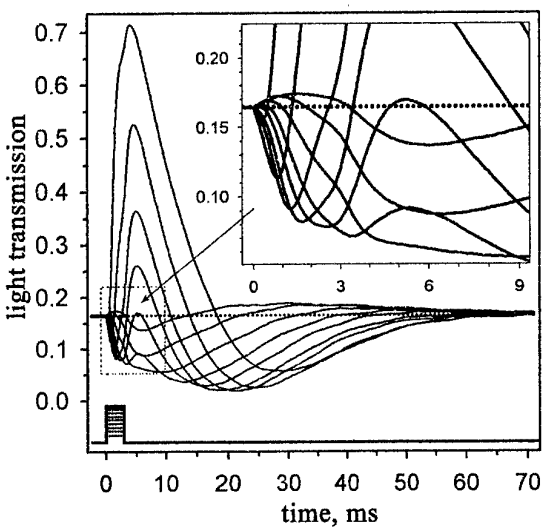

Figure 2. Oscillograms of optical response of PDNLC film for a series of square pulses with amplitude 3-15 volt.

Conclusion

The observations of oscillatory character of the optical response of uniaxially oriented PDNLC films at effect of rectangular electrical signal are represented. The comparison with the data of works [1-6] confirms the interference nature of the detected oscillations. It is necessary to underline, that the dynamic pattern of optical response of composite films generally may have very complicated form since the influence of the different phenomena is possible. For example, the action of an electric field induced by spatially separated charge of impurity ions [9, 10], appearance of defects and domains [11], re-structuring of a droplet-polymer boundary [12, 13] and others. Thus, the outcomes of this research show the necessity to take into account the contribution of interference effects for the complex analysis of dynamic electrooptical characteristics of PDLC films.

References

1. Zyryanov V.Ya., Presnyakov V.V., Shabanov V.F. Fredericksz effect in polymer dispersed nematic droplets. Tech. Phys. Lett., V.22, No14, p.22-26 (1996).
2. Shabanov A.V. Presnyakov V.V., Zyryanov V.Ya., Vetrov S.Ya. Characteristics of the process of reorientation of bipolar drops of a nematic with rigidly fixed poles. JETP Letters, V.67, No9, p.733-737 (1998).
3. Shabanov A.V., Presnyakov V.V., Zyryanov V.Ya., Vetrov S.Ya. Bipolar nematic droplets with rigidly fixed poles in the electric field. Mol. Cryst. Liq. Cryst., V.321, p.259-270 (1998).
4. Presnyakov V.V., Zyryanov V.Ya., Shabanov A.V., Vetrov S.Ya. Friedericksz threshold in bipolar nematic droplets with rigidly fixed poles. Mol. Cryst. Liq. Cryst., V.329, p.27–34 (1999).
5. Konkolovich A.V., Presnyakov V.V., Zyryanov V.Ya., Loiko V.A., Shabanov V.F. Interference quenching of light transmitted through a monolayer film of polymer dispersed nematic liquid crystal. JETP Letters, V.71, No12, p.486-488 (2000).
6. Zyryanov V.Ya., Presnyakov V.V., Serebrennikov A.N., Shabanov A.V., Loiko V.A., Konkolovich A.V. High contrast light modulator based on PDNLC monolayer. Mol. Cryst. Liq. Cryst., V.368, p.3983-3990 (2001).
7. Barannik A.V., Shabanov A.V., Zyryanov V.Ya. Interference oscillations in the dynamics of the optical response of polymer dispersed nematic liquid crystals. Tech. Phys. Lett., V.28, No8, p.675-677 (2002).
8. Zharkova G.M., Sonin A.S. Liquid crystal composites. Novosibirsk, Nauka, 214 p. (1994).
9. Aphonin O.A., Nazvanov V.F., Novikov A.V. Modulation on double frequency in encapsulated nematic liquid crystals. Tech. Phys. Lett., V.15, No6, p.33-37 (1989).
10. Zhujkov V.A., Shabanov V.F., Zharkova G.M., Vladimirov V.M. Electrooptic effects in encapsulated liquid crystals. Mol. Cryst. Liq. Cryst., V.179, p.377-381 (1990).
11. Shimada E., Uchida T. Control of polymer dispersed liquid crystal (PDLC). Jpn. J. Appl. Phys., V.31, Part.2, No3B, p.L352–L354 (1992).
12. Barannik A.V., Smorgon S.L., Zyryanov V.Ya., Shabanov V.F. Stability of light transmission of optical shutters based on PDNLC. J. of Optical Technology, V.64, No5, p.99-101 (1997).
13. Cupelli D., Macchione M., Nicoletta F.P., De Filpo G., Chidichimo G. Electrically induced changes in polymer dispersed liquid crystals. Appl. Phys. Let., V.76, No20, p.2856-2858 (2000).

NED-P10. Texture and Optical Properties of Stretched Composite Films Doped by Lecithin

O.O. Prischepa, V.Ya. Zyryanov*
SKTB «Nauka» SB RAS, Krasnoyarsk 660049, Russia
*L.V. Kirensky Institute of Physics, Akademgorodok, Krasnoyarsk 660036, Russia

Abstract

Uniaxially oriented films of polymer dispersed liquid crystals based on polyvinylbutyral-5CB composition doped by lecithin were prepared. Texture and optical properties of the films depending both on elongation parameter and concentration of lecithin were studied. Specific features of electrooptical response of the samples are discussed.

Keywords: polymer dispersed liquid crystals, nematics, director configuration, homeotropic anchoring, light polarization, electrooptical materials

Introduction

Uniaxially oriented films of polymer dispersed nematic liquid crystal (PDNLC) with tangential interface have been investigated in detail earlier [1-4]. Nematic droplets in such films have a bipolar director configuration and are oriented in the same direction, laying in film plane [1-4] or under a small angle to it [5]. Uniaxially oriented PDNLC films evince a number of interesting properties. They can have the large anisotropy of light scattering (light transmission), which magnitude can been operated by applied electric or magnetic field [6]. Interference oscillations of volt-contrast curve [7, 8] are clearly shown in them, and the effect of interference quenching of light [9] can be observed. Due to these properties such materials are large interest for display application.

The addition of various surfactants in PDLC film allows to change essentially boundary conditions, to form new director configurations and, hence, to change macroscopic optical and electrooptical characteristics of a material qualitatively. This work aims at researches of PDNLC films with addition of lecithin which is well-known surfactant, providing homeotropic anchoring of nematic molecules on the interface [10].

Sample preparation

Polyvinylbutyral (PVB) of 1PP mark (Russia standard) was used as a matrix polymer. This polymer is dissolved in many solvents, is transparent in visible range of a spectrum and provides planar anchoring with molecules of mesomorphic derivatives of alcylcyanobiphenyls. Glass-transition temperature of PVB is $T_g = 57°C$, temperature of chemical decomposition at contact to air is 160°C. A refractive index $n_p = 1.488$ at $T_c = 22$ °C ($\lambda = 0.633\mu m$). Widely used nematic 4-n-penthyl-4′-cyanobiphenyl (5CB) has been chosen for LC component. It has temperatures of transitions crystal-(22 °C)-nematic-(35 °C)-isotrop and $\Delta\varepsilon > 0$. At T = 22 °C ($\lambda = 0.633\mu m$) refractive index of 5CB $n_{\parallel} = 1.717$ and $n_{\perp} = 1,531$.

The samples of PDNLC film have been prepared by SIPS method with the use of ethyl alcohol (spirit) as the common solvent for all used components. In process of phase separating a part of NLC (up to 20 %) remains dissolved in polymer, matching a refractive index of a matrix to $n_{\perp}$ 5CB. Besides dissolved nematic plasticizes a polymer matrix so that at room temperature the composite film remains plastic, allowing to modify it easy in uniaxially oriented state by the stretching. or shear. Lecithin was used in the form of the alcohol solution of 2.5 % concentration. The contents of each component: $C_{LC} = 55$ %, $C_{PVB} = 41.5 \div 45$ % and $C_{lec} = 0 \div 3.5$ %. Adjusting speed of evaporation of solvent, and also a composition, it is possible to vary the size of droplets and morphology of PDNLC film. On the average the droplets diameter was equal 1÷5μm.

Results and discussion

In PDNLC films under study the director configuration inside nematic droplets strongly depends on the concentration of lecithin (see Figure 1). Thus it is possible to define three various intervals of concentration of the lecithin, characterized by specific orientational structures of droplets. At a small concentration of lecithin (< 0.1 %) formed droplets basically have a classical bipolar configuration of director (see Figure 2). In the range of middle concentrations (0.1 % < C_{lec} < 3.5 %) formation of droplets with different orientational structures (Figures 2-5) is possible. In the whole of ensemble the bipolar droplets (Figure 2) remain in a small amount (less than 5 %). Besides the droplets with a radial configuration of director (Figure 3), a toroidal configuration (Figure 5) and having a structure of surface hedgehog (Figure 4) are observed.

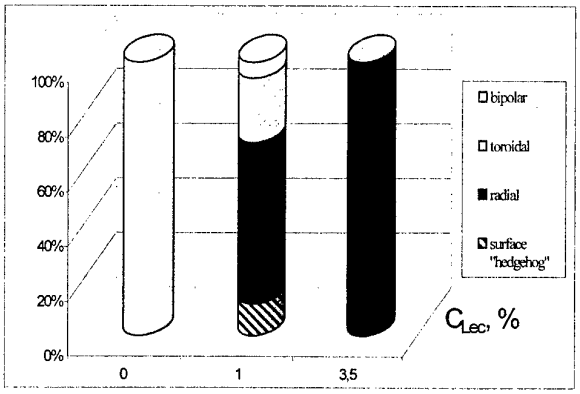

Figure 1. Diagram of relative content of NLC droplets with a different director configuration in PDLC film depending on concentration of lecithin.

Bipolar configuration

Here poles (two point defects or so-named «boojums» [11]) are localized on the opposite sides of droplets. In the crossed polarizers dark strips in the form of hyperboles are seen, they proceed gradually extending from point defects. If the axis of symmetry of a droplet coincides with a direction of any polarizer (Figure 2a-b), dark strips merge in a cross with the expanded central part.

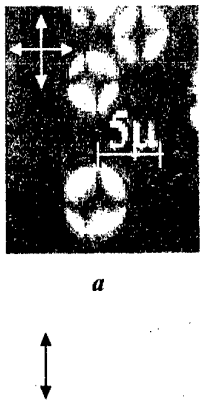

a

b

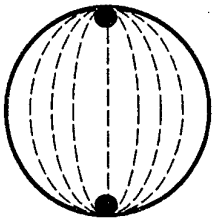

c

Figure 2. Texture of bipolar nematic droplets, **a**, in geometry of crossed polarizers; **b**, with only a single polarizer; **c**, bipolar configuration of the director inside a droplet.

Point defects are especially distinctly visible at observation with a single polarizer (Figure 2b).

Radial structure

The formation of a radial configuration (Figures 3a-b) is caused by homeotropic orientation of the nematic on the interface due to the addition of lecithin. Here each droplet at observation in a polarizing microscope in geometry of the crossed polarizers (Figure 3a) show four dark zones forming a figure of the Maltese cross which orientation does not change at turn of the PDNLC sample. In the center of droplets a point defect, so-called «a radial hedgehog» [11] (Figure 3b) locates. It should be noted that a weak bend of the cross figure may be evidence of the presence of a small amount of chiral impurity in lecithin since it was received from a biological material for the medical purposes.

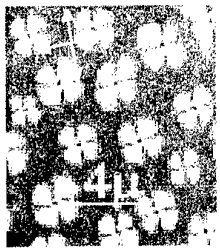

a

b

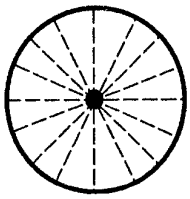

c

Figure 3. Texture of radial droplets of LC 5CB doped by lecithin (C = 0.5 %), **a**, in crossed polarizers; **b**, observation with a single polarizer; **c**, radial configuration of director inside nematic droplet.

Configuration of surface «hedgehog»

Earlier [11] it has been shown, that for homeotropic anchoring the formation of another orientational structure in which point defect is located on a surface of nematic droplet (Figures 4a-b) is also possible. Apparently, the reason of formation of such a structure in the same film, in common with structure (Figures 3a-b), can be the difference of both the form of LC droplets and the local concentration of surfactant.

Toroidal structure

The droplets shown in Figures 5a-d, have the most complicated structure which has not been described earlier. In this case in the center of droplet the dark area is seen in crossed polarizers. In the lateral areas of droplet the concentric lines similar to lines observed in the spherulite structure of cholesteric droplets [12,13] are seen. However radial disclination in the nematic droplets is absent. Such a texture can be formed by the toroidal configuration of director submitted in

Figures 5a,b. In the center of droplets the area where nematic director is oriented perpendicularly to a plane of PDLC film is formed. On a lateral surface of droplet director is oriented tangentially and lies in the plane of film. Along radius the chiral torsion deformation of director is realized. In the shown case the turn of director is approximately equal 270° (the reasons of chirality of used lecithin were discussed above). The toroidal configuration is observed in the droplets having the maximal size for the given sample. It is possible, that this type of orientational structure is caused by strongly flattened form of droplets.

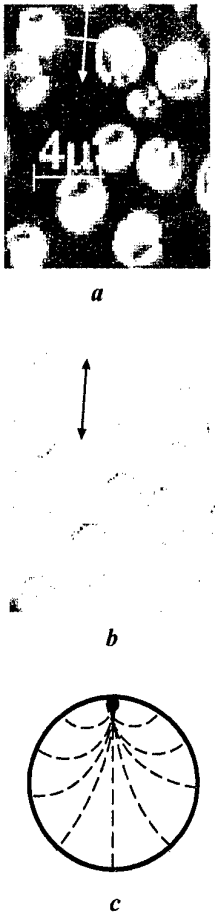

a

b

c

Figure 4. Texture of nematic droplets doped by lecithin (C = 1%) with a structure of surface «hedgehog», **a**, in crossed polarizers; **b**, with a single polarizer; **c**, director configuration of nematic droplet with surface point defect.

For the range of concentrations of the lecithin exceeding 3.5%, the majority of nematic droplets have a radial configuration (see Figure 3a-c).

Stretching deformation of PDNLC films results in a transformation of orientational structures of all droplets. At that the bipolar configuration of director is formed in the most part of droplets ensemble, as well as in PDNLC films without lecithin. Therefore, for stretched PDNLC films doped by lecithin the anisotropy of light scattering (light transmission) is also characteristic.

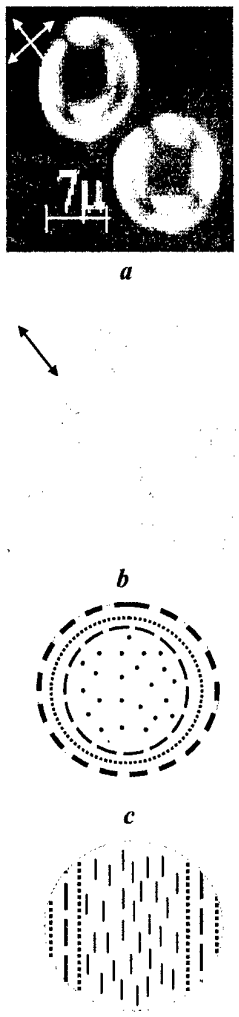

a

b

c

d

Figure 5. Texture of toroidal droplets of NLC doped by lecithin (C = 1 %).**a**, in crossed polarizers; **b**, only with a single polarizer; **c**, director configuration inside droplets for plane and **d** for lateral cross-section of toroidal droplet of nematic.

The elongated nematic droplets doped by lecithin are shown in Figure 6. Here two point defects localized on the end of long axis of droplets are seen clearly.

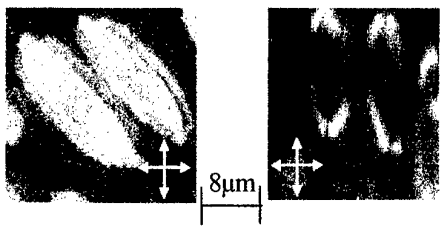

Figure 6. Texture of stretched PDNLC film doped by lecithin (C = 2 %) in crossed polarizers. The initial thickness of the prepared film was near 18μm., a strain consists of 170 %.

Light transmission of stretched PDNLC film doped by lecithin on applied voltage is presented on Figure 7.

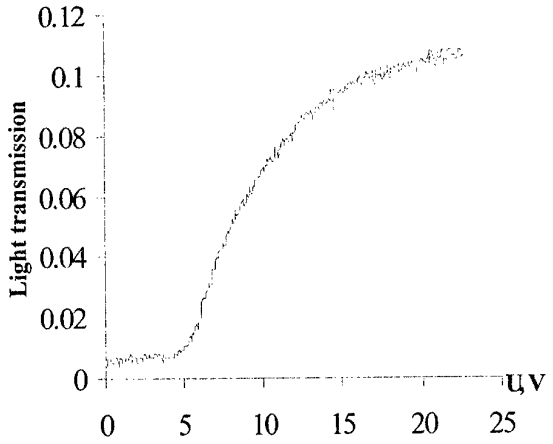

Figure 7. Transmittance of parallel component of the light passed through the stretched PDNLC film (thickness is 9μm, droplets size 3 ÷ 5μm) depending on applied voltage.

Here, a threshold character of dependence is observed, as well as in uniaxially oriented PDNLC films without lecithin. For the film under study light transmission remains constant up to voltage 5V, further sharply grows and reaches the saturation in a translucent state. It should be noted, that uniaxially oriented nematic PDLC films in our case show a reduction of the threshold and saturation fields more than 20 % in comparison with the similar parameters obtained for same films without a lecithin.

Conclusion

Textures and director configurations of nematic droplets which can be formed in PDLC films doped by various amount of lecithin are described.

Besides well-known types of orientational structures, the toroidal configuration of director can be formed inside the droplets. At stretching of PDNLC film the most part of the droplets becomes bipolar, and composite film therefore, shows a great macroscopic anisotropy of optical properties.

New specific feature of electrooptical materials and devices based on such PDNLC films may be a low control voltage due to a weakening of tangential anchoring of nematic at the interface.

References

1. Pat. 4.685.771 US, МКИ G02F 1/13. Liquid crystal display material comprising a liquid crystal dispersion in a thermoplastic resin / J.L. West, J.W. Doane, S. Zumer. -- Publ. 11.08.87.
2. Zyryanov V.Ya., Smorgon S.L., Shabanov V.F. Elongated films of polymer dispersed liquid crystals as scattering polarizers. Molecular Engineering, V. 1, №4, p. 305–310, 1992.
3. Aphonin O.A., Panina Yu.V., Pravdin A.B., Yakovlev D.A. Optical properties of stretched polymer dispersed liquid crystal films. Liq. Cryst., V. 15, No3, p. 395–407, 1993.
4. Amimori I, Priezjev N.V., Pelcovits R.A., Crawford G.P. Optomechanical properties of stretched PDLC films for Scattering polarizer applications. J. Appl. Phys., V. 93, No6, p. 3248-3252, 2003.
5. Whitehead J.B., Zumer S., and Doane J.W. Light Scattering from a Dispersion of Aligned Nematic Droplets. J. Appl. Phys., V. 73, No3, p. 1057--1065, 1993.
6. Zyryanov V.Ya., Presnyakov V.V., Shabanov V.F. Fredericksz effect in polymer dispersed nematic droplets. Tech. Phys. Lett. (Rus), V.22, No14, p.22-26, 1996.
7. Shabanov A.V., Presnyakov V.V., Zyryanov V.Ya., Vetrov S.Ya. Specific features of reorientation process of bipolar nematic droplets with rigidly fixed poles. JETP Letters, V.67, No9, p. 733-737, 1998.
8. Shabanov A.V., Presnyakov V.V., Zyryanov V.Ya., Vetrov S.Ya. Bipolar nematic droplets with rigidly fixed poles in the electric field. Mol. Cryst. Liq. Cryst., V.321, p.245-258, 1998.
9. Konkolovich A.V., Presnyakov V.V., Zyryanov V.Ya., Loiko V.A., Shabanov V.F. Interference quenching of the light passed through the monolayer film of polymer dispersed nematic liquid crystal. JETP Letters, V.71, No12, p. 486-488, 2000.
10. Cognard J. Alignment of nematic liquid crystals and their mixtures. Gordon and Breach Science Publishers, Paris, 1982, 104 p.
11. Volovik, G.E, and Lavrentovich O. D. Topological dynamics of defects: boojums in nematic droplets. JETP, V. 85, No85, p.1159-1166, 1983.
12. Robinson C., Ward JC., Beevers R.B. Liquid crystalline structure in polypeptide solution. Discuss. Faraday Soc., V.25, p.29-42, 1958.
13. Candau., Le Roy P., and Debeauvais F. Magnetic field effects in nematic and cholesterics droplets suspended in an isotropic liquid, Mol. Cryst. Liq. Cryst., V.23, p.283-297, 1973.

NED-P11. Uniaxially Oriented Films of Polymer Dispersed Liquid Crystals: Preparation, Physical Properties and Display Applications

V.Ya. Zyryanov

L.V. Kirensky Institute of Physics, Akademgorodok, Krasnoyarsk 660036, Russia

Abstract

The brief review on uniaxially oriented films of polymer dispersed liquid crystals including nematics, cholesterics and ferroelectric smectics are presented. Various methods of the modification of composite films in uniaxially oriented state, their structure, electrooptical properties and the projection of these materials for the future application in display devices are discussed.

Keywords: polymer dispersed liquid crystals, nematics, cholesterics, ferroelectric smectics, light polarization, light modulation, electrooptical materials

Introduction

For the first time the uniaxially oriented films (UOF) of polymer dispersed liquid crystals (PDLC) have been prepared and investigated by Sonin et. al. [1]. They have found that uniaxially stretched films of polymer dispersed cholesterics liquid crystals (PDChLC) show anisotropy of selective light scattering and transmission spectrum.

The idea to use a similar effect in uniaxially stretched or sheared films of polymer dispersed nematic liquid crystals (PDNLC) for manufacturing a scattering polarizer has been patented in [2]. In this case the bipolar nematic droplets in composite film have ellipsoidal form with the long axes oriented along a direction of deformation (Fig. 1). As follows from [3,4], the bipolar axes of director configuration in such droplets coincide with their long axes. If a refractive index of polymer n_p is equal to perpendicular component of refractive index $n_{\perp lc}$ of LC,

$$n_p = n_{\perp lc} \qquad (1)$$

light polarized perpendicularly to the stretching passes through a film and light polarized along the stretching, is intensively scattered.

It should be noted, that a shear deformation of composite film generally results in orientation of ensemble of LC droplets not in a plane of a film, but under some angle to it, for example, near 30° [5].

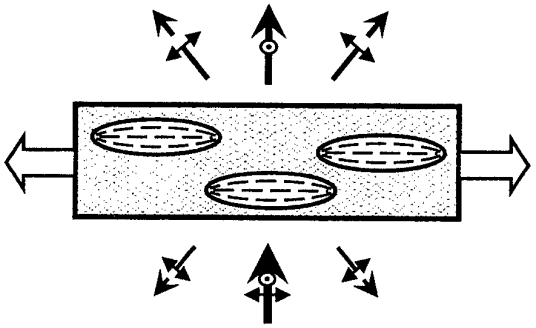

Fig. 1. Polarization of light passed through the stretched PDLC film with uniaxially arranged ensemble of elongated bipolar nematic droplets [2].

There are also other ways to create uniaxially arranged ensemble of LC droplets. For example, if to apply electric or magnetic field in a plane of composite LC film during the polymerization of a matrix, there will be the unidirectional orientation of ensemble of LC droplets after switching off a field [6], but in this case not due to deformation of droplets, and to orienting influence of polymeric walls which macromolecules are aligned alone a field.

Another way of manufacturing of UOF PDLC with using of anisotropically photocured polymer matrix [7,8] in which an uniaxially ordering of macromolecules occurs under exposure to a linearly polarized light is very promising for the display applications.

The paper presents the brief review on the research and development of UOF PDLC carried out mainly in L.V. Kirensky Institute of Physics by author with the collaborators [9-31].

Uniaxially oriented films of nematic PDLC

We carried out special works on optimization of manufacturing techniques and study of performance of UOF PDNLC [7, 9-16]. Fig. 2 shows perpendicular $T_\perp$ and parallel $T_\parallel$ component of light transmission and contrast ratio $T_\perp/T_\parallel$ in dependence of elongation parameter $\Delta L/L_0$. The value of $T_\perp/T_\parallel \approx 410$ at $\Delta L/L_0 = 0.5$, that corresponds to an efficiency of high-quality conventional polarizers based on light absorption anisotropy. This value is not a limit, it may be raised, for example, in more thick films, but the transmittance of perpendicular component will decrease. Reduction of the $T_\perp/T_\parallel$ ratio at $\Delta L/L_0 > 0.5$ is entirely caused by thinning of composite film, since the anisotropy of light scattering coefficient $(k_\parallel - k_\perp)$ in this interval of elongation values smoothly grows [9].

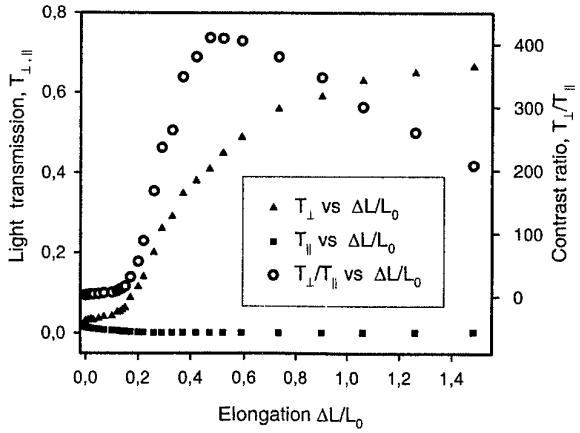

Fig. 2. Anisotropy of transmittance of He-Ne laser beam in stretched PDNLC film [9].

The operational temperature range of the scattering polarizers correlates with an interval of LC mesophase. As against the prism polarizers, UOF PDLC film are compact and simple in manufacturing, as well as absorbing polarizers. But in comparison with the last they have conclusive advantages. Firstly, PDLC films can be used for polarization of powerful radiation, because "unnecessary" light component scatters by this material, and it is heating less, than absorbing polarizers in which such component of light is absorbed causing their destruction. Secondly, PDLC films effectively polarize light in all visible and near infrared range (where condition (1) remains valid), while absorbing polarizers only inside absorption band of dichroic dyes.

Nevertheless the most interesting difference from absorbing polarizers is the opportunity to operate polarizing efficiency of UOF PDLC by using electric field. The typical kind of transmittance curves and $T_\perp/T_\parallel$ ratio of scattering polarizers depending on applied voltage are shown in Fig. 3.

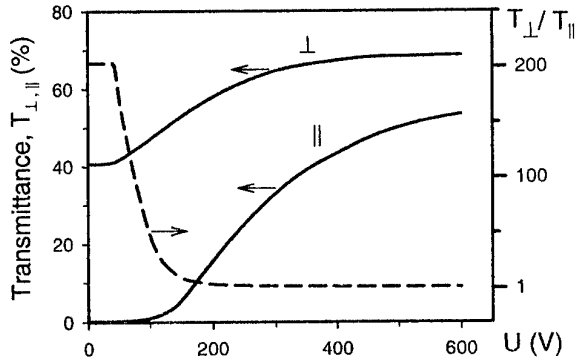

Fig. 3. Anisotropy of light transmission of UOF PDNLC depending on applied voltage.

Another effect having a great potential for display applications is an interference oscillation of volt-contrast curves in monolayer arranged LC droplets having sufficiently large size [10-16] (see Fig. 4). We have demonstrated considerable increase of contrast ratio due to effect of interference light quenching in monolayer UOF PDNLC with low-voltage operation [14,15].

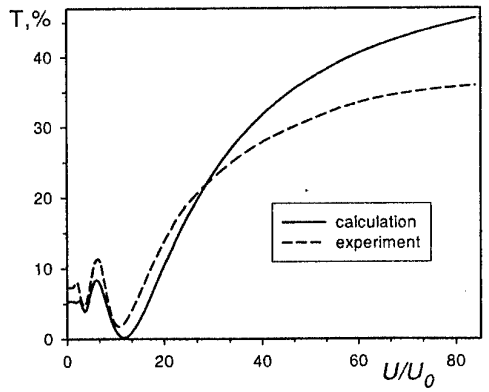

Fig. 4. Calculated and experimental curves of parallel component of light transmission in monolayer UOF PDLC film depending on applied voltage divided by threshold field [14,15].

Uniaxially oriented films of cholesteric PDLC

More complicated effects are observed in UOF of polymer dispersed cholesterics (chiral nematic) liquid crystals (PDChLC) [17-20]. Director configuration, its transformation in electric field, optical response of such films dependent very strong on the concentration C_{ch} of chiral dopant in nematic. For small C_{ch} value the droplets structure and volt-contrast curves of composite films is similar to the one without dopant. Dramatic changes of these parameters reveal for the middle C_{ch} values [17-19]. Figure 5 shows the transmittance properties of light polarized component and their ratio for UOF PDChLC based on butyral resin and cyanobiphenyls mixture with 5 % of cholesterylacetate as a chiral dopant As can see, these films can be in three different optical states: to scatter the light of any polarization, to scatter only one linearly polarized component, to be transparent for the whole of light beam. Thus we have developed the electrooptical material for polarization-selective modulation of light. For the high C_{ch} value volt-contrast curves of UOF PDChLC have additionally the range characterized by inversion of $T_\perp/T_\parallel$ ratio [20].

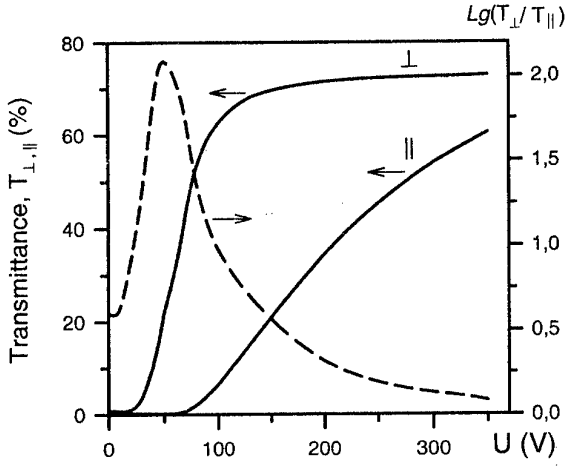

Fig. 5. Anisotropy of light transmission in UOF PDChLC depending on applied voltage [19].

Strainless PDChLC films reveal big hysteresis of the volt-contrast characteristic that allows using them effectively in displays with the passive-matrix addressing. Besides we have found out the effect of electro-thermooptical bistability in such films and shown the opportunity of its use for thermooptical reversive recording of the information [21,22]. By using this data the method of laser-addressed recording of the information in bistable PDChLC films doped by dye in normal and inverse scattering mode was developed [22].

Uniaxially oriented PDLC films based on ferroelectric smectics

Novel high response composite material representing an uniaxially oriented films of polymer dispersed

ferroelectric liquid crystals (PDFLC) has been developed by us and for the first time presented in [23,24]. Characteristics of PDFLC films depending on material constants of FLC and polymer, smectic layers configuration inside droplets, morphology of a film (the size, form of droplets and their relative arrangement), parameters of control field have been studied. The manufacturing techniques of the films are necessary to optimize so that anisotropy of transmittance will be maximal. The information on specificity of manufacturing methods, used composition of UOF PDFLC films, their structural, optical and electric properties is submitted in [25-31].

The high optical anisotropy of PDFLC film is achieved only in the samples with the droplets possessing a wavy type structure (Figure 6a,b). If a long axis of such droplets is aligned along one of the crossed polarizers, the brightness of the droplets is minimum and the texture presents two and more dark lines which are oriented parallel or at a small angle to the long axis. The droplets show the maximum brightness if its long axes form an angle 45° with the polarizers.

In geometry of a single polarizer the interface of elongated FLC droplets with wavy type structure is looked as a solid line, if the long axes is oriented parallel to the light polarization [29,30]. It means that there is a high gradient of refractive index on the droplets boundary and corresponds to the intensive scattering of the incident light. For the perpendicular orientation of light polarization, the interface line smears due to the optical homogeneity of the structure. In this case, the light passes through the film without considerable scattering.

a)

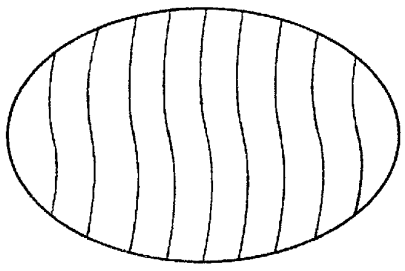

b)

Fig. 6. Microphoto of FLC droplet (a) with wavy type disclinations and corresponding arrangement of smectic layers (b) inside the droplets [29,30].

There are two basic ways to modulate the light intensity by using PDFLC films. Firstly, PDFLC films can be used as a phase plate placed in traditional layout between two polarizers. The second method is based on the using of light scattering effect [23-31]. The design of light scattering PDFLC modulators in its turn may be both with a single polarizer [23-27,31] and polarizer-free [28].

The PDFLC modulator with a single polarizer [23-27,31] (see Figure 7) consists of two glass substrates with transparent electrodes on the internal surfaces and uniaxially oriented PDFLC film between them. Light polarizer places before or after the sandwich. The components of PDFLC material are chosen so that the refractive index of polymer is equal to the index of ordinary ray (in uniaxially approximation) in liquid crystal. Owing to this, the light passes through the cell without scattering if the polarizer orients perpendicularly to the director inside FLC droplets (Figure 7b). If $\alpha = \theta = 45°$ (where α is an angle between light polarization and strain direction, θ is molecular tilt angle), the opposite pulse of electric field reorients the director of FLC parallel to the light polarization (Figure 7a) resulting in the intensive scattering of the radiation due to the high gradient of refractive index at the droplet interface.

We have proposed three different modifications of PDFLC light modulators without the using of polarizers [28]: based on binary PDFLC cells, on bilayer PDFLC films and on liquid crystal polymer matrix. Additional advantage of the polarizer-free PDFLC devices is determined by an opportunity to use commercially available ferroelectric LC mixtures with an angle θ equal 22.5° (in contrast to the exotic FLC with $\theta = 45°$ required for the design of Figure 7) as such value of tilt angle is optimum for these designs.

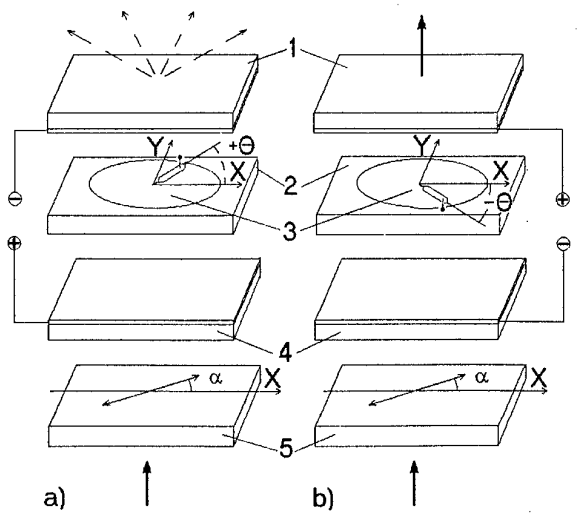

Fig. 7 The design and operation principle of a single-polarizer PDFLC light modulator. 1 and 4, substrates

with transparent electrodes; 2, polymer; 3, FLC droplet; 5, polarizer [25].

Pilot samples of light modulating PDFLC cells with the following performance parameters have been made: contrast ratio 22:1, saturation voltage 25÷30 V, reswitching time 30 μs in smectics C* phase and less than 1 μs in smectics A* phase, maximal transmittance up to 35 %, limiting density of radiation power 4 kW/cm^2.

References

1. Sonin A.S., Shibaev I.N. Structural order and properties of cholesterics encapsulated films. J of Physical Chemistry (Rus), V.55, No5, p.1263–1268, (1981).
2. Pat. 4.685.771 US, МКИ G02F 1/13. Liquid crystal display material comprising a liquid crystal dispersion in a thermoplastic resin / J.L. West, J.W. Doane, S. Zumer. – Publ. 11.08.87.
3. Koval'chuk A.V., Kurik M.A., Lavrentovich O.D., Sergan V.V. Structural transformations inside nematic droplets in external electric field. JETP, V.67, p.1065 (1988).
4. Wu B.-G., Erdmann J.H., and Doane J.W. Response times and voltages for PDLC light shutters. Liq. Cryst., V.5, No5, p. 1453–1465 (1989).
5. Whitehead J.B., Zumer S., and Doane J.W. Light Scattering from a Dispersion of Aligned Nematic Droplets. J. Appl. Phys.,. V.73, No3, P. 1057–1065 (1993).
6. Margerum J.D., Lackner A.M., Ramos E, Lim K.-C., Smith W.H. Effects off-state alignment in polymer dispersed liquid crystals. Liq. Cryst., V.5, No5. p. 1477–1487 (1989).
7. Nazarenko V.G., Reznikov Yu.A., Reshetnyak V.Yu., Sergan V.V. and Zyryanov V.Ya. Oriented dispersion of LC droplets in a polymer matrix with light induced anisotropy. Molecular Materials, V.2, p. 295–299 (1993).
8. Jain S.C. and Kitzerow H.-S. Bulk-induced alignment of nematic liquid crystals by photopolymerization. Appl. Phys. Lett., V.64 (22), p. 2946–2948 (1994).
9. Zyryanov V.Ya., Smorgon S.L., Shabanov V.F. Elongated films of polymer dispersed liquid crystals as scattering polarizers. Molecular Engineering, V.1, No4, p. 305–310 (1992).
10. Zyryanov V.Ya., Presnyakov V.V., Shabanov V.F. Fredericksz effect in polymer dispersed nematic droplets. Tech. Phys. Lett., V.22, No14, p.22-26 (1996).
11. Shabanov A.V. Presnyakov V.V., Zyryanov V.Ya., Vetrov S.Ya. Characteristics of the process of reorientation of bipolar drops of a nematic with rigidly fixed poles. JETP Letters, V.67, No9, p.733-737 (1998).
12. Shabanov A.V., Presnyakov V.V., Zyryanov V.Ya., Vetrov S.Ya. Bipolar nematic droplets with rigidly fixed poles in the electric field. Mol. Cryst. Liq. Cryst., V.321, p.259-270 (1998).
13. Presnyakov V.V., Zyryanov V.Ya., Shabanov A.V., Vetrov S.Ya. Friedericksz threshold in bipolar nematic droplets with rigidly fixed poles. Mol. Cryst. Liq. Cryst., V.329, p.27–34 (1999).
14. Konkolovich A.V., Presnyakov V.V., Zyryanov V.Ya., Loiko V.A., Shabanov V.F. Interference quenching of light transmitted through a monolayer film of polymer dispersed nematic liquid crystal. JETP Letters, V.71, No12, p.486-488 (2000).
15. Zyryanov V.Ya., Presnyakov V.V., Serebrennikov A.N., Shabanov A.V., Loiko V.A., Konkolovich A.V. High contrast light modulator based on PDNLC monolayer. Mol. Cryst. Liq. Cryst., V.368, p.3983-3990 (2001).
16. Barannik A.V., Shabanov A.V., Zyryanov V.Ya. Interference oscillations in the dynamics of the optical response of polymer dispersed nematic liquid crystals. Tech. Phys. Lett., V.28, No8, p.675-677 (2002).
17. Zyryanov V.Ya., Presnyakov V.V., Smorgon S.L., Shabanov V.F. Electrooptical properties and orientation-structural transformations in the ensemble of ellipsoidal cholesterics droplets. RAS Report (Rus), V.354, No2, p.178-181 (1997).
18. Presnyakov V.V., Smorgon S.L., Zyryanov V.Ya., Shabanov V.F. Polyfunctional optoelectronic elements based on oriented PDCLC films. SPIE Proceedings, V.3348, p.98-102 (1998).
19. Presnyakov V.V., Smorgon S.L., Zyryanov V.Ya., Shabanov V.F. Volt-contrast curve anisotropy in planar-oriented PDChLC films. Mol. Cryst. Liq. Cryst., V.321,. p.259-270 (1998).
20. Presnyakov V.V., Shabanov V.F., Zyryanov V.Ya., Komitov L. Chiral additive effects on electrooptical response and droplet structure in uniaxially oriented films of polymer dispersed nematic. Mol. Cryst. Liq. Cryst., V.367, p.3157–3165 (2001).
21. Zyryanov V.Ya., Smorgon S.L., Zhuikov V.A., Shabanov V.F. Memory effects in polymer-encapsulated cholesterics liquid crystals. JETP Letters, V.59, No8, p.547-550 (1994).
22. Barannik A.V., Zyryanov V.Ya., Shkuryaev P.G., and Shabanov V.F. Thermooptical information recording in the bistable films of polymer dispersed cholesteric liquid crystals. Proceedings SPIE, V.3347, p.107–112 (1998).
23. Zyryanov V.Ya., Smorgon S.L., Shabanov V.F. Light modulation by polymer dispersed ferroelectric liquid crystals. Summer European Liquid Crystals Conference, Abstracts, Vilnius, V.1. p.141 (1991).
24. Zyryanov V.Ya., Smorgon S.L., Shabanov V.F. Electro-optics of polymer dispersed ferroelectric liquid crystals. IV International Conference on Optics of Liquid Crystals, Abstracts, Florida, USA, p.70–71 (1991).
25. Zyryanov V.Ya., Smorgon S.L., Shabanov V.F. Polymer dispersed ferroclectric liquid crystals as display materials. Digest SID, V.23, p. 776–777 (1992).
26. Zyryanov V.Ya., Shabanov V.F., Smorgon S.L. Electrooptics of polymer dispersed ferroelectric liquid crystals. Ferroelectrics, V.143, p.271–276 (1993).
27. Zyryanov V.Ya., Smorgon S.L., Shabanov V.F. Light modulation by a planar-oriented film of a polymer-encapsulated ferroelectric liquid crystal. JETP Letters, V.57, No1, p.15-18 (1993).
28. Zyryanov V.Ya., Shabanov V.F., Smorgon S.L., Pozhidaev E.P. Polymer dispersed ferroelectric liquid-crystal light valves. Digest SID, V.25, p.605–607 (1994).
29. Zyryanov V.Ya., Smorgon S.L., Shabanov V.F., Pozhidaev E.P. Orientational structures of elongated droplets of ferroelectric liquid crystals in polymer matrix. Molecular Materials, V.9, No2, p.139–145 (1998).
30. Zyryanov V.Ya., Pozhidaev E.P., Smorgon S.L., Barannik A.V., Presnyakov V.V., Andreev A.L., Kompanets I.N., Shevtchenko S.A., Ganzke D., Haase W. Light modulation characteristics of single-polarizer PDFLC cells. Ferroelectrics, V.243, P.179–188 (2000).
31. Zyryanov V.Ya., Pozhidaev E.P., Smorgon S.L., Andreev A.L., Ganzke D., Shabanov V.F., Kompanets I.N., Haase W. Light modulation characteristics of a single-polarizer electrooptical cell based on polymer dispersed ferroelectric LC. Liq. Cryst., V.28, p.741–748 (2001).

NED-P12. **Structure and Electrooptical Properties of Unoriented Films of Polymer Dispersed Ferroelectric Liquid Crystals**

V.Ya. Zyryanov, A.V. Barannik, R.D. Ilvutikov, V.F. Shabanov, E.P. Pozhidaev*

L.V. Kirensky Institute of Physics, Akademgorodok, Krasnoyarsk 660036, Russia
*P.N. Lebedev Physical Institute, Leninsky pr. 53, Moscow 117924, Russia
zyr@iph.krasn.ru

Orientational structure of the droplets of ferroelectric liquid crystals dispersed inside unoriented polymer films both for homeotropic and planar anchoring conditions have been studied. Macroscopic optical properties of the films under the action of electric field are analyzed. The light intensity may be modulated with the help of this material, but the efficiency of the modulation is too small for electrooptical applications.

NED-P13. **High azimuthal index doughnut beam generated by liquid crystal spiral phase plates**

P. Shum, Q. Wang and X.W. Sun

School of Electrical and Electronic Engineering, Nanyang Technological University,

Nanyang Avenue, Singapore 639798, Singapore

fax: 65-67920415, e-mail: epshum@ntu.edu.sg

The doughnut beam of higher azimuthal index have larger orbit angular momentum, this is an advantage while applying doughnut beam to the rotation of microscopic particles. A novel technique of producing azimuthal index l>1 doughnut beam of good quality by use of multi-liquid crystal cells is presented, the experimental results is in consistent with the simulation. The advantages of this technique are the high conversion efficiency and flexibility. The doughnut beam's azimuthal index can be easily changed with different driving voltage scheme. We also obtained the interference patterns made by a doughnut beam and a plane wave, which is useful in optical tweezers.

NED-P14. **Fabrication of ITO thin films by filtered cathodic vacuum arc deposition**

X.W. Sun, B. J. Chen, P. Shum

School of Electrical and Electronic Engineering, Nanyang Technological University,

Nanyang Avenue, Singapore 639798, Singapore

fax: 65-67920415, e-mail: exwsun@ntu.edu.sg

Polycrystalline indium tin-doped oxide (ITO) thin films have been fabricated on Si (111) and quartz substrates by filtered cathodic vacuum arc (FCVA) technique for the first time. The ITO thin films were deposited at different substrate temperature and oxygen gas flow rates into the reactor chamber. The optimized ITO film has a high transmittance of about 95% in the wavelength range of 400 nm to 800nm, the volume resistivity is 6.57×10^{-4} Ωcm and the electron carrier concentration is as high as 1.62×10^{21} cm^{-3}. Atomic force microscopy (AFM) images show that the surface of ITO film is very smooth both on silicon and quartz substrates, the RMS average roughness is 2.24 nm for silicon substrate and 2.43nm for quartz substrate respectively. These smooth ITO films are suitable for long lifetime organic light-emitting devices.

NED-P15. **Two-parameters optimization procedure of TN display**

Marek Olifierczuk and Jerzy Zieliński
Institute of Applied Physics, Military University of Technology
2 Kaliskiego St., 00-908 Warsaw, POLAND

keywords: TN display, contrast ratio, luminance, optimization procedure, dye-doped layer

In our work the two-parameters optimization procedure of TN display has been done. This procedure has depended on the numerical calculations of the optical parameters of a TN display such as contrast ratio and luminance as a function of the both arguments: LC layer dichroic properties and polarization coefficient of used polarizers. The calculations have been done for:

- human eye sensitivity;
- real spectral characteristics of lighting source (the both internal and external ones);
- the both positive and negative modes of the display;
- real director profile into the LC layer;

Additionally, our procedure has taken into account the interference phenomena into the display and quasi-real properties of the polarizing films.

As a result of our work the close relationships between the TN display optical parameters and used dichroic LC layer and polarizing films have been obtained. These information make possible to done the initial choice of the display elements for different display application and users requirements.

NED-P16. **Multi-parameters optimization procedure of the contrast ratio in TN two-polarizer reflective display**

Jerzy Zieliński and Marek Olifierczuk
Institute of Applied Physics, Military University of Technology, 2 Kaliskiego St., 00-908 Warsaw, Poland

keywords: TN effect, numerical optimization, dye-doped display

The aim of our work has been to work out the multi-parameters procedure for the contrast ratio optimization process in a TN reflective display. The requirements range for the contrast ratio value for different display applications has been presented. The measurements procedures for different elements of the TN display have been described. These procedures have been worked out especially for application in the computer program worked by authors earlier. Using this computer program the procedure makes possible to obtain the contrast ratio of the display for different:

- spectral characteristics of the lighting source;
- human eye sensitivity;
- anisotropic and dichroic (dye-doped layer) properties of the liquid crystal layer;
- polarization properties of the used polarizing films.

The calculation done by this program take into account the reflection and interference phenomena and also the real curve of the director profile in the liquid crystal layer. In this case the results obtained by this program are very similar to the real experimental results.

Using this computer program the multi-parameters optimization procedures for reflective TN two-polarizers display have been done. The properties of individual display elements have been established for the optimized display used for different application. The influence of the display elements properties for finally contrast ratio has been described. The difference of optical parameters obtained for real director profile and ideal profile has been shown.

As the finally result of our work one has obtained the close relationships between the properties of individual display elements and the display optical parameters, especially contrast ratio value. This knowledge makes possible for correctly choice of the display elements for different application of the two-polarizers TN reflective display.

NED-P17. Oblique Reactive Cathode Sputtering as a Method for Creation of OrientingLiquid Crystal Microrelief

Yu.Kolomzarov, P.Oleksenko, V.Sorokin, P.Tytarenko, R.Zelinskyy
Institute of Semiconductor Physics, NAS Ukraine, 41, prospect Nauki, 03028 Kyiv, Ukraine

Abstract

A mechanism for creation of microrelief surface anisotropy of amorphous films oxides materials such as Si, Ge, Al, In, Ta, Ti, Ni, etc., which are obtained by oblique reactive cathode sputtering method is described. The influence of technological parameters of sputtering on the LC orienting parameters is investigated. The dependencies of the target material, angle of material emission and reemission processes under the substrate negative ion bombardment is shown. The application of oblique reactive cathode sputtering method for creation of LCD with different size is demonstrated.

Keywords: liquid crystal, alignment, reactive cathode sputtering

1. Introduction

Scientific-and-technical reviews devoted to orientational effects at the interface "liquid crystal (LC) – solid", methods of preparing various types of orientants [1-4] as well as to problems of interrelations between physical properties of surfaces with electrooptical parameters of devices based on LCs [5-7] allow critical analysis of orientational methods, when taking into account currently industrial requirements. Nowadays, in industry, the technological orientation process is realized using both vacuum technologies of orienting film deposition [8] and vacuumless ones based, for example, on the specific mechanical rubbing of organic films [9]. In this case, vacuum methods have some limitations as to the possibility to automate the process of orienting film deposition onto large substrate areas, which are related to specificity of thin film vacuum deposition methods. For vacuumless methods, the main problem is to control anchoring energy and orientation parameters of LC, in particular, pre-title angles of LC molecules. Wide perspectives can be provided by the effect of induced anisotropy of microrelief on the orienting surface when exposing it by polarized light [10-12]. This method has no deficiencies inherent to the method of the mechanical rubbing and enables to effectively control orientation parameters. However, before its wide application in practice, it is necessary to solve a set of problems associated with thermal stability, reproducibility of orienting films and reliable

In this work, we represent investigation results of new original way to prepare oriented LC structures based on reactive cathode sputtering (RCS) method [13-14].

2. Experimental setup

Our setup for deposition of orienting films by using the method of reactive cathode sputtering is shown in Fig. 1. A special water-cooled cathode unit 1 was mounted at the top part of VUP-5 installation jar.

As target material, we used wafers of silicon, germanium, nickel, tantalum, titanium, aluminum and indium that possess a good thermal contact with cathode plane. The total area of the sputtered target was approximately 50 cm^2. The sputtering of targets was carried out in atmosphere of argon-oxygen mixture. Substrates were mounted in the special holder enabling to change the slope angle between normal to plane of the target and substrates within the range 0 to 90°. The discharge voltage was varied from 1 to 5 kV.

Deposition of orienting layers was performed using the pressure of operating gas mixture withing the range $6x10^{-2}$ to $8x10^{-3}$ Torr. We used industrial LCs based on cyanobyphenyls. The quality of homogeneous as well as twist orientations was estimated using methods of polarization microscopy. The parameter of twist orientation k_t was determined via the following expression

$$k_t = \log \frac{I_o}{I_t} \qquad (1)$$

where I_o and I_t are the values of light flow transmitting through the cell when polarizers are parallel and the cell is not filled with LC and did with the twist orientation one, respectively.

3. Results and discussion

Our analysis of physical processes taking place under preparation of thin films by thermal sputtering and RCS shows that there is no direct similarity between them. While using RCS, the structure of the deposited film is determined by two main factors: deposition of substance onto the substrate and re-emission of the latter in the consequence of efficient bombardment by negative ions. Contribution of the separate factor is determined by plasma beam parameters. The bombardment by negative ions takes place just under the angle α relatively to the substrate surface, while condensation angles of sputtered substance have larger infinity through its collisions with gas ions and atoms as well as due to the fact that cathode dimensions are considerably larger than substrate projections onto the cathode. Being based on numerous experiments, we ascertained that the infinity in condensation

angles for orienting substance can be essentially decreased if using the screen with a slot of the rectangular shape placed under the target at the distance 3 to 5 mm, which enables to form the narrow plasma torch (Fig. 1).

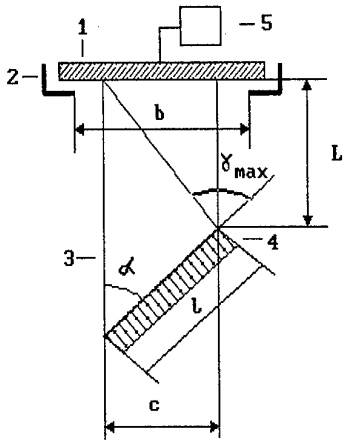

Fig.1. Schematic of the cathode unit for deposition of orienting layers. 1 – cathode, 2 – screen, 3 – plasma torch, 4 – substrate, 5 – high voltage supply.

The symmetry axis of the slot should coincide exactly with the target centre and that of the substrate holder. As it follows from Fig. 1, the condensation angles of sputtered substance will be limited by the well determined condensation angle γ_{max}, while substrates will be treated in the plasma torch with the width c, and c being always less than the slot width b. It is conditioned by screwing the plasma torch by the screen, as it is placed within the range of dark cathode space.

It was ascertained that the orientation worsened with exceeding the substance maximal condensation angle. The peak value of the allowed substance condensation angle can be defined in the following manner:

$$\gamma_{max} = \alpha + arctag\frac{c}{L_o} \qquad (2)$$

where α is the angle of the substrate slope relatively to the normal to cathode surface, c is the width of the plasma torch, L_o is the minimum allowed distance from the cathode to the upper substrate edge (the length of the dark cathode space).

Changing the plasma torch width, one can change the substance condensation angle and control, in this manner, the orientation parameters of LC films. It is experimentally found that the plasma torch width c is the function of at least four technological parameters, namely: the cathode voltage U_k, gas pressure in the operating mixture p, oxygen concentration in this mixture k_o and the screen slot width b.

The deposition scheme shown in Fig. 1 possess one essential deficiency – a low package density for substrates under the cathode and, as a consequence, an insufficiently high productivity of this technological facility. For instance, if considering the substrates with sizes 25x15 mm^2 under given technological regimes for orienting layer deposition that provides the high quality of LC orientation, then the necessary plasma torch width c = 8 mm is reached with the slot width b = 28 mm, i.e., practically 60% of the cathode area is used inefficiently.

To avoid this deficiency, we developed the second way. Fig. 2 shows the scheme of appliance capable to realize the developed way of orienting coating deposition, and Fig. 3 represents the deposition scheme using to this way. In according with Fig. 2, the screen is designed in the form of sections with the height and length limited by the cathode dimensions.

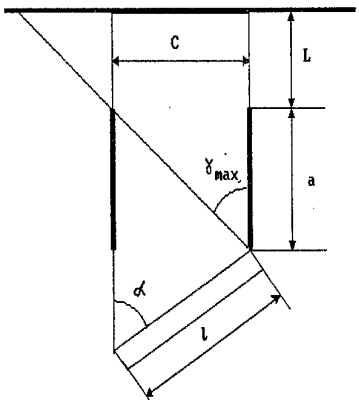

Fig. 2. Scheme of the facility for deposition of orienting layers, which is suitable to optimize substance condensation angles.

The separation between sections was chosen as equal to $l \sin\alpha$, where l is the substrate length. The distance L between the screen 2 and cathode 1 was chosen in such a manner that it were larger than or equal to the length of the dark cathode space in this glow discharge. The substrates 3 were mounted into the holder 4 in the manner that their plane made the angle α relatively to the plasma torch direction.

To determine the screen section height, we shall use Eq. (2) and Fig. 2. Taking into account that in the first way c = 8 mm L = 48 mm, let us deduce the maximum substance condensation angle for this substrate:

$$\gamma_{max} = \alpha + 13.2^{o} \qquad (3)$$

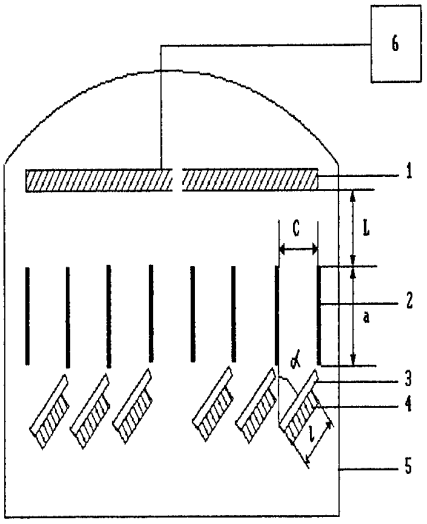

Fig. 3. Scheme of an under-jar setup in the industrial unit for deposition of orienting structures: 1 – cathode, 2 – screen system, 3 – substrate, 4 – substrate holder, 5 – jar, 6 – high voltage supply

On the other hand, it follows from Fig. 2 that the expression for the maximum substance condensation angle in the second way of orienting coating deposition has the following form:

$$\gamma_{max} = \alpha + arctag\frac{l\sin\alpha}{a} \qquad (4)$$

Having jointly solved Eqs (3) and (4), we get

$$a = 4.3l\sin\alpha \qquad (5)$$

Validity of the equality (5) is one of the necessary conditions for the offered way to be realized.

In this case, with decreasing the screen section height, γ_{max} is increased. As a consequence, LC orientation is worsened. Therefore, in a common case, when realizing the offered method, the value a should be chosen using the following inequality

$$a \geq 4.3l\sin\alpha \qquad (6)$$

The second necessary condition to realize this way is the necessity to place the screen at the distance L from the cathode, which is large or equal to the length of the glow discharge dark cathode space L_0:

$$L \geq L_o \qquad (7)$$

As compared with the first way, the productivity of the installation is approximately three-fold increased when deposing these orienting coatings.

To solve the tasks of orienting layer deposition onto substrates with a large area, we have developed the scheme of a cathode unit enabling to scan the substrate in the plasma torch (Fig.4). This modification of the cathode unit provides formation of a narrow plasma torch with 5...8 mm width and 150 mm length as well as the possibility of substrate alternate motion with the velocity 0.5 to 5 mm/s, the substrate being mounted at the angle $\alpha = 5 - 30^{\circ}$.

This configuration provides the possibility to obtain an equal-thickness coating over the whole area of the substrate with large sizes (150x150 mm^2) as well as the potential to simultaneously deposit the orienting coatings onto large quantity of substrates with a small area.

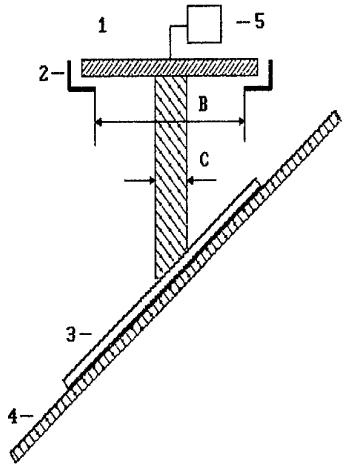

Fig. 4. Scheme of the cathode unit with configuration enabling to scan substrates in the course of orienting layer deposition: 1 - cathode, 2 – screen, 3 - substrate, 4 – scanning system, 5 – high voltage supply.

Our investigations of orienting properties inherent to oxides films of indium, aluminum, germanium, silicon, tantalum, titanium showed that SiO_X and GeO_X layers, as to the above properties, are capable to compete with thermally deposited ones. Experiments showed that the quality of twist orientation promoted by SiOx and GeO_x films is k_t~2.5, which meets well the requirements to LC indicators. However, SiO_x orientants are more transparent and less hydrated. Therefore, these were preferred in our investigations. The performed study showed that the orientation quality depends on a great amount of technological parameters in the course of SiO_x layer deposition (the cathode voltage, discharge current density, operating gas

pressure, oxygen concentration in an operating mixture, angle and time of deposition, *etc.*).

Our analysis of technological regimes suitable for deposing these orienting layers, which provide the high quality of twist orientation, enabled to ascertain the main regularities represented in Fig. 5. Any point of the dashed area in this figure corresponds to deposition parameters that provide the twist orientation factor $k_t = 2.5$. For example, at the given deposition angle $\alpha = 15^\circ$ and the voltage $U_k = 3$ kV, the deposition process should be carried out at the current density $j = 3.2$ mA/cm^2 . The voltage or discharge current density increase results only in growing k_t.

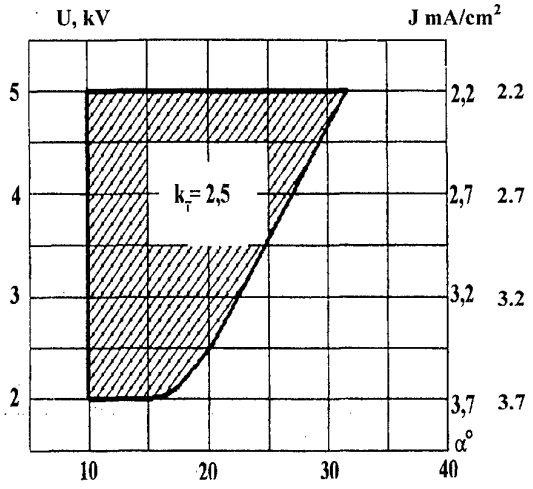

Рис.5. Nomogram for determination of the technological parameters.

4. Conclusions

The experimental investigations of the developed method applicability to deposing oxides of such materials as silicon, germanium, aluminium, tantalum, indium *etc.* showed the possibility to form oxide structures of above materials capable to orient molecules of nematic LCs in the direction coinciding with that of ion bombardment in the course of material deposition. The substrate plane should be oriented at the definite angle to the cathode plane normal.

The study of orienting layer capabilities and optical properties of these layers showed that formation of the orienting structure is determined by two main processes: emission (the sputtered substance is deposited onto a sustrate after its oxidation in plasma) and re-emission (the deposited layer is under bombardment by negative ions).

It is these two processes that provide formation of the material oxide structure that is capable to orient a wide class of LC substances. The offered method opens a direct way to create ecologically pure technology of LC displays without using harmful chemical compounds.

References

[1] Luk'yanchenko E.S., Kozunov V.A., Grigos V.I. Orientation of nematic liquid crystals//Uspekhi khimii **54**, N 4, p. 214-238, 1985 (in Russian

[2] Ctoosens W.J.A. Bulk interfacial and anchoring of liquid crystals// Mol. Cryst.Liq.Crys.- 1985.-vol.124.- N 1-4.- p.305-319.

[3] Chigrinov V.G., Korkishko T.V. Role of surface in electrooptics of liquid crystals // Abstracts of the Fifth All-Union Conference "Liquid Crystals and Their Practical Application", Vol. 2, Books 1 and 2, p. 6-51. Ivanovo, 1985 (in Russian).

[4] Konyar Zh. Orientation of of nematic liquid crystals and their mixtures. "Universitetskoye", Minsk, 1986 (in Russian).

[5] Chigrinov V.G. Orientational effects in electric and magnetic fields//Kristallographiya 27, N 2, p. 404-430, 1982 (in Russian).

[6] Kozunov V.A., Chigrinov V.G. Electrooptics of the twist effect in liquid crystals//Obzory po elektronnoi tekhnike. Ser. 3. Mikroelektronika, N 8, 1988 (in Russian).

[7] Berreman D. AAlignment of liquid crystals by groved surfaces// Mol.Crys.Liq.Crys.- 1973.- vol.23.- N 3-4.- p.215-231.

[8] Gorbunov O.V., Kurchatkin S.P., Mukhayev A.A. et al. Orientation of liquid crystals using germanium monooxide// Izvestiya AN SSSR. Ser. Neorganich. Mater. Vol. 19, N 3, p. 467-471, 1983 (in Russian).

[9] H.Tabira, T.Inoue, Y.Yahagi, H.Imayama, M.Morimoto. Precision rubbing supported by fine process analysis// J. of the SID.-2002 .-V.10.-N.4.-p.329-337.

[10] Fedorenko D., Ouskova E., Reznikov Yu., Su L., Shiyanovskii S., Kuksenok O., Wesi J., Francescangeli O., Simoni F. Hidden Photoalignment of Liquid Crystals in isotropic Phase // Phys. Rev. E. - 2001. - Vol.63, 021701. - P.) -5.

[11] Andrienko D., Fedorenko D., Uskova O., Reshetnyak V., Reznikov Yu.. Slussarenko S., Voloshchenko D., Lavrentovich O. Light-induced Alignment and Reorientation Effects in Liquid Crystals Doped with Azo-dyes // Ukr. Journ. of Phys. -1099. - Vol.44, JV»l-2. - P. 149-157.

[12] Fedorenko D., Ouskova E., Reznikov Yu., Reshetnyak V., Shiyanovskii S., Frarirescangeli O., Simoni F. Properties of Bulk-mediated Photoalignment of Doped Liquid Crystal // Mo!. Cryst. Liq. Cryst. - 2001. - Vol.359. - P.137-145.

[13] Sorokin V.M., Oleksenko P.F., Ovsyannikov V.D. The method of orienting film preparation. Author's certificate 1009109.

[14] Anoshkin A.V., Zelinskyy R.Ya., Kuz'min N.G., Sevostyanov V.P., Sorokin V.M. The facility for deposition of orienting films. Author's certificate 1492736.

NED-P18. Two-Row Addressing Method For Cholesteric LCD

A. Rybalochka, V. Sorokin, S. Valyukh

Institute of Semiconductor Physics, NASU, Kiev, Ukraine

Abstract

One from the ways to increase the addressing speed of Cholesteric LCD is an implementation of multiple-row addressing methods. In these methods the addressing of several rows at a time to decrease the addressing time is used. For practical using of drive schemes with multiple-row addressing methods simplicity of the driving voltage waveforms is necessary. Only in this case the standard LCD drivers can be used. In this paper the new dynamic drive scheme for Cholesteric LCD with the simple driving voltage waveforms and two rows at a time addressing are presented.

Keywords: cholesteric, bistable LCD, drive scheme

Introduction

Cholesteric liquid crystals (ChLCs) are widely used in display technologies due to inherent them two main properties: bistability and Bragg reflection for light in visible spectral range [1]. Bistability of ChLCs lies in a presence of two stable textures of such liquid crystal materials: planar texture and focal conic texture. In the planar texture the helical axes of a ChLC are more or less perpendicular to the cell surface. This cholesteric structure has the pitch P_0 that are determined by the physical properties of a ChLC. In the planar texture a ChLC crystal exhibits Bragg reflection at the wavelength $\lambda_0 = n \times P_0$ for normally incident light, where n is an average refractive index. If λ_0 is in the visible light region, the display cell has a bright colored appearance. The reflection spectrum has a bandwidth that determined in the following: $\Delta\lambda = \Delta n \times P_0$, where Δn is a birefringence. In the focal conic texture the helical axes are more or less parallel to the display cell plate and ChLC in this texture becomes scattering. In this case an incident light are partly scattered and partly absorbed by background of a display. Due to these specific properties bistable reflective cholesteric displays have intrinsic low power consumption. This fact in the aggregate with high reflectivity, wide viewing angle, technological simplicity production and possibility of information representation with high information content does Cholesteric liquid crystal displays (ChLCDs) a good candidate for applications such as different schedules, timetables, pointers, electronic books, electronic newspapers etc.

For the addressing of a ChLCD transitions between the stable planar and the stable focal conic textures of a ChLC in display's pixels must be realized [2]. A low voltage pulse can realize the transition from the planar texture to the focal conic texture. The transition from the focal conic texture to the planar texture is more complicated. First, the cholesteric-nematic transition must be realized. It can be achieved (for a ChLC with $\Delta\varepsilon_0>0$) by applying of external electric field that exceeds the threshold value $E_C = (\pi^2 / P_0)\sqrt{K_{22} / (\varepsilon_0 \times \Delta\varepsilon)}$, where K_{22} – is a twist elastic constant, ε_0 – is a dielectric constant and $\Delta\varepsilon_0$ – is a dielectric anisotropy. In this case helical structure is unwound and all liquid crystal molecules are aligned parallel to external electric field. This texture of ChLC is called homeotropic texture. At the absence of the external electric field this texture is unstable. Final stable texture of ChLC obtained from homeotropic texture depends on how the external electric field is turned off [3]. When the external electric field is turned off slowly the final stable texture of ChLC is the focal conic texture. When the external electric field is turned off quickly ChLC first of all transforms from the homeotropic to the transient planar texture. The transient planar texture has a helical structure similar to the stable planar texture with the pitch $P_0^* = (K_{33}/K_{22}) \times P_0$. The homeotropic – transient planar transition (H-P_0^* – transition) is very quickly. For different liquid crystal materials the time of H-P_0^*-transition can be from hundreds of microseconds to milliseconds. The transient planar texture is also unstable and finally a ChLC relaxes into the stable planar texture.

The cholesteric-nematic transition has hysteresis properties [4]. In detail these properties of cholesteric materials have been considered in the next section of this paper. Due to investigations of hysteresis properties and texture transitions of ChLC a number of dynamic drive schemes (DDSs) for cholesteric displays had been developed [5-10].

Cholesteric displays are addressed by DDSs with the speed that approximately is about time of the homeotropic-transient planar transition per row. However such addressing speed is slow for video application. On the other hand the main application of a bistable ChLCD with very low power consumption is a cases where a high resolution is combined with low update rate. But even in this case for comfort using of ChLCD the addressing time is necessary to reduce to its minimum value. One from the ways to solve this problem is application of multiple-row addressing (MRA) to the ChLCD. Possibility to reduce the addressing time by MRA with the three-phase addressing scheme were presented by *Roosendaal' at al* [11]. But the drive sequences that are applied to rows and columns of a display for realization of this drive

principle are sufficiently complex and it is necessary to use the special complicated and expensive drivers.
In this paper we demonstrate the two-row addressing of a ChLCD by a new DDS that has very simple driving voltage waveforms. In this new DDS the driving voltage sequences that are applied to rows and columns of a display consist of unipolar voltage pulses with only two values of amplitude: U and 0. In this case simple two-level LCD drivers can be used.
We performed all our measurements on the display cell filled with the liquid crystal mixture BL126 (Merck), cell thickness d=4,4 μm.

Hysteresis properties of ChLC

For consideration and analysis of hysteresis properties of the ChLC the experimental investigation of a response of the liquid crystal to voltage pulses have been carried out. The voltage waveform that was used for measuring of the electro-optical response of the ChLC is shown in Figure 1.

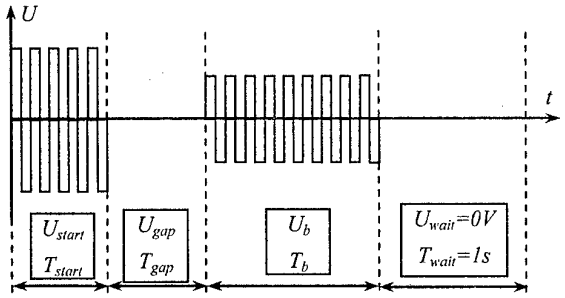

Figure 1. The voltage waveform to measure the electro-optical response of the ChLC.

First, to transform the ChLC to the homeotropic texture, a high voltage U_{start} is applied to the display cell irrespective of the initial texture of liquid crystal. Then during the time T_{gap} a voltage U_{gap}=0V is applied to the display cell. After that the bias voltage pulse (U_b, T_b) is applied for studying of the response of the cholesteric material. The final reflectance of the ChLC is measured in one second (T_{pause}) after the bias pulse when the reflectance no changes more with time. Figure 2 shows four dependences of the stabilized reflectance of the display cell vs. the effective value of the bias voltage U_b for different values of some parameters of the voltage waveform that have been demonstrated on Figure 1. For all curves on Figure 2 values of the next parameters of this voltage waveform is identical: U_{wait}=0V, T_{wait} =1s, T_{start}=0,5s, U_{gap}=0V and T_b=0,3s. For these curves only parameters U_{start} and T_{gap} have different values. For the curve "FC" – U_{start}=20V and T_{gap}=1s. This curve shows a response of the ChLC in the stable focal conic texture to the bias voltage pulse. The curve "P" shows a response of the ChLC in the stable planar conic texture to the bias voltage pulse (U_{start}=50V and T_{gap}=1s). For cholesteric material used here the time of the H-P_0^* transition is $T_{H\text{-}P^*}$=2,8ms at room temperature. Therefore the curve "P*" shows a response of the cholesteric material in the transient planar texture to the bias voltage pulse at U_{start}=50V and T_{gap}=2,8ms. And finally, the curve "H" shows a response of the cholesteric material in the field induced homeotropic planar texture to bias voltage pulse (U_{start}=50V and T_{gap}=0s). Some threshold voltage levels that are very important for determination of parameters for any dynamic drive scheme are also presented on Figure 2. The voltage levels U^c_{FC}, U^c_P and $U^c_{P^*}$ – are threshold voltages of the focal conic – homeotropic, planar – homeotropic and transient planar – homeotropic transitions respectively. The voltage levels U^{max}_{FC-FC}, U^{max}_{P-FC} and $U^{max}_{P^*-FC}$ – are the maximal voltage levels that address the cholesteric material in the final stable focal conic texture that has minimal reflectance from the initial focal conic, planar and transient planar states respectively. The voltage level U^c_H is the minimal voltage level that holds the field induced homeotropic texture of the ChLC in the display cell during the bias time T_b.

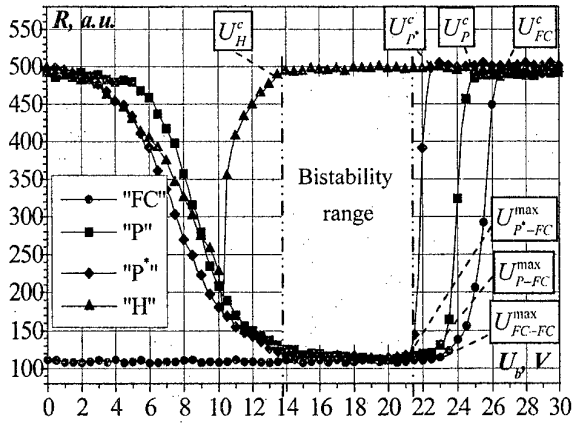

Figure 2. The response to bias voltage pulses and some threshold voltage levels of the cholesteric display cell.

There is the bistability range $U^c_H < U_b < U^{max}_{P^*-FC}$ where the field induced homeotropic texture is held and the focal conic, the planar and the transient planar textures are addressed into the focal conic state. Such behavior of the electro-optical characteristics of the cholesteric display cell demonstrates the hysteresis properties of cholesteric liquid crystal materials.

Two-Row addressing method

In the new DDS with simultaneously addressing of two rows of a display at a time the standard principle of the dynamic addressing of cholesteric displays by two-level DDS are used [8-10]. In two-level dynamic drive schemes the driving sequences of voltage pulses that are applied to rows and columns of a display consist of unipolar voltage pulses with amplitudes U and 0 but the resultant effective voltage levels on pixels during the addressing are changed. The changing of the resultant effective voltage levels on pixels has appointed form. It is determined by summarized across pixels voltage waveforms.

The pipeline algorithm that is used to drive a ChLCD by the new DDS is shown on Figure 3.

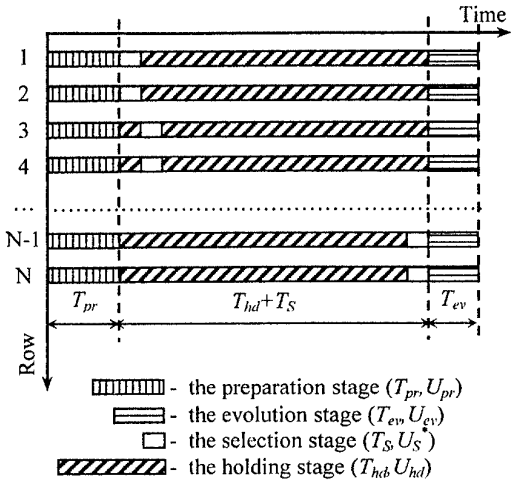

Figure 3. The pipeline algorithm used to drive a N-row passive matrix ChLCD.

At the beginning, the preparation voltage $U_{pr}=U$ is applied to all display pixels during the preparation stage. The value of the preparation voltage is enough to transform the ChLC into the homeotropic texture, independent of its initial texture. In the first part of the holding stage that follows the preparation stage before the selection stage, the ChLC is kept in the homeotropic texturee by the holding voltage $U_{hd}=U/\sqrt{2}$. During the selection stage (T_s) the final texture of the ChLC in two rows of a display is determined. In selected pixels the ChLC is kept in the homeotropic texture and in non-selected pixels the ChLC transforms into the transient planar texture. In the second part of the holding stage that follows the selection stage before the evolution stage (T_{ev}, $U_{ev}=U_{hd}$) the ChLC remains in the homeotropic texture if it was kept in this texture during the selection stage. From this argumentation follows that the effective value of the holding voltage level U_{hd} must be chosen from the bistability range (see Figure 2). In the case when the ChLC transformed into the transient planar texture during the selection stage, it evolves to the focal conic texture. After the end of the evolution stage the stable focal conic texture of the cholesteric material is formed in non-selected pixels and the ChLC transforms from the homeotropic to the stable planar texture in selected pixels .

For voltage waveform that shown in Figure 1 the stabilized reflectance of the display cell vs. the duration of the gap time (T_{gap}) is presented on Figure 4 (U_{start}=50V, T_{start}=0,5s, U_{gap}=0V, U_b=20V, T_b=0,3s, U_{wait}=0V and T_{wait} =1s). From this dependence we can see that the reflectance of the display cell is maximal at $T_{gap}\geq T_{H\text{-}P^*}$=2,8ms and it is minimal at $T_{gap}<T^*$=2,45ms.

The voltage waveforms applied to rows (R_{pr}, R_{ev}), columns (C_{pr}, C_{ev}) and resultant across pixels (P_{pr}, P_{ev}) during the preparation and the evolution stages for the new DDS are presented on Figure 5. Thereby the effective voltage level across all displays pixels in the preparation and evolution stages is $U_{pr}=U$ and $U_{ev}=U/\sqrt{2}$ respectively.

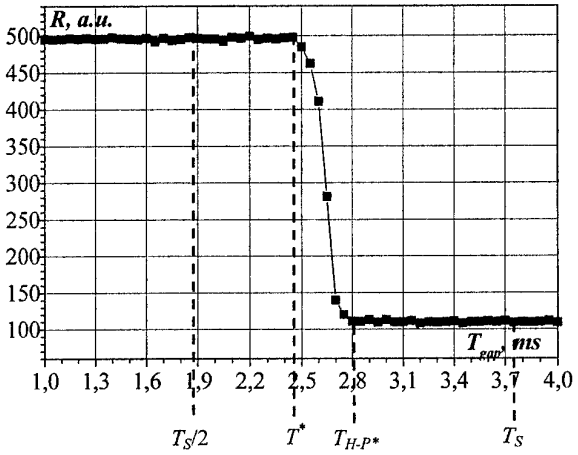

Figure 4. The stabilized reflectance of the display cell vs the gap time interval.

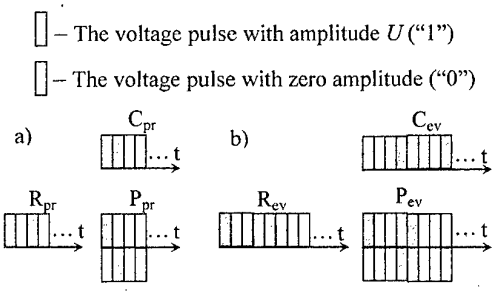

Figure 5. The voltage waveforms that are applied to rows, columns and resultant across pixels in the preparation (a) and the evolution (b) stages for the new DDS.

There are different effective voltage levels on different display's pixels during the holding and selection stages simultaneously. When pixels from two display rows are in the selection stage then the others pixels are in the holding stage simultaneously. Moreover, there are four different pairs of pixels in the stable states at combination from the final planar and focal conic textures on intersection of one column and two rows of a display at two-row addressing (Figure 6).

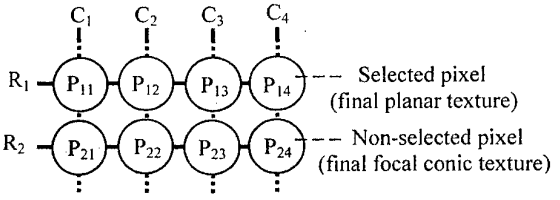

Figure 6. Four different pairs of pixels in the stable states on intersection of one column and two rows of a display at two-row addressing

For the realization of simultaneous addressing of these final states of a cholesteric mixture in a matrix display

we have developed the next voltage waveforms that are applied to rows (R_{S1}, R_{S2}, R_{NS}) and columns (C_{S1}, C_{S2}, C_{S3}, C_{S4}) during the selection and the holding stages for the new DDS (see Figure 7). They give the next resultant across pixels voltage waveforms: P_{11}, P_{12}, P_{13}, P_{14}, P_{21}, P_{22}, P_{23}, P_{24}, P_{Hd1}, P_{Hd2}, P_{Hd3}, P_{Hh4}. As we can see from the Figure 7 during the holding stage the effective voltage level on all pixels is $U_{hd}=U_{ev}=U/\sqrt{2}$. In the selection stage there are eight different resultant voltage waveforms across display pixels. The waveforms P_{11}, P_{21} have parts with permanent zero amplitude during time durations T_0^{11} and T_0^{21} correspondingly ($T_0^{11}=T_0^{21}=(3/4)\times T_S$). For others waveforms analogous parameter is $T_0^{13}=T_0^{24}=T_S$, $T_0^{14}=T_0^{23}=(1/2)\times T_S$ and $T_0^{12}=T_0^{22}=T_0^{Hd1}=T_0^{Hd2}=T_0^{Hd3}=$ $=T_0^{Hd4}=(1/4)\times T_S$.

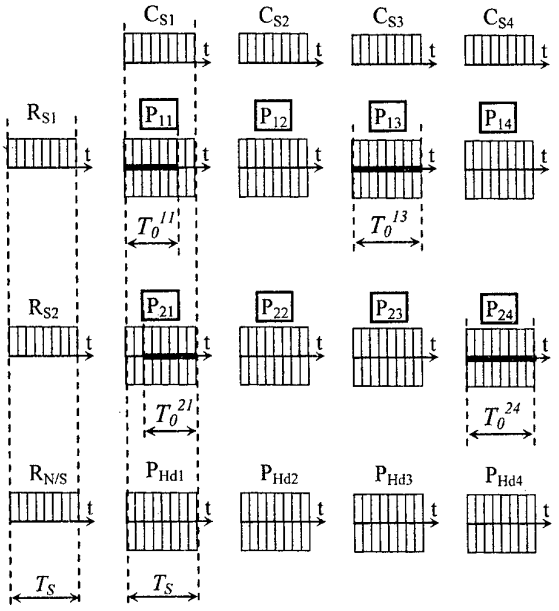

Figure 7. The waveform of the voltage that are applied to rows, columns and resultant across pixels during the selection and the holding stages for the new DDS.

For the addressing of a display by the new DDS the next conditions must be executed:

1) T_0^{11}, T_0^{21}, T_0^{13}, and T_0^{24} must be more or equally to $T_{H\text{-}P^*}$;
2) T_0^{12}, T_0^{14}, T_0^{22}, T_0^{24}, T_0^{Hd1}, T_0^{Hd2}, T_0^{Hd3} and T_0^{Hd4} must be less or equally to T^*.

As we can see from Figure 4, these conditions are fully satisfied. It means that two-row addressing method for a cholesteric display can be realized by the new simple two-level DDS. With this DDS we can address passive matrix cholesteric display with a speed about time $(3/4)\times T_{H\text{-}P^*}$ per line. This DDS have the maximal addressing speed from all two-level DDS for cholesteric bistable displays.

Conclusion

In this paper we have analyzed hysteresis properties of cholesteric liquid crystal materials. Also the new two-level DDS for the fast dynamic addressing of bistable cholesteric displays have been demonstrated. In this new DDS two-row at a time addressing method is used. All others two-level DDS have on 33 percents smaller addressing speed in comparison with the new DDS. Thus we have the new simple dynamic drive scheme for a cholesteric display with the simple drive sequences and high addressing speed.

Acknowledgements

The authors would like to gratitude Mr. P. Titarenko and Mr. Yu. Kolomzarov for their help in preparation of liquid crystal display cells.

This work was supported by STCU under the project No. 2025.

References

[1] D.K. Yang, J.L. West, L.-C. Chien and J.W. Doane, Control of Reflectivity and Bistability in Displays Using Cholesteric Liquid Crystals, J. Appl. Phys., 76 (2), p. 1331-1333, 1994

[2] X.Y. Huang, J.W. Doane, D.K. Yang, The Transient Response and Dynamic Drive of Cholesteric Liquid Crystal Displays, Journal of the SID 5/3, p. 179-187, 1997

[3] D.K. Yang, Z.J. Lu, Switching Mechanism of Bistable Reflective Cholesteric Displays, SID 95 Digest, p.351-354, 1995

[4] M. Kawachi, O. Kogure, Hysteresis Behavior of Texture in the Field-Induced Nematic-Cholesteric Relaxation, Japan J. Appl. Phys., Vol.16, No. 9, p. 1673-1678, 1977

[5] X.Y. Huang, D.K. Yang, P. Bos and J.W. Doane, Dynamic Drive for Bistable Reflective Cholesteric Displays: A Rapid Addressing Scheme, SID 95 Digest, p.347-350, 1995

[6] X.Y. Huang, M. Stefanov, High-performance Dynamic Drive Scheme for Bistable Reflactive Cholesteric Displays, SID 96 Digest, p.359-362, 1996

[7] Y.M. Zhu, D.K. Yang, High-Speed Dynamic Drive Scheme for Bistable Reflactive Cholesteric Displays, SID 97 Digest, p.97-100, 1997

[8] A. Kozachenko, P. Oleksenko, V. Sorokin, V.Nazarenko, Histeresis as a Key Factor for the Fast Control of Reflectivity in Cholesteric LCDs, Conference Record of the IDRC 97, p.148-151, 1997

[9] A. Rybalochka, V. Sorokin, S. Valyukh, A. Sorokin, V.Nazarenko, Dynamic Drive Scheme for Fast Addressing of Cholesteric Displays, SID 2000 Digest, pp. 818-821, 2000

[10] A. Rybalochka, V. Sorokin, S. Valyukh, A. Sorokin, Simple Drive Scheme for Bistable LCDs, SID 01 Digest, pp. 882-885, 2001

[11] S.J. Roosendaal', L.M. Hage, K.E. Kuijk, L.J.M. Schlangen and J.A.M.M. van Haaren, Fast Addressing of Cholesteric Texture Liquid Crystal Displays, SID 01 Digest, p.1268-1271, 2001

NED-P19. A Method for Measuring a Reflective Twist Nematic Liquid Crystal Cell Properties

S. Valyukh, A. Rybalochka, V. Sorokin, P. Tytarenko, K. Skarp*

Institute of Semiconductor Physics NASU, Kyiv, Ukraine
**Dalarna University, Borlänge, Sweden*

Abstract

We propose an optical method for simultaneous measuring the cell gap, twist angle, and wavelength dispersion of the birefringence of a reflective liquid crystal cell. It is based on spectral measurements of light reflected from the cell that illuminated by polarised light and passed through the exit polarizer. The measurements are made for three different orientations of the exit polarizer with the angles 0^0, 45^0 and 90^0. In order to determine unknown parameters, the inverse optical problem is solved. The proposed method may be applied for the low cell gap as well as the high cell gap.

1. Introduction

Recently reflective liquid crystal displays (LCDs) have been found wide applications in verious mobile devices, because of their low power consumption and light weight. The twist angle, cell gap, and the birefringence are important parameters that determine the optical and electro-optical properties of conventional twisted nematic (TN) and super twisted nematic (STN) LCDs. In order to get an image of preferred quality, the precise control of these parameters is necessary. Therefore a simple, fast and accurate method to measure the twist angle and the retardation of filled reflective TN (or STN) cells is highly desirable.

Various methods for measuring reflective twist nematic liquid crystal cell properties have been proposed [1-5]. Some of them use a single wavelength as an optical probe, the others based on analysis of spectral distribution of light. A major disadvantage of the monochromatic methods is impossibility to find the wavelength dispersion of the retardation (or birefringence). To derive the cell gap, it is necessary to know the liquid crystal (LC) birefringence for the wavelength of light used in the measuring. Most materials are only supplied with the principal refractive indices at one wavelength (typically 589 nm). If this wavelength differs from the exploitable one, an additional measurement of the birefringence is needed. The same problem exists for the spectral methods which use certain special points in the spectrum of observed light, for example, the wavelength of null transmittance [4] or variation points in the spectrum [5]. Moreover, for some configurations of the LC cell it is difficult to find these spectral positions accurately, and, as a rule, they have to be determined manually. A common drawback of both methods is that they cannot be rendered fully automatic.

In this paper we propose a method for measuring retardation of the LC cell, its wavelength dispersion and the twisted angle. We use the same geometry of the experimental setup as in the monochromatic method introduced by H. L. Ong [2]. Retardation, its wavelength dispersion and the twisted angle are derived from three spectra of light passed through the LC cell in configuration, where the entrance polarizer is always oriented at 45 degreases to the entrance LC director, and the exit polarizer is oriented at the angles 0^0 (parallel), 45^0 (diagonal) and 90^0 (perpendicular) to the entrance polarizer direction. The cell gap is got, if the birefringence is known for some wavelength. In comparison with Ong's monochromatic method, spectral measurements provide a large array of experimental data that makes the spectroscopic method more accurate.

The main idea of the proposed method is to find the unknown parameters of the LC cell from quantitative comparison between theoretical calculations and experimental data. This allows us to determine the wavelength dispersion of the birefringence. The proposed approach can be used for finding the tilt angle and input director orientation. In addition, our method is not such sensitive to noise or to contribution caused by multi-reflections between layers of the sandwiched structure of the LC cell as the monochromatic method is, when coherent light source is used.

2. Theory

Intensity of light reflected from uniformly twisted nematic LC cell at normal can be calculated using the Jones 2x2 matrix technique [6]. The Jones matrix of the reflected LC cell is:

$$\hat{G} = r\hat{M}^T\hat{M}, \quad (1)$$

where r is reflectivity of the cell reflector, $\hat{M}$ is the Jones matrix of the LC layer, the index T means transparent. The matrix $\hat{M}$ is given:

$$\hat{M} = \hat{R}(\varphi)\begin{pmatrix} \cos X - i\frac{\Gamma \sin X}{2X} & \varphi\frac{\sin X}{X} \\ -\varphi\frac{\sin X}{X} & \cos X + i\frac{\Gamma \sin X}{2X} \end{pmatrix}, \quad (2)$$

where matrix $\hat{R}(\varphi)$ is a coordinate rotated matrix, φ is the twisted angle, $X = \sqrt{\varphi^2 + \left(\frac{\Gamma}{2}\right)^2}$, $\Gamma = \frac{2\pi(n_e - n_o)d}{\lambda}$; n_e, n_o are principal refractive indexes of LC, d is the cell gap, λ is the wavelength. Intensity of light reflected from the cell is

$$I_r(\lambda) = I_o(\lambda)(1 - r_h(\lambda))\left|\vec{E}_{ex}\hat{G}\vec{E}_{in}\right| + I_o(\lambda)r_h(\lambda)\left|\vec{E}_{ex}\vec{E}_{in}\right| \quad (3)$$

where I_o is intensity of light passed through two parallel polarizers, r_h is the harmful reflectivity from the top cell surface, $\vec{E}_{ex}$, $\vec{E}_{in}$ are the unit Jones vectors that describe state of light polarisation passed through the entrance and exit polarizers, respectively.

The wavelength dispersion of the birefringence (Δn(λ)) can be approximated by the Cauchy formula [7]

$$\Delta n(\lambda) = A + \frac{B}{\lambda^2}, \quad (4)$$

where A, B are constants. If the birefringence is known for a wavelength λ_0 (for example λ_0=589 nm), one of the coefficients can be expressed through the other:

$$A = \Delta n(\lambda_0) - \frac{B}{\lambda_0^2} \quad (5)$$

3. Experiment

The optical setup for measuring cell gap and twist angle of reflective TN LC cells is shown in Fig.1. The collimated light from a lamp that has a broad light spectrum passes through the entrance polarizer and after the beam-splitter falls on the cell. The reflected ray, after passing through the beam-splitter and the exit polarizer, is registered by the computer controlled spectrometer.

In order to neglect the sensitivity of the spectrometer for state of light polarization, we rotate the entrance polarizer only.

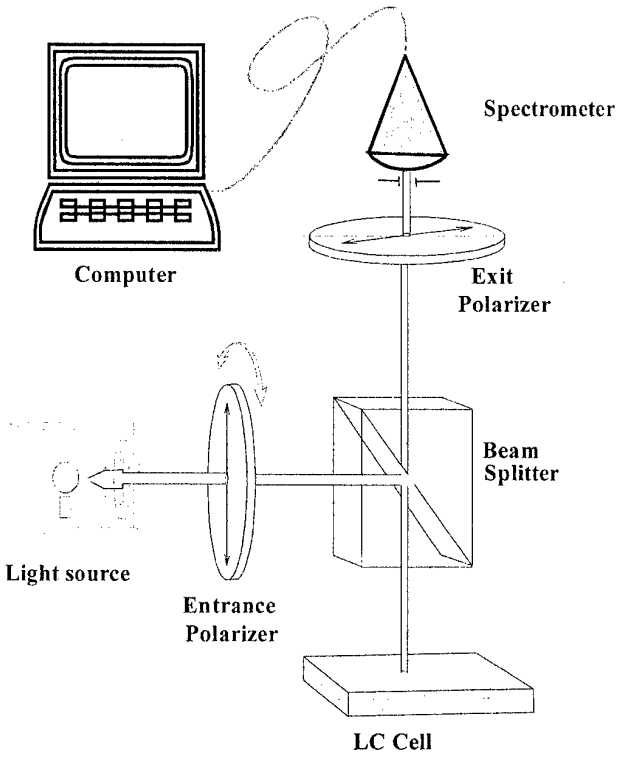

Fig.1. Experimental setup.

4. Algorithm

The procedure of measurements contains the following steps:

1) Evaluating the reflectivity caused by interfacial reflections (r_h).

2) Measuring of light spectra for the three positions of analyzer: $\Phi_{exit} = 0^0$, $\Phi_{exit} = 45^0$, $\Phi_{exit} = 90^0$. Taking into account the Eq.3, the spectral distributions of light passed through the LC cell ($I_o(\lambda)\left|\vec{E}_{ex}\hat{G}\vec{E}_{in}\right|$) is recalculated for three orientations of the entrance polarizer. The results are saved as the numerical functions: $S_0(\lambda), S_{45}(\lambda), S_{90}(\lambda)$.

2) Normalisation of obtained spectra by formulae:

$$S_0^*(\lambda) = \frac{S_0(\lambda)}{S_0(\lambda) + S_{90}(\lambda)},$$

$$S_{45}^*(\lambda) = \frac{S_{45}(\lambda)}{S_0(\lambda) + S_{90}(\lambda)},$$

$$S^*_{90}(\lambda) = \frac{S_{90}(\lambda)}{S_0(\lambda) + S_{90}(\lambda)} \qquad (5)$$

3) Compilation a new function

$$F(d,B,\varphi) = \sum_{\lambda=\lambda_{min}}^{\lambda_{max}} ((s^c_0(\lambda,d,B,\varphi) - S^*_0(\lambda))^2 + (s^c_{45}(\lambda,d,B,\varphi)$$

$$- S^*_{45}(\lambda))^2 + (s^c_{90}(\lambda,d,B,\varphi) - S^*_{90}(\lambda))^2) \qquad (6)$$

where d, B and φ are varying parameters; $s^c_0, s^c_{45}, s^c_{90}$ are the light spectra calculated according to mathematics described above with the variables d, B and φ, $\lambda_{min}, \lambda_{max}$ are, respectively, the minimal and maximal wavelengths in the measured spectra. The function $F(d,B,\varphi)$ is always positive and reaches its global minimum (zero value for an ideal case) when the varying parameters are equal to the LC cell parameters. Thus, to get the unknown values it is necessary to find the global minimum of the function $F(d,B,\varphi)$. To do this it is nessasary to use the standard numerical methods [8,9]. In fact, from mathematical point of view such founding of the minimum is the method of least squares.

The another way for obtain unknown parameters of the LC cell, when both theoretical and experimental data are in a good agreement, is to use the procedure of resorting.

5. Results and discussions

From mathematical point of view the problem under consideration is an inverse task. In order to examine the number of solutions that this task can have, we study dependencies of light intensity in the proposed above experimental setup versus parameter $\frac{\lambda}{\Delta nd}$ for different twisted angles. The calculated distributions of light intensity versus the ratio between the wavelength and retardation for different twist angles are shown in Fig.2. After numerical analysis of these results we have concluded, that three spectra of visible light which got in as it is described above, are unique and depend on the ratio $\frac{\lambda}{\Delta nd}$ and the twist angle. For evaluating the harm light reflectivity from the top surface of the cell, reflectivity of a glass plate, that used as a cover in the LC cell, is measured in the experimental setup shown in Fig.1.

In order to reach the best coincidence between experimental and calculated results, the value of entrance director orientation and tilt angle can be varied.

Accuracy of our method, in principle, cannot be less than proposed by H. L. Ong monochromatic one [2] that is considered as a quite accurate method. Moreover, a large set of experimental data allows one to find the wavelength dispersion of the birefringence and the other parameters of the LC cell.

6. Summary

In summary, we have proposed and demonstrated a method for measuring the cell gap, wavelength dispersion of the birefringence and the twist angle. It is also suitable for fitting the tilt angle or entrance director orientation. Moreover, the proposed method can be used for measuring the cell gap variation (Δd).

The method can be easily implemented in commercial instruments. It is fully computer controlled, which makes it especially attractive for LCD mass production.

7. References

[1] H. L. Ong, *New Simple Cell Gap Measuring Method With Three Transmission Measurements* //SID'00 Digest, p.79-81 (2000).

[2] H. L. Ong, *Simple and Accurate Optical Reflection and Phase Compensation Methods for Reflective LCD Cell Gap* // SID'01 Digest, p.430-434 (2001).

[3] S. Valyukh, A. Rybalochka, V. Sorokin,K. Skarp, A.Slobodyanyuk *Spectroscopic method to measure the cell gap of TN LC cells//* The 22nd SID conference, Nice (France), 433-436 p., 2002.

[4] S.T. Tang, H.S. Kwok, *A New Method for Liquid Crystal Cells Twist Angle and Cell Gap Measurement//* SID'98 Digest, p.552-556 (1998).

[5] J.S. Gwan, D.C. Jeong, C.G. Jhun, K.Y. Han, T.H. Yoon, J.C. Kim, *Cell Gap Measurement of a Twisted-Nematic Liquid Crystal Cell by Using Spectroscopic Method* // Asia Display/IDW'01, p.189-192 (2001).

[6] Yeh P. Optical waves in layered media . – John wiley & Sons Ltd., 1988. – 403p.

[7] I.C. Khoo and S.T. Wu, Optics and Nonlinear optics of Liquid Crystals// World scientific, 1993.

[8] Korn G.A., Korn T.M, Mathematical handbook for scientists and engineers // McGraw-Hill Boook Company,1968.

[9] N. I. Malysh, V. P. Kunets, S. I. Valyukh, Vas. P. Kunets *Saturation of optical absorption in CdS single crystals* // Semiconductor Physics, Quantum Electronics & Optoelectronics. V.2, No 1. P.31-34.

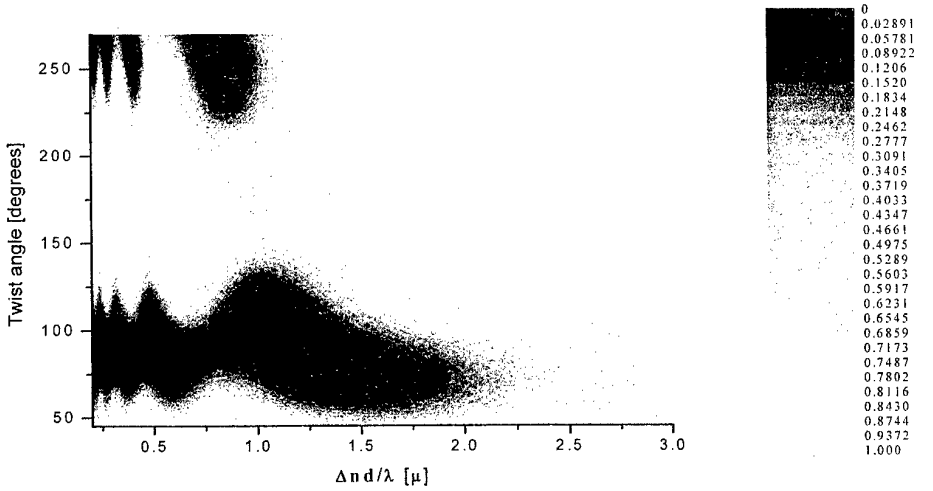

Fig. 2. Distribution of light intensity for parallel polarizers.

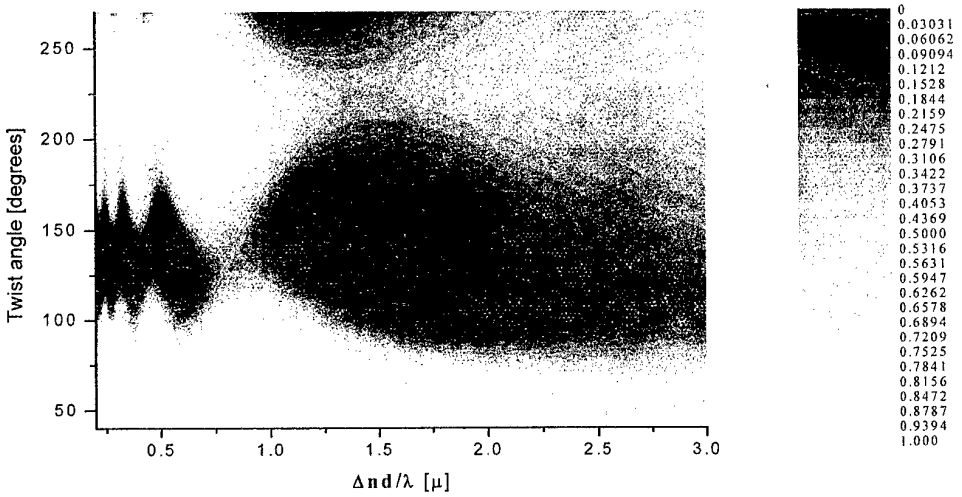

Fig. 3. Distribution of light intensity for diagonal orientated polarizers.

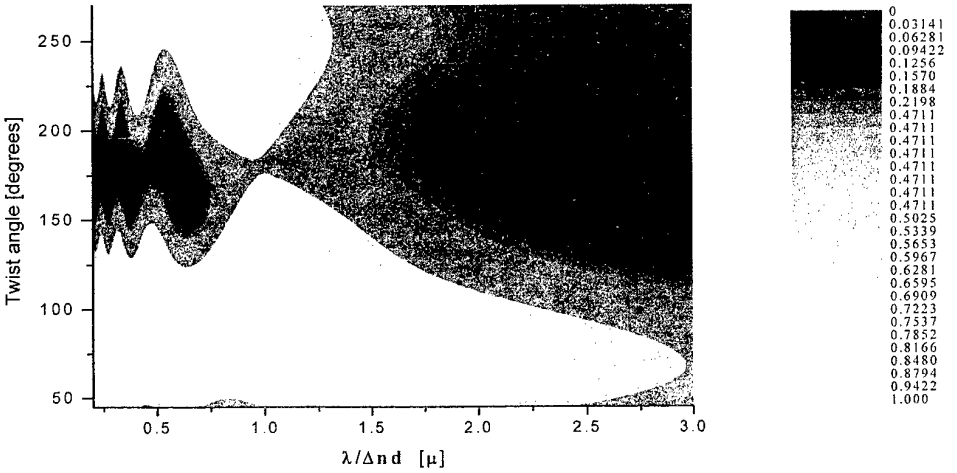

Fig. 4. Distribution of light intensity for crossed polarizers.

NED-P20. Numerical Study of Reflectivity of Monochrom Double-Layer Cholesteric Liquid-Crystal Displays

I.Valyukh[1,2], A. Slobodyanyuk[1], R. Lymarenko[2], K. Skarp[3]

[1]*National Taras Shevchenko University, Kyiv, Ukraine*
[2]*Institut of Applied Optics, Kyiv, Ukraine*
[3]*Dalarna University, Borlänge, Sweden*
E-mail: ivalyukh@ua.fm

Abstract

We consider two constructions of double-layer monochrome cholesteric liquid-crystal displays that allow in principle to reach the reflectivity twice as much as for the single-layer ones. In the first construction both layers are made from enantiomorphic cholesteric liquid crystal materials that have the same pitch but opposite handedness. Two layers of the second construction are made from the same liquid-crystal material, but they are additionally separated by a half wave plate for wavelength of maximum selective reflection of cholesteric liquid crystal. Reflectivity of the said displays versus an angle of incidence and retardation of the birefringent plate were obtained numerically. Ellipticity of the eigenmodes of CLC in the double-layer constructions are analyzed too.

1. Introduction

Reflective liquid crystal displays (LCDs) have favorable properties which make them an attractive alternative for transmissive LCDs. During the last years especial attention was focused on cholesteric LCDs (CLCDs) due to their important display features such as selective reflection of light, good contrast, large viewing angles, and bistability. Luminance and contrast ratio of CLCD are defined by reflectivity of planar texture of the cholesteric liquid crystal, when a pixel is in the bright state. One of the integral parts of nematic LC displays is a polarizer that except of rising in display price districts luminance, because natural light passing through a polarizer loses at least 50% of power. From this point of view the absence of the polarizers in a CLCD is its advantage. On the other hand a cholesteric liquid crystal (CLC) is in the planar texture itself can be considered as a circular polarizer. That is why its reflectivity cannot be more than 50% too.

In an attempt to reach the reflectivity of CLCD more than 50% the double-layered CLCDs have been proposed [1-3]. There are two constructions of double-layer cholesteric liquid-crystal displays that allow us to reach reflectivity up to 100%. In the first construction both layers are made from enantiomorphic cholesteric liquid crystal materials that have the same pitch but the opposite handedness (Fig.1a). Two layers of the second construction are made from the same liquid-crystal material, but they are additionally separated by a birefringent plate, retardation of which is half wavelength of the peak selective reflectance of CLC (Fig 1b).

Reflective properties of the double-layer CLCD can be explained in terms of normal modes that propagates in CLC. Incident unpolarized light excites in gyrotropic-anizotropic medium of CLC two mutually orthogonal normal waves that have in the general case elliptically polarizations. The state of light polarization (ellipticity) of the normal modes depends on the angle between the direction of light propagation inside CLD and helical axis.

One mode with sign of rotation of the $\boldsymbol{E}$ vector coincided with the sign of the helical pitch totally reflectes from the periodic medium of CLC. The other one transmits it without losses. The idea of the both mentioned above constructions is to reach maximum reflectance in such manner when the wave transmitted

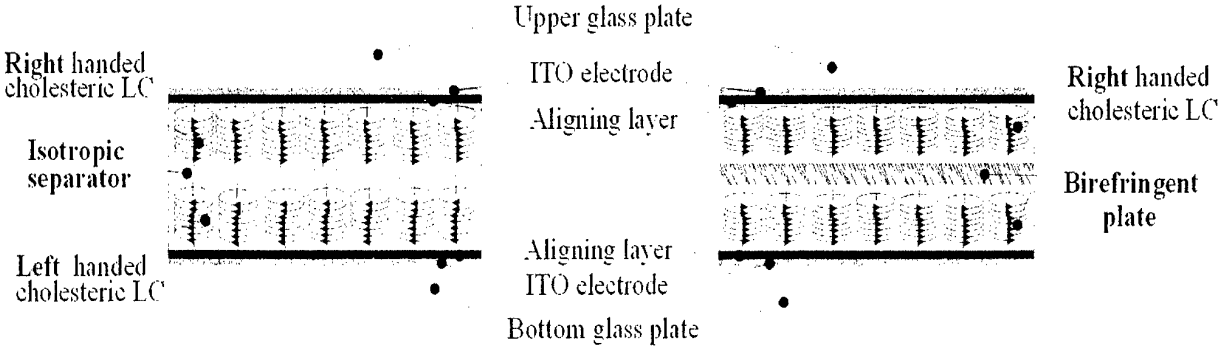

Fig. 1. The double-layer structures of cholesteric liquid crystal displays.

through the first layer totally reflects from the second one. In the construction shown in Fig. 1a, this is realized, because of opposite handedness of the CLC in layers. In the other construction (Fig. 1b), the wave passed the first layer changes its polarization on opposite, because of the half-wave plate, and after that totally reflects from the second layer. Thus, the maximum reflection can reach unity in this case too.

In the paper we consider reflectivity of both mentioned above double-layer constructions of CLCD for normal and oblique light incidences, study the dependence of the light reflection versus the phase retardation of the separated plate. We deal with CLCs that have the ideal planar structure. The case of unperfected planar will be considered in another paper.

2. Normal incidence

Let us consider the reflectivity of both mentioned above constructions of CLCD (Fig. 1) for the simplest case of normal incident light. To do this we use the well-known Berreman 4x4 matrix method [4]. The obtained reflectivities of the single and double-layer CLCD versus a wavelength are shown in Fig.2. Principal refractive indices of CLC in the calculations were no=1,48, ne=1,54, and the pitch - 333 nm.

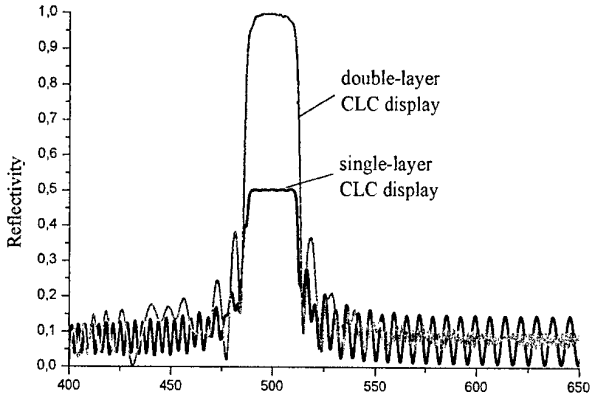

Fig. 2. Reflectivity of the single and double-layer CLC displays versus wavelength

These dependencies demonstrate that reflectivity of the double-layer structure in the spectral region satisfied to Bragg condition is twice as much as for single-layer one.

It is noted that 100% reflection is always achieved theoretically by stacking enantiomorphic material with opposite handedness (Fig. 1a). In this case the normal mode that passes through the first slab reflects from the second one. The advantage of the first construction (shown in Fig.1a) is that the maximal reflectivity for wavelength satisfied to the Bragg condition always is unity. On the other hand, in practice it is very difficult to make chiral mixtures that have the same pitch but opposite handedness and possess similar temperature and electro-optical properties. This may be the essential disadvantage of the considered construction for practical applications.

As for the construction presented at Fig.1b, both slabs consist of the same material. In ref. [1] it was concluded that this is not well suited for the practical applications, because the half-wave plate has retardation only for the fixed wavelength, and the half-wave plate is quite expensive. To get a more detail understanding concerning the practical applications, let us study the dependence of maximal reflectivity versus the phase retardation of the separated plate and evaluate how its retardation affects on reflectance. Using the Berreman method [4] again and studding the reflectivity for the wavelength 500 nm (the other parameters are the same as were before) we obtained the dependence plotted in Fig.3.

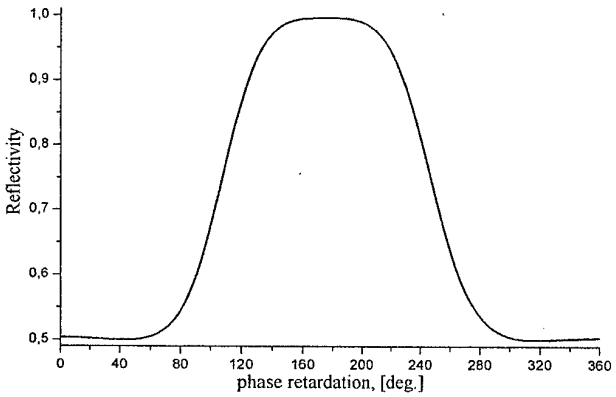

Fig. 3. Reflectivity versus the retardation of the birefrigent plate.

According to this graph the reflectivity changes from unity, when the phase retardation of the birefrigent plate is around 180^0 ($\pi(1+2N)$ where $N=0,1,2...$) to 0.5, when the phase retardation of this plate equals to 0^0 or 360^0 ($2N\pi$). It is easy to see that the reflectivity is near 1 when the retardation of the birefrigent plate differs from $\lambda/2$ up to 15% (λ is the peak of wavelength given by Bragg formula). This fact allows us to confirm that the requirements for birefrigent plate are not quite essential as they are usually for the half-wave plate in optical setup. We can use an ordinary anisotropic film here that has the retardation near $\lambda/2$. In addition, it should be noted that we could replace the birefringent plate by electrically controlled twisted nematic slab. In this case it is possible to change the display luminance automatically.

3. Oblique incidence

Let us examine the reflective properties of both constructions of the CLCD (Fig.1) in case of oblique incident light. Again, the simplest way to do this is to analyze the normal modes of CLC. As it was

mentioned above, unpolarized light incident onto chiral medium excites in CLC two mutually orthogonal elliptical polarized normal waves. One mode passes through the layer of the CLC whereas the second one reflects according to the Bragg condition. The ellipticity of the normal waves depends on the incident angle on CLC. The main idea of the considered in the paper double-layer CLCDs is to achieve conditions when the mode passed through the first slab totally reflects from the second one. The construction presented in (Fig.1a) possesses this property for all incident angles.

As for reflectance of the CLCD with the birefrigente plate, the situation is not such good. The point is that the state of light polarization of the wave passed through the birefringent plate depends on the angle between the optical axis of the birefringent plate and the direction of wave propagation. That is why the reflectance of the double-layer CLCD shown in Fig. 1b changes versus the angle of incidence. To understand this more detail, we found the angles of ellipticity [5] of the waves passed through the first CLC layer and the birefringent plate for two perpendicular orientations of the optical axis of the plate, and compared with state of light polarization that totally reflects from the second CLC layer. In order to find the ellipticities of the normal modes, we investigated dependencies of maximum selective reflections and minimum transmittance versus the state of light polarization of the incident ray. Calculations were made for the wavelength satisfied to Bragg conditions. Ellipticity of the incident light was changed from linear to circular. When reflectance reaches its maximum value (transmittance is minimum), the state of light polarization of the normal mode that totally reflects coincides with the polarization of incidence light. In case of minimum reflectance and maximum transmittance, the normal mode that transmits has the same state of light polarization as incident light. Obtained results as functions of the angle of light incidence are shown in Fig.4.

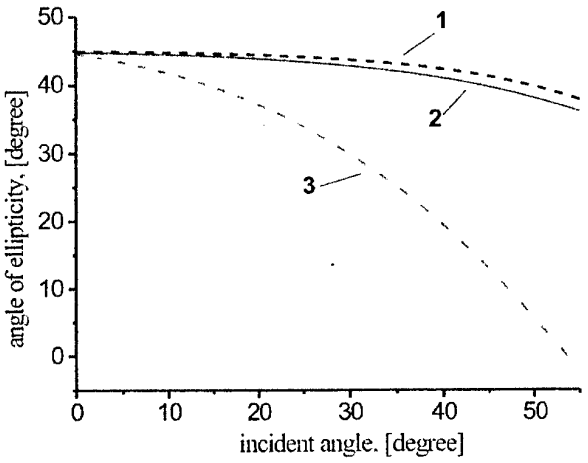

Fig. 4. The angle of ellipticity versus an angle of incidence.

The curve denoted by the number 1 (Fig. 4) corresponds to the ellipticity of the wave that totally reflected from the second layer of the double-layer CLCD. The curves of the number 2 and 3 (Fig. 4) correspond to cases when the optical axis of the birefringent plate lays in the plane of light incidence and perpendicular to it, respectively.

According to obtained curves the maximum reflectance for case of oblique incidence depends on the direction of observation. As an example, we calculated the reflectance of the considered CLCD versus azimuthal angle (φ in Fig.5) when the polar angle (Θ in Fig.5) is 50^0. Obtained results are shown in Fig. 6.

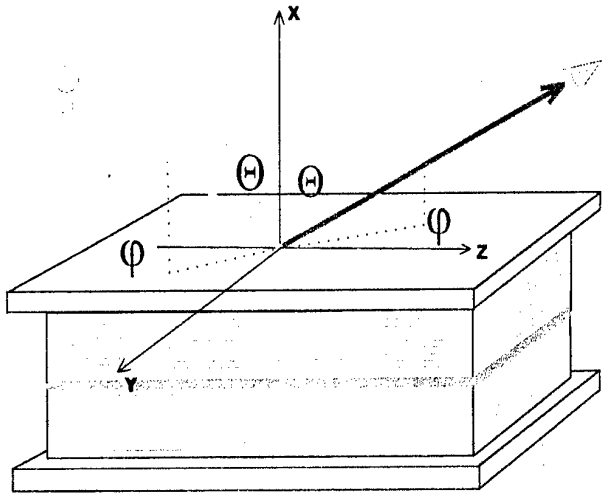

Fig. 5. The polar and azimuthal angles in the laboratory system XYZ.

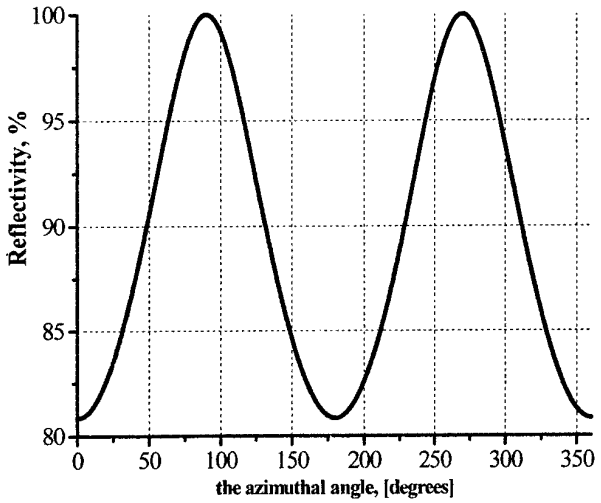

Fig. 6. The reflectivity of the peak versus the azimuthal angle.

Minima of this dependence (Fig. 6) correspond the case when the optical axis of the birefringent plate is perpendicular to the plane of the light incidence. Respectively, reflectance of maxima correspond the case when optical axis of birefringent plate is parallel to the incidence plane of light. Such dependence is disadvantageous for this structure. On the other hand, the construction (Fig. 1b) with established the orientation of optical axis of the birefringent plate for preferable section for observation can be applied in some deices.

In order to find the optimal luminance conditions of double-layer CLCD it can be applied the same approach as for single-layer one [6, 7].

Conclusions

Two constructions of the double-layer monochrome CLC displays were considered. The reflectance of such displays is twice as much as for single-layer ones.

Using Berreman method the dependencies of reflectivity of the mentioned displays versus an incident angle of light and parameters of the birefringent plate were obtained. The merits and limitations of each of CLCDs were discussed. It was shown that in the double-layer construction where both layers are made from the same material the ordinary birefringent plate with retardation differs from $\lambda/2$ up to 15% can be used (the wavelength is satisfied Bragg formula). So that both of monochrome CLCDs are tolerance in manufacturing. Results of this paper can be applied to optimize the reflective properties of the CLCDs.

Acknowledgments

We gratefully acknowledge Dr. S. Valyukh and Dr. A. Kozachenko for helpful discussions.

References

1. E. Lueder, *Liquid Crystal Displays Addressing Schemes and Electro-optical Effects*//John Willey & Sons, 2000.
2. A. G. Kozachenko, A. I. Kryvutenko, L. Komitov, *Formation and Properties of Double Layer Chiral Slabs*// Pros. SID'2002, 453-456 (2002)
3. Y. Kawata, H. Yamaguchi, T Yamaguchi et al., *A high reflective LCD with double cholesteric liquid crystal layers*//IDRC'97, P. 246-249, (1997)
4. Berreman D.W., *Optics in stratified and anisotropic media: 4x4-matrix formulation* // J. Opt. Soc. Am. – 1972. – v.62, №4, – P. 502-510.
5. R. Azzam, N. Bashara, *Ellipsometry and polarized light*/ North-Holland, 1977.
6. Valyukh S., Slobodyanyuk A., Sorokin V., *Viewing characteristics of reflective cholesteric liquid crystal displays // Proc. of the* 8th Int. Symp. *Advanced display technologies*, Crimea, Ukraine. – 1999. – P. 287-294.
7. Valyukh S., Slobodyanyuk A., Sorokin V., *Optimization of illumination conditions for reflective cholesteric liquid crystal displays //* proc. of 20th IDRC, Florida, USA.– 2000. – P.213-216.

NED-P21. **Thermo-optical properties of polyvinyl alcohol films modificated by dichroic dyes**

S. Shahab, V. Agabekov, N. Ariko, N. Ivanova

Institute of Chemistry of New Materials of the National Academy of Sciences of Belarus,
Staroborisovski Trakt 36, 220141, Minsk-141, Belarus
E-mail: agabekov@nf.ichnm.ac.by

Abstract

Polarizer films based on absorption dichroism of anisotropic system: polyvinyl alcohol (PVA) – dichroic agent (iodine or organic dye) are traditionally used in display units.
The analysis of scientific and patent literature shows that spectral- polarizing properties, thermal stability and light stability depend on a nature of the dichroic agent. Film painted molecular iodine have high effect of polarization practically in all range of a seen part of a spectrum, but at exploitation of films in conditions of the high temperatures and humidity of air iodine containing chromophores were destroyed[1].
The replacement of iodine by organic dyes has allowed raising termostability and moisture resistance of polarizers, however their polarizing ability in most cases has appeared below iodine containing films and besides was limited to area of absorption of dye.
Was established earlier that uniaxially oriented polyvinyl alcohol film colored by dichroic azodyes containing 2 or 3 N=N of group have effect of polarization sufficient for creation of polarizer for a range 450-650 nm. In the given work the results of study of the spectral-polarizing characteristics and thermal properties such films are given.

Experimental

Water-soluble azodyes

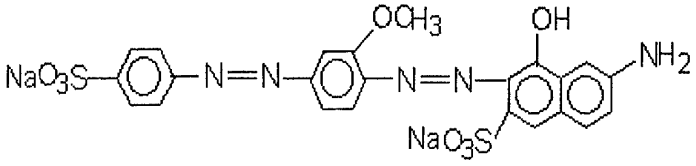

M₁

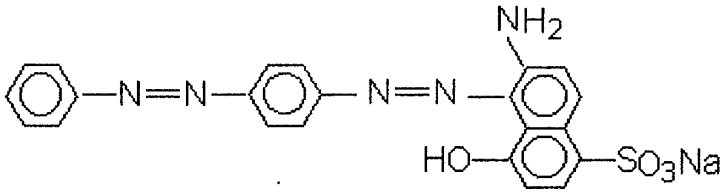

M₂

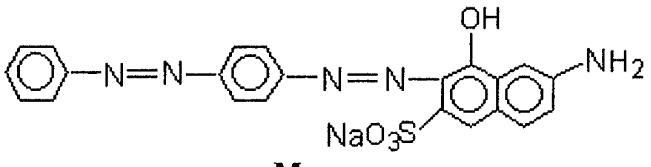

M₃

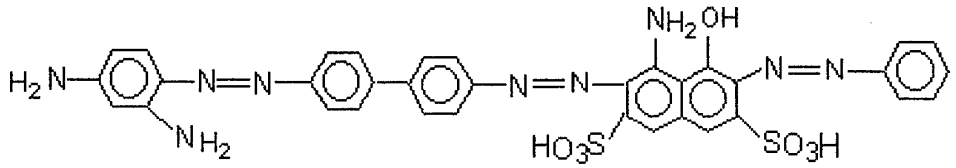

M_4

were synthesized in accordance to a known procedure usually used for preparation of azocompounds [3].

The methods of preparation and dyeing of PVA-films as well as the absorption measurements are described in [2,4].

Heat conductivity was determined by indicated method of definition of a degree of its anisotropy of polymers on the complex equipment (mark LC-201) of firms Frinkle (Sweden).

Results

Azodyes M_1, M_2, M_3 and M_4 taking place in volume of uniaxaily stretched of PVA-films differently absorb in a seen part of a spectrum[2], despite of similarity of a structure of their molecules. Greatest and less dependent from length of a wave optical density is characteristic for a film containing M_3. The film with M_1 absorbs less intensively, is especial in the field of 400 nm. Two absorbed of a maximum M_1 and M_3 are expressed indistinctly: in a film with M_1 they are at 505-510 and 598-600 nm, in a film with M_3 at 435-490 and 575-580 nm. The dye M_2 absorbs basically in the field of 550-600 nm where at 575-580 nm is located its absorbed maximum. Least coefficient of extinction is observed at M_4 which has three maxima of absorption at 500-530, ~ 600 and 638-640 nm.

Polarizing ability of films containing the investigated dyes also depends on a nature of dye. If films have comparable EP at maxima of absorption than on ability to polarize light in a wide range of a spectrum from 350 up to 675 nm dyes can be arranged in a range $M_3 > M_1 > M_2 > M_4$.

For all investigated connections EP grows with increase of quantity of dye in a film (tab. 1).

Table. 1

Influence of concentration of dye on polarizing ability

C, %	Dye	EP, %					
		350 nm	400 nm	450 nm	500 nm	550 nm	600 nm
0,1	M_1	29	20	49	53	80	65
	M_2	38	27	20	49	79	63
	M_3	46	61	78	71	79	70
	M_4	5	7	18	37	40	67
0,2	M_1	49	42	70	82	83	88
	M_2	42	28	26	55	85	71
	M_3	71	83	94	89	94	88
	M_4	22	11	27	54	63	87
0,4	M_1	62	58	87	90	93	95
	M_2	48	61	47	85	96	96
	M_3	81	92	99	97	98	98
	M_4	48	30,8	49	64	78	96

The molecular structures M_1, M_2, M_3 differ only by quantity of the assistants and situation of azogroup in naphthalene range. Hence, the distinctions in polarizing ability of films are connected to orientation of dye in a polymeric matrix, which is determined by a condition of dye, interaction of its molecules with circuits PVA and ability to be built along an axis of stretching. The dye M_4 containing three N=N of group polarizes light only in peak of maximum, that testifies axis of long-wave oscillator is rather close to an axis of orientation of film.

It is known that the dye can react with molecules of environment[5]. Such interaction with the extended fragments of molecules of PVA promotes orientation of molecular axis of dye along an axis of stretching of film. It is possible to assume that M_1 and M_3 cooperate with circuits of PVA in comparison with M_2 and M_4 more actively. The hydrogen connection in molecules of the last weakens on all probability their interaction with a polymeric matrix.

At introduction of dye in PVA-film its heat conductivity has changed (tab. 2), thus along an axis of orientation it has increased, and in perpendicular axis reduced. Heat conductivity poorly depends on nature of dye - only for M_4 it is a little bit higher in comparison with M_1, M_2 and M_3, in parallel and perpendicular directions. According to the theory of Airman thermal resistance of sample represents a grid of elementary thermal resistance with atoms located in units[6], which depends on force of connections: than more strongly connection, is less resistance and more heat conductivity. Hence, at the presence of dye there is hardening connections caused by the main valence, which settle down along the basic circuit of polymer and easing of connections in a perpendicular direction. Taking root between circuits of polymer, the molecules of dye reduces free volume and average distances between circuits that promote increase of elastic constant connections along an axis of orientation are exploited. The resistance of sample is reduced and heat conductivity grows. In perpendicular direction of axis of orientation, the dye, on the contrary, weakens interaction: the resistance grows and heat conductivity falls.

Thus data on heat conductivity of films painted by azodyes testify to interaction of dye with molecules of PVA that will be coordinated to conclusions made of results of research of the spectral-polarizing characteristics the films.

Table. 2

Heat conductivity of films containing azodyes

Dye	Quantity in film, %	Heat conductivity, W/ m.°C	
		In parallel axes of orientation	Perpendicularly axes of orientation
–	–	0,788	0,455
M_1	0,1	0,865	0,154
	0,2	0,851	0,150
	0,4	0,844	0,146
M_2	0,1	0,877	0,160
	0,2	0,871	0,152
	0,4	0,863	0,141
M_3	0,1	0,884	0,150
	0,2	0,877	0,142
	0,4	0,864	0,139
M_4	0,1	0,916	0,167
	0,2	0,906	0,160
	0,4	0,884	0,157
Mix of M_1, M_2, M_3	0,1×3	0,884	0,143

Reference

1. Sherkliff. Polyarizovanni svet. M., 1965. C.48.
2. V.Agabekov, L.Filippovich, S.Shahab, N.Ariko, N.Ivanova. Proc. XI-the International Symposium «Advanced Display Technologies». Crimea, Ukraine. 2001. P 164.
3. B.F.Porai-Koshits. Azokrasiteli. "Khimiya".,1972.
4. L.Filippovich, N.Ariko, V.Agabekov. Vesti NAN B, cer. khim. navuk. 2002. № 3. C.168.
5. N.Yamaoka, S.Takatsukit, M.Miura. Bull.Chem.Soc.Japan. 1975, V.48, № 10, P.2739.
6. I.Perepechko. Vvidenie v fiziku polimerof. "Khimiya".,1978. C.105.

NED-P22. REFLECTANCE OF ALUMINIUM REFLECTORS FOR LCD

N.Ivanova, V.Agabekov, V.Verbitski, A.Tsaruk *, V.Hreben *, V.Dlugunovich *

Institute of Chemistry of New Materials of the National Academy of Sciences of Belarus,
36 Staroborisovski Trakt, 220141 Minsk, Belarus
E mail: agabekov@nf.ichnm.ac.by
* B. I. Stepanov Institute of Physics of the National Academy of Sciences of Belarus,
68 F. Skarina Ave., Minsk, 220072, Belarus

Abstract

In this paper ability of aluminium surfaces with a various microrelief to reflect, scatter and transform linearly polarized radiation of a visual region is investigated. It has allowed to present operation aluminium coats in a composition of polarizers of reflecting type, "mirror" reflectors in a construction of liquid crystal displays (LCD) and purposefully them to use on manufacture, in view of presented consumer requirements.

1. Introduction

Now for manufacture of devices and apparatus with light indication on LC as reflectors are widely applied light reflecting coats on polarizers, plates and films. They are the binding and important LCD elements creating a phone for mapping of numerals, letters, figures and other indication and work on reflection and a dispelling of linearly polarized light. However more often in the modern references such mirrors are mentioned as "specula" and there is no particular information on their manufacturing and specification of use. At the same time, there are USA patents [1,2], developments of plant "Kron" (Vladikavkaz) [3] and catalogues of leading firms of manufacturers of film polarizers: "Nitto Denko" (Japan), "Polaroid " (USA), "Ace Digitech. Ltd" (South Korea), in which not at all "specula" but faster the question is "directly diffuse" or "diffuse" reflectors are described.

2. The experimental part

Objects of investigation were the aluminium reflecting coats designed in Institute of Chemistry of New Materials of the National Academy of Sciences of Belarus and used as reflectors for polarizers of reflecting type [4,5]. On structure and geometry reflecting surface and method of its formation the coat can be divided into four groups:

1. **sample 1**-coat is formed by plasma **sputtering of Al** on a matte surface of polyethylene therephthalate (PET) film;
2. **sample 2** – coat is formed by plasma **sputtering of Al** on a smooth surface of the PET film;.
3. а) **sample 3** – aluminum **foil GOST 745-75** with "groove" matte surface, formed during its manufacture;
   б) **sample 5** – the Japanese **foil**, which has been taken off from reflective type polarizer NPF-F-3205 ("Nitto Denko");
   в) **sample 6 –foil TU 1811-001-45011923-99** with "groove" microrelief;
4. **sample 4 – enamel coat** with pigment in form of Al powder.

Polarization ability of coats, their possibilities to reflect and radiation scatter depending on a observation angle were studied on methods designed in Institute of Physics of the National Academy of Sciences of Belarus with use goniophotometric laser stokes–polarimeter [6,7]. Setup, which schema is submitted on fig. 1, consists from He-Ne laser LG-126 *(1)* generating multimode linearly polarized radiation with diameter of a beam 5 mm. Radiation transited through the polarimetric plate *(4)* and correcting polarizer *(5)* which formed the linear polarization as in a plane of incidence, or orthogonal to it. Radiation reflected and scattered by a sample *(6)* placed on a goniometric table was collected by a lens *(15)* and was directed by a lens *(17)* to photometer sphere *(18)*. A part of the radiation getting in sphere was registratied by photomultiplier FEU-79 *(10)*. The electrical signal from FEU-79 was amplified by the electronic device *(12)* and measured by the digital voltmeter *(19)*. For the account of fluctuations a part of laser radiation was directed by the divided plate *(3)* to the basic channel. It consisting of a lens *(8)*, the filter *(7)*, photometic sphere with the detector *(9)* (the photodiode in a regime of photoresistance), the electronic device *(11)* and the digital voltmeter *(13)*. The plane of incidence coincided with a plane of observation.

Rough surfaces of above-mentioned light reflecting coats were exposed by laser radiation (λ = 0,63 μm), linearly polarized in a plane of incidence or perpendicular to it.

For obtaining of the complete information on all surface roughness (the reflecting micro flats directed under different angle to the interface of a coat), a bidirectional reflectance indicatrixes of orthogonal polarized component of radiation

were constructed $R_{\|,\perp} = \frac{I_{\|,\perp}(\text{и})}{I^0_{\|,\perp}}$ and polarizing ability $q = \frac{I_\perp - I_\|}{I_\perp + I_\|}$ at angles of irradiation φ = 5° and observation θ = 5 – 75° accordingly, where $I_\|$, $I_\perp$ - intensities of scattered radiation polarized in a plane of incidence or perpendicular to it, and $I^0_\|$, $I^0_\perp$ -intensities of a incident radiation. The intensities of radiation are measured with relative accuracy 3 % [6].

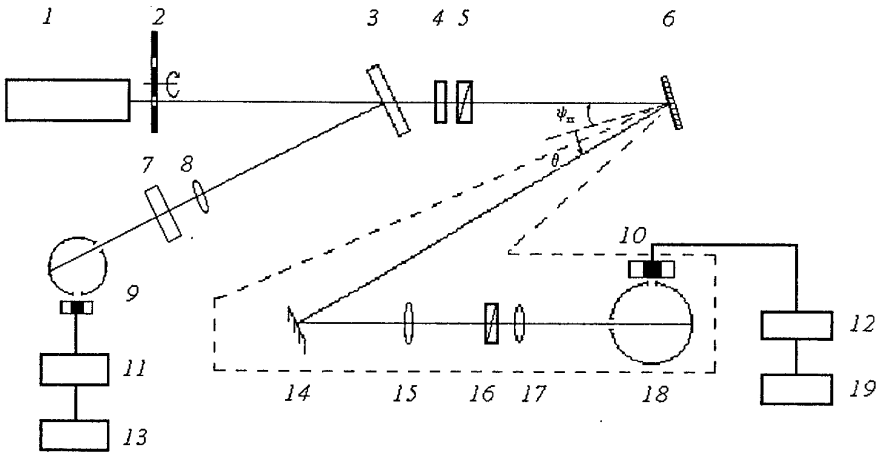

Fig. 1

3. Results and discussion

Dependencies of $R_{\|,\perp}$ and q values for all samples vs. angles of observation are submitted on fig. 2, 3.

Samples 1 – 5 of first three groups represent reflecting coats in which rough reflecting surface contacts only to the air and has no any protective film or other elements from the investigated side. The fourth group includes a sample 6 which is the reflecting enamel coat put on a polymeric film, and the working side of a surface is interior, i.e. is closed from an incident light stream by a film.

For samples 1-5 profilometersation was carried out by profilometer-profilograph of model 252 ("Kalibr", Moscow) and R_a – an average deviation from a middle line of a profile is measured. However for characterization of a surface roughness standard deviation of roughness – σ is used more often [8], which calculated under the formula $\sigma = \sqrt{\frac{\pi}{2}} R_a \approx \frac{1}{0{,}8} R_a$ and its values are given in the table. Besides according to reflecting coats imagines of a raster-type electronic microscope "Hitachi", the sizes and the quantitative relation of roughness in a plane of external sample surface were evaluated.

This has allowed estimating the sizes of reflecting coat roughness in three dimensions. Results of the investigations and observations carried out are presented in the table.

The data of reflecting surface profilometry and electronic microscopy (Table) satisfactorily correlate with results of definition of $R_{\|,\perp}$ (Fig. 2).

Comparison of results for samples of the first group shows, that reflecting coats equally reflect radiation of orthogonal components and there for they weakly polarize incidence radiation, that is shown in a small quantity of q for all registration angles (Fig. 3).

Radiation scattering by the sample 1 is close to the scattering by ideal diffuser (Fig. 2). The electronic microscopy of this sample surface shows presence of roughness of the various sizes (Table). It must be note, that this coat has matte surface view. The sample 2 has the smallest roughness, both on depth, and in other dimensions. It is characterized by specular brilliance at visual viewing and its bidirectional reflectivity indicatrix (Fig. 2) is closest to a specular one (the greatest values of a bidirectional reflectivity at angles close to specular direction and the small-scale values for angles far from specular direction).

Comparative characteristics of a roughness of light reflecting surfaces Table

№ sample	Profilometric date	Electronic microscopy date			Polarimetric date
	$\sigma = \frac{R_a}{0,8}$, μm	Presence of directivity	Roughness along a preferential direction, μm	Roughness across a preferential direction, μm	Change of a signal at scanning in one direction
1.	0,465	No	0,3±0,1÷10±1	0,3±0,1÷1,0±0,1	No observed
2.	0,071	No	0,1±0,05 and smaller	0,1±0,05 and smaller	Observed (rough surface)
3.	0,313	Yes	10±0,5	5±0,5	Observed
4.	1,326	No	3±0,5÷10±0,5	3±0,5÷10±0,5	No observed
5.	0,431	Yes	18 ± 3	10 ± 3	Observed (rough surface)
6.	–	Yes	3±0,5÷30±5	3±0,5÷8±0,5	Observed (rough surface)

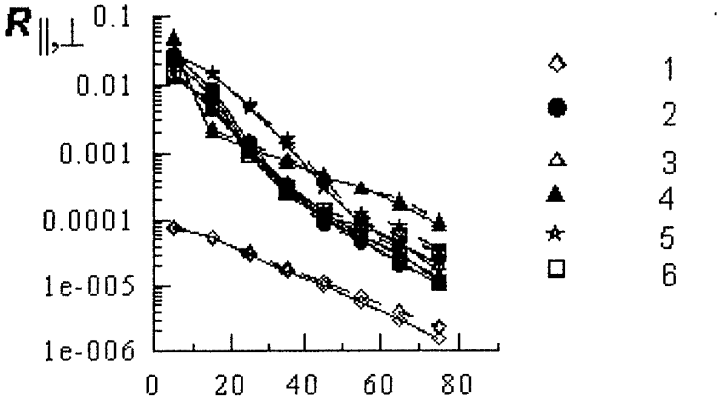

Fig. 2

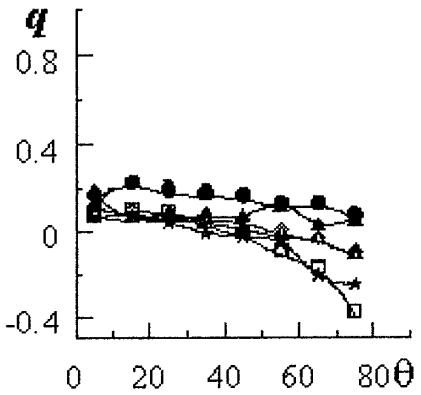

Fig. 3

Sample 3 according to profilometry and electronic microscopy results (Table) has only one size roughness, close on quantity and character to roughness of 2-nd sample. Visually it is characterized by specular brilliance and its bidirectional reflectance indicatrix (Fig. 2) is close to there for the sample 2.

Sample 4 according to profilometry is characterized by the greatest sizes of roughness depth. Viewing of electronic microscopy imagines confirms it, showing presence of cavities sins it has the flake structure caused by the shape of particles of a pigment – Al powder. These roughnesses have one size high by order of probe radiation wavelengths. Despite of homogeneity of a sample 4 relief, presence of the deep cavities causing multiple reflection of radiation by its walls has caused closeness of its indicatrix (Fig. 2) to the indicatrix of the sample 1.

Similarly to samples 2 and 3, the sample 5 is characterised by larger size one scale roughness (Table). Its indicatrix of a bidirectional reflectivity (Fig. 2) is similar to indicatrixes of sample 2 and 3, but its reflectivity is higher. It is caused by one scale roughness of the sample 5, which larger than probing radiation wavelength (λ=0,63μm) in contrast to samples 2 and 3.

One scale roughness of the sample 6 is larger than λ and roughness of the samples 2, 3, 5. Its indicatrix of a bidirectional reflectivity (Fig. 2) is closest to indicatrixes of samples 2, 3. But reflectance for observation angle close to specular (15°) coincides with those for a sample 4.

Thus, it is shown, as structural features of rough aluminium surfaces are connected with their ability to polarize, reflect and scattered under certain angles linearly polarized radiation.

4. Conclusion

Samples 1 and 4 with different roughness, accordingly larger and smaller of probing radiation wavelength and cavities in a coat causing multiple reflections scattered polarized radiation more uniformly, diffusely, and in the larger interval of observation angles. It means that such coats can be used at the construction of displays working at good irradiation conditions and in difficultly available places to review.

Reflecting coats as a matte foil 3, 5, 6, with roughness larger than λ scattered radiation in larger interval of observation angles close to the specular direction. Therefore their using as LCD reflectors does not require additional illumination but have ergonomic restrictions because of a small viewing angle.

References

1. Patent USA № 4 286 127 from 19.05.1981, МКИ^3 G02F 1/13.
2. Patent USA № 4 025 688 from 24.05.1977, МКИ^2 C09J 7/02.
3. C.c. USSR N 1819280 from 30.05.93, МПК^5 C 09 D 131/04, 133/08, 5/33.
4. N.Ivanova, V.Daineko, V.Agabekov etc. //News of NAS Belarus. Ser. of Chem. Sciences, №1, P.125-128, 1999.
5. V.Agabekov, N.Ivanova, V.Verbitski etc. //Proceedings of the 7th International Symposium «Advanced display technologies», December 1-5 1998, Minsk, Belarus, P.171-173.
6. V.Dlugunovich, L.Simonchik, V.Snopko, O.Tsaruk //Measuring technique, №1, P.22-26, 2001.
7. V.Dlugunovich, V.Snopko, O.Tsaruk // Jorn. appl. Spectros., V. 66, №6, P.869-874, 1999.
8. A.Toporets Optics of a rough surface. Leningrad. Mechanical engineering, 1988, 191p.

NED-P23. RESEARCH OF EFFECT PRETILT OF MOLECULES ON REORIENTATION AND OPTICAL PROPERTIES OF THE PLANAR ORIENTATION NEMATIC IN LC-MIKROLENS

A.A.Shevchenko, G.E.Nevskaya, A.V.Morozov, A.Gvozdarev

Novosibirsk State Technical UniversityK. Marx prosp. 20, Novosibirsk, 630092, Russia
E-mail:kof@ref.nstu.ru

Abstract

The effect pretilt of molecules on a focal length LC-microlens with planar orientation is reviewed. The comparative analysis of quality of the map is conducted, depending on a type pretilt. Shown, that the focal length depends on a direction rubbing of footprints.

Keywords: liquid crystal microlens

Introduction

In liquid-crystal microlens the structure (profile) of an index of refraction shapes at the expense of a non-uniformity of an electrical field. This non-uniformity was obtained with the help of an asymmetrical design of electrodes: conducting stratum of a substrate is contained a hole, and other electrodes is solid and transparent.

Experiment

We home made researches of asymmetrical LC-microlens with diameters of holes from 50 up to 800 microns. The welding rods around the holes were divided into sections. It allowed to change operational modes: to submit identical or different voltage to sections of electrodes Researched LC-microlens were manufactured identically in a unified work cycle. The width of LC-layer was 70 microns for all cells. The attitude of diameter of a hole to width of a LC-layer

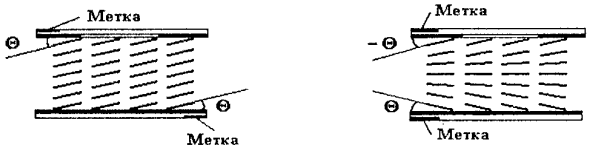

Fig.1. Distribution of the director of molecules NLC in a microlens at a zero potential on control electrodes: а) identical pretilt of molecules; б) opposite pretilt.

varied from 0,7 to 11,4. The LC-cell with different orientation LC on a surface is shown in fig.1. The angle of initial pretilt was 4-5 grades. A qualitative estimation of a angle pretilt conducted with the help of a method described in [1]. Difference of microlenss, introduced in a fig. 1a and 1b that the director NLC is oriented on substrates on one direction (fig. 1a) and opposite (fig. 1b). The liquid crystal with a positive dielectric anisotropy (LC-1289) was used in cells.

The frequency of given sinusoidal voltage was 2 kHz. The focal length was determined with the help of microscope. Quality of the obtained map was evaluated simultaneously. With the help of the digital chamber have been received interference patterns of phase profiles. Laser emission with wavelength λ = 660 nm. Microlens were placed under the angle 45^0 on attitude to a plane of polarization of light, and analizator was 90^0 it.

The results of measurements of focal length for microlens with different parameters L/d and with different pretilt of molecules are shown in a fig. 2; 3. As

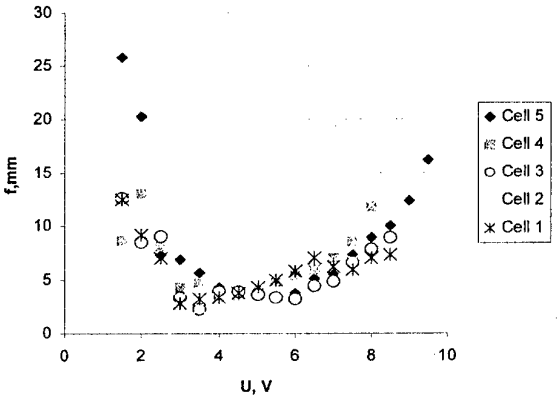

Fig.2. Relation of focal distance to the affixed voltage for lenses of diameter 400 microns and attitude(relation) L/d = 5,7.

an example the dependences of a focal length from fixed voltage for microlens a 600 and 400 μm are shown with L/d 8,6 and 5,7 accordingly with diameter. Number 1,2 indicated on figures, correspond to LC-cells introduced in a fig. 1b; and number 3, 4 and 5 LC-cells introduced in a fig. 1a. Obtained by us independence, will be agreeed the data of other researches [2]. Energizing the focal length at first decreases fast. Then reaches a minimum and starts increasing. High qualita-

tive map of subjects obtained with the help of microlens, is watched in range of voltage of appropriate areas of minimum focal lengths. The range of smooth modification of a focal lengh at large attitude t_0 L/d is decreased. Also see, that the focal length for lens with

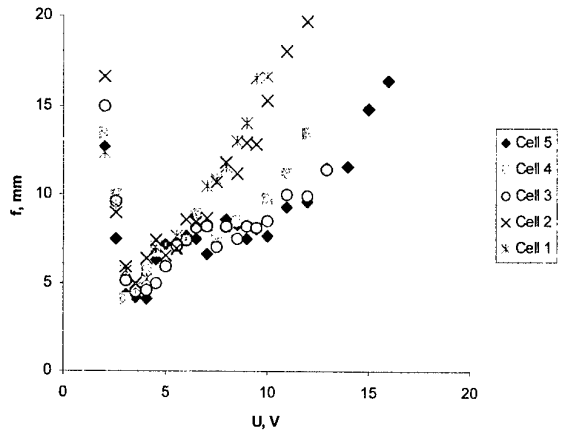

Fig.3 Relation of focal distance to the affixed voltage for lenses of diameter 600 microns and attitude(relation) L/d = 8,6.

parameter L/d difference between values of a focal length becomes less noticeable. For microlens with parameter L/d = 2,9 these distinctions differences disappear absolutely. All data are obtained for one potential on the upper electrode. The time of an output in a mode (take on time) for opposite angle pretilt is significant more, than such angle. It is called by appearanced disclination, which has large time of a resorption. At different energizing on the decomposed electrodes it is possible to avoid disclination. Reducing time of an output LC-microlens in a demanded mode of focusing. Also decreasing time of an output in a mode have achieved by submission(supply) on short time of heightened voltage.

different pretilt has small differences. The focal length of microlens with opposite pretilt (fig.1a) will be more, than for microlens with identical pretilt (fig.1b). It more precisely is expressed for microlens with a large parameter value L/d (fig.2). With decreasing of this

The conclusion

The obtained independence of a focal length from applid voltage allow to define (determine) ranges of modification of focal lengths. At attitudes of width of a LC-layer to diameter of holes such the same as 2-5 have received close to quadratic phase delay. The disclination is detected in microlens opposite pretiltis. The way of the ascent LC-microlenss in nondisclination a mode is offered.

References

1. A.V.Morozov. A technique of an estimation of a corner(angle) pretilt of the director NLC on footprints., Transactionses APEIE-2000, vol. 3, 2000, seconds 99 - 101.

2. A. Gwozdarev, G. E. Nevskaya. Optical properties of Liquid crystal microlenses with variable focus legth. KORUS, 1997, 304 - 307.

NED-P24. The Comparison Of Electrooptical Properties Of LC-Microlenses With Different Nematic Alignment.

G.E. Nevskaya, A. Gvozdarev
Novosibirsk State Technical University,
Novosibirsk , Russia;
E-mail: nevskaya@ref.nstu.ru

Abstract

We have carried out the researches of optical properties of homeotropical, homogeneous and hybrid LC-microlenses. The observation of an interference picture under various applied voltages has allowed to obtain the profiles of a phase retardation for different microlenses. The range of voltage values for holes of different diameters has been determined in the case when a microlens is close to spherical lens and has good optical properties. Under low voltages the LC-microlenses with homeotropical alignment possess defocusing properties and the microlenses with planar and hybrid alignments possess focusing properties. Next voltage increase causes planar- and hybrid-alignment LC-microlenses to become defocusing.

. We have carried out the researches of numerical aperture for all types of microlenses dependens on the voltage and geometrical parameters of microlenses. The comparison of the resolved microlenses ability showed, that the best optical properties in focusing regime possess microlenses with planar alignment, and in defocusing regime – with homeotropical.

Introduction

Liquid crystal optics with variable parameters is one of the perspective directions for optical systems development. LC-microlens is a cell the upper electrode of which has round holes and the lower one is coated by a transparent layer of indium dioxide *(In_2O_3)*.
The hole diameters have values from 170 to 800 urn. Under a voltage applied to the LC-cell an axially-symmetrical electrical field causing a deformation of a nematic director is produced. In result the radially symmetrical refractive index distribution is formed and LC-cell obtained the properties of a lens.

Experimental results

We have carried out the researches of optical properties of homeotropical, homogeneous and hybrid LC-microlenses [1], [2], [3]. The observation of an interference picture under various applied voltages has allowed to obtain the profiles of a phase retardation for different microlenses. The range of voltage values for holes of different diameters has been determined in the case when a microlens is close to spherical lens and has good optical properties.

The Table 1 represents the comparative characteristics of LC-microlenses with different nematic alignment and various ratios of the microlens diameter (L) to the LC layer thickness *(d)*. Used LC-materials are following: for the homeotropical alignment - a mixture *of MBBA* and *EBBA (N-8)* with $\Delta\varepsilon$ =-0.43, Δn = 0.25; for the planar alignment - *GhKM-1289* with $\Delta\varepsilon$=9.8, Δn = 0.17; for the hybrid alignment – *5CB* with $\Delta\varepsilon$=*12.6,* and Δn = 0.18.

Table 1. Comparative characteristics of LC-microlenses

Alignment	Properties	L/d	Range of applied voltage, V	Optimal voltage, V
Homeotro-pical	defocusing	3.2 7.4 11.5 15	3-10 5-11 6-15 6-20	7 10 14 18
Homogenous (planar)	focusing	1.5 3.2 5 7	0.5-3 1-3 3-4 3-6	1.5 3 3,5 4
	defocusing	1.5 3.2 5 7	5-25 6-25 10-70 20-70	maximal
Hybrid	focusing	3.5 7.4 11 15	0.1-2.5 0.1-6.0 0.1-7.0 3.0-11.0	1.2 4.0 5.0 8.0

Under low voltages the LC-microlenses with a homeotropical alignment possess defocusing properties and the microlenses with planar and hybrid alignments possess focusing properties. With the increasing of a ratio L/*d* the values of applied voltage increase.

The optimal voltage value (under which the best optical properties are obtained) increases also.

A voltage increase causes planar- and hybrid-aligned LC-microlenses to become defocusing. The researches of various microlenses focal lengths on voltage are carried out. It is obtained that these dependencies for all microlenses in the range of low voltage values are similar: under voltage increasing the focal length at first decreases attaining the minimum at certain voltage value and after that it increases.

The maximum value of a numerical aperture (NA_{max}) has been calculated for all types of microlenses. The dependency NA_{max} on a LC-microlens diameter is shown at Fig. 1 a, b. As it is shown at Fig.1

the LC-microlenses with planar alignment in the case of focusing regime have a greater numerical aperture (NA_{max} = 0.21) than the microlenses with a hybrid orientation.

In the case of a defocusing properties (see Fig. 1b) LC-microlenses with homeotropical alignment have greater numerical aperture: NA_{max}= 0.25.

The results of researches of LC-microlenses resolution ability are represented at Fig.2. The resolution ability decreases with a growth of L/d parameter for different nematic alignment of LC-microlenses. The greatest resolution ability is observed in the focusing regime for planar LC-microlenses and it takes place in the defocusing regime for homeotropical LC-microlenses.

Conclusion

The researches performed allowed us to make conclusion that focusing planar LC-microlenses are perspective. They have small operating voltage values and greater numerical aperture. The homeotropical LC-microlenses are more perspective under the defocusing regime. They have a great numerical aperture and under certain range of values have a smooth parabolic phase profile.

Represented results confirm the perspective of non-symmetrical LC-microlenses using in the field of microoptics for the problems of a fiber optics, a transformation of a ray polarization and etc.

References

1. A. Gvozdarev, G.E. Nevskaya. *Optical properties of homeotropically-aligned liquid crystal microlenses //* Mol. Cryst. Liq. Cryst., vol. 304. pp. 423-428, 1997.

2. A. Gvozdarev, G.E, Nevskaya. *Optical properties of liquid crystal microlenses with variable focus length //* Proc. of the First Korea-Russian International Symposium on Science and Technology KORUS'97, Ulsan, Korea, pp. 304-307, 1997.

3. A. Gvozdarev, G.E. Nevskaya. *Optical properties of homogeneously- and hibrid-aligned liquid crystal microlens*es // Mol. Cryst. Liq. Cryst., Vol 329. P.81-88, 1999

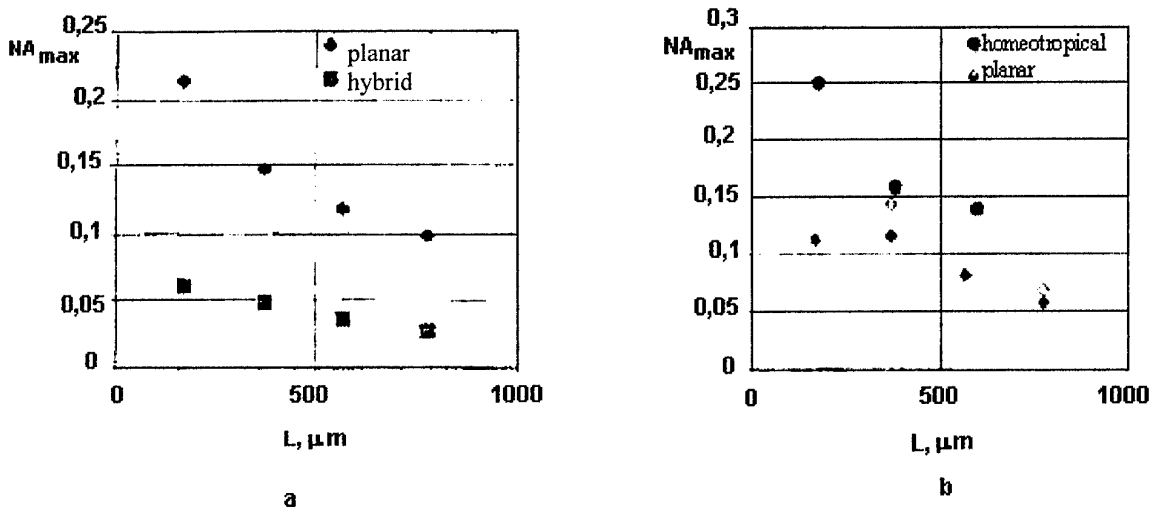

Fig.1. The numerical aperture of LC-microlenses: a - the focusing properties, b — the defocusing properties.

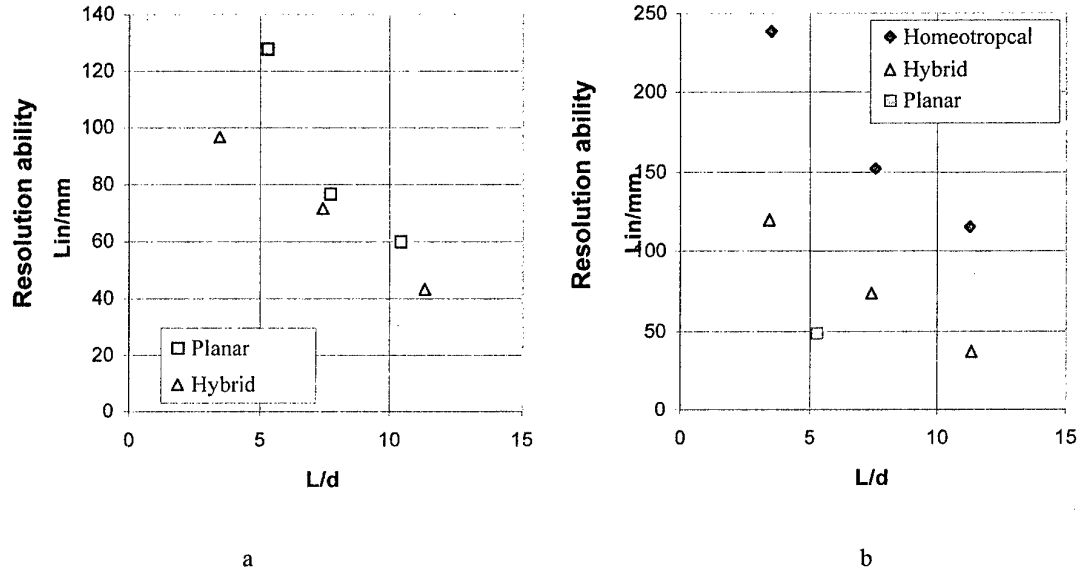

Fig2. The greatest resolution ability of the different LC-microlinses. a – the focusing properties, b — the defocusing properties.

NED-P25. MEMOMI-SCREEN: A HIGH CONTRAST PASSIVE MATRIX LC DISPLAY WITH TV FAST RESPONSE

S.A. Studentsov, V.A. Brezhnev, B.I. Gorfinkel, N.D. Zhukov,
(all from R&D Institute VOLGA, Saratov),
I.S. Bezludnaya, G.V. Simonenko
(all from Satatov State University),
V.A. Ezhov
(Institute of General Physics of Russian Science Academy, Moscow)

A new method of elimination of the STN-screen frame response providing high contrast ratio (higher than 100:1) and total fast response (less than 25 ms) was proposed. All results were obtained with STN standard technology, with serially produced LC materials and did not require development of specific aligning materials.

1. Introduction

Creation of a high information content passive matrix screen requires a maximum slope of the contrast vs voltage characteristic. It is provided due to creation of conditions of the highest interference. In order to increase the slope of the of contrast vs voltage characteristic in such screen, a twist angle α_0 differs from that required for a wave guide mode, polaroid optical axes make an angle $\beta \neq 90°$, and an input polaroid is aligned with a narrow angle γ to the rubbing direction. For example, for OMI effect [1] the following optimum combination is recommended: $\alpha_0 = 175°$, $\beta = 70°$, $\gamma = -10°$. In the classical STN with an ideal compensation $\Delta nd = 0.85$; $\alpha_0 = 240°$, $\beta = 90°$, $\gamma = 30°$. Then the slightest variation in the molecule configuration influences the intensity of the transmitted light. However, the residual birefringence in this case is quite high even for higher voltages, which prevents achievement of the wave-guide mode contrast level, used in TN-effect.

Active matrix screens operate actually with direct driving of the screen elements and do not require a high slope of the of contrast vs. voltage characteristic. The residual twist of AM screens is very low and for the most highly mass-produced TN AM-screens it provides essentially more high contrast (about 300:1). The total fast response of such screens is 25-45 ms. However, it is believed that that valuable TV image is provided with fast response not less than 12 ms [2].

Recently many companies conduct research in the field of bistable twist nematics (BTN), for instance BiNem. According to [3], the initial voltage pulse realigns molecules from the initial 180° twisted structure to the vertical direction. Then the element is driven into one of the stable states: achievement of a stable configuration with an increased twist angle of molecules requires sharp voltage drop, and for the state with a twist angle reduced up to zero the voltage should be lowed gradually. Thus division of elements into switched on and switched off ones is realized not at the expense of the slope but by change of LC configuration. It allows to minimize interference and to reduce contrast losses. Bistable displays show high contrast ratio (more than 100:1), long memory and excellent response time (less than 10 ms). Their main disadvantage is associated with conditions of bistability existence. Hence it results in strict requirements to the gap precision and a helix pitch. By the same reason the lower limit of the BTN operation temperature reaches sometimes 35°. [4].

2. MEMOMI screen structure

Another version for solving the problem is suggested in [5]. The initial 180° twisted LC structure under effect of the voltage is transformed in a self-compensating one [6]. In this configuration optical activities of the upper and lower halves of LC layer are similar by a module, but are opposite by a sign. Self-compensation occurs not only under voltage, it is shown by intermediate configurations formed in the relaxation process. One can say that compensation occurs till there is at least one molecular vertically aligned LC layer. In other words the maximum contrast is maintained for 10-40 ms after cessation of saturation voltage supply. For visualization of the self-compensation it is necessary to follow a number of the optical conditions: polarizers must be strictly orthogonal, and their optical axes must coincide with rubbing directions of LC molecules (or be normal to them). This differs MEMOMI from π-cells where crossed polaroids are aligned 45° to the rubbing direction, and from OMI (see above).

As in OMI here we speak about maintenance of conditions of the interference minimum of optic beam interaction. However, maintenance (that is storage) of this minimum within a time period between switching pulses allows to call this structure MEMOMI.

After cessation of supply of the high voltage pulse, the switched on element of STN-screen begins to return to the initial state.

In *slow* STN during the time between frames an element remains in the state of high (for STN) contrast though it drops. In *fast* STN an element every time has enough time to return in the initial state and again switch on during row scan time. It results in fast contrast drop of STN. The phenomenon of the contrast

drop between switching row pulses is called *frame response*. For elimination of this phenomenon it is suggested either to increase essentially by factor 10-20 the frame frequency (but it will result in a problem of elimination of the occurring parasitic effects), or to output within a frame period some lower voltage row pulses (multiline addressing) but it requires calculation of their shape depending on the displayed data, which is rather difficult. [7].

Due to the optic response delay in MEMOMI the contrast drop between frames is not observed. Thus MEMOMI gives one more method of overcoming the frame response without problems which are caused by high frame frequency.

It is worth to note that at the same time response times are improved. Firstly, unlike in a typical STN screen, low viscosity LC materials may be used without apprehension of fast contrast drop between frames. Secondly, usually self-compensation of MEMOMI is maintained for about a half of the total time of return to the initial state, i.e. visible relaxation time decreases at least two times.

Division of the classic STN screen elements into on and off ones is realized, according to Alt-Pleshko theory, by the value of rms frame voltage. High contrast of MEMOMI is maintained even without intermediate (column) voltages. It means that rms saturation voltage decreases and a slope of the contrast vs. voltage characteristic will be higher.

Because the amount of the MEMOMI delay is determined also by frame duration and voltage amplitude, the multiplex level is set also by a mode and not only by LC parameters. And LC characteristics optimization must be conducted not for providing of the high slope as in STN (this method is exhausted), but for increase of the inertness in τ_{reac} and delay time in τ_{relax}. It is clear that the appropriate requirements differ significantly. For instance in a typical STN screen the slope is improved with increase of the twist angle. On the contrary, for MEMOMI screen there is an optimum angle, the deviation from which to any side, even by 5°, results in the contrast drop by an order of magnitude.

Since division of the elements into on and off ones must be done within row scan time, in MEMOMI screen the instant amplitude begins to play the most important role. If it is only slightly higher than threshold, the typical for STN behavior is maintained. If the amplitude level is higher, the self-compensating configuration is formed. Duration of self-compensation depends on LC material and number of molecular layers, forming this configuration. That is the storage depends on the voltage value. At sufficiently high voltage amplitude the maximum contrast ratio will be maintained till the beginning of the next frame. It is clear that with this the slope of the contrast vs. voltage characteristic will be higher than in the typical STN screen, where due to the frame response it is necessary to supply continuously some voltage for support of the high contrast ratio.

3. *Experiment results*

A MEMOMI screen prototype with 60x30 dots was made of two glass plates with ITO-electrodes which were successively coated with an isolation SiO_2, ~ 100 nm layer and an aligning polyamide, 40 nm layer (a pretilt angle 2-3°). The plate-to-plate gap was set by glass fiber of Ø2.75 μm (screen type A), Ø3.5 μm (screen type B) and Ø6.2 μm (screen type C). Outer surfaces of the plates were covered by film polaroids of NPF-G1229DU type of *Nitto Denco* (Japan). As LC materials, LCM-3089 (Δn=0.21) with an equal helix pitch p_o =5.0 μm (screen of type A) and 7.0 μm (screen of type B) of *R & D Institute of Optical Polymers and Dyes* (Moscow); MLC6219-000 of *Merck* (Germany) with an equal pitch p_o =12.5 μm (screen of type C), MLC7600-000 of *Merck* with the same equal pitch p_o =12.5 μm (screen of type D) were used.

For comparison similar samples were manufactured by standard technologies TN, STN (240°) and OMI (180°). In all these cases MLC-6219-000 with thickness d=6.2 μm, p_o =100 μm, was used for TN and p_o = 12.5 μm - for other effects. As a compensator for STN, a similar cell with an opposite twist angle (alignment direction orthogonal to that near the adjacent operating cell surface) was used. Twist angles and polaroid alignment angles corresponded to the above specified recommended values.

For driving of samples the following modes were used:

- direct (U=10 V, 1280 Hz)
- isolated polarity variable 40 μs meanders with period 10 ms
- multiplex (row voltage 12 V, column voltage ± 1.5 V) with duty ratio 1/32 for the frame duration 2.5 ms.

The results of measurement of the electro-optical parameters of various LC matrix versions are given in a table:

Table

Version	Static mode		Isolated pulse with duty ratio 1/250		Multiplex 1/32	
	CR a.u.	τ_Σ, ms	CR, a.u.	τ_Σ, ms	CR, a.u.	τ_Σ, ms
DSTN	35:1	80	10:1	200	7.1:1	200
TN	760:1	20	1,5:1	800	10.2:1	800
OMI	300:1	12	15:1	180	40:1	160
MEMOMI (D type)	1600:1	25	250:1	120	240:1	200
MEMOMI (C type)	1500:1	12	240:1	40	135:1	80
MEMOMI (B type)	1600:1	12	200:1	22	120:1	3
MEMOMI (A type)	1600:1	7	180:1	15	110:1	23

Only MEMOMI showed contrast ratio higher than 100:1 and the total response time lower than 25 ms. For some materials the contrast reached about 250:1. STN is significantly inferior to other effects even in maximum high voltage direct driving conditions.

Optical screen response of A type in multiplex driving mode (16 frames "ON" + 16 frames "OFF") is shown in Fig.1. It is seen that response time by 10-90% level is 2.8 ms. After cycle 4 the frame response is not practically observed.

An optic response of the same screen in this mode is shown in Fig.2. Relaxation time by the level from 90% to 10% is 20 ms.

At this stage we verified MEMOMI idea, having selected some LC's from those produced in the world, and obtained reassuring results. Today we have worked out some requirements, which should be met by the ideal LC material. If necessary we could develop a specific LC material, and its parameters will not be unique, not occurring in practice.

Using standard completing parts we have developed a unit for screen driving. In this term the situation differs beneficially from BTN, driving of which differs principally from capabilities of available STN drivers.

4. Summary

Possibility of manufacturing of passive matrix screens on the basis of the optical self-compensation with parameters close to those of active matrix ones was proved. It will allow to restore positions of STN displays being lost within recent years under impact of AM technologies.

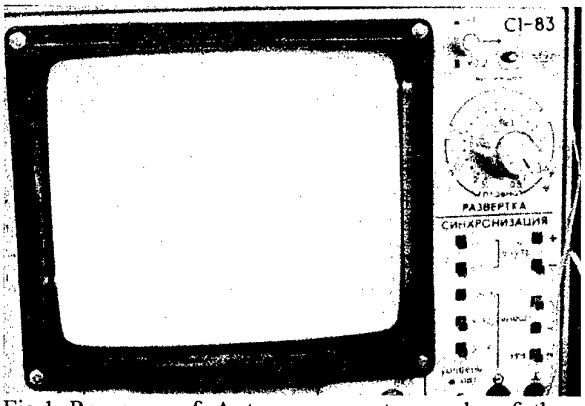

Fig.1 Response of A type screen to supply of the switching on pulse in the multiplex mode 1/32. Value of a division - 2 ms/square. Response time by the level 90-10% is 2.8 ms

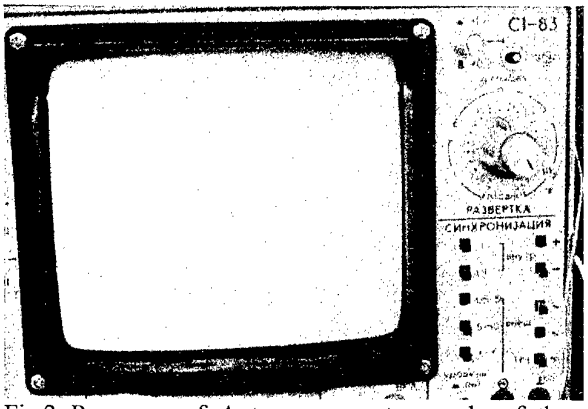

Fig.2 Response of A type screen to supply of the switching off pulse in the multiplex mode 1/32. Value of a division - 5 ms/square. Relaxation time by the level 90-10% is 20 ms.

5. References

1. M.Schadt, F.Leenhouts, Appl. Phys. Lett., V.50, № 5, 1987, pp.236-238
2. SID 2000 Digest, pp.410-413.
3. I.Dozov, A.Boissier, T.Laboureau, Information Display, V.18, No.1, 2002, pp.10 – 13.
4. Z.L.Xie, H.S.Kwok, V.37, 1998, pp.2572-2578.
5. S.Studentzov et al., Euro Display, 2002, pp. 437 – 440.
6. P.Bos, K. Rickey Koehler/Beran, Molecular Crystals & Liquid Crystals, v.113, №1/4, 1984, pp. 329-340.
7. T.Scheffer, Information Display, V.14, No.10, 1998, pp.12 – 17.

NED-P26. Liquid Crystal Photo-Alignment Induced by Azodyes

Boris A. Umanskii[a,c], Sofia I. Torgova[a,c] Nikolai V. Novoseletskii[a,c], , Galina N. Dorozhkina[a,c] and Alfredo Strigazzi[b,c]

[a] Federal State Unitary Enterprise "State Research Center "NIOPIK" B. Sadovaya 1/4, Moscow 123995, Russia
[b] Dipartimento di Fisica, Politecnico di Torino,C. Duca degli Abruzzi 24, I-10129 Torino, Italy;
[c] Joint Laboratory of Orientationally Ordered Media (OOM-Lab),C. Duca degli Abruzzi 24, I-10129 Torino, Italy

Abstract

The photo-generation of optical anisotropy by irradiation of linearly polarized light was investigated for azodyes insoluble and soluble in liquid crystals (LC). Insoluble dyes were used as individual films or incorporated in polymer films. The photo-alignment of soluble azodyes was studied in the bulk of guest-host LC samples in the cells with different surfaces of glass plates. It was investigated the influence of azodye molecular structure on the photo-induced optical anisotropy. The reason of the orientation was explained in the terms of hydrogen bonding.

Keywords: chemical structure, azodyes, liquid crystals, photo-alignment, hydrogen bonds

1. Introduction

The proper orientation of liquid crystals in a cell is a prerequisite condition for the correct performance of any liquid crystalline device (LCD). Mechanically surface rubbing technique is generally used to achieve the uniform alignment [1,2]. For this purpose as aligning layers are usually used polyimide films. This method, has several problems such as the generation of dust particles and electrostatic charges, so rubbing-free techniques are desired.

The aligning methods without rubbing were intensively investigated during the last years, due to the reason that they have many advantages. The photo-induced orientation is the most promising among the contactless methods [3-6]. It gives the most successful repeatability of the liquid crystal alignment.

Recently, it has been reported many investigations of LC alignment obtained by irradiation of linearly polarized UV light [3,6-8]. The main type of photo-aligning materials is based on photo-isomerization of azo-compounds. Such materials are used as orienting films, which can be individual azodyes, polymers with azodye fragments and azodyes incorporated in polymer matrix. For such films were used azodyes insoluble in LC. Moreover LC alignment could be achieved on non-photosensitive substrates by azodyes dissolved in LC matrix [9-11].

We have investigated the orienting ability of different soluble and insoluble in LC matrix azodyes. The last ones were used as orienting films deposited on the surface by spin-coating technique. It was also investigated the influence of chemical structure of different solvents used for spin-coating on the LC photo-aligning characteristics and electro-optic properties of twist nematic photoaligned cells [12-15]. The influence of chemical structure of soluble in LC azodyes on their aligning capability was also investigated [16-17]. The aim of this work is to systemize our results and to try to understand the mechanism of the orientation processes.

2. Experimental

Some of the chemical structures of azodyes investigated are given in the table. All compounds were synthesized in NIOPIK except 10 and 18 that are standard chemical indicators (products of NPO "Biochemreactive"). The dyes (1-14) are soluble in liquid crystals. For our experiments they were dissolved in LC with different percentage. The other dyes (15-18) are insoluble in liquid crystals therefore they were

used either as individual dye films or they were incorporated into polymer matrix (polyamide acid - PAA).

As a nematic liquid crystal material was used ZhK-1289 (commercial product of NIOPIK). For soluble dyes we have investigated the influence of dye concentration on the type of LC orientation. For other experiments we used 0.4% solutions of azodyes in LC matrix.

For investigation of aligning capability of azodyes insoluble in LC they were either incorporated in polymer matrix or used as individual films. The aligning films of individual azodyes or their compositions of with PAA were formed on glass substrates by spin-coating. For these purposes, three different solvents, namely dimethylformamide (DMF), N-methyl-pirrolydone (N-MPD) and ethylcellosolve (ECS) were used. Then coated substrates were annealed at 180°C for 1 hour.

For the investigation of aligning capability of soluble azodyes glass substrates coated by pure PAA were prepared. For the compound 10 (Methyl Red) we have investigated the influence of the cell surface nature on its ability to orient LC. We prepared six different surfaces of the cell: glass plates coated with indium-tin oxide (ITO), polyamide acid (PAA), polyacrilic acid (PAcA), polyvinylalcohol (PVA), bare glass plates and bare quartz plates.

LC cells were fabricated by assembling of two substrates by gluing with epoxy glue. Calibrated spacers gave the cell's thickness equaled 12 μm. The empty cells with photosensitive substrates (containing insoluble azodyes) were irradiated by a polarized light beam directed normally to the glass plates and

Table. Chemical formulae of investigated azodyes

N	Chemical formulae	Orientation
1	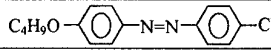	no
2	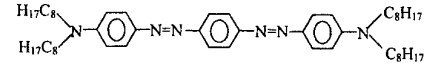	no
3	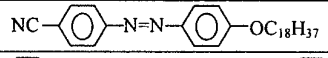	no
4	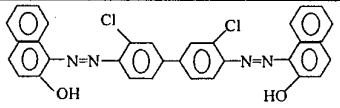	no
5	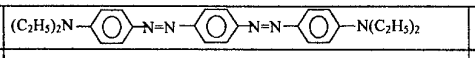	no
6	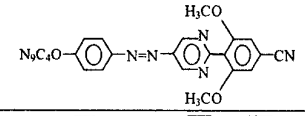	no
7		no
8		no
9	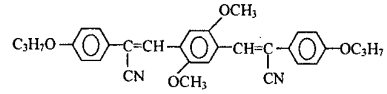	no
10	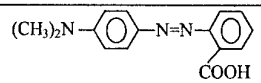	yes
11	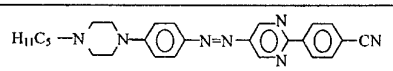	yes
12	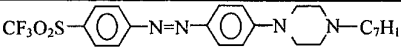	yes
13	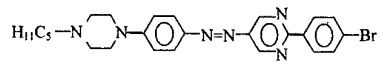	yes
14	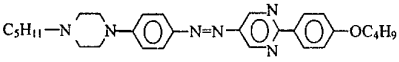	yes
15	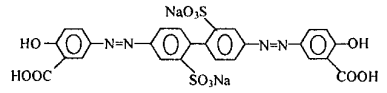	yes
16	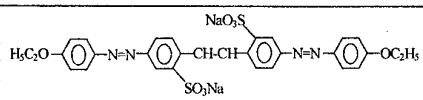	yes
17	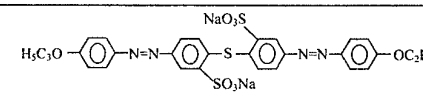	yes
18	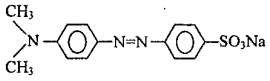	no

then they were filled with LC material. Another group of LC cells without photosensitive substrates were filled with LC dopped by azodye. Then they were irradiated by a polarized light.

For irradiation we used 250 W high-pressure mercury lamp. The irradiation time was 1 - 30 min, the light intensity was 60 mW/cm^2. The dose of radiation was varied by changing of the time for exposure. The band-pass filter (460 nm) and Glan polarizer were used for getting required light conditions.

3. Results and discussion

Some authors explained the mechanism of photo-alignment with azodyes, as the resullt of cis-trans isomerisation under UV-light [6]. According to our experimental results this

property is necessary, but not enough. As one can see from the table, the irradiation by linearly polarized UV light of the compounds 1–9 and 18 doesn't show any LC alignment while irradiation of the compounds 10-17 results in LC alignment. Moreover, when insoluble azodyes were used as individual orienting films even the chemical structure of the solvents for spin-coating played a very important role. For example, the dyes 16, 17 with the solvents N-MPD and DMF lead to homeotropic LC orientation, while solvent ECS results to planar orientation. The dye 15 leads to planar orientation with every solvent mentioned above.

The chemical structure of compound 15 differs from compounds 16, 17 by the presence in the first one the substituents which are the donors of the protons for hydrogen bonds (H-bonds) formation, namely carboxyl and hydroxyl substituents (Table). From the point of view of H-bonds formation it is also possible to explain the influence of the solvents. Solvent ECS is the strong donor of protons, so it is able to form H-bonds with the surface and with compounds 16 and 17 as well. In the case of incorporation of the dyes (15-17) in PAA the irradiation by linearly polarized light leads only to planar alignment of nematic LC. This result can be explained due to the fact that PAA is able to organise hydrogen bonds with the surface and with dyes as well.

From these facts follow that formation of H-bonds plays an important role on the aligning capability of azodyes due to the ability to preserve orientation by the increasing of anchoring energy. Thus the chemical nature of the substituents in the photosensitive molecule and the chemical nature of the solvent used for spin coating as well determine the type of LC orientation.

When azodyes are soluble in LCs the probability of their practical application as orienting agents in LCD manufacturing is negligible. However, the investigation of the LC photoinduced alignment on nonphotosensitive substrates of the cell filled with LC dopped by photosensitive dye is very useful for understanding the mechanism of alignment by photosensitive molecules.

It is evident from the table that among investigated soluble azodyes some of them result to LC alignment (compounds 10-14) while others don't exhibit any photoinduced alignment (1-9). Analysis of the structures of these dyes makes it possible to relate the presence of some substituents with the aligning ability of the dyes. Among dyes investigated we have revealed only two such substituents: piperasene fragment and carboxyl one. Both of these fragments are able to form H-bonds with the surface containing hydroxyl. As it was mention above we used LC cells with different type of surfaces. On the substrates coated with PAA, PVA, PacA and for bare glass and bare quartz which have hydroxyl-groups on the surface after irradiation with linearly polarized light the photoinduced alignment arise due to the photoisomerization of dye molecules attached to the surface by H-bonds. While on the substrates coated with ITO, which don't form H-bonds with azodyes no alignment arises under irradiation by linearly polarized light. We can conclude, that photoisomerisation of dye molecules in the bulk of LC doesn't cause LC alignment.

We have also investigated some derivatives of stilbene soluble in LC matrix (compounds 8, 9), which also exhibit cis-trans isomerisation under UV light. No any photoinduced alignment with stilbene derivatives has been found.

It is interesting to mention that azodye Methyl Red (compound 10) results to photoinduced planar or twist orientation only if its concentration is less than 0,5% (wt). For 1% (wt) concentration after irradiation with linearly polarized light the homeotropic LC orientation arises. For concentrations more than 1,5% (wt) the homeotropic orientation arises after a time without any irradiation. The dyes with piperasene fragment (compounds 11 - 14) always result to planar orientation. According to our opinion the peculiarity of compound 10 behavior also can be explained in the terms of hydrogen bonds formation. In this case it occurs the complicate competition between inter- and intra-molecular hydrogen bonds. In order to give the correct explanation it needs additional investigations.

4. Conclusion

We have investigated the influence of chemical structure of azodyes on their aligning capability for soluble and insoluble in LCs dyes. It was shown that formation of H-bonds between azodyes and surfaces plays an important role for the aligning capability of azodyes.

Acknowledgements
The work was partially supported by European Community in the frame of the INCO Copernicus Concerted Action "Photocom", under Contract No. IC15-CT98-0806.

References

[1] J. Cognard, Mol. Cryst. Liq. Cryst., **78**, Suppl.1, 1 (1982).
[2] J.M. Geary, J.W. Goodby, A.R. Kmetz, J.S. Patel, J. Appl. Phys., **62**, 4100 (1987).
[3] M. Schadt, K. Schmidt, V. Kozenkov, V. Chigrinov. *Jpn. J. Appl. Phys.*, **31**, 2155 (1992).
[4] V.M. Kozenkov, A. Dyadyusha, T. Marusii. *Ukrainskii chim. zhurnal*, **36** (7), 1059 (1991).
[5] V.G. Chigrinov, V.M. Kozenkov, *SPIE*, **3318**, 454 (1995).
[6] M. Hasegawa, Y. Taira, J. Photopolym. Sci. Technol., **8**, 241 (1995).
[7] J. Chen, D.L. Johnson, P.J. Bos, X. Wang, J.L. West, Phys. Rev. **E 54**, 1559 (1996).
[8] W. Gibbons, P. Shannon, S.T. Sun, B. Swetlin, Nature, **51**, 49 (1991).
[9] Shao-Tang Sun, W. Gibbons, P. Shannon, Liq. Cryst., **12**, 869, (1992).
[10] D. Voloschenko, A. Khizhnyak, Yu. Reznikov, V. Reshetnyak, Jpn. J. Appl. Phys., **34**, 556 (1995).
[11] D. Fedorenko, O. Francescanngeli, E. Ouskova, V. Reshetnyak, Yu. Reznikov, F. Simoni, S. Shiyanovskii, Mol. Cryst. Liq. Cryst., **359**, 137 (2001).
[12] N. Novoseletski, G. Dorozhkina, S. Torgova, B. Umanski, Mol. Cryst. Liq. Cryst., **352**, 27 (2000).
[13] E. Prudnikova, G. Dorozhkina, N. Novoseltskii, S. Torgova, B. Umanskii, Mol. Cryst. Liq. Cryst., **352**, 119 (2000).
[14] S. Torgova, N. Novosetskii, G. Dorozhkina, B. Umanskii, A. Strigazzi, Mol. Cryst. Liq. Cryst., **360**, 81 (2001).
[15] B. Umanskii, G. Dorojkina, N. Novosetskii, S. Torgova, Mol. Cryst. Liq. Cryst., **368**, 387 (2001).
[16] B. Umanskii, N. Novoseletskii, S. Torgova and G. Dorozhkina, ILCC-2002 (Edinburg) Proceeding (ref. ILCC-121), Mol. Cryst. Liq. Cryst (in press)
[17] B. Umanskii, N. Novoseletskii, S. Torgova, SID-2003 (Baltimore) Proceedings, P.103.

NED-P27. Printed Optical Components for Liquid Crystal Displays

Pavel Lazarev, Victor Nazarov, Natalia Ovchinnikova and Sergey Remizov

Optiva, Inc., 377 Oyster Point Blvd, Unit 13, South San Francisco, CA, USA

Tel (650) 616-7600; Fax (650) 616-7602; www.optivainc.com

plazarev@optivainc.com, Victor.Nazarov@optiva.ru, Natalyov@optivainc.com, Sergey.Remizov@optiva.ru

Abstract

Optiva, Inc. has developed a new technology for Thin Crystal Film (TCF) polarizers and retarders produced by deposition, molecular alignment and drying of water-based lyotropic liquid crystal (LLC) materials. The preferable deposition methods, for applying shear force for LLC molecular orientation, are slot-die or Mayer rod. This paper presents these coating methods of obtaining anisotropic crystalline films and characterization of resulting TCF.

1. Introduction

TCF technology [1-6] is based on self-assembling disk-shaped molecules. TCFs are produced by deposition of water based lyotropic liquid crystal (LLC) formed by rod-like Supramolecules of organic sulfonic acids. These Supramolecules, which have a columnar structure with an aspect ratio of more than 100, form by interactions between disk-shaped molecules [7,8]. Within a certain temperature and concentration range, the supramolecules form mesophases. The rheological behavior associated with liquid crystallinity is essential for the processing of these materials into the structure to exhibit desirable polarizing properties. The material in this LLC state can then be printed directly onto virtually any substrate by a variety of existing commercial wet coating methods, such as slot die extrusion, offset gravure, Mayer rod and doctor blade. The common factor in every method is the application of a uniform shear force in the coating process, as well as a thin and uniform material layer. The shear force during the coating process provides the required energy for alignment to occur. The long rod structures align along the shear force direction in a wet layer about 10 microns thick. While drying, the layer crystallizes to a sub-micron thick semi-crystalline thin film functional layer with dichroic molecules aligned over the entire coated surface.

The strong anisotropy of refraction and absorption indices [9,10] make TCF very attractive for use in liquid crystal display (LCD) and organic light emitting device (OLED) related applications [1-6, 11-14]. The first industrial application of TCF is a polarizer for LCD.

TCF properties are defined to a great extent by the coating technology. The preferable deposition methods are slot-die or Mayer rod. Optiva, Inc. and Nakan Corporation have developed a coating process and equipment based on a Mayer Rod shearing technique [15-17]. Here we consider the basic features and advantages of the slot-die coating method of TCF manufacturing. Optical performance and environmental stability of resulting TCF (produced with Mayer rod and slot-die coating technique) are discussed.

2. TCF coating technique

We designed a new method of crystallization to create anisotropic crystalline films from LLC systems, formed by the Supramolecules (kinetic units) distributed in a liquid dispersion medium (water). The method is characterized by simplicity and economy, ensuring a high degree of anisotropy and ordering of films.

The method includes the following steps:

a. Molecular design of plate-shaped conjugated amphiphilic compounds

b. Self-assembly of the molecules into a Supramolecule

c. Formation of Lyotropic Liquid Crystalline system by the Supramolecules in liquid

d. Printing of wet LLC layer with global order created by mechanical/hydrodynamic process

e. Drying the layer into a crystalline film.

Drying is preferably conducted at humidity levels of no less than 50% and at room temperature.

At this point in technology development, we have experience with two major types of deposition devices: Mayer rod and slot-die coating technique. A TCF coater based on Mayer rod shearing technique is shown in the Fig. 1a. LLC material is deposited onto the substrate 1 (plastic or glass) using dispenser 2. The next operation is the process of alignment of the kinetic units (Supramolecules) of the LLC. To implement the external aligning impact to LLC we use a Mayer rod. This is a rod wound with a wire, which doctors off excess coating liquid. The amount of liquid remaining in the coating is related to free space between the high points of the wires, thus the diameter of the wire determines the thickness of the wet layer. A uniform wet coating of 7 to 15 μm thick [2] allows producing TCF from 100 to 900 nm thick. Shear stress generated by the rod results in lowering of the viscosity of the thixotropic LLC system (Fig. 2). The substrate holder may be heated so as to raise the temperature of the deposited wet layer to 50°C.

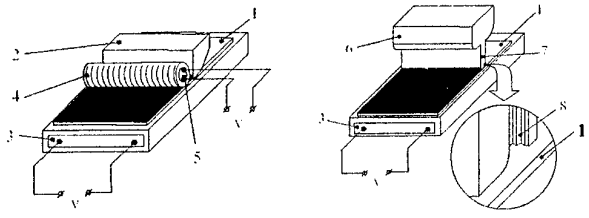

a b

Fig. 1. TCF coaters based on Mayer rod (a) and slot-die (b) shearing technique.

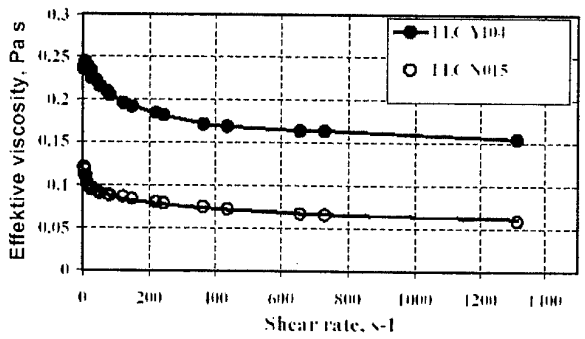

Fig 2. Viscosity vs. shear rate curves for different LLC Optiva materials.

The final operation of the method is drying. The rate of drying should be optimized in order to prevent cracking and misalignment of the previously aligned structure of the layer. Usually, drying is done at room temperature and humidity at about 60%.

A slot-die coating method is schematically illustrated in Figure 1b. The solution is placed in the reservoir 6. Extrusion of Supramolecules from the slot 7 under pressure produces alignment. The gap between the walls of the slot is 50 μm. During the printing procedure, the slot moves over the substrate, and an extruded layer is uniformly deposited onto the substrate. The drying operation is performed as described above in Mayer rod coating technique description.

The resulting anisotropic crystalline films have optical parameters similar to those obtained using the Meyer rod method. The dependencies of contrast ratio vs. transmittance are shown in Fig. 3 and Fig. 4 for samples of TCF N015 coated onto plastic and glass substrates with slot-die and Mayer rod technique. Both coating methods provide the same optical performance of the finished polarizing films.

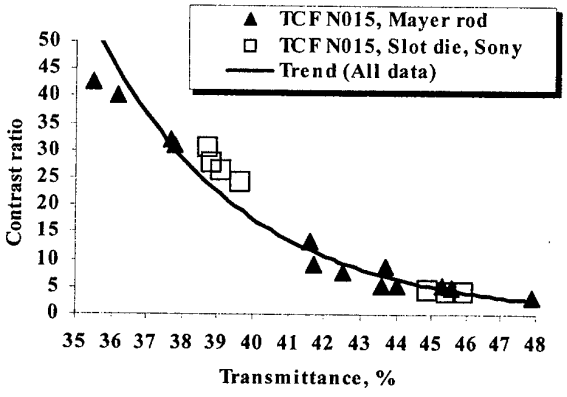

Fig. 3. Contrast ratio vs. Transmittance for TCF N015 coated on PET substrate usingdifferent coating techniques.

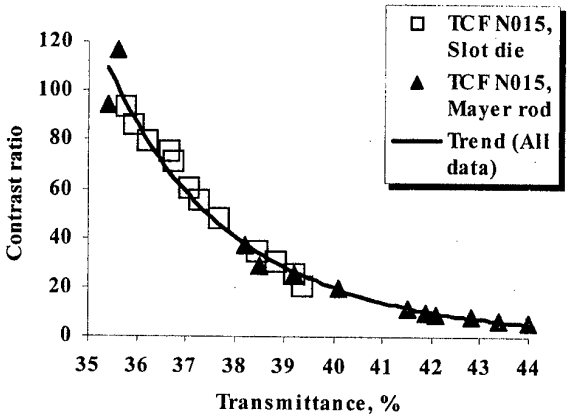

Fig. 4. Contrast ratio vs. Transmittance for TCF N015 coated on glass plates using different coating techniques.

The main advantages of the slot-die method over Mayer rod coating technique are: 1) option to form large-area crystalline films; 2) possibility of TCF coating on roll-to-roll film at a high coating line speed (125 feet per min); 3) better reproducibility; 4) higher uniformity resulting in better appearance / cosmetics; 5) availability of wider thickness range starting at 100 nm. Absence of contact between a coating tool and a substrate also allows avoiding damage of vulnerable surfaces and defects related to interactions between the wire spacing and the coating hydrodynamics [18].

Geometric dimensions (thickness) and surface morphology of the film change in the course of drying. This leads to elastic stresses during the crystallization process, which can result in geometrical deformation of the film. A low rate of crystallization creates favorable conditions for maintaining Supramolecules in their aligned state. Redistribution also takes place in the structure of the Supramolecules, which also favorably affects perfection of the crystalline structure of the forming film.

3. Optical performance and environmental stability of Polar Film.

The first commercial applications of TCF technology are Plastic Film Polarizers for the flat panel display market. New technology allows production of printed polar films by slot-die coating. Optiva, Inc. has developed a polarizer plastic film set intended for use in TN displays that has fewer component layers, resulting in a less expensive substitute for conventional LCD polarizers. The new design avoids the conventional costly "cellulose triacetate (TAC) film sandwich" needed to protect the delicate PVA film with an optically neutral substrate. The polarizer plastic film set is composed of a low-reflection PET substrate coated with TCF, a PSA and a release liner. The TCF TN transmissive film utilizes a single, low cost PET substrate as the external layer. Since this layer is outside the display optics, the birefringence properties are not relevant for most TN applications. While TAC film could be used in this design, PET provides a more durable substrate alternative that does not require hard coatings.

Sony Magnetic Products of America has started TCF Plastic Sheet Polarizers production based on the slot-die coating method. TCF deposited by Sony on PET film (of 100 μm thickness) were tested

in Optiva's lab. We measured the polarizing transmission spectra of samples of polarizing film laminated onto soda-lime glass in depolarized light with no substrate correction at 58% relative humidity (RH). Polarizing parameters were calculated for the visible region of the spectrum 400-800 nm with CIE-Photopic weighing with the spectrum of illuminant C. We present the polarizing characteristics and spectra of the tested samples in Table 1 and Fig. 5.

Table 1. Polarizing parameters and color coordinates of TCF N015 Plastic Sheet Polarizers produced by Sony using slot-die coating technique.

Sample number & thickness, nm	Transmission, %			Ep	C/R	Kd
	T	H_0	H_{90}			
1 - 310	45.9	34.1	8.2	78.3	4.2	11.6
2 - 310	45.4	34.0	7.3	80.4	4.7	12.2
3 - 560	38.7	29.0	0.9	96.8	30.5	16.1
4 - 560	38.8	29.1	1.0	96.5	27.7	15.8
5 - 460	40.8	31.7	1.6	95.2	20.2	17.2
6 - 460	40.9	31.6	1.8	94.5	17.6	16.5

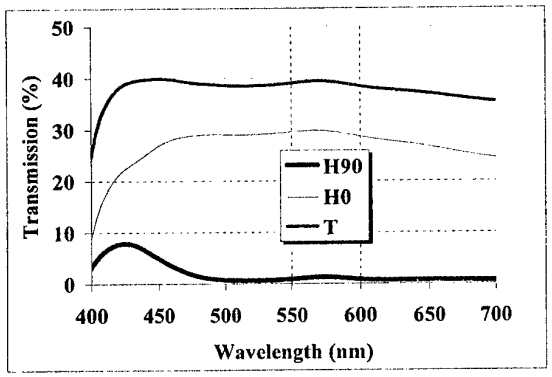

Fig. 5. Spectra of TCF N015 (thickness 560nm) deposited on PET-film.

TCF Plastic Sheet Polarizers were tested under high humidity (50°C/95%RH) and dry heating (60°C/dry) conditions for 1,000 hours in an environmental chamber. The test procedure was reported earlier [12].

The results of environmental testing of TCF N015 polarizers are presented in Fig. 6-9.

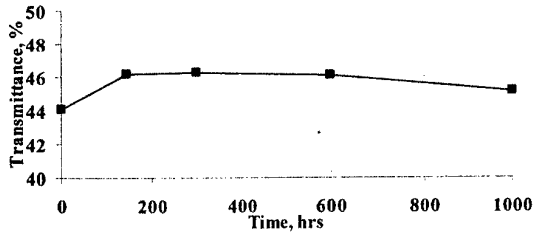

Fig. 6. Transmittance of the single Sony TN Reflective Mode TCF Polarizer (50°C /95% RH).

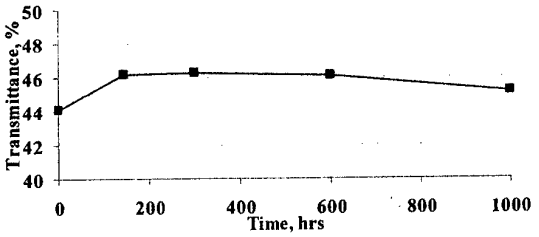

Fig. 7. Contrast ratio of Sony TN Reflective Mode Polarizer (50°C /95% RH).

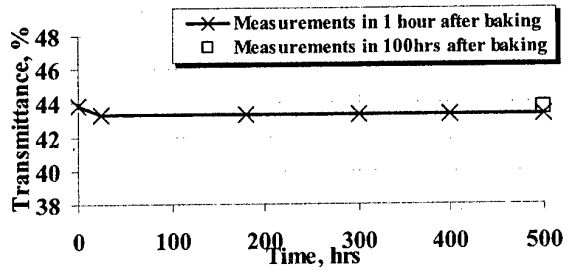

Fig. 8. Transmittance of the single Sony TN Reflective Mode Polarizer (60°C/dry).

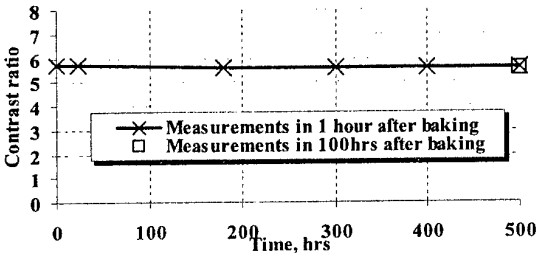

Fig. 9. Contrast ratio of Sony TN Reflective Mode Polarizer (60°C/dry).

This data confirms the high stability of transmittance and contrast ratio of TCF Plastic Polarizers during long-term environmental tests.

5. Conclusion

Conventional printing methods like Meyer rod and Slot-die coatings can be used to produce large-area Thin Crystal Film polarizers. Printing demonstrates reproducible optical properties and high environmental stability of optical components.

These printing methods can be used with either plastic or glass substrates. TCF Plastic Sheet Polarizers are currently being introduced to the market and offer advantages that result in a less expensive substitute for conventional LCD polarizers. Printing directly onto glass also offers advantages over conventional technology and will be discussed further in future papers.

6. References

[1] OPTIVA, Inc. (www.optivainc.com).

[2] U.S. Patent 5,739,296.

[3] U.S. Patent 6,049,428.

[4] WO 00/25155.

[5] WO 97/39380.

[6] U.S. Patent 6,174,394.

[7] A. Dembo, A. Ionov, P. Lazarev, A. Manko and V. Nazarov, Lyotropic Dye-water Mesophases Formed by Rod-like Supramolecules, *Molecular Materials* **14**, 275 (2001).

[8] S. Remizov, A. Krivoshchepov, V. Nazarov and A. Grodsky, Rheology of the lyotropic liquid crystalline material for thin film polarizers, *Molecular Materials* **14**, 179 (2001).

[9] P. Yeh, M. Paukshto, Molecular crystalline thin-film E-polarizer, *Molecular Materials*, **14**, 1-19 (2001).

[10] Y. Bobrov, V. Novak, Determination of anisotropic complex refractive indices of thin film E-polarizers, *Molecular Materials*, **14**, 21-31 (2001).

[11] Y. Bobrov, P. Lazarev, D. McMurtry, S. Remizov, Incorporation of Optiva Polarizers in LCD Production Line, SID'01 Technical Digest, 639-641.

[12] Y. Bobrov, L. Blinov*, L. Ignatov, G. King, P. Lazarev, V. Nazarov, N. Ovchinnikova, S. Remizov, Environmental and optical testing of Thin Crystal Film™ polarizers, *J. of the SID*, 11/1, 63-70, (2003).

[13] T. Sergan, T. Schneider, J. Kelly, O.D. Lavrentovich. Polarizing-alignment layers for twisted nematic cells, *Liq. Cryst.*, **27**, 567-572 (2000).

[14] T. Sergan, J. Kelly. Negative uniaxial films from lyotropic liquid crystalline material for liquid crystal display applications, *Liq. Cryst.*, **27**, 1481-1484 (2000).

[15] Fennell, L., Lazarev, P., Ohmura, S., Paukshto, M., Thin Crystal Film Polarizers™, Asia Display/IDW'01, *Proceedings of The 21st International Display Research Conference in conjunction with The 8th International Display Workshops*, Nagoya, Japan, October 16-19, 2001, p. 601-603.

[16] Y.Bobrov, L.Fennell, P.Lazarev, M.Paukshto, S.Remizov, Manufacturing of a Thin-Film LCD, *J. of the SID*, 10/4, 317-321 (2002).

[17] Y. Bobrov, L. Fennel, T. Ganpule, P. Lazarev, S. Ohmura, Manufacturing and Coating Equipment Development for Thin Crystal Film Printing, *Proceedings of The 9th International Display Workshops*, Hiroshima, Japan, December 4-6, 2002, 405-408.

[18] E.G.Gutoff, E.D.Cohen, Coating and Drying Defects: troubleshooting operating problems, Wiley-Interscience (1995) 287p.

DISPLAY ERGONOMICS AND APPLICATIONS

DEA-1. **Display Technologies for the Mobile Information Society**

Jyrki Kimmel
Senior Research Manager
Nokia Research Center
Tampere, Finland

Mobile telephony has advanced in the last few years to the edge of the capabilities of present GSM networks. As the next phase in network evolution, the third generation mobile communications networks are being installed in many countries. The increased capabilities of the new networks and associated mobile terminals enable new applications for the benefit of the user of tomorrow. The worlds of Internet computing and cellular telephony merge in this market, creating a new Mobile Information Society through the digital convergence. New display technologies are in a central role making this development a reality with true benefits for the user.

The evolution of digital communication networks

The installation of the GSM (Global System for Mobile Telecommunications) networks first in Europe, later globally, enabled elementary digital data applications for the mobile user since 1992. The first applications were the use of the short message service (SMS) allowing the user to send and receive messages up to 160 characters long. This service has been a great success and a revenue maker for operators everywhere. The demands on the displays were evident from the start of these applications. Larger displays with more lines of text appeared first, then with the first games on the mobile terminals, graphic displays were required. For the business user, Nokia was first to introduce Communicator models, starting with the Nokia 9000 communicator in 1997. The Communicator already had an additional graphic display with 640 by 200 pixels. Towards the end of the decade, additions to the GSM phase 2 standard were the high speed circuit switched data (HSCSD) and general packet radio service (GPRS). These additions increased the basic data channel bandwidth of the GSM (9.6 kbit/s) first to 14.4 kbit/s and later to maximum user modem speeds of 115 kbit/s. The next step along this path is enhanced data rate GSM (EDGE) that speeds up the practical data connection even more.

The third generation mobile services will utilize new networks that allow a theoretical data rate of 2 Mbit/s to a stationary user. In practice, it is estimated that a mobile user will be able to utilize a bandwidth of about 128 kbit/s, on the average. This is already better than the internet experience obtained by home users today. The services will evolve along with the network capabilities, enabling new uses for the mobile terminals.

It is evident that the full exploitation of these data speeds will be for exceedingly visual content. Already for GPRS phones, Nokia is offering products with built-in cameras. The image transmission is handled via the Multimedia Message service (MMS) that allows the user to send and receive image content to and from the mobile terminal, exchanging data with other mobile users, or with a PC or a server. New user interface styles have been defined for these applications utilizing both Nokia proprietary and Symbian operating systems. This development sets new demands for the displays as well. These challenges have been solved today by using transflective active and passive matrix liquid crystal displays (LCD's), except for the Communicator 9210 display, which is transmissive (see Table 1).

Table 1. Nokia user interface styles and key characteristics

User Interface Style	Resolution (pixels)	Color depth (bits)	Platform
Series 40	128x128	4096	Nokia proprietary
Series 60	176x208	4096	Symbian
Series 80	640x200	4096	Symbian

Digital Convergence and Mobile Information Society

Digital convergence brings together many previously unrelated applications in a mobile device. The first convergence products from Nokia, in addition to the mobile computing enabled Communicator family, were the 5510 phone with an integrated MP3 player, the 7650 imaging phone, and the 7210 smart phone with an integrated stereo FM radio. The immediate followers are the 3650 and 7250 camera phone models, with the Series 60 and Series 40 user interfaces, respectively. The next development includes embedding games with a game user interface in a mobile phone in the upcoming Nokia N-Gage. This is only the beginning of the development, as these products are centered on the individual user benefiting from the new integrated applications in a single device.

The next phase in the development of digital convergence is the Mobile Information Society. When the convergence products and associated services enable the user to seamlessly be connected to the services anywhere, with anyone utilizing the same services, at any time, we have realized the ultimate connectivity of the user. The services provide both utility and entertainment, and the mobile terminals will have to be designed to provide the best possible user experience.

Displays and the Mobile Information Society

Displays are key components in making the new generation of mobile terminals work for the user. The basic requirements include increased resolution and visual quality in terms of brightness or reflectivity, contrast, and color purity. The basic Internet page today is usually designed to accommodate an 800 by 600 pixel, 4:3 form factor. It is quite obvious that with current displays, the mobile terminal would become cumbersome and too large for everyday mobile use. Therefore, for portable terminals in the convergence products for the Mobile Information Society, the display needs a higher resolution in a size similar or smaller than what is found in mobile phones today – and because of the increased visual content in the display, the image quality must not be compromised. This demand can be realized either by manufacturing direct view displays by e. g. low temperature polysilicon technology (LTPS), with resolutions of up to 220 dots per inch (dpi), or by utilizing virtual displays.

LTPS allows high resolutions for both LCD's and organic light emitting displays (OLED's). The common active matrix LCD employs amorphous silicon as the backplane of the display. If the amorphous silicon is heated up to melting point with a laser and allowed to anneal, the result will be a polycrystalline structure with higher carrier mobility than in the amorphous silicon backplane. This in turn allows faster and smaller transistors in the display, with included benefits of the ability to integrate row and column drivers, and possibly other functions as well, directly as integrated circuits on the glass substrate. A 800 pixel wide web page then could be shrunk to be shown on a 3.5"...4" diagonal display, suitable for a notepad-like device today.

Virtual displays are based on making either an LCD on a silicon backplane (LCOS) or by depositing organic or polymer emitting layers on silicon. The resulting displays, typically 0.3" to 0.8" diagonal, must be then enlarged by optical means to function as displays meaningful to humans. User comfort issues are crucial in order for the mobile phone manufacturer to be

able to gain any benefit from using virtual displays. These include the field of view, size of the exit pupil, and size and weight of the optics. In the simplest sense, a magnifying glass could be used, but this results in a bulky and heavy optical part. Diffractive and holographic elements have been proposed to alleviate this problem. Further user comfort issues arise if data is shown to both eyes of the user, mainly as a result of alignment errors.

There are three ways to apply virtual displays in a mobile device: as a monocular, biocular, or as a binocular display. In the monocular case, only one eye is used for viewing the display, in the biocular case the same information is shown to both eyes, and in the binocular case, information content imaged from two laterally different points of view are shown for each eye separately, giving an illusion of three-dimensional content. In the monocular case, the eyes get fatigued easily due to the unnatural way of accessing information. While one eye is actively studying the content on the display, the other must be physically or mentally blocked from seeing distracting content in the surrounding environment. In the binocular, stereoscopic case, further complications result from the misalignment of focus and vergence points of the display axes and the content shown on the displays. A good compromise is the biocular case, where essentially two-dimensional content is shown for the both eyes. While the visual effect might not be as striking as in the stereoscopic case, the alignment problems are restricted to aligning the optical axes to a comfortable focus distance.

Conclusions

From the Mobile Information Society standpoint, it can be seen that the visual content of the applications and services available to the future mobile user, new technologies in displays have to be able to provide a good visual user experience. These technologies include advanced active matrix LCD's, OLED's and virtual displays. Other new technology areas such as flexible LCD's, bistable LCD's, and microelectromechanical system (MEMS) based displays have applications in mobile terminals that require extremely low power consumption, where image quality can be sacrificed either in the number of colors and grayscale to be shown, or in the display speed.

The proposed new technologies for the new era are still expensive, and as the cost of the displays generally tend to decrease over time, so do the prices of the cheaper, mainstream alternatives as well. The adoption of new display technologies is synergistic with the advances in the penetration of the third generation cellular networks and terminals, and for the user to get the best possible experience from the new services, the displays, services, and the networks need to develop all together.

DEA-2. **Aviation Display Devices and Market**

Darrel Hopper

Air Force Research Laboratory
AFRL/HECV Bldg 248 Rm 300
2255 H Street
Wright-Patterson AFB OH 45433-7022
< darrel.hopper@wpafb.af.mil>

Paper is not available

DEA-3. 3-D DISPLAY TECHNOLOGIES

Igor N. Kompanets

P.N.Lebedev Physical Institute of RAS
53, Leninsky pr., Moscow 119991 Russia
<kompan@sci.lebedev.ru>

Abstract.
Requirements and possible methods of creating the 3-D display are discussed. Progress in the 3-D medium based displays is demonstrated including the «Perspecta Spatial 3D Platform» system. Forecast of 3-D display developments is presented.
Keywords: 3-D display, 3-D medium, laser beam scanning, light scattering, two-photon absorption, holographic display, optical-mechanical display, optical-electronic display.

1. Introduction.

Creating the systems of mostly complete – 3-demensional displaying of the real world will influence cardinally (straightly or by indirection) on all spheres of human practice and initiate the development of whole series of research directions and technologies. Actually, the field of 3-D display application is extremely wide: displaying the complicated technologic processes and dynamic scenes in video information systems, computer simulation and design, navigation, visualization of tomographic information in medicine, simulation of different tasks in science and technology, computer trainers and games, advertisement and entertaining actions.

Attempts to develop 3-D display do not interrupt for many years, since 2-D displays have been developed. This problem is under investigation in many companies such as Naval Command, Control and Ocean Surveillance Centre, National ATC Association, StereoGraphics (all they are from the USA), Siemens (from Germany), Sony (Japan), Samsung (Korea) and others. However they have not created any effective 3-D display until now though there are many 3-D working samples and some of them are used.

Main obstacles to create 3-D display are highest information capacity of a 3-D image ($N_x \cdot N_y \cdot N_z$ of elements – voxels instead of $N_x \cdot N_y$ elements – pixels conditionally) that demands essentially much more capacity of signal transmission channels for real time operation as well as a lack of the appropriate easy addressed 3-D medium.

A possibility to create 3-D display on the base of different approaches is discussed regularly in press (for example, see "Airtraffic management", pp.18-21, 1997), and the brief review of modern state in this field is presented below. Note devices considered do not use spectaculars because the last ones compose 3-D illusion only as well as tire eyes and nervous system.

2. Requirements and ways to 3-D display realization.

It is known that trained eyes of an expert are able in favorable conditions to distinguish up to 200 distance planes (scales) while 3-D image quality is satisfactory accepted as wholly if one can distinguish 8-9 planes only. A system displaying 16-20 different planes provides good quality of 3-D image. Of course, it is impossible to shorten a number of distance planes or to present a scene simplistically if we mean not subjective 3-D sensing by an observer but displaying the real space in definite scale and coordinates that is necessary for solution of practical tasks in air-navigation, object breadboarding, computer sophistication, tomography and other fields. Then a number of distance planes N_z in 3-D display must approximate to $N_x \approx N_y$.

The next requirement concerns to smooth looking around an object, or so-called parallax. An observer sees the object displayed in 3-D medium like natural one if he can observe it not only from different distances but also from different directions i.e. points of view. The more a number of points of view in the object

displaying and the closer N_z to $N_x \approx N_y$, the smoother looking around and the better a quality of 3-D object presentation. Thus, for N_x,N_y and N_z as high as 10^3 (each) it takes about 10^9 bits to form qualitative monochromic 3-D image.

If to say about 3-D sensing the volume object or scene it is easy to do this due to 3-D medium which displays them in the form of slices (Z-cuts) according to given coordinates. When all slices are displayed for 1/25 sec and less a man perceives them as a single whole i.e. as 3-D image of this object or scene.

Since the effective 3-D medium is absent 2-D display screen to represent 3-D object or scene is used really until now. In this case such a display forms 2-D image corresponding to one point of view (i.e. one direction and one distance planes) for present position of observer eyes. When the position is changed a new 2-D image is formed for it and so on. Looking around is considered as smooth if a step between neighbor points of view does not exceed 10'-20' both along the horizontal and vertical lines. Thus, when the view angle is ±30° along the horizontal line and ±20° along the vertical line then the multi-plane system forming 3-D images of high quality must represent a huge amount– minimum 60 thousand points of view of about 10^6 bit each.

The creation of such display systems is rather complicated technologic problem demanding a special-purpose computer equipment to form, transfer and display every current point of view, for example, given by the position of observer eyes relative to the display center. Actually, the bandwidth of 10^{11} Hz and more is required to transfer multi-plane 3-D image of high quality. Therefore 3-D display creators try constantly to find any essential simplification of 3-D display system or/and to improve methods of data transmission keeping an appropriate image quality.

Looked around 3-D pattern can be formed holographically. Of course, real time information displaying supposes using the computer-generated holograms reconstructed in some amplitude-phase dynamic medium. This method could be related to multi-plane methods also. The difference is that separated points of view do not demand to be specially composed, and neighbor ones transfer each other smoothly (not discontinuously). However, the angle of looking around is limited (it equals 20-30° usually, maximum 40°). The acoustooptical crystal was used as such a medium in 3-D display system of Massachusetts Institute of Technology (USA). Rather power computer station has allowed recording and reconstructing the only simple linear digital holograms with parallax in one plane (horizontal).

Thus, taking into account a computer resource that can be given to concrete 3-D system, which displays the multitude of different points of view, such a multi-plane system is suitable for representation of simple objects and scenes only. In opposite cases it possesses low rate (a few frames per second) or low angle of looking around (up to 30°) that means a small number of points of view accordingly in horizontal and/or vertical planes (tens - hundreds, not more). Besides, complicated software and additional optical and technical elements are necessary for composing the 2-D images when such an approach is used.

Note, the information capacity $N_z \cdot N_x \cdot N_y$ is much less (3 orders minimum), than capacity, required for forming the adequate multitude of points of view formed on 2-D display screen, since different planes are not formed in 3-D media specially but are observed naturally at the looking an object (scene) around.

In spite of evident disadvantages of 3-D systems based on 2-D display use, only these systems are commercially available today for 3-D individual and collective displaying the objects and scenes. Different 2-D screen design and different schemes of detecting the position of an observer head are used in these systems. Mostly spheres of such a system application are video games and trainers, composing the space illusion for users, as well as this method based computer design and tomography.

3. Possibilities of 3-D display creation on the base of 3-D media.

So, 3-D object, scene or other 3-D information represented mostly close to 3-D image and smoothly looked around can be only formed on the base of 3-D medium. Three following methods of visualization and accordingly of addressing the voxels in 3-D

medium are suggested: two-laser beam scanning in orthogonal planes, optical-mechanical and optical-electronic methods.

When voxels are addressed by two laser beams (see Laser focus world, November 1994, p.28 and Applied Physics Letters, v.74, №3, pp.329-331, 1999) 3-D image is formed dot by dot directly in radiating (fluorescent, to be precise) transparent 3-D medium (gas, liquid or solid-state), for example, possessing the effect of two-photon absorption of radiation of two crossed laser beams that are scanned in two orthogonal planes. The use of such a photo-excited medium is characterized with most reliable displaying the 3-D scene and view angle closed to 360°. To reach the high spatial resolution in such a display it is necessary to provide two-beam time matching with 10^{-12} sec accuracy. However the main disadvantage of this method is the very low light efficiency (10^{-3}... 10^{-4}), and even this value is achieved only under definite conditions, namely, at the ideal spatial coincidence of beams and their polarization as well as the lack of exciting radiation absorption out the beam coincidence zone. There is also the problem in full-color display creation because of difficulty in the selection or synthesis of a material possessing two-photon fluorescence in red, green and blue spectral regions at once.

Optical-mechanical method to create 3-D display which was described first at «Aviation week», v.73, № 8 (1960) proposes using the free space where periodical translations of 2-D fluorescent or light scattering screen take place, if this screen is fastened on the screw butt-end or rotated disc. Voxel visualization is realized due to 2-D laser beam scanning at the screen plane. One of last variants of 3-D optical-mechanical display («Electronics», № 18, 1990) consisted of 2-D laser beam scanner (in X-Y plane) and an opaque plate which scattered an incident beam and shifted along axis Z being fastened on a rotated disk. To take into account the shift continuity and difference in linear velocities of plate points, differently distant from the disk center, the very complicated plate profile or/and additional software for laser beam addressing must be used. To create full-color display one can use here three laser beams of different colors or three plates covered with different phosphors. Unfortunately, the presence of fast moving unit and «dead» zone at the plane of beam scanning, highest requirements to profiling precision and positioning of the movable plate, visualization of voxels on one side of a plate and disk (i.e. at 1/4 of space) as well as only consecutive (along Z axes) slice addressing limit seriously possibilities of optical-mechanical method.

Nevertheless namely this method have been used recently in the first created 3-D medium based 3-D display system «Perspecta Spatial 3D Platform» of Actuality Systems, Inc. (Berlington, Massachusets) demonstrated on Boston display exhibition (UK, June 2002). A disk with a plate was placed under transparent semi-sphere of 50-cm height, and image visualization volume was about 25-cm diameter. This image was formed from 198 slices of 768x768 pixels each and looked like a whole one at disc rotation rate of 24 cycles per second and more. The creation of «Perspecta Spatial 3D Platform» means significant break in 3-D information displays, and this fact will determine a development level in this field for a long time.

The 3-D display system with optical-electronic voxels addressing has been described recently in the Russia patent application (No. 2002111262 of April 26, 2002). Like the optical-mechanical variant a laser beam scans at 2-D plane, but a slice is selected due to electrical field supplying to selected electrooptical (scattering a light) layer of multi-layer composite medium. Such a system has not moving unit, and visualization volume can be observed from all sides practically. Evidently, three laser beams of different colors can be used in full-color 3-D display. Basic requirements to 3-D display system of optical-electronic type are small time of on/off switching the light scattering and minimization of light reflection on layer boundaries. A few composite media satisfy to these requirements including media on the base of ferroelectric liquid crystals and electrooptical ceramics (additional immersion and antireflection layers are necessary).

4. Future prospects of 3-D display developments.

Besides 3-D display of «Perspecta Spatial 3D Platform» type taking only first steps

in the display market and applications, there are no other displays based on 3-D medium. Therefore one can expect that 2-D screen based 3-D multi-plane information displays using a power computer and additional optical elements will dominate up to 2010. Among such 3-D displays the spectacular free multi-plane systems of collective using, run slit or lenticular raster based will be widely distributed. It is supposed that 3-D scene images with a few hundreds of distance planes and tens thousand points of view (up to 100 000) will be visualized to this time, optimal codind/decodind of points of view will be realized to diminish requirements to the transmission channel, recording equipment and fast algorithms of real time video-information processing will be developed, and head facilities free viewers (ten and more simultaneously) will watch high quality 3-D images on 2-D screens of 1200x1000 pixels (SXGA size).

It is supposed that interactive video-systems with multi-dimension remote control information input will be developed to 2010, and they will allow creating 3-D competition games of "player-player" type due to the play situation control by both players simultaneously. Expected parameters of such a system are the following: the number of players - up to 4, the control panel with 4-6 degrees of freedom and 600 horizontal and 300 vertical resolvable positions, remoteness from 0.5 to 4.0 m, information update rate not less than 50 Hz.

Computer progress will allow creating rather effective 3-D display of the holographic type. Perhaps, first commercially available systems will come to 2010 to the market and occupy some application niche, perhaps, in trainers, video games, and advertising.

Concerning to 3-D medium based displays one can expect that more than one hundred such displays of the optical-mechanical type like «Perspecta Spatial 3D Platform» system will be produced to 2010. First of all they can be used in airplane navigation, 3-D task computer simulation, in medicine. The first 3-D display with optical-electronic voxel addressing can be produced in 2007 only. However as early as in 2010 it can compete with optical-mechanical displays. Within the next few years soft- and hardware for data recording, processing and transmission will be elaborated intensively to provide subsequent displaying the data by the slice method in both types of displays. Perfection of fast laser scanner for them will allow increasing the slice number up to 300. Both 3-D displays will be monochromic mainly in 2010. Then color ones will be available also and will become accustomed to users for next ten years.

All mentioned above types of 3-D displays – multi-plane (including interactive ones) with 2-D screens, holographic, and multi-cat ones (optical-mechanical and optical-electronic) will be used widely to 2020. Their part on the world display market can be quite significant and reach a few percent (in money).

In principle, in further future the most important task could be solved, perhaps. Namely, 3D-display could be created with electronic only addressing the voxels in 3-D medium, if such a medium could be lucky grown layer by layer (like in IC technology) from separate 2-D fast flat display screens with transparent elements luminescent under the electrical voltage.

DEA-4. **The comparative analysis of information perception quality on screens of CRT and TFT LC displays.**

Konstantin Bogachov, Igor Litvak

Moscow State Technical University of Electronics & Mathematics, Russia

Paper is not available

DEA-5. **Aviation Display Devices in Russia**

Vladimir Feofanov

R&D Institute "Electroautomatika", S.-Peterburg, Russia

Paper s not available

DEA-6. Electroskin Substitution Of Human Vision (Display For Low Vision And Blind Persons)

G.G. Demirchoglyan, V.I. Verkhoturov, S.M. Verkhoturov, V.B. Filippov, and V.A. Kundik

Russian Foundation for Engineering Rehabilitation of Low Vision and Blind Persons, Moscow, Russia
Russian Research Institute of Physical Training and Sports, Moscow, Russia

A device (display for blind persons) makes it possible to transform optical images into electric signals that are fed to a matrix of the needle-like silver electrodes retained against the skin of a blind person. The blind person is trained to perceive signals of these electrodes as visual images. Thus, an area of the skin (for example, on the human back) replaces the retina and the brain generates an image of external objects, which the blind person is not able to see in the usual manner, i.e., through the visual channel.

Recently the pilot (only 100 channels for the present) device was assembled. This mains-operated device has a high-sensitive matrix that differs advantageously from the prior art devices by unconventional engineering solutions and lower cost [1]. After certain training of the blind and low-vision persons, the device is simple enough to be used by them in practice.

Results of the experiments performed showed the following:

(1) Based on the criteria of minimum sensation threshold, maximum efficient range, and maximum differential spatial sensitivity, the area of human back may be taken the best one. The areas of shoulder and knee did not differ significantly from the area of the back in absolute values of the sensation threshold, but the upper limit of the efficient range was lower.

(2) The stomach area is distinguished by a lower perception threshold and a more narrow efficient range, but the use of this area as a location of the stimulating matrix is undesirable, because the reflex projections of the internal organs are located in this area (the Zakhariin-Ged zone).

(3) Among persons under test, the differential spatial sensitivity was higher upon localization of the stimulus in the areas of the shoulders; but the thresholds in stimulating both left and right shoulders markedly differed, which poses an additional problem of the choice of the side of application of the stimulus.

Further, the possibility of a simple coding of information was studied with varying parameters of the electroskin irritation. Thus, four bipolar electrodes located in the vertices of a 2-cm square were fixed on the skin of the person under test. The task to interpret these electrodes as the upper right, upper left, lower right, and lower left was given to such persons. In doing so, the thresholds of sensation and pain were determined, and then the middle of the range obtained was taken as the optimum stimulation.

In our new version of the device under development (see Figs. 1 and 2), the signals involving the above parameters come via actuator elements (6) to electrostimulating electrodes (7) that contact with the skin of the blind or low-vision person and thus create distinct skin physiological sensations therein.

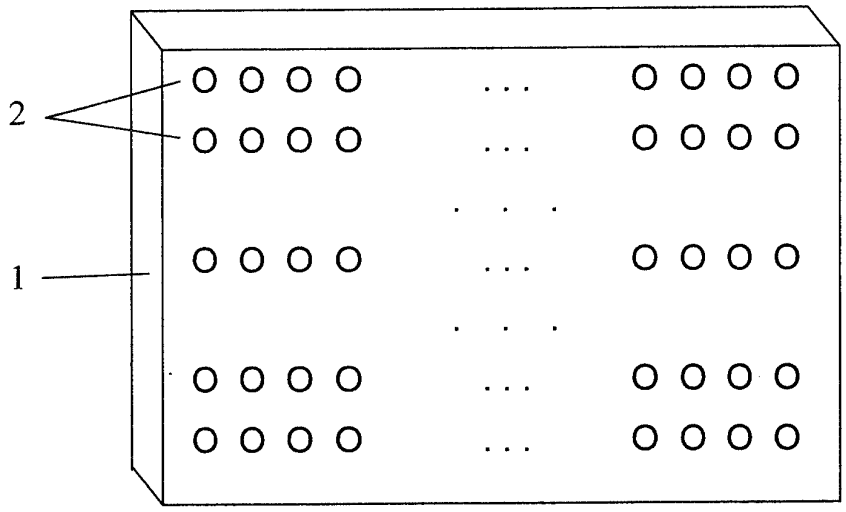

Fig.1. Display for blind and low-vision persons. 1- photoelectric matrix, 2 – photo-receivers.

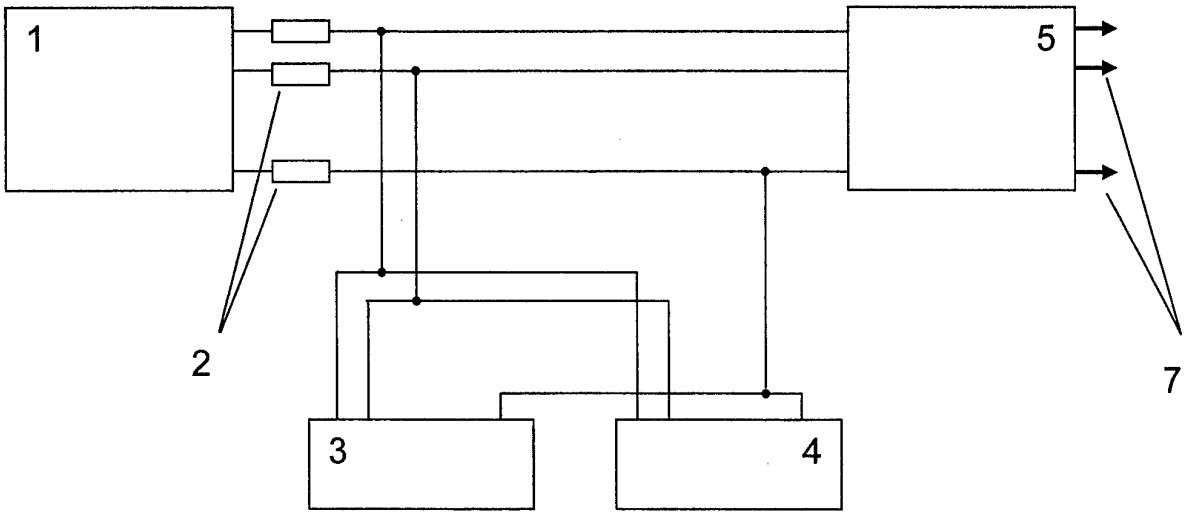

Fig.2. Scheme of the signals formation in the display for blind and low-vision persons. 1- photoelectric matrix, 2 – resistors, 3 - amplitude modulators , 4 - frequency modulators, 5 - actuator elements, 6 - electrostimulating electrodes.

The following examples of the display functioning are given below:

(A) An object with respect to the viewer is located at a large distance to the right. In this case, the viewer feels a weak electrostimulation from the side of the right electrodes.

(B) A traffic light with the switched-on red light is located in the frontal plane forward of the viewer. In this case, the vertical row of elements (2) of the photoelectric matrix (1) fixed to the person's forehead is darkened; the post of the traffic light and the red light are displayed on the corresponding photoelements by different values of the photoelement currents correlating with their color. These signals first pass through amplitude modulators (4) and frequency modulators (5) and then come to the corresponding actuator blocks (6) thereby reproducing an upward-elongated figure with red light in the upper part. The skin perceives this image, which will certainly be associated with the forbidden red light of the traffic light.

Thus, such a display for blind persons makes it possible to determine the following parameters of objects located in the frontal plain: the dimensions, the color, the direction of motion, the velocity of motion, the distance from an object to the viewer, etc. Our further investigations for obtaining a higher resolving power are scheduled in 2003-2004.

REFERENCE

1. G.G. Demirchoglyan and V.B. Filippov Application to Patent of the Russian Federation No.20011117340, filed May 5, 2000.

DEA-7. **Information display large screen projection systems**

A.V. Sadchikhin, A.G.Morozov, S.B.Sozinov

AR Technologies Corp., Russia

Paper is not available

DEA-8. A New Approach To The Design Of Highly Efficient Large Size LED Displays With Improved Ergonomics

Yu. V. Trofimov, V. S. Posedko, V. K. Sivenkov,
I. M. Mironenko, S. I. Lishik
Institute of Electronics NASB, Logoiskii trakt 22,
220090 Minsk, Belarus

We have proposed a new approach to engineering and manufacturing of indoor type of indicators on the base of the energy effective super-bright LEDs. In our design the light from a small number of such LEDs is uniformly redistributed using a special lightguide. Recently we developed a multi-segment (40) LED indicator with improved ergonomics with the brightness up to 4000 cd/m^2. This indicator is also capable of displaying (apart from the digits) some special service symbols

Ketwords: superbright LED, ergonomic, display, seven-segment, multi-segment, indoor, outdoor

The continued electronization and informatization of the society makes the display devices even more important. Amongst these devices the highly efficient large size LED displays with improved ergonomics will play a significant role. Depending on the operating conditions, mainly on the level of illumination at the place of installation and climate conditions, the displays fall into the two groups. In the first group the displayed image is formed from uniformly illuminated segments; in the second – from a large number of separate LEDs.

Let us consider the two groups in more detail. One has to note that there are similarities as well as differences in the properties and characteristics of these two types of indicators. In both cases it is required to achieve correct and reliable readability of the information under various combinations of ergonomic parameters, what in many respects is determined by the quality of the graphical representation of a character. As the size of the display is concerned, for indoor use it does not, as a rule, exceed 20 cm and the sufficient brightness level is at about 300 cd/m^2. In the second case the character height can reach 1 m and more, and the brightness exceed 10000 cd/m^2. However, lately for use in sport buildings (stadiums, swimming pools) as well as in stock exchange and auction halls, the displays of the first type with the character size 25-35 cm, brightness level 1500-2000 cd/m^2 are required. Such displays are easily readable from the distance of 150 m.

For the seven-segment indicators, which are the most widely used ones, the parameters also very important for the readability are: the height-width ratio of the display, the gaps between segments, the brightness and uniformity of the segment illumination, and the slanting angle. The main disadvantage of this type of displays is the limited character set, that is why the development of multi-segment displays of high importance.

Let us consider the indicators from the first group based on the information presented in [1].

The need to increase the size of the display and at the same time limit the number of the LEDs to decrease the cost led to the development of the hybrid devices based on the dispersion of light. In such devices the illumination of the segment is realized with the help of the semiconductor LEDs, situated the light-diffusing cavity of the lightguide. In this case the size, shape of the segment and the uniformity of its brightness are determined by the dimensions and the configuration of the lightguide. At present it is possible to distinguish three different approaches to the design of the lightguide:

- plastic lightguide with top dispersing layer (Fig. 1a);
- hollow lightguide with dispersing film (Fig. 1b);
- plastic lightguide with the reflective mirror walls, the plastic material of lightguide contains a dispersing additive (Fig. 1c).

During the development of such light-dispersion based indicators the uniformity of the brightness throughout the light-emitting surface is required. In the first of the above mentioned types the light coming from the LED chip after multiple reflections from the plastic-air interface leaves the lightguide through the top dispersing layer. The uniformity is then achieved by controlling the distribution of the dispersing glass or quartz particles in the top layer.

An alternative solution to the uniformity problem is realized in the devices of the second type. In this case the emitted light after multiple reflections now from the side surfaces of the hollow lightguide enters the dispersing film and leaves the system. To increase the efficiency of the display it is imperative to have a high reflection coefficient of the lightguide sidewall surfaces. This is normally achieved by depositing of a gold or aluminum layer with a high reflection coefficient in the visible light wavelength range.

The design of the third type is a synthesis the two above mentioned technologies.

DEA-9. **Beyond 3D Television: The Multi-modal, Multi-viewer TV System of the Future**

Phil Surman, Ian Sexton, Richard Bates,
Wing Kai Lee, Michael Craven, Kam Chaun Yow
De Montfort University, Leicester, The Gateway, Leicester LE1 9BH, UK
Email 3DTV@dmu.ac.uk

Abstract

Under the European Union funded Advanced Three-dimensional TElevision System Technologies (ATTEST) project, De Montfort University is developing a 3D display system targeted specifically at the domestic television market. This uses a modified commercially available LCD panel combined with novel backlighting and optics to project multiple viewing regions, or exit pupils, into the viewing space. These exit pupils are located in space using a head tracker.

The display accommodates multiple viewers simultaneously and imposes no physical constraints, such as special goggles or glasses. Viewers may move freely over a 'typical' room sized area.

The novel backlighting system is particularly versatile. Used in conjunction with high resolution transmissive LCDs, many other display regimes are possible beyond the 'standard' 3DTV mode in which each viewer sees the same image-pair. These modes include many completely different monoscopic scenes, a mixture of monoscopic and 3D, and full motion parallax, amongst several others.

The underlying optical principles of this display system are presented along with a description of its current manifestation.

Keywords
3D Television, Autostereoscopic, Multi-viewer, Liquid crystal display

A New Approach

Our display uses a new approach to generating 3DTV and consists of two main components, a spatially multiplexed front screen and a novel optical steering array and light sources that directs light through the screen to the viewers, thereby enabling 3D to be seen without the use of special glasses.

The steering optical system is controlled by the output of a head position tracker to locate the viewers' eyes in space. As head tracking work is being carried out by several other groups throughout the world [1][2][3], our research concentrates only on the display optics.

Spatial Image Multiplexing

In order to perform spatial image multiplexing on the front LCD screen, light from two distinct sets of *steering optics (left and right eye) must be directed to the appropriate pixel rows on which the left and right images are displayed on the LCD. Figure 1 indicates how this is achieved.*

The figure shows that light from two separate sets of

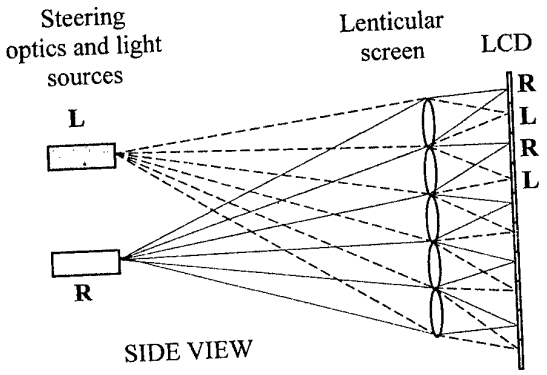

Figure1. Spatial Image Multiplexing

steering optics is directed to the alternate left and right image rows on the LCD by using a horizontally aligned lenticular screen. The figure is not to scale; the lenses shown are, in fact, very small in relation to the arrays of steering optics.

Note that the lenticular screen is not used for directing the left and right eye images in space, but is only used for interlacing the two images on the front screen. Hence a stereo image-pair is produced on alternate pixel rows enabling the same pair of stereo images to be seen by every viewer.

Steering Optics

The steering optics comprise of two distinct arrays of coaxial optical elements arranged behind the screen as shown in figure 2.

Each array consists of multiple optical elements and illumination sources arranged in stacks across the back of the screen. This approach allows the full width of the screen to be illuminated by the steering optics. Using an array of small optical elements obviates the need for a single large lens and illumination source, as shown in figure 3a.

With a single large lens, an exit pupil, which is the real image of an illumination source, can be steered by moving the light source position.

This approach has been used in several 3D display

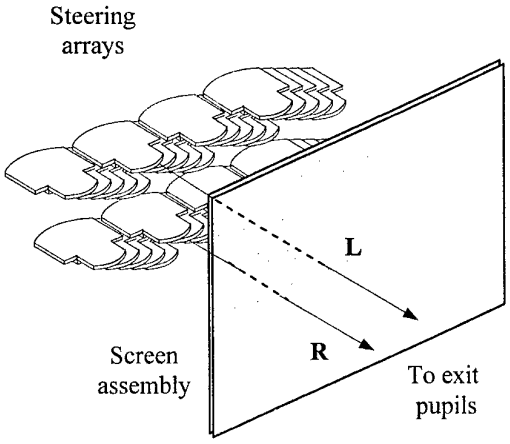

Figure 2. Steering optics

systems [4][5][6]. Generally, TV viewers should be free to move over a large viewing area; hence exit pupils need to be produced at large angles from the screen. With a single large lens this is clearly not practicable because the illumination sources would need to move over a very large region behind the lens. Also, in this arrangement the spherical aberration of the large lens would severely limit the angles over which the exit pupils could be formed.

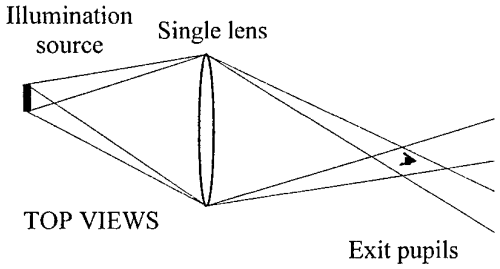

Figure 3a. Single lens

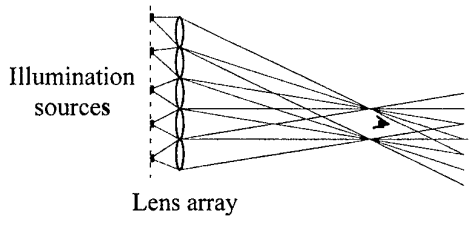

Figure 3b. Multiple lenses

The problems associated with a single large lens are overcome with the use of the lens array, as shown in figure 3b. The array uses small movements of multiple light sources behind the multiple lenses instead of large (impractical) movements of a single light source. In addition several illumination sources can be lit simultaneously, producing multiple exit pupils for multiple viewers. Hence the steering optics do not impose a restriction on the number of viewers the display can accommodate; this is only restricted by the number of viewers who can physically fit into the viewing field.

The use of multiple light sources also facilitates the steering of exit pupils fore and aft in front of the screen. Hence, as a viewer moves closer to or further from the screen, the spacing between the light sources changes to accommodate the convergence or divergence required for the projection of the exit pupils.

Rather than physically move each illumination source behind each lens of the steering optics, high-brightness white LEDs are arranged closely behind each lens and movement is accomplished by switching LEDs on or off to steer the exit pupils.

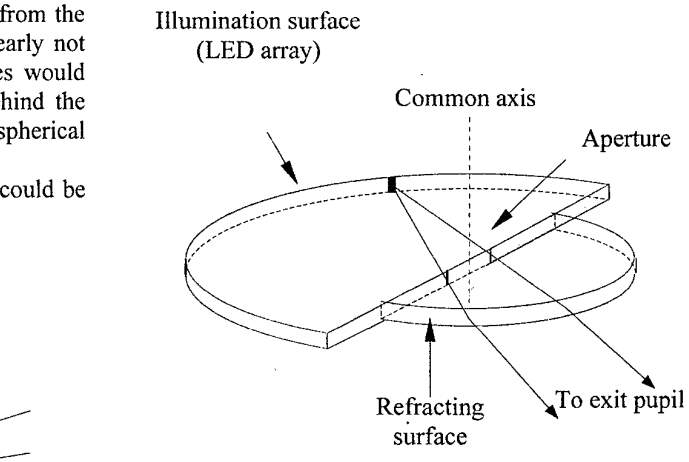

Figure 4. Co-axial optical element

To overcome the spherical aberration associated with a single large lens, the lenses of the steering optics use optics that do not exhibit off-axis aberrations. This is achieved by using a cylindrical lens and a curved illumination source that have a common axis, with an aperture that is centred on this axis. The optical elements are therefore termed 'coaxial'. An element is shown in figure 4.

Light from the illumination sources is contained within the two D-shaped components by total internal reflection. After passing through the aperture, it is formed into a parallel beam by the front refracting surface. The illumination LED array has a pitch of around one millimetre. This enables

the exit pupil position to be controlled in small increments relative to the interocular distance.
Each optical element uses an aperture that is faded at the edges rather than having an abrupt cut-off. When the lenses are placed in the array, these apertures are aligned in series, with overlapping faded regions, and hence form a contiguous exit pupil light source across the full width of the screen.

As the steering optical arrays are not as high as the screen, a vertical diffuser is used on the lenses to fully illuminate the complete height of the screen, consequently the steering optics are situated at some distance behind the screen. This might require the housing size to be impracticably large, however the display dimensions can be kept to a reasonable size by using folding mirrors, as shown in figure 5. This reduces the size of the display to that of a typical domestic wide-screen television.

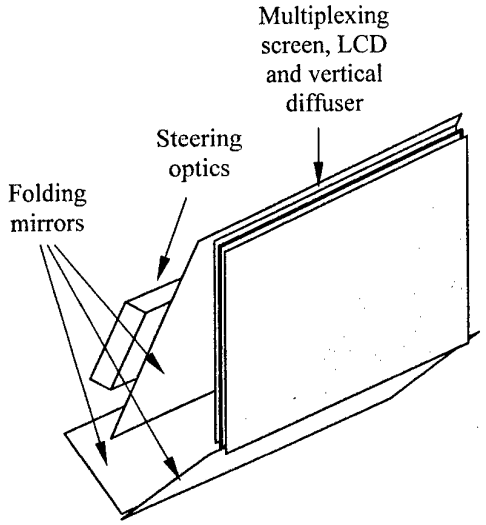

Figure 5. Optical folding

Beyond 3D Television

The design outlined here allows two different images to be produced on a single screen, giving 3DTV to multiple viewers. However, the operation of the steering optics is sufficiently flexible for it to be used for the presentation of many different images when used in conjunction with a modified image multiplexing arrangement, with the resolution of the front LCD as a limiting factor. Since the resolution of LCDs is gradually increasing, and currently nine million pixel devices are available, this would, for example enable four standard resolution images to be displayed.

This scalability of design presents the possibility for an entirely new form of screen that can present completely different views to different viewers.

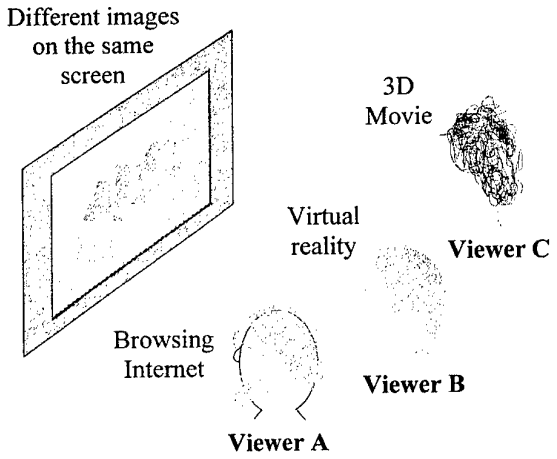

Figure 6. Display possibilities

For example, 3D full motion parallax can be presented to viewers, or viewers may watch different TV channels simultaneously, or some use the screen as a computer monitor or virtual reality display whilst other viewers watch TV, as shown in figure 6.

In an increasingly interactive future, it is envisaged that other modes of operation will be used in addition to the standard TV mode. Hence the display can be considered as a practical 'one-for-all' solution, or 'super-screen' for a variety of future display requirements

References

[1] Harman P. "Autostereoscopic Teleconferencing System", SPIE Proceedings, "Stereoscopic Displays and Virtual Reality Systems VII", Vol.3957, pp 293-301., 2000

[2] Heidrich H., Schwerdtner A., Glatte A. and Mix H. "Eye Position Detection System", SPIE Proceedings, "Stereoscopic Displays and Virtual Reality Systems VII" Vol.3957, pp 192-197, 2000

[3] Morishima H., Nose H., Yaniguchi N., Inoguchi K and Matsumura S. "Rear Cross Lenticular 3D Display without Eyeglasses", SPIE Proceedings, "Stereoscopic Displays and Applications IX", Vol.3295, pp193-201. 1998

[4] Benton S.A. "Autostereoscopic Display System", United States Patent No. 6,351,280. 2002

[5] Son J.Y., Smirnov V. V., Asnis L. N., Volkonsky V. B., Chun J. H. and Kuznetzov S. V. and Lee H. S. "Real-time 3D Display with Acousto-optical Deflectors", SPIE Proceedings, "Stereoscopic Displays and Virtual Reality Systems VI", Vol.3639, pp 137-142. 1999

[6] Woodgate G.J., Ezra D., Harrold J., Holliman N.S., Jones G.R. and Moseley R.R. "Observer Tracking Autostereoscopic 3D Display Systems", SPIE Proceedings, "Stereoscopic Displays and Virtual Reality Systems IV", Vol.3012, pp187-198. 1997

DEA-10. Application Of Waveguide Holograms In Displays And Planar Illuminators

Putilin A., Gustomiasov I., Chernopiatov A.
Lebedev Physics Institute of Russian Academy of Science (LPI)
Laboratory for superfast optoelectronics and optical processing
117924, Moscow, Leninsky prospect 53,
tel: 132-6491, fax: 132-5363
E-mail: w_hologram@mail.ru

Abstract

The recording and reconstruction of waveguide holograms for optical plane illuminators and lenses are discussed. The part of the paper is devoted to the investigation of the specific noises and distortions of the waveguide hologram reconstruction. These noises arise due to the non-uniform illumination of the hologram by waveguide modes.

A prototype device for the LC Display that uses a waveguide hologram as a part of the acromatic illuminator unit is described. The use of waveguide holograms enables reduction in size, weight and energy consumption of the illumination unit.

The virtual displays are another area of waveguide hologram application. We have recorded several schemes of virtual holographic display for multicolor viewing. The specific feature of these achromatic holographic head mounted displays is different optical passes that different illumination wavelengths have in the optical scheme described.

Keys: plane illuminators, integrated optics, holography, waveguide hologram.

...

Some specific noises and distortions arise when waveguide holograms of two-dimensional images are recorded. Formerly we supposed the reasons of these noises to be mistakes in the recording process, but it happens rather regularly and that's why we decided to investigate in details the linearity of the hologram recording and reading process in order to understand the peculiarities of the waveguiding mode reconstruction

In this paper we investigated the relief type waveguide holograms (WGH) /1/. The recording setup is a Fourier hologram recording scheme with an angle of the reference beam incidence matched with the waveguide mode propagation constant, that is used for reconstruction. The recording material was evaporated on the top of the planar waveguide. After exposing and selective etching we obtain thin relief type waveguide hologram. In experiments we use ion-exchange glass waveguides, amorphous As_2S_3 layers and photoresist films as a recording materials. He-Cd laser was used for recording, He-Ne and semiconductor red lasers for reconctruction. The spatial frequency of the recorded holograms was about 2500 mm^{-1}, information capacity of the holograms didn't exceed 10^3 bit/mm^2.

In experiments on waveguide holograms recording (for matched filtering, hologhaphic memory and displays) we observed very high noise level, or even entire information loss, while in conventional (non-waveguiding) reconstruction schemes the images were rather good. The waveguide reconstruction adds some new nonlinearities in reconstruction, because of the distributed interaction of holographic grating with waveguide mode. Grating is strongly influenced not only by an imaginary part of the mode propagation constant but also by the real part when the diffraction efficiency of the hologram arises. Some parts of the hologram will not be reconstructed because the light will be coupled out of the waveguide before it reaches these areas of the hologram.

The typical noises of the waveguide reconstruction are shown in fig.1, binary and grey-scale test images have been used . Another specific feature of the waveguide hologram is the influence of the diffraction efficiency upon the direction of the reconstructed beam incidence angle, and one can distinctly observe it for the asymmetric Fourier spectrum of the recorded information.

a)

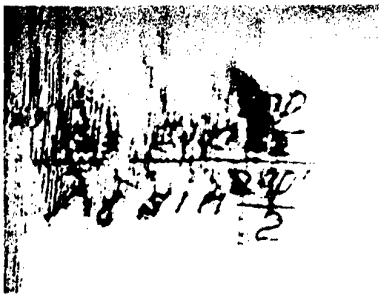

b)

Fig.1 a) typical noises of the binary image waveguide reconstruction
b) typical noises of the grey-scale image waveguide reconstruction

The computer model of the reconstruction of the waveguide holograms was constructed in order to investigate the influence of the parameters of the waveguide on the image quality.

We try to make the qualitative analysis of the reasons of the noises and to suggest the methods of their elimination. It was shown, that the increasing of the amplitude of the grating strongly influences the root-mean-square error (MSE) of the reconstructed image because of the multiplicative noises. The specific influence of the waveguide hologram reconstruction may be thought of as the adding of two filters to a conventional holographic process. The first one - the phase filter, that has a modulation proportional to the square-root of the Fourier transform of the recorded information, and the second one - the one-dimensional exponential amplitude filter, that takes account of the decreasing of the waveguide mode power due to the coupling out the light on the holographic grating. The calculation shows that for the MSE about 10^{-2} the diffraction efficiency of the waveguide Fourier hologram will be no more than 5% for binary and 0.01% for the gray-scale images. The vertical oriented fragments of reconstructed images are more noisy then the h orizontal lines (basic direction is a direction of the waveguide mode propagation). High spatial frequencies are more noisy because the corresponding information is located on the outlying area of the hologram where the gradients in disturbed phase and amplitude have a maximum.
Then we tried to examine the influence of the parameters of the spatial light modulators used for hologram recording on the MSE. This analysis may be very actual for the development of compact holographic memory. The binary random images were used as test objects for hologram recording modeling. The shape of the pixel and period-to-pixel duration ratio (R) can be varied. Fig. 2. shows the signal-to-noise ratio (MSE) versus R for the round pixel shape.

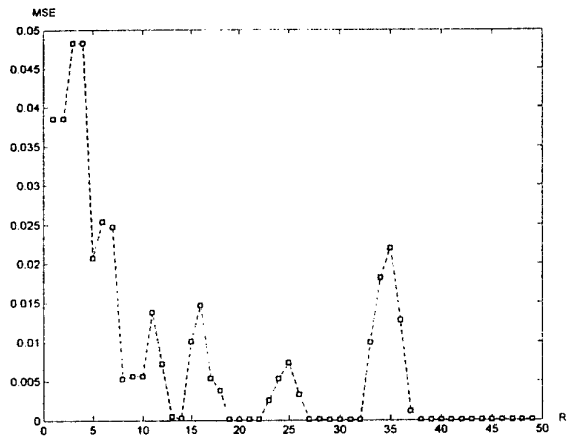

Fig.2 Signal to noise ratio (MSE) versus the size of the single pixel (R), period of the pixels position in the matrix - 50, the probability of the transparent pixels in the random image is 0.8

The noise oscillation for soe period-to-pixel duration ratio is rather high, so in practice the physical parameters of the SLM must be adjusted for the concrete design of the holographic integrated memory.

We assume the size of the photodetector on the reconstruction step to be equal to the size of the pixel whale recording. MSE is rather low for the large R, but for good electrical separation the small size is preferable, so the optimal R/Rmax must be defined in the area far from the noisy peaks on the MSE graph.

The strong dependence between the signal-to-noise ratio and the type of information recorded on the waveguide Fourier holograms is the main result of our investigation. The waveguide holograms efficiency increasing acts differently on the reconstruction of the low and the high spatial frequencies, because of the exponential decreasing of the light mode power in the grating area. The recording of gray-scale images is more sensitive to this kind of distortions, so the maximum diffraction efficiency of the free of noise gray-scale holograms will be rather low.

Application of phase random masks and recording of non Fourier holograms will perform the mixing of the spatial frequencies in the recording holograms, so the distortions mentioned above will be significantly decreased.

Applications of waveguide holograms in display design.

1

In our previous paper /2/ we have described the waveguide illuminator for the LCD displays, which performs at the same time the color coding. The light efficiency of these displays is three times higher than the conventional one. Here we want to describe the further development of the idea of the holographic color masks for LCD displays. One of the main drawback of the color LCD and CRT tubes is a spatial separation of the colors (color subpixel structure) in the color pixel, which leads to the taking painting of the outline of the gray-

scale image fragments.

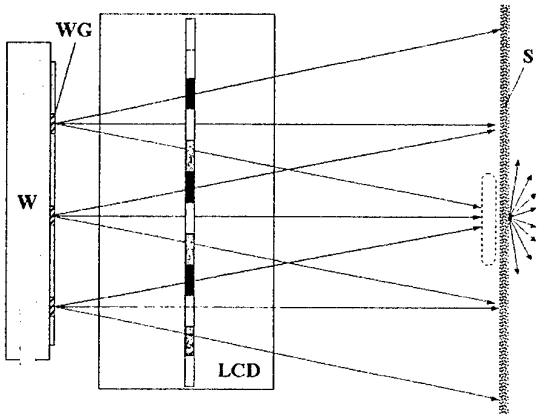

Fig.3 LCD display with holographic achromated color coding, WG - waveguide hologram , S- diffuser.

The size of the pixels must be less than the resolution of the human eye for perfect viewing, but in practice, the most of the people fall into the way of watching closer the rated distance. The holographic illuminator scheme for the LCD displays, which forms "white" (achromated) pixel is proposed. Fig.3 Shows the optical scheme of the "White" pixel waveguide holographic illuminator. Waveguide hologram forms the series of micro-rainbows which are spatially matched to the color subpixel structure of the LCD display. Monochrome or color LCD display can be used in this optical scheme, in both cases the light efficiency of the display will be three times higher than the conventional color coding scheme.

LCD is placed at the distance where colors are spatially separated. Triads of the color beams are focused over the LC layer and optical substrates of the panel. Unlike conventional color subpixel structure our triad is formed by the second neighbors in the matrix. The optical scattering layer S is placed in the plane of focusing for complete spatial color mixing and viewing diagram forming. Such optical scheme forms the color image with constant color and contrast for all angles of viewing. The narrow range of incidence angles permits to obtain high contrast and transparency of the LC layer.

This scheme of LCD illuminator forms achromated pixels of enlarged size in front of the active LC layer, so it needs precise components positioning in the arrangement.

2

Achromatization of the holographic images is the most complicated problem of holography. Here we describe the new method based on the waveguide holography approach. Originally it was proposed for operation improvement of integrated illuminators /3/. The design of the achromated holograms begins with the selection of the lasers that will be used for reconstruction, because of the limited amount of laser wavelengths. We propose the scheme which requires rather precise adjustment of the laser wavelength according to the parameters of the hologram and waveguide. We see that a semiconductor laser wavelength can be shifted a little for the concrete application. Fig.4 shows the scheme of substrate mode hologram reconstruction.

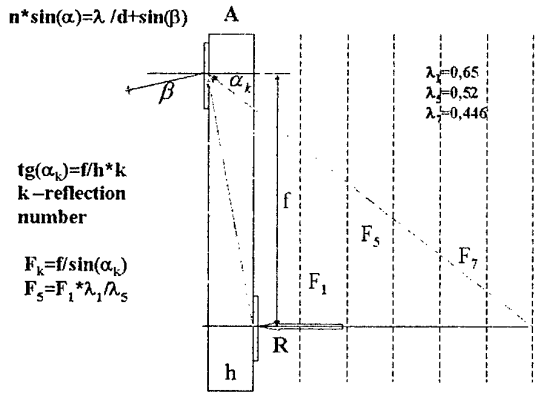

Fig.4 Achromated reconstruction of the hologram by the substrate modes

h- the thickness of the substrate, f- the distance between the holograms A and R, α- the angle of light incidence on the hologram A, β- the diffraction angle, F - focus distance.

For waveguide hologram the angle of incidence for blue light differs greatly from the green and especially from red lights because of the high spatial frequencies of the grating. The light of different wavelengths will have a different passes in the substrate in order to reconstruct color image, and the focus distances of the holographic lenses are inverse ratio to the wavelength. This conditions can be fulfilled simultaneously while the optical paths have a multiple reflection in the substrate. The second hologram R with the same spatial carrier was used for coupling light beams into the substrate. Corresponding color rays paths are shown by dashed lines (fig.4). For example, the color beams will have one(red), five (green) and seven (blue) reflections in the substrate if the wavelength of the laser sources will be 0.65, 0.52 and 0.446 micron, the thickness of the substrate must be 8 mm and distance between holograms 40 mm. This three colors forms rather good color triangle, so the image will have natural colors.

This method permits to construct robust and integrated color holographic displays, because all optical elements can be placed on the sides of substrate and optical transformation is performed inside this substrate.

Conclusion

In spite of the rather strong interaction betweeen the quality of the reconstructed image and the type of information recorded, waveguide holograms obtain several useful properties, such as high efficiency, integrated design, wide viewing angle and non-diffracted beams separation.

Application of waveguide holograms in LCD illuminators increases the optical efficiency three times and improves viewing properties.

We've proposed the new scheme of color

holographic illuminator for holographic displays and LCD on the base of hologram reconstruction by substrate modes .

Reference

1. Putilin A.N., Miler M. Perculiarities of two - dimensional objects waveguide hologram recording, Photonics and Optoelecrtonics, 2, 21-28 (1994).

2. A.N.Putilin, Y.P. Borodin, A.V.Chernopiatov Waveguide holograms in LCD illumination units, Proc SPIE, v.4511, p144-148, 2000.

3. Caulfield H. John, Huang Qiang, Putilin Andrei, Morozov Valentin, Shamir Joseph, Waveguide hologram illuminators, US Patent # 5,515,184, May 7, 1996

DEA-11. **Tunable Spectral Filters Based on Photonic Crystals with Liquid Crystal Defect Layers**

A.V. Shabanov, V.F. Shabanov, V.Ya. Zyryanov, S.Ya. Vetrov*

L.V. Kirensky Institute of Physics, Akademgorodok, Krasnoyarsk 660036, Russia

*Krasnoyarsk state technical university, Kirensky str., 26, Krasnoyarsk 660074, Russia

nikel@akadem.ru

One of the important features of photonic crystals is the opportunity to form photonic band gaps and defect levels of energy inside them. Such one-dimensional structures may reflect a light in sufficiently wide spectral range, but at the same time have a narrow spectral band of a transparency inside this range due to a defect mode. The use of liquid crystals as defect layers enables to operate spectral properties of photonic crystals structures, for example, with the help of various electrooptical effects in liquid crystal layers. It should be noted a prospect of this phenomenon for various applications, for example, in tunable spectral filters, narrow-band polarizers, light modulators.

DEA-P1. Investigation of the methods of estimating a visual fatigue when working with displays.

K.A. Bogachov
Moscow State Institute of Electronics and Mathematics (Technical University).

In order to solve the problem of work that is safe from the ergonomics viewpoint, the knowledge is necessary which concerns not only the theoretical basics of constructing perception models but also a considerable body of experimental data relevant to features of the dynamics of fatigue and relaxation of operator.

At present, there are several techniques of estimating fatiqueability of human operator. Some of these procedures allow one to continuously estimate the physiological state of his organism, i.e., the monitoring.

It is these techniques that are of prime interest to researches, since they make it possible to construct an individual fatigue curve for a particular time interval.

The purpose of studying different techniques of assessment of operator's fatigability was to compare the results obtained and to find the most sensitive and accurate technique that ensures both minimum estimation time and minimum interruption time under working conditions of user.

The methods that allow one to analyze a general functional state of operator's organism (for example, the indices such as periods of visual and motor reactions of operator) and the professional ophthalmological methods that allow one to estimate the efficiency of visual operation and the process of visual load and fatigue were tested in the course of our experimental investigations.

In our investigations, evaluation tests of the following techniques of estimating fatigability were performed:

1. "Bio-test" as a reference technique.
2. Critical flicker-fusion frequency (CFFF) test that is realized with the help of software-hardware complex involving a personal computer.
3. CFFF test that is realized with the help of an independent instrument developed at the ELITA Testing Center.

The "Bio-Test" technique is based on the measurement of a latent period of visual-motor reaction of operator to a given stimulus.

When the visual stimulus appears on the monitor screen, operator should react to this stimulus as quickly and accurate as possible. In doing so, the latent periods of visual and motor reactions of operator and recorded by a timing device with an accuracy of milliseconds. From those times and the recognition errors recorded as well as from the results of passage of a set check point, the indices of working capacity of operator are calculated using a special program. One measurement takes about 1 min, which allows this test to be employed in the course of operator's work.

The software-hardware complex for estimating CFFFs is a device that has external visual stimuli of red and green colors and is connected to a personal computer via a serial input-output port. The device is controlled by a special program of testing and recording the data obtained. The program makes it possible to fill the user's data base, with recording time and conditions of testing. In the course of testing, the critical flicker-fusion frequencies are also recorded.

The independent instrument for estimating CFFFs developed at the ELITA Testing Center ensures automatically the count and record of CFFF and time and conditions of experiments. The advantages of this instrument are the full automation of testing, a high accuracy of specifying and recording the critical frequency, and the quickness of testing. The instrument contains a risk single-crystal processor that controls the operation of stimulators and a liquid-crystal display and programs the count of the critical frequency with a high accuracy. The test time is 30 s. Depending on the functional state of operator, the design of the instrument allows the operation of different external devices to be controlled.

The experiments were performed in the following time sequence: 2-h work, 15-min interruption, 2-h work, 15-min interruption, and 2-h work. The total duration of one cycle of experiments was 6 h 30 min.

Testing with the use of all the techniques mentioned were performed at the start of working day, then at intervals of 30 min, and at the finish of working day. The number of check points of testing for each technique is 288, the total number of these points is 1152.

In order to reach the necessary accuracy, the work of operator as applied to its two main types was investigated: the work with text, i.e., a conventional type of activity of many users, and the computer game, i.e., a simulation of intense activity that requires a decision making under the conditions of limited time (an analog of the working process on consoles of control of deferent objects).

The example of summary diagrams of the dynamics of fatigue upon employment of different estimation techniques is given below a stable tendency for decreasing operator's working capacity from the start of work to its finish is clearly traced.

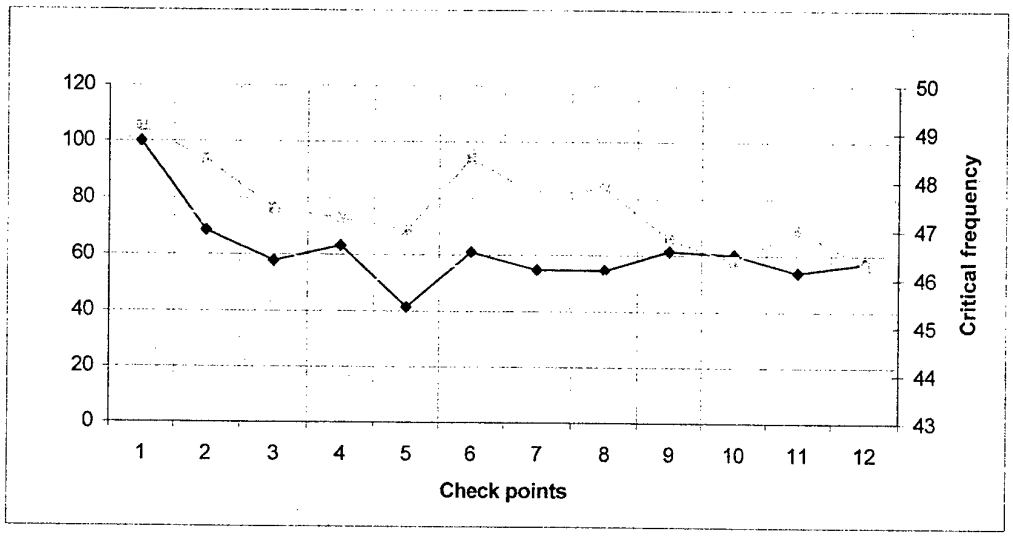

Fig. 1. Diagrams of the dynamics of the process of fatigue.
Bio-Test; software-hardware complex for estimating CFFF; independent instrument for estimating CFFF.

Conclusions

1. As is shown experimentally, the "Bio-Test" technique that takes only 1-3 min when testing can be recommended for estimating and measuring a degree of operator's fatigability.
2. Our experimental investigations confirmed that the CFFF technique may be used for estimating a degree of operator's working capacity when working with a personal computer.
3. Comparison of the results obtained by the "Bio-Test" technique with the result of the software-hardware complex for estimating CFFFs showed their weak correlation.
4. The technique for estimating CFFFs with the use of the independent instrument developed at the ELITA Testing Center (Moscow Institute of Electronics and Mathematics) yields the result of the "Bio-Test" technique and ensures high accuracy and quickness of testing operators.
5. The results of our investigations make it possible to solve the problem realizing the working conditions that are safe from the ergonomics viewpoint when operators can work with different image devices and displays. At present, this problem is solved by using the unified time quotas of working conditions for all operators. Such an approach completely rules out the flexibility of changes in the working conditions for each concrete operator, since an individual dynamics of the process of operator's state makes it possible to construct for each operator the individual working conditions that correspond to his minimum fatigue. This, in its turn, assures the fast, reliable, and accurate work of operator with the man-machine interface.

DEA-P2. The estimation of self-descriptiveness of symbols' elements of synthesized alphabets and the possibility of it's application.

Denis V. Feldman
Moscow State Institute of electronics and mathematics
(Technical University)

Abstract.

Character information displayed by modern electronic display units is formed on the basis of matrix (5x7, 7x9, 8x11, etc.). Symbols that are built in a matrix have special topology different from typographic fonts. In this connection there comes up the problem of increasing of perception quality of displayed character information, i.e. it is necessary to develop methods of analysis of symbols' configuration of matrix alphabets and methods of synthesis of optimal symbols' forms. The estimation of self-descriptiveness of elements of investigated symbols is the one of criterions of analysis of symbols' configuration.

There was proposed and approved the method of estimation of self-descriptiveness of symbols' elements of matrix alphabets. The "weights" of separate parts of symbols and they're influence on reliability, speed and comfort of perception were determined. In the process of developing of the method there was used the concept of "basic character" we proposed previously.

The method allowed to synthesize symbols with increased quality and reliability of perception. The number of perception mistakes of renewed symbols was 3 - 10 times less.

1. Introduction.

There are two types of fonts in modern electronic display units that are competing one with other. They called vector and matrix fonts. Vector fonts are applied for displaying symbol information by PC monitors or in systems that include OS Windows. These fonts are intended for working with high resolution displays. And matrix fonts are intended for working with low resolution display units (e.g. displays of mobile telephones, illuminated indicator boards at a stadiums and railway stations etc.). The symbols made in matrix are different by form from their original topology. In this connection it is necessary to consider the problem of increasing the self-descriptiveness of matrix alphabets' symbols.

2. The concept of "basic character".

The concept of "basic character" was used for analysis of matrix alphabets' symbols. The basic character for a certain matrix alphabet is a symbol containing elements that are common for more than defined percent of symbols (50-80%). In other words the basic character consists of most often encountered elements of symbols of the alphabet. In that way the basic character characterizes the similarity degree of alphabet symbols: the more elements the basic character consists the more similarity of symbols of the alphabet . Finally it leads to increasing of probability of confusing symbols of the alphabet by operators.

3. Dividing to groups.

There are certainly unlike symbols (e.g. such as I and O) in the Latin and Cyrillic alphabets. Therefore the basic character for whole alphabet characterizes the similarity degree of the alphabet symbols not adequately. In order to avoid this it is necessary to divide symbols of alphabet to several groups according to their exterior similarity and analyze several basic characters for each group of symbols. In this case calculation of basic characters for all combinations of pairs of alphabet symbols enables to define the similarity degrees between all

pairs (using the 50% basic characters) and in the basis of the criterion divide the alphabet to groups of symbols that are similar by their configuration.

4. Searching the informative features.

Considering symbols in the groups it is possible to declare that the probability of confusing symbols of same group higher than probability of confusing symbols of different groups. Calculated basic character for a group is a symbol that consist of common elements of symbols of the group. Comparing calculated basic character with each symbol of the group it is possible to find such fragments of symbols that are not the parts of the basic character. These fragments are informative features of symbols of the group. That fact enables to conclude that it is necessary to decrease the volume of a basic character for a group of symbols and to increase the volume of informative features of symbols of the group for decreasing the probability of confusing symbols of the group.

5. Our developments.

5.1. The analysis of alphabets.

The program for analysis of matrix alphabets was developed and approved.
It enables:

- to calculate a basic character for any alphabet or group of symbols;
- to divide alphabets to groups according to symbols similarity;
- to search informative features;
- to make changes of configuration of alphabet symbols.

5.2. Experimental developments.

The firmware for experimental searching symbols similarity (confusing by operators) for certain alphabet was developed. The firmware intended for experiments with several operators. During the experiment the control of latent reaction periods and confusing errors of operators is made. The symbols are displaying in tahistoscopic mode with different frequencies and porosities of showing symbols. The matrixes of confusing symbols and mean speeds of operators' reactions are made on the basis of obtained data.
The firmware enables to modernize serially in several iterations alphabets' symbols that are slowly and confusingly perceived by operators.

6. Results.

During creating and approving of the program of alphabets' analysis and of the firmware the testing experimental investigation was made. There was used Latin and Cyrillic alphabets. Four operators participated in the experiment. As a result of investigation the speed of operators' reaction increased and confusing errors are 5-10 times less.

Fig. 1. The basic character for Latin alphabet.

Fig. 2. The firmware.

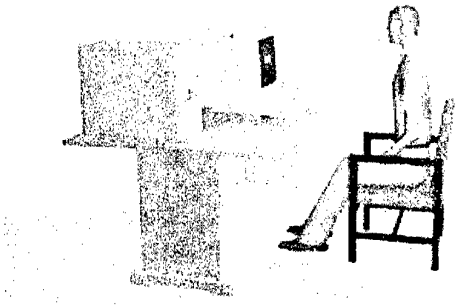

DEA-P3. **Research of Type and Choice Parameters' Optimization Possibility Means of Information Display**

Terent'ev A. U.
Moscow State Institute of Electronics & Mathematics
(Technical University)

While solving a task on choosing the best means of display for a technical task, that really exists, a project manager deals with a task, known as a task of optimal projecting or task of multy-criteria optimization. Until recently, a search for optimal solution for multy-parameter and multy-criteria systems due to the absence of an effective method faced serious technological problems, based on high costs and time spent on research. Most frequently, a 3-d model is used. But 3-d modeling requires a lot of time and finance resources.

Almost every complicated technical decision making task proves to be multy-purpose, because while choosing the best variant one has to consider a lot of various requirements towards the system, among which contrary ones occur. Though almost all of mathematical optimization methods are targeted at finding of one function's extreme point - i.e. for one purpose. That is the reason, why one most often tries to bring a multy-purpose task to a single- purpose one. This procedure in most cases leads to serious alterations in core problem, and thus leads to an incorrect task substitution.

Although while solving a single- purpose task no methodological problems arise, and only calculation problems might occur, multy-purpose solutions are another story. Main nuances here are based on the following alternative: what to consider the best choice in a task with a couple of contrary target functions and reach maximum in various points of multiply alternatives. One of the possible decisive points could be a transit from an absolute value to a relative evaluation, which means evaluation of display equipment based on a complex effectiveness criteria, in other words - complex quality mark. Method transforms into a complex system quality mark determination for each of the considered means and explaining the preference of one quality mark to another.

Software being created allows solving the following tasks: choosing an appropriate means of information display for a stipulated technical task, optimal working mode calculation for existing means of display, construction recommendations for new means of information display.

DEA-P4. **Research of adaptive opportunities of the multimedia equipment**

Morozov I.Yu.
The Moscow state institute of electronics and mathematics
(Technical university)

For any equipment of display of the information the problem of qualitative perception of the information, absence of "losses" of perception of the information the operator in process of dynamically varying external light exposure is actual. Such operating mode is characteristic not only for instrument panels of the automobile and the plane, but also for street advertising and information boards, videowalls (or videocubes), for portable computers (notebooks), used outside of rooms, etc.

At sharp changes of light exposure while in service devices of display occurrence of mistakes of perception because of long readaptation sight of the operator is possible. There are various ways of reduction the influence of jumps of light exposure on reliability of perception of the information the operator. Most perspective of them is the method of change brightness of the image depending on light exposure.

The idea of this method consists that the display units working in conditions of unpredictable varying light exposure, are equipped with system of automatic adjustment of brightness of the image. And, essential difference of the system developed in Research Centre "Elite" from other, already existing systems, that the basic attention is directed on creation of an *intellectual* control system, in view of features of perception of the information the person in concrete conditions, kinds of information models, colors of signs and a background.

For revealing laws of perception of the information by the person at various light exposure in Research Centre "Elite" experiments with various kinds of the Display Units which ultimate goal is revealing dependence according to which it is necessary to change brightness of the display unit at changing external light exposure for the best recognition of the information are carried out.

DEA-P5. **Calculation and designing of the reflecting and transmission displays for achieving the maximal contrast.**

E.A. Naumov
Moscow State Technical University of Electronics & Mathematics, Russia

Paper is not available

DEA-P6. Estimation Of Human-Engineering Characteristics Of Work Of Operator With Display Devices Of Shipboard Control Systems

V.I. Gol'traf, T.A. Goncharova, V.V. Kobzev, and A.V. Nefedovich
AVRORA Corp., Russia

Shipboard systems of control of equipment are the complex engineering systems that ensure running of all-ship systems (heating, ventilation, water supply, etc.), powerplant, electric-power system, and motion control.

Numerous equipment distributed in rooms and located in inconvenient and even inaccessible places and severe service conditions (motions, vibration, noise, long-term operation in sailing conditions, etc.) with limited crew determined the structure of constructing ship systems that are united in the form of a high-automated complex system of control of equipment (CSCE).

The resulting contradiction between, on the one hand, the need for processing a great amount of information in the short time and increasing emotional and psychological loads and, on the other hand, the possibility of human functioning under such conditions necessitated realizing the automated work stations (AWSs) which, apart from conventional elements of the human-machine interface, contain an intellect system of support of decision-making and elements of functional diagnostics.

The operator functions consist mainly in the areas of monitoring operation of the equipment and the decision-making when nonstandard situations arise. The operator work is particularly responsible in localizing emergency situations and in the presence of bad shortage of time for the decision-making when the value of responsibility for the concequences increases. Under these conditions the fraction of mistaken decisions may amount to 10-30% depending on the state, capacity for work, and moral and psychological stability of the concrete operator [1].

From different estimates, up to 40% of all failures of complex engineering systems occur through operator's fault [2]. There are following reasons for mistaken actions [3]: personal qualities (including inattention, unpunctuality, irresponsibility, carelessness, and violation of operative instructions); insufficient level of professional skill and training; improper organization of the work station; and imperfect human-machine interface. The latter reason is related to the most significant sources for mistaken actions of the operator (about 20%).

It is worth noting that when the possibilities for monitoring and control with the use of modern display devices (DDs) are multiply increased, amounts of information flows grow (by a factor of 10-15 as compared to those of the ship systems of the preceding generation) and, correspondingly, the level of intensity of work of operator of control systems grows several times.

Operator works at a control console located in main control room, conning room, or another relatively comfortable room. This console involves the following controls: buttons (buttons-tableau), keyboards, switchs, strain-gage or ball manipulators, and display devices in the form of scattered tableaus and from one to four displays.

Typical problems that are realized using the AWS are the following:

- operative automated equipment control;
- individual remote equipment control;
- representation of information about parts of the running equipment and modes of its operation;
- representation of information about current values of the parameters;
- alarm and warning signalling;
- issue of recomendations;
- input of preset values of the parameters;
-representation of information about parts and state of equipment of CSCE;
- representation of information about values of the parameters in specified time intervals (recording the parameters);
- support of communication between the operators (between control consoles, the consoles and rooms);
- support of call for information when viewing rooms;
- logbook-keeping.

The color displays are used as devices for data representation; together with the keyboard or the strain-gage or ball manipulator, these displays are also employed as control hardware. In the latter case, operator controls the displays using virtual buttons activated by the cursor on the display screen.

Upon such organization of the control and monitoring, the reliable and efficient work of the operator is largely determined not only by the characteristics of the displays, or the imaging terminals, and the computers but also by human-engineering characteristics of interaction between the man and the display.

The color displays, which are used in the shipboard automatic equipment in the Russian Federation, are manufactured in this country or imported. In their characteristics, they meet the requirements for visual human-engineering parameters and parameters of radiation. Their design characteristics comply with the normative documentation: state standards, guide documentation, medical norms and rules for operation with the display devices for the personal use.

In the Russian Federation, the State Standard GOST R 50948-2001 coordinated in visual parameters with the International Standards ISO 9241-3:1996 and ISO 9241-8:1997 is extended to the display devices; its requirements are obligatory upon design, manufacture, service, and certification of displays.

By definition, the human-machine interface is a complex of the software and the hardware whereby the dialog mode of the executing functions is realized in the automated control systems. Development of the interface is based on the criterion of an estimation of the operator's functions. The efficiency (accuracy) of the perception (reading) of information by the operator and the rate of his reaction to the incoming signals are taken as such a criterion. The problem that is related to the maintenance of the optimum conditions for the execution of the operator's control actions on an object is solved in the interests of reliability and in some cases (emergency situations) survivability of the whole ship.

The efficiency of the perception of the visual information as a constituent part of the efficiency of the operator's work depends on a number of the conditions:

- a specified level of the luminance of the visual field;
- a sufficient brightness of an object or a surface, i.e., the proportionality of luminance to the object size, and the required contrast of the background (a difference in the brightness between the object examined and the background);
- a sufficient object size as a relation of the linear object size to the object-observer distance.

The above components of the efficiency are defined in normative documentation, their numerical values given for particular service conditions are determined at the stage of obtaining request for proposal on the development of system as follows:

- level of luminance of the display screen 150-250 lx;
- brightness of an image 80-150 cd/m^2 at image contrast 0.6-0.8.

As to the object size, the human vusual field is limited by the angular dimensions and the accuracy of the reading information is determined by the distance between the screen and the center of the visual field and the distance from it to the operator's eyes. The advisable angles of view in the vertical and horizontal planes from the sight line are reported in some specialized literature [4, 5]. For CSCE when operator sits at a control console at the distance approximately 700 mm from the display screen, the linear dimension of basic prints should be 3-14 mm, which corresponds to the angular dimensions of a symbol in a range of 16-60 ang. min.

Factors in which the process of solving problems by operator manifests itself are the following:

- routes of the motion of a look over the screen;
- duration of the hold of the look at an object;
- frequency of addresses to the object (the absolute number of the holds of the look at the object).

The above factors may be established only in the course of experimental investigations when given regimes are realized by the operator.

Of special urgency is conducting experimental human-engineering estimations in the engineering-decision-making relative to organization of the control when new hardware is developed, in order to determine:

- efficiency of the actions of the operator when solving functional problems including antiemergency problems;
- character and causes of the possible difficulties and the mistaken actions of the operator when interfacing the AWS;
- dynamics of the functional state and the intensity of the operator work in the process of his activity.

The result of our investigations performed on a model (pilot) specimen must form the basis for design of the information-control fields of the consoles and methods of organization of the data representation for the specimens ready to use.

The tests that were performed with participation of permanent operators on one of the model specimens of the CSCE when the consoles set to object simulators reproduced the real situations with monitoring of the actions and states of the operators, suggested that the realization of the human-engineering estimation of the interfacing of the operator with the console in solving his typical professional problems is possible.

In the course of the experiments, the nonstandard and emergency situations related to the failures of the equipment were introduced without warning. The operator's task involved the maintenance of the preset parameters when controlling the objects and monitoring states of the equipment and devices, the reading (with the greatest possible rate and accuracy) of values of the parameters (on inquiries of the experimenter), and the execution of actions in solving antiemergency problems. Sometimes the task to change one or other operative parameter of the equipment was given to the operator.

Upon the simulation of the emergency situations the operator's task was as follows:

- timely detection of an alarm signal;
- identification of the emergency situation;
- execution of the required antiemergency actions.

Before the start of the experiments the operators were acquainted with their tasks and information-control fields of the consoles, were instructed how to act in the simulated nonstandard and emergency situations, and studied the content of the experimental tasks.

The quality of the implementing a task was estimated on the five-mark scale:

- "5", excellently (easily, reliably, and without interferences in the operator's activity);

- "4", well (insignificant interferences and discomforts);
- "3", satisfactorily (interferences and discomforts that hinder non-radically the operator's activity);
- "2", unsatisfactorily (significant interferences and discomforts that lead to the operator's mistakes and hinder his activity);
- "1", badly (drawbacks reducing substantially the operator's activity).

The final estimate is calculated by the following formula:

$$P = \frac{1}{n}\sum_{1}^{n} P_i$$

where P is the average value of human-engineering characteristic (average mark), P_i is the expert estimates of the human-engineering characteristic; and n is the number of experts (a group of experts should be no less than 6 persons).

Then, the values of the efficiency of the operator's activity relative to the system of control of motion which had been obtained experimentally were presented.

The routes of motion of operator's look over the screen with a distribution of attention to the pixels were determined from analyzing the results of a look-recording instrument when the operator solved typical and antiemergency problems of control. The structure of information acquisition was estimated from the videorecording data on motions of the operator's eyes obtained with the help of an instrument (Japan, NAC incorporated firm) fixed on the operator's head.

The duration of the hold of the look made it possible to judge the clearness of information and the easiness of perception of readings, while the routes of the motion of the look were employed for analyzing the process of information retrieval both under standard operative conditions and when nonstandard and emergency situations arose.

With different variants of control from displays using keyboards or manipulators (strain-gage or ball manipulators) and the look-recording instrument, the professiographic analysis of the operator's activity showed that an average time between the presentation of the command and its execution with the strain-gage manipulator exceeded by a factor of 2-2.5 the corresponding time with the keyboard because of the established holds of the look. Implementing typical operations with the cursor update using strain-gage manipulator requires greater visual monitoring and implementation of a significant number of coordinated, differently directed motions of the hand as compared with the actions executed using the buttons of the functional keyboard.

It turned out that the most attention (from 51% to 71,5%) was concentrated on the central part of a videoframe where the mnemonic circuit, which is topologically connected to an object, as well as the current, preset, and predicted control signals are presented graphically. The average duration of the hold of the look ranged from 1 to 1.9 s. With the short holds (0.4-0.6 s), the operator used an additional information from the indicators located in a peripheral part of the screen; in doing so, the routes of the look usually passed through the central part.

It is worth noting that the duration of recording the parameters that fall in the range of the current and preset values is by a factor of 1.5-2 larger than the time of recording analogous parameters that have images in the form of the indicator scales represented on the display screen.

The time characteristics of the actions when operating with menu and inputting preset parameters were also recorded in the course of experiments. Operation of transition from one videoframe to another took, on the average, from 3 to 4 s.

The distinguishability of information when reading information was estimated from the interrogation of the operator relative to values of the parameters imaged on the display screen. An experimenter named the wanted parameter in random order The task of the operator was the fastest search for the given parameter and an accurate answer. In our investigation the readout time (from the beginning of the search to the answer) and its content were recorded. The criterion was the probability of correct answers according to the formula

$$P_{cor} = N_{cor}/N_0 \; x \; 100\%,$$

where N_{cor} is the number of correct answers and N_0 is the total number of answers.

The degrees of the distinguishability of information were estimated on the five-mark scale.

At the same time, with the use of a cardiomonitor, the dynamics of functional state and intensity of work of the operator in the process of his activity was estimated from the data of recording cardiac rhythm. A special computer program of processing these data allowed us to obtain indices of scatter and concentration of the cardiac rhythm. As evidenced by the recorded indices, the operator experienced a moderate intensity when interfacing the control console.

When estimating an efficiency of the work of the operator of the control system for the ship's motion, the problem of precise maintenance of preset parameters was solved when controlling an object and making maneuvers within minimum time. The operations in solving functional problems of stabilization and heading control are rigorously regulated. A predicted information about the tendency for a change in the object's position in space imaged on the display screen favored a more precise control of motion to a great extent.

When analyzing physiological parameters, insignificant changes in the level of nervous and emotional load corresponding to the complexity of

implemented task were revealed. The maximum values of frequency of systols did not exceed 97 beats per minute, which corresponded to the 15-20% increase relative to the background values.

In this experimental investigation the problem of protection of mistakes associated with the shortcomings of design the of displays on the work station was also set.

The characteristic of the distribution of the operator's attention with determination of reserve of attention was constructed by an example of a "Heading manouver" problem. At one time with implementing typical tasks, it was suggested to solve an additional problem. Thus, the color signals on a special tableau were presented in the random order to the operator. With the appearance of such a signal, the operator must react by pressing the button of corresponding color. The time intervals necessary for searching color signals by the operator were recorded with the help of a motion-picture camera.

$$t = \sum \cdot \Delta \cdot \frac{t}{T} \cdot 100 \quad \%,$$

The volume of reserves of attention was calculated by the following formula:

where $\sum \cdot \Delta \cdot t$ is the total reaction time and T is the duration of filming.

The experimental estimation of the reading parameters on the scales from the display screen was performed through the interrogation of the operator in the process of the control of an object. These parameters were interrogated in the random order. The task of the operator involved the most accurate and fastest determination of a value of the parameter. In this case the latent time of the operator's reaction (from the interrogation to the beginning of the answer) and its content were recorded.

The characteristic of the reading parameters from the scales on the display screen when solving the problem of the motion indicates a sufficiently reliable distinguishability of values of the parameters on the scales. In all cases the time of the reading a specified value of the parameter does not exceed 3 s.

When analyzing physiological parameters, insignificant changes in the level of nervous and emotional load, which corresponds to the complexity of implemented task and does not exceed the 20% increase relative to the background values, were revealed.

The dynamics of functions of visual analyzer is determined by the duration of implementing his professional functions by the operator. After continuous 4-h-work (watch) in studying contrast-frequency characteristics of the vision (videograms), no significant changes in the light sensitivity and deep-seated vision occurred, which suggested that the light-engineering and visual characteristics of images of information frames ensure a reliable perception of visual information when the operator works under the conditions of simulated situations.

An analysis of the quality of implementing typical tasks when working with different systems showed that the operators correctly acted on the controls and timely monitored the state of systems in the information field of the displays. The average estimate obtained in the course of experiment on the quality of the control was 4.6 marks.

In the process of implementing typical tasks, however, the experts found some shortcomings:

- information overloading of a number of videoframes with auxiliary information;
- a high videoframe frequency in the process of solving one typical problem;
- complex algorithm of solving the antiemergency problem with insufficient information support of the operator's activity when solving it.

CONCLUSIONS

The use of modern display devices and controls in the shipboard AWSs provides new possibilities for the work of the operators and simultaneously makes necessary a thorough test of human-engineering characteristics by experience.

This test must be realized in the following two directions:

- check of an agreement between the DD characteristics and the requirements of normative documents;
- experimental check of the efficiency of operator's activity when solving the most complex and responsible problems.

The realized estimation of human-engineering characteristics of the work of the operator with the display devices of the shipboard control systems suggested an optimum control with the use of a keyboard-display combination and design of information-control field with allowance made for psychological and physiological characteristics of human-operator.

REFERENCES

1. S.A. Bagretsov "Principles of designing and practical realizing of integrated work-stations of fast control systems" // Problems of psychology and human engineering. No.3. P.58-64 (2001).
2. A.I. Gubinsky "Reliability and quality of functioning of ergatic sytems". Nauka Publishers, Leningrad, 1982.
3. A.N. Anokhin, V.A. Ostreykovsky // Problems of psychology and human engineering. No.1. P.57-61 (1999).
4. M. Schmid "Ergonomic parameters". Mir Publishers, Moscow, 1980.
5. P.Y. Shlayen, V.M. Lvov, P.M. Elizarov "Handbook of engineer and designer on human engineering sciences. Ch.3. Methodology of ergonomic provision of development and exploiting systems controlled and served by a human". Ergotsentr Publishers, Tver, Russia, 1997.

DEA-P7. Graphic Forms of Operating Monitoring and Prediction of Orbital Structures of Satellite Systems

M.Burdaev[a], A. Aylamazyan[b], V.Khachumov[b]

[a]Yu.Gagarin Cosmonaut Training Center, Zviozdnyi Gorodok, Moscow Region, Russia
[b]Program Systems Institute of RAS, Moscow, Russia

One of the most important factors that influence the efficiency of functioning of regular systems of satellites is the stability of their orbital structures. The stability of orbital structures of satellites is the preservation of relative positions in space of all the satellites that enter into system within the prescribed limits on coordinates and time.

The spatial orbital structures of such systems are three-dimensional and dynamic. For this reason, the problem of visual presentation of the relative positions of the satellites in the systems is not only urgent, but also difficult for solution.

One of possible ways of its solution may be the following:

1. The orbital motion of each satellite of the satellite system is represented analytically and geometrically with respect to the conditional orbital coordinate system (COCS) that accompanies the satellite and follows a circular orbit of the radius equal to an average rated value of the major semiaxis of orbits of all satellites of the system. The start of motion of the COCS on this circular orbit is related in time to the instant t_0 with argument of latitude ω_0.

2. The mutual arrangement of circular orbits, on which the COCSs move, and the reference of motions of the COCSs to time correspond to the rated theoretical characteristics of the orbital structure of the satellite system predicted for the time instant relative to which the monitoring is performed. According to the design structure of the system, the unified rated circular orbit is introduced for the satellites that should move in one plane. For each satellite the motion of the COCS on this orbit differs only in the time of passage of preset points (or point).

3. For simultaneous representation and monitoring of relative positions of the system's satellites in all their orbital planes, the COCSs of these satellites are transformed, on the screens of displays, into the unified horizontal orbital coordinate system (UOCS).

The mathematical software for solving the problem involves the analytical and visual parts.

The analytical part contains:

1. Standard algorithms of the information system that is used for solving the problem under consideration, namely:

- the algorithm of calculation, for given time instants, of the osculating elements of circular orbits on which the COCS moves, for all n satellites of the system:

$$\Omega_{0_1}, i_{0_1}, \omega_{0_1}, t_{n_{0_1}}, a_{0_1}$$

.....

$$\Omega_{0_i}, i_{0_i}, \omega_{0_i}, t_{n_{0_i}}, a_{0_i}$$

.....

$$\Omega_{0_n}, i_{0_n}, \omega_{0_n}, t_{n_{0_n}}, a_{0_n}$$

(in particular cases, these parameters in columns can be equal to each other (i_0, ω_0, a_0) or differ by a constant magnitude (Ω_0, t_{n_0}));

- the algorithms of prediction, for given time instants, of the basic elements of real orbits of the system's satellites

$$\Omega_1, i_1, \omega_1, t_{n_1}, a_1, e_1$$

.....

$$\Omega_i, i_i, \omega_i, t_{n_i}, a_i, e_i$$

.....

$$\Omega_n, i_n, \omega_n, t_{n_n}, a_n, e_n$$

2. Its own algorithms of the method for solving the problem:

(a) the algorithm of calculation of the rectangular coordinates {X, Y. Z} of the satellite in the COCS that accompanies the satellite (Fig. 1), in the form of a function of time t.

(b) the algorithm for solving a problem of the fastest calculation of the same coordinates of a satellite in the COCS required for the formation of lines that describe the calculated and real motions of the satellites in the system (Fig. 2).

In order to reach the maximum speed, the eccentric anomaly E is used as an independent variable in this algorithm instead of time. To save the program size, this algorithm can be employed together with the previous algorithm, because some common relationships are used in them.

From a set of the points calculated by the algorithms (a) and (b), the geometrical images are formed which represent the basic characteristics of mutual arrangement and motion of satellites in the system given in the compact and visual form that is convenient for a fast and reliable comparative analysis. These images are the following:

- the synchronous constellation of the satellites representing their mutual arrangement in the orbital plane in the OCS that is unified for all satellites at a single time instant. This constellation is calculated by the algorithm (a).

The position of each satellite in the unified OCS is displayed by a point with coordinates $\{r_i, u_i\text{-}u_0\}$;

- the reference trace of motion of the satellites in an orbital plane in the unified OCS of the system is the basic geometric image. The deviations of the satellite from a given position in the system are visually estimated with respect to this image (Fig. 2, position 1). The trace calculated by the algorithm (b) for $a_i = a_0$ is formed by a set of the points for different values from $0 \le E \le 2\pi$. The number of rated points is chosen practically; these points differ from the points of the previous group by the color and shape of symbols for the trace-forming points;

- the trace of the single satellite, for which a significant deviation of the sizes of basic elements from the average ones of the system (Fig. 2, position 2) is found, is predicted in the unified OCS. The trace is calculated by the algorithm (a) or (b) depending on the available time. This trace is a set of rated points; these points likewise should differ from the points of the previous group by the color and shape of symbols for trace-forming points;

The exact calculation of the relative positions of the system's satellites according to the outlined procedure with regard for real perturbations requires the largest size of the computer program and the greatest computation time in comparison with other computational procedures. For enhancing efficiency of the method examined, the simplifications that insignificantly reduce the accuracy of operative estimations are introduced in it. These are the following:

1. The elimination of considering the perturbations from the algorithms (a) and (b). Such an assumption is based on the fact that a change in the relative positions of the satellites in the system is determined by influence not of absolute perturbations but of their differences that are much smaller.

2. The simplification of considering noncoplanarity of the osculating real orbits of the satellites in the orbital planes of the COCSs corresponding to them. The planes of these orbits are taken to be coplanar. The correction is made only to longitudinal motion to account for the longitudes of ascending nodes. The magnitude of the correction is calculated by the following approximate formula:

$$\Delta u = (\Omega_{osc} - \Omega_{real}) \cdot Cos\, i_0$$

where Δu is the correction to the position of the satellite in the COCS on the orbit and i_0 is the inclination of the conditional circular orbit.

The flow chart and calculation relations of the simplified method for the i-th satellite (Fig. 3) were used by us as a basis for the development of an algorithm and program of operating monitoring and prediction of the orbital structure of the system's satellites.

The visual part of the method including a set of the computer-free operations performed independently by the user is the visual analysis of geometrical images on the screen of display.

An operator estimates visually the following:

- the general mutual arrangement of the satellites in the system by the form of synchronous constellation of the satellites and, more precisely, by comparing this constellation with the reference trace in the unified OCS;

- the correspondence of the maximum and minimum altitudes of the satellite's orbits to the region between their limiting allowable values represented on the screen as two lines of rated altitudes (Fig. 2, position 3);

- the evasive motions of the satellites in their orbits as estimated from the distance between them on the reference trace. For enhancing accuracy of such an estimation, the mask, for example, in the form of a grid of isolines of true anomalies ϑ can be superimposed onto the image;

- the lateral deviations of satellite's positions from the rated ones in the system determined on the separate scale of direct ascentions of the ascending nodes, which indicate the values of Ω for all satellites of the system;

- the approximate value of the allowable time or the angular position for the next correction for the orbit of the satellite deviated from the average orbit as determined from the predicted deviations.

All operations of the visual part of the method can be executed with a computer. The appropriateness of the developed form of indication and the availability of visual part of the method involve: (1) the maintenance of reliable and operating user-computer interfacing; (2) the increase in efficiency of the calculations due to reducing analytical part of the method; and (3) the increase in efficiency and reliability of the estimation of orbital structure of the system due to the compactness and visualization of information presented in the geometric forms.

For convenience of the work with a display, it is necessary to provide, in analytical algorithms of the method, the adjustment of parameters of a rated average circular motion of the COCS, the scales of the images, and the choice of operative regimes as follows:

- -indication of the orbital structure of the constellation for a given time instant;

- -indication of the reference trace for average osculating of motion in the system;

- indication of the predicted trace of the single satellite;

- combined regimes (constellation + reference trace, predicted trace + reference trace, traces of the group of satellites);

- dynamic indication of the synchronous constellation of the satellites for the current time instant;

- modes of the changed time scale.

In order to simplify the construction of visual images and to save the size of the computer programs, the quantities r_i and $u_i - u_0$ can be represented on displays not in polar but in orthogonal systems of coordinates.

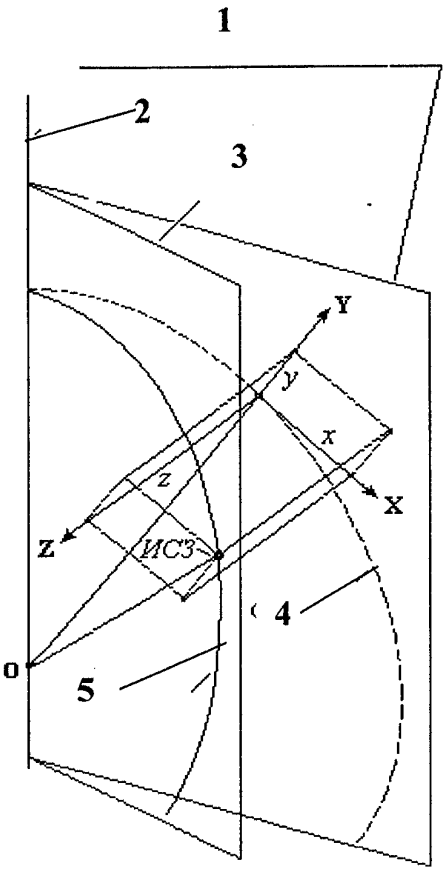

Fig. 1. Rectangular coordinates of the real orbit of the satellite in the conditional orbital coordinate system (COCS). 1. Plane of the orbit of the COCS; 2. Line of the ascending nodes; 3. Plane of the real orbit of the satellite; 4. Orbit of the COCS; 5. Real orbit of the satellite

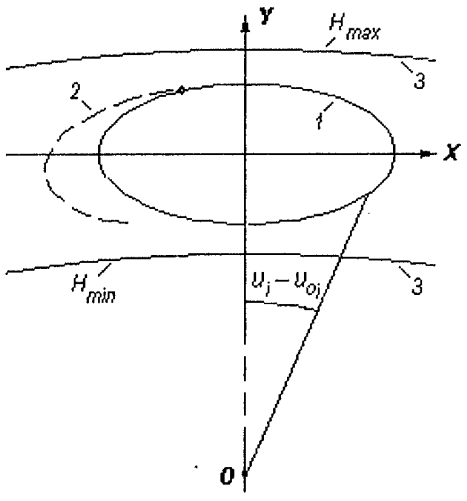

Fig. 2. Lines describing the calculated and real motions of t satellites relative to the COCS. 1. Reference trace; 2. Real t 3. Limitations on altitude

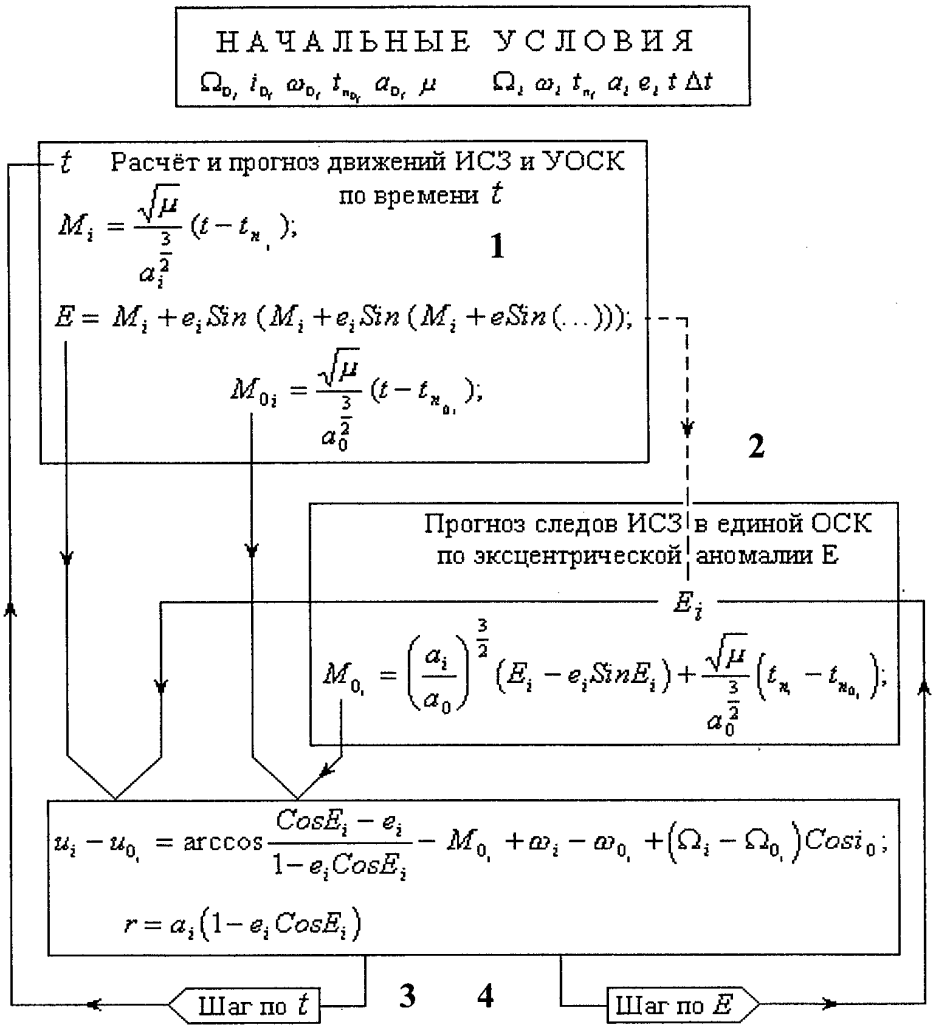

Fig. 3. Flow chart of the algorithm of monitoring and prediction of the orbital structure of the satellite system. 1. Calculation and prediction of motions of the satellites and the COCSs with time t; 2. Prediction of the traces of the satellites in the unified OCS from the eccentric anomaly E; 3. Step in t; 4. Step in E

DEA-P8. **The dynamic architectural display**

Alexander M. Ilyanok,
Atomic and Molecular Engineering Laboratory
220050, St. Kirova 1-50, Minsk, Belarus, Ilyanok@bsu.by

The new paradigm of a large size display construction switching from matrix type light emitting to flat RGB displays controlled by external reflected light with the frame frequency over 75 Hz and self-scanning regular feature is proposed. It allows to create dynamic architectural display for design as instant change of external and internal appearance of buildings without change of the form. The decorating of appearance of the building and its internal rooms is made directly with the help of the computer, using library of the ready images or own models. Architectural display carries out the role of electronic-controlled "wallpaper", made on the base of glass blocks from a usual window glass with a special covering developed on the base of nanotechnology.

Keywords: architectural display, dynamic design, electron cluster

The existing tendencies in architecture and construction are based on harmony of the forms, figures and color spectrum. Thus the design is static. Therefore, at changing of style and fashion the reorganization of buildings and interior of rooms is required. In result it leads to significant financial expenses. We offer the new concept in architecture, which is the "dynamic" design. The "dynamic" is design as instant change of external and internal appearance of buildings (without change of the form) at will and mood of a person. That is, the decorating of appearance of the building and its internal rooms is made directly with the help of the computer, using library of the ready images or own models. And the computer model of the chosen design can instantly be transferred on walls and windows of rooms actually without financial expenses. This idea is somewhat similar to the well known Dr. Zvi Yaniv's kinetic artworks but the technical realization is different and is based on an so called "architectural" display.

In essence, this "architectural" display carries out the role of electronic-controlled "wallpaper", made on the base of glass blocks from a usual window glass with a special covering developed on the base of nanotechnology. The size of the glass blocks can be varied from 1 m^2 up to 10 m^2 and more. Using such glass blocks it is possible to decorate any rooms, not being limited neither size, nor form. It is important, that the materials and paints used in displays, are inorganic and not reduced under solar ultra-violet radiation. The image of such "wallpaper" is formed under action of electrically controlled elements. Thus the energy is consumed only during creation of image (appr. 1 J/m^2). Simultaneously these glass blocks carry out a role of thermal and noise isolation, by analogy with vacuum window glass pack.

It is a flat color display of an unlimited format, and its cost will be in the order of 100$ per sq. meter. Moreover, in contrast to television and computer displays, they operate in reflected light under external illumination. That is, they look like the color polygraphic image that does not tire eyes. It is connected with that the physiological features of a human sight is its perception of the environmental world in reflected light. Therefore, such displays do not have alternative on a problem of preservation of sight and health of the user.

The architectural displays are operating also as electronic-controlled filters, no any more with reflection, but with transmission of light. Such a window can carry out two functions. In the afternoon it forms the desirable image with given transmission factor of solar light. During night it carries out the role of a light screen reflecting light inside of a room. Additionally one can be noted, that this window reflects light in infrared region as well. It allows to reduce sharply the thermal losses from rooms at a cold weather. At a hot weather it on the contrary reflects solar light that prevents superfluous heating of rooms. That is, in essence such windows are electronic-controlled jalousie. And, besides they are good thermal and sound isolators.

We stressed that such architectural display can be used as a car window with controlled light transmission, as well as in advertising industry, in publishing for replacement of paper carriers. And their updatings for the moving images one can use for computer and television displays.

We have developed a hybrid of LCD-CRT having simplified streamer rotation with self-scanning which substantially improved the Shoulder's display technology using electronic clusters (EC) [1]. EC represents spatial formation from several billions of electrons and can move on a surface of dielectric under an external electric field. However, Shoulders's EC is destroyed at emission of electrons on a luminophor. We have found conditions when ECs are stable [2,3]. On the Fig.1 a movable driver from the stable electronic cluster of 30-100 μm in diameter right inside the nanostructured material is shown. Such a cluster can generate average current of 10-100 mA all along the length.

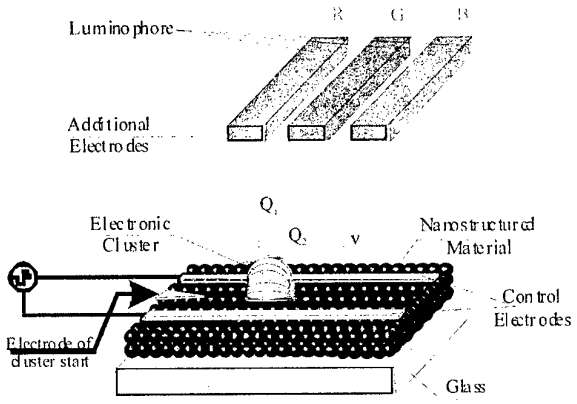

Fig. 1 Electronic cluster row movement.

One or three EC can be use as the movable electronic cluster as an RGB display control element in the self-scan mode. It will travel along a nanostructured film placed on a dielectric substrate at a pace high enough to form the frame frequency up to 120 Hz. The substrate is also connected with control electrodes forming an unbroken "snake" allowing streamer rotation (Fig.2). This bring down the number of control electrodes from 1280X1024 in the HDTV standard to just 15 making the electronic control unit much simpler and less expensive and lowering the level of the display's electromagnetic radiation.

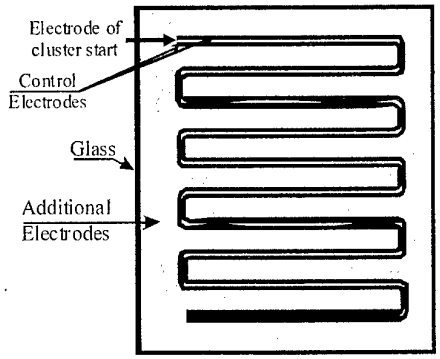

Fig. 2. Constructive version of the display cathode with self-scanning evolvement.

The electrodes can control the pace of the electronic cluster traveling along the nanostructured coating. At the same time additional more electrodes can modify the total amount of the cluster charge or the current going through it which simplifies image formation

The electronic cluster can move in two ways. One way allows the movement within the film itself. When making contact with a light active environment it can control the brightness of electroluminescent materials like, say, in ELD, or change the reflecting/absorbing properties, like in LCD. In the other option, the electronic cluster breaks down into two parts, with one Q_2 still moving within the coating while the other Q_1 emitting into gas or vacuum (Fig. 1). In the latter case, the cloud of free electrons can excite luminofors the way it happens in PDP at the emission into gas, or in the vacuum FED

The color control is carried out with the help of switching of electrodes R, G, B, located on the anode (fig. 3, 4).

Structurally anode and cathode is compounded as glass block, convenient for architectural works. Such glass block simultaneously is perfect thermoisolator and not degrades under action of an environment.

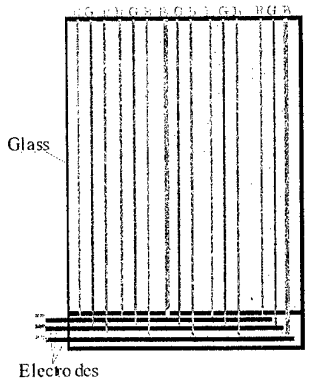

Fig. 3. Constructive variant of monitor anode.

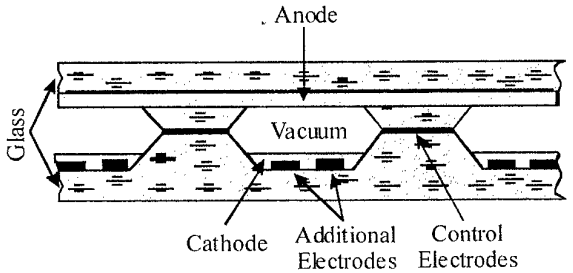

Fig. 4. Constructive variant of the segment of display

At present we have developed the new class of inorganic materials. They are controlled by external electric current and effectively absorbing or reflecting light. It is very important, that in such materials the charge and, hence, image up to the following circle is kept. The static image they can keep long enough. These can be produced only with nanotechnologies, providing for optimization of ergonomic and electrophysical parameters directly at the molecular level. Such materials can completely replace luminofors. The main disadvantage of the streamer rotation currently in use is a frame and line rotation standard mismatch with the prevailing TV and PC standards, requiring a standard matching device. Digital matching presents no problem while analog would have to keep in memory the rotation line which would make TV sets a bit more complicated. The generation of any image is carried out with the help of the computer. More detailed information by principles of work and technology of manufacturing can be received from [2,3]".

We propose to change radically the paradigm of a large size display construction switching from matrix type light emitting to flat RGB displays controlled by

external reflected light with the frame frequency over 75 Hz and self-scanning regular feature [4]. Existing technologies make no room for this paradigm, so new principles of physics as well as advanced technologies, particularly nanotechnologies, must be adopted.

1. K. R. Shoulders, US Patent № 5,018,180
2. A.M. Ilyanok, EA patent № 003164 «Quantum-Size Electronic Devices and Operating Conditions Thereof».
3. Patent application: Ilyanok A.M., PCT/EA02/0008 "SELF SCANNING FLAT DISPLAY" (WO 03/003335 A1 http://www.ipdl.wipo.int). On this application the EA patent are taken out;
4. http://www.e-pag.com/nanotechnologies/display.htm

DEA-P9. **Perspectives of applications of illuminated indicator boards for visual information displaying**

N.S.Severinovsky, K.G. Simforov
JSC «Kiev Factory of Relay and Automatic Machinery», Ukraine

Paper is not available

DEA-P10. **The screen for symbol data representation**

A.N. Shesterkin, O.V. Kuznetzov
Ryazan, Russia

Paper is not available

DEA-P11. **Liquid Crystals 3D Displays**

J. Parka
Institute of Applied Physics, Military Academy of Technology,
2 Kaliskiego Str. 00-908 Warsaw, Poland

Physiological investigations have suggested that some aspects of humane performance are enhanced by the provision of stereopsis. Recent research concerning the evaluation of a variety of stereoscopic displays. Experiments originally intended to explore the superiority of stereoscopic presentation over conventional monoscopic displays have shown improvements in positioning accuracy. A number of peripheral benefits may be realized when empliong stereoscopic CRT video and other techniques. One of them is "LC technique". The TFT-LCD based 3D display system. These kind of LCD panels are operated in a normally white mode to produce a high contrast picture, and a maximum brightness of 150 cd/m^2 [1]. Very interesting proposition was given by Boulder Nonlinear System. High resolution analog spatial modulator (SLM) are widely three-dimensional display industry. The other propositions are to generate the real-time holograms using Optically Addressed Spatial Light Modulators [2].

In this paper we present properties of large optical anisotropies of nematic and smectic liquid crystals which are a very attractive class of materials for dynamic holography applications and other optical devices. Properties of these kind of materials has been studied theoretically and experimentally. Enhancement of ultraphotorefractivity properties of these LC systems in static and dynamic regime will be discussed. The results of our main investigations concentrated on the behavior of thin ($5 \div 20$ μm) cells with pure isothiocyanate nematic liquid crystal with high optical anisotropy ($\Delta n > 0.35$) and doped materials will be presented.

Strong diffraction efficiency dependence on the cell construction was observed. The above mentioned LC mixtures in cells with different photoconductive layers were tested. Our experiments were aimed at optimization of various cell construction parameters, LC mixtures and photosensitive admixtures in respect to demand the highest diffraction efficiency and shortest write/erasing times. Few millisecond writing/erasing times holograms were obtained.

Investigated LC cells seem to be very promising media for optoelectronic dynamic image reconstruction and real-time holograms and optically addressed devices [3, 4]. The first 3D holographic movie with simple object will be presented.

1. D. Song, *3D display systems*, SID Asia Display, pp. 483 – 486, (1998).
2. F. Simoni, O. Francescoangeli, Y. Reznikov, S. Slussarenko, *Dye-doped liquid crystals as a high-resolution recording media*, Opt. Lett. Vol. 22, No 8, (1997).
3. A. Miniewicz, J. Parka, S. Bartkiewicz, A. Januszko, *Liquid crystals as materials for real time holography*, Pure and Appl. Opt. Vol. 7 (2), pp. 179-189, (1998).
4. T. Grudniewski, M. Sutkowski, J. Parka, A. Miniewicz, *The digital holograms projected onto LC cells*, Biuletyn WAT, Vol. LI, Nr 01 (2002).

DEA-P12 Model of Lens Integrator of Projection Systems

S.V. Smagin[a], V.V. Belyaev[b], A.V. Sadchikhin[c], S.N. Sozinov[c]
[a]Moscow Technical University for Radio Engineering, Electronics & Automation,
78, Vernadsky prospect, 117454, Moscow, Russia
[b]Cometa Central R&D Institute, 5, Velozavodskaya str., Moscow, 115280 Russia
[c]AR Technology Co., 1/3, 3rd Kabelnaya str., Moscow, 111024, Moscow, Russia

In projective systems of information displaying one of most important tasks is to achieve good uniformity of the light flux. So-called integrators are used to achieve the uniformity.

The integrator is one of key optical elements in projective system for collective use. It has two functions: a) maintenance of homogeneous distribution of light, and, hence, and almost homogeneous illumination of the screen; b) transformation of circular section of a beam to the rectangular form.

There are two basic designs of such integrators: lens and rod designs.

The rod integrator is a rectangular element with the same aspect ratio as the matrix light modulator. The walls of the rod are high-quality mirrors. The integrator can be filled with air, or can be cast, but the principle of its action is based always on complete internal reflection.

There are two main drawbacks of the rod integrator:

- Optical path required for the integrator and a lens, occupies the most part of optical length of the projection system.
- The multiple reflections can result in essential loss of light in the system, depending on a type of the mirror used.

One of variants of the lens integrator is represented in Figure 1.

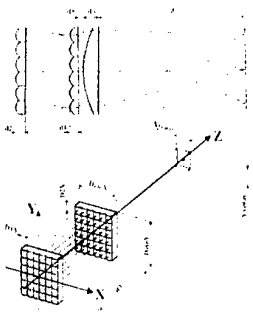

Fig 1. The optical circuit of the lens integrator.

The lens integrator consists of two plates, which can be identical each other or not. The integrator structure includes also an auxiliary lens.

The integrators with two different plates can be more efficient than integrators with two identical plates, but because of manufacture cost the integrators with two identical plates are used more often. Each plate presented on figure 1 is a file of 6x6 of microlenses, where each element has aspect ratio 3x4.

Usually a parallel light beam is required at the input of the lens integrator. Each of 36 microlenses in the first file displays the image of a light source onto the center of a microlens in the second file. It forms the file of 36 virtual sources. Each of microlenses in the second file works as a field lens and, in connection with the auxiliary lens, displays the beam onto the light modulator. For correct functioning of the given system it is necessary to observe a condition of equality of a focal length of the microlenses in each file. The distance between lens files should be equal to the focal length of the microlenses.

A modern projective system of the information displaying is represented at figure 2. The design has the lens integrator raising uniformity of the projection system.

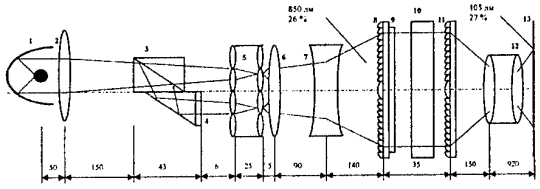

Fig. 2. 1 - parabolic; 2, 6 - lens; 3 -polariser; 4 - l/2 a plate; 5 - integrator; 7 - lens disseminating; 8, 11 - Frenel's lens ; 9 - plate - analyzer; 10 - modulator of light; 12 - objective.

It has performances listed below:

- Non-uniformity of the light flux in a plane of an LCD-matrix is 26 %.

- Non-uniformity of the light flux from the center to the edges is 60 %.
- The size of the LCD-matrix is 6.4 inches (160 mm).

For optimization of parameters of the projective system it is necessary:

- To reduce up to the minimum the heterogeneity of the light flux at the output of the system;
- To remove divergence at the input;
- To ensure changes of the light beam diameter at the input of the lens integrator;
- To ensure necessary aspect ratio at the output of the lens integrator;
- To optimize the number of elements of the integrator.

The purpose of the work is to create a model of the lens integrator with an opportunity of change of any parameter of its optical system in connection with a concrete design of an optical system of the projector.

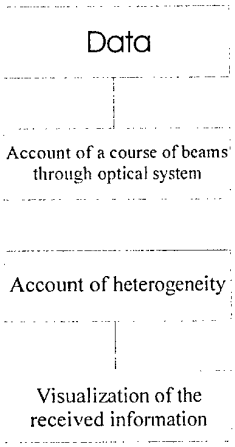

Fig.3. A block diagrams of the model of the lens integrator.

In figure 3 there are given a block diagrams of the model to account the optical system of the lens integrator and to account the beam propagation through all system of the lens integrator with the subsequent visualization. In the given program there are five mainframes:

- Specification of data of the optical system of the lens integrator.
- Calculation of the beam propagation through the optical system.
- Calculation of the beam propagation through the optical system in that case, when the beam is incident onto the boundaries of the lenses.
- Displaying the auxiliary information on graphic objects.
- Development of a program of visualization of the system on two- and three-dimensional diagrams.

In the mathematical model of the lens integrator the optical system, i.e. two files of microlenses and the auxiliary lens, is described through matrixes of moving and refraction, which assist to calculate the beams propagation through the system. As the beam passes through the system of refracting lenses, it is necessary to consider only two basic processes:

- Moving between two refracting surfaces - optical interval.
- Refraction on a boundary surface between two areas with various refraction indices.

Also a calculation of parameters intended for additional service, facilitating perception (recognition) of the graphic information is carried out. This calculations includes following actions:

- Automatic displaying the file of the microlenses at change of parameters;
- Check of a hit of the light beam onto the edges of the microlenses;
- Definition of a type of this hit;
- Check of a hit of beam coordinates onto the illumination area of the first file of microlenses of the integrator;
- Displaying of both basic planes and coordinates of the input and output on 2D diagrams of files of microlenses and the beam propagation in the planes;
- Displaying of basic planes and beam propagation in the optical system on a 3D diagram.

Using the data of the block-programs in one general program, it is possible to not block up all model, and display all stages of calculation on the

monitor, that results in optimization and maximal presentation of both program and model as a whole.

The results of the program are represented in figure 4.

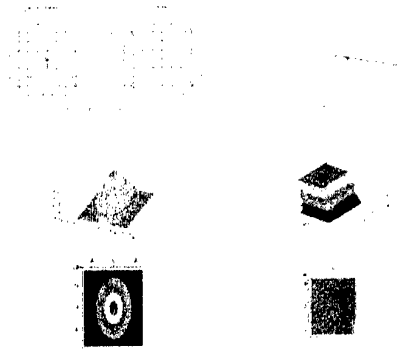

Fig. 4. Display of a course of a beam at hit on a side on 2D and 3D the diagrams. Distribution of intensity on an input and output of optical system линзового of the integrator

At creation of model of the integrator the following task is a calculation of non-uniformity of the light flux from the center to edge on the screen. To solve the task additional programs, specifying and reading files were developed.

The structure of the programs for the calculation of heterogeneity and intensity distribution on the screen is practically identical, but it includes data files of both input, intermediate, and output parameters.

Further, with the help of the programs listed above we define optimum number of microlenses for the parameters given and calculate output parameters of intensity distribution on the screen, and subsequently display the calculation results on 3D and 2D diagrams (figure 4 bottoms).

After displaying input and output distribution of intensity the final calculation of heterogeneity in the screen plane follows.

Results of modeling of a projection system presented at figure 1 are shown in the Table.

Output parameters of the optical system the lens integrator	
Uniformity of the light flux on the output of the system	7 %
Optimum number of microlenses	8 x 8
Aspect ratio on the output of the lens integrator	4 x 3
Transformation of circular section of the beam to the rectangular form	100 %
Minimal structure of the lens integrator	1. Two identical files of microlenses of the integrator 2. Auxiliary projective lens

It is to conclude that a mathematical model of a projection system element (the lens integrator) and a software was developed for the first time to calculate the formation of the homogeneous light flux in the projection systems of the information displaying.

The model developed is universal, i.e. it includes an opportunity to change all input data and parameters of elements of the optical system, such as:

- Focal lengths,
- Refraction indices,
- Curvature radii,
- Thickness of optical elements and distances between them,
- Apertures,
- Distribution of intensity on the input of system.

The model developed allows easily to perceive all deduced information, its reviewing does not block up the calculations.

By using the model the optimum number of microlenses in the lens integrator was found, the heterogeneity of the light flux on the output of projection system is calculated

DEA-P13. Research of an electromagnetic susceptibility of computer displays to magnetic fields of industrial frequency of 50 Hz

Afanas'ev A.I., Krichevsky V.I.
GNPP "TSIKLON-TEST", Russia

Abstract: The research of CRT display electromagnetic susceptibility to magnetic fields of industrial frequency are performed. It is established, that an external magnetic field level, which produce positional instability (jitter) of image on screen, in an essential measure depends on vertical frequency of the display (refresh rate). If the refresh rate is increased from 60 Hz up to 100 Hz, the susceptibility of the display to an external magnetic field is reduced more than on the order.

It is known, that CRT displays are sensitive to external magnetic fields.

In the actual operating conditions with availability of an increased hum noise of a magnetic field of industrial frequency of 50 Hz, it is resulted in emerging such harmful production factor, as positional instability (jitter) of image on a screen.

The situation largely becomes complicated by that in the acting in Russia standards and hygienic norms has a place a discordance of requests on electromagnetic compatibility (electromagnetic stability) displays and requests to environmental conditions on workplaces, where the displays should be used.

The jitter of an image on screens arises already at level of magnetic fields from 200 nT up to 500 nT.

At the same time, the norms on low-frequency magnetic fields in workroom (СанПиН 2.2.4.723-98) suppose levels of these fields up to 100000 nT, and norms on low-frequency magnetic fields in living quarters (СанПиН 2.1.2.1002-00) - up to 10000 nT.

Based on these norms, the power supply systems both industrial, and residential buildings are designed and are accepted in operation now.

The jitter of an images arising during use of displays, at their official certified tests is not revealed (and it can not be revealed).

It happens because now in Russia the check of positional and temporary stability of an image on exposure to low-frequency magnetic fields is not specified.

In the given situation any is not infringed from the normative documents, acting now in Russia.

The manufacturers producing production in the correspondence with established norms of safety and confirming this fact by availability of the certificates of the correspondence and the hygienic conclusions are right.

The trading organizations selling certificated displays are right.

The building organizations realizing mounting of power systems of buildings in the correspondence with the acting sanitarian and building norms are right.

The consumers suffer, and the chiefs of organizations cannot in such situation ensure the safe working conditions on workplaces with PC.

The claims could not be presented.

It is natural, that a cardinal solution of the problem is the decrease of a magnetic hum noise of industrial frequency at 50 Hz by own forces or forces of specialized laboratories.

Source of this hum noise can be power cables and switchboards of a power supply system located near to workplaces.

Besides the reason of origin of a hum noise can be the not compensated currents originating because of incorrectly executed grounding, etc.

The methods of struggle with an increased magnetic hum noise exist.

But frequently they demand the significant financial costs connected to essential reorganization of systems of the power supply - and not only workplaces with PC, but also workrooms, and sometimes and buildings as a whole.

At the same time, to reduce essentially sensitivity of the display to an external magnetic field of industrial frequency at 50 Hz it is possible by only hardware.

The research, conducted by us, show, that this sensitivity depends largely on refresh rate of an image on a screen of the display.

During research the displays are located in the test facility (A Helmholz coil with an external diameter of one meter), which gives on all volume of the display a uniform magnetic field at 50 Hz adjustable in limits up to 100000 nT.

Results of research:

1. A threshold level of a magnetic field (level at which the operator begins visually to fix a jitter of an image) depends on a direction of a vector of a magnetic field in relation to a direction of movement of an electron beam. The maximum sensitivity of the display to a magnetic field (minimum level of a magnetic field) is observed in case, when the vector of a magnetic field is parallel to a direction of movement of an electronic stream. This sensitivity approximately twice is higher, than at other orientation of a magnetic field.

2. The minimum detected threshold level of a magnetic field for displays with a screen 17 " is 180-250 nT, for displays with a screen 14 " - 400-500 nT.

3. As the refresh rate increases the jitter of an image is fixed visually at much higher external fields. The allowable (threshold) level of an external magnetic field for a concrete sample of the display is increased more, than by the order. The experimentally established dependence of a threshold level on a refresh rate for one type of displays with a screen 17 " is represented on Figure.

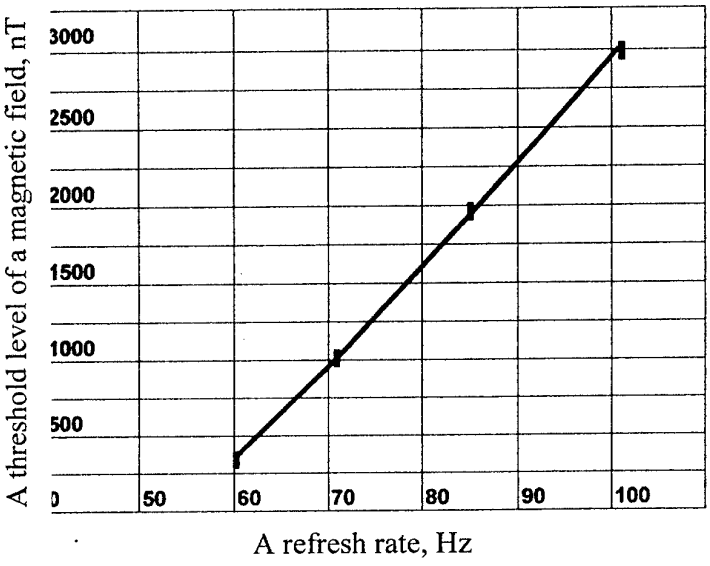

Figure 1. Dependence of a threshold level of a magnetic field on a refresh rate of an image for one from types of displays with a screen 17".

AUTHOR INDEX OF THE CONFERENCE "BASIC STUDIES OF PROBLEMS FOR INFORMATION DISPLAYING" (FLOWERS'03)

PS	-	**Plenar Session**	**p. 15**
ED	-	**Session "Emissive Displays"**	**p. 27**
ED-P	-	**Poster Session "Emissive Displays"**	**p. 40**
NED	-	**Session "Non-Emissive Displays"**	**p. 89**
NED-P	-	**Poster Session "Non-Emissive Displays"**	**p. 111**
DEA	-	**Session "Display Ergonomics and Applications"**	**p. 191**
DEA-P	-	**Poster Session "Display Ergonomics and Applications"**	**p. 216**

Abramov V.	ED-P20
Abanshin N.	ED-5
Afanas'ev A.	DEA-P13
Agabekov V.	NED-P21, NED-P22
Akmaeva T.	ED-P8
Alexeev A.	ED-P16
Andreev A.	NED-P3
Anikin K.	ED-P1
Ariko N.	NED-P21
Aylamazyan A.	DEA-P7
Barannik A.	NED-P9, NED-P12
Bates R.	DEA-9
Belyaev V.	PS-2, NED-P4, NED-P5, NED-P6, DEA-P12
Berdnik V.	NED-P8
Bezludnaya I.	NED-P25
Bobylev Yu.	NED-P3
Bogachov K.	DEA-4, DEA-P1
Bresler M.	ED-P6, ED-P7
Brezhnev V.	NED-P25
Burdaev M.	DEA-P7
Chen B.	NED-P14
Chepeleva L.	NED-P2
Chernopiatov A.	DEA-10
Chigrinov V.	NED-1
Chuvashov A.	ED-P20
Craven M.	DEA-9
Davidov R.	ED-P5
Demirchogljan G.	DEA-6
Denisova Z.	ED-P19
Dlugunovich V.	NED-P22
Dmitrienko A.	ED-P8, ED-P9, ED-P10
Dmitrienko V.	ED-P9
Doroshenko A.	NED-P2
Dorozhkina G.	NED-P26
Efremov M.	NED-6
Ejenkova L.	ED-P16
Ezhov V.	NED-P25
Fedosenkova T.	NED-P3
Fel'dman D.	DEA-P2
Feofanov V.	DEA-5
Filippov V.	DEA-6
Froitzheim A.	ED-P7
Frolov V.	ED-5
Fuks W.	ED-P7
Gerasimov V.	NED-P4
Gerasimova T.	ED-P9
Goltraf V.	DEA-P6
Goncharova	DEA-P6
Gorfinkel B.	ED-3, ED-5, ED-P8, ED-P9, NED-P25
Grebyonkin M.	NED-P5, NED-P6
Gribkova O.	ED-P17
Gusev O.	ED-P6, ED-P7
Gushcho Yu.	NED-11
Gustomiasov I.	DEA-10
Gvozdarev A.	NED-P24
Hazanov A.	ED-P10
Hatanaka Y.	ED-P15
Hopper D.	PS-1, DEA-2
Hreben V.	NED-P22
Ilvutikov R.	NED-P12
Ilyanok A.	ED-P17
Ivanov V.	DEA-P8
Ivanova N.	NED-P21, NED-P22
Ivlyushkin A.	ED-2
Jo W.-H.	ED-P12
Kalashnikov A.	NED-P5, NED-P6
Kalenkov V.	ED-7
Kalinin M.	ED-P14
Kang J.-W.	ED-P12
Karabutov A.	ED-5
Kazarin L.	NED-P4
Khachaturjan V.	NED-8
Khachumov V.	DEA-P7
Kimmel J.	DEA-1
King G.	NED-10
Kirillov S.	ED-P18
Klosowicz S..	NED-5
Kobzev V.	DEA-P6
Kolomzarov Yu.	NED-P17
Kominami H.	ED-P15
Kompanets I.	NED-P3, DEA-3
Kononets Ya.	ED-P19
Konov V.	ED-5
Kornilov V.	ED-6
Korostelin Yu.	ED-4
Korsakov V.	ED-P16
Kozlovsky V.	ED-4
Kosyakov Yu.	ED-P14

Krichevsky V. NED-P1, NED-P2
Krivoshey A. DEA-P13
Krysa A. ED-4
V.Kulishov NED-P1
Kundik V. DEA-6
Kutulya L. NED-P1, NED-P2, NED-P3
Kuznetsov A. NED-P6
Kuznetzov O. ED-4
Kuznetsov P. DEA-P10
Lachinov A. ED-6
Lazarev P. NED-10, NED-P27
Lee Y-K. ED-P12
Lee W. DEA-9
Limonova T. ED-P1
Lin V. ED-P3
Lishik S. ED-7, DEA-8
Litvak I. DEA-4
Loiko V. NED-P7, NED-P8, NED-P9
Lyabin A. ED-P14
Lymarenko R. NED-P20
Lypenko D. ED-P18
Makienko O. ED-P4
Manko A. NED-10
Maltsev E. ED-P18
Martynov V. ED-P8
Mashchenko V. NED-P4
Mikhailova V. ED-P9
Mironenko I. ED-7, ED-P11, DEA-8
Mironov A. ED-P18
Morozov A. NED-9, NED-P23
Morozov A.G. ED-P15
Morozov I. DEA-P4
Nakanishi Y. DEA-7
Nasibov A. ED-P2
Naumov E. DEA-P5
Nazarov V. NED-10, NED-P27
Nefedovitch A. DEA-P6
Neizvestnii I. NED-6
Nekrasov A. ED-P17
Nevskaya G. NED-9, NED-P23, NED-P24
Nikolaev Yu ED-P6, ED-P7
Novoseletskii N. NED-P26
Obraztsova E. ED-5
Oleksenko P. NED-P17
Olifierczuk M. NED-P15, NED-P16
Osipov G. DEA-P7
Ovchinnikova N. NED-P27
Parka J. NED-8
Petrov A. DEA-P11
Petrushenko Yu. ED-P14
Pimenov S. ED-5
Pivnenko M. NED-P1, NED-P2
Pozharov A. ED-5
Popov Yu. ED-4
Posedko A. ED-P11
Posedko V. ED-7, ED-P11, DEA-8
Pozhidaev E. NED-4, NED-P3, NED-P12
Prischepa O. NED-P10
Puisha A. ED-P20
Putilin A. DEA-10
Remizov S. NED-10, NED-P27
Rhee B.-J. ED-P12
G. Rode NED-P1
Rodionov A. ED-P16
Rumyantseva V. ED-P18
Rybalochka A. NED-P18, NED-P19
Sadchikhin A. DEA-7, DEA-P12
Samokhvalov M. ED-P5,
Samorodov V. ED-2
Samsonov V. PS-3
Samsonova I. NED-8
Severinovsky N. DEA-9
Sexton I. DEA-P9
Shabanov A. DEA-11
Shabanov V. NED-6, NED-P9, NED-P12, DEA-11
Shahab S. NED-P21
Shapiro B. ED-P18
Shein I. ED-P10
Shesterkin A. DEA-P10
Shevchenko A. NED-9, NED-P23
Shkolnikova N. NED-P2
Shmakov S. ED-P10
Shoshin V. NED-P3
Shum P. NED-P13, NED-P14
Simforov K. DEA-P9
Simonenko NED-P25
Sivenkov V. ED-7, ED-P11, DEA-8
Skarp K. NED-P19, NED-P20
Skasyrsky Ya. ED-4
Slobodyanyuk A. NED-P20
Slominsky Yu. ED-P18
Smagin S. DEA-P12
SmirnovA. NED-2
Sorokin V. NED-3, NED-P17, NED-P18, NED-P19
Sostchin N. ED-P13
Sozinov S. DEA-7, DEA-P12
Strel'tzov S. NED-8
Strigazzi A. NED-P26
Studentsov S. NED-P25
Sun X. NED-P13, NED-P14
Surman P. DEA-9
Survilo L. ED-P11
Sychov M. ED-P15, ED-P16
Tchurlina E. ED-6
Terekhov S. ED-5
Terent'ev A. DEA-P3
Terukov E. ED-P6, ED-P7
Titarenko P. NED-P17, NED-P19
Tolmachev A. ED-P18
Tolner H. ED-1
Tolochko A. NED-P1
Tomilin M. ED-P20, NED-7
Torgova S. NED-P26
Trofimov Yu. ED-7, ED-P11, DEA-8
Tsaruk A. NED-P22
Tsyrkunov Yu. ED-P19
Udra S. NED-P4
Umanskii B. NED-P26

Valyukh I. NED-P20
Valyukh S. NED-P18, NED-P19
Vannikov A. ED-P17, ED-P18
Vashchenko V. NED-P1
Veligura L. ED-P19
Verbitski V. NED-P22
Verhoturov S. DEA-6
Verhoturov V. DEA-6
Vetrov S. DEA-11
Vishnyakov A. NED-6
Vitukhnovsky A. ED-P1
Vlasenko N. ED-P19
Volodin V. NED-6
Wang Q. NED-P13
Weon S. ED-P12
D. Yastrebov NED-P7
Yoo E.-H. ED-P12
Yow K. DEA-9
Yumaguzin Yu. ED-6
Zelinskyy R. NED-P17
Zharkova G. NED-6, NED-8
Zhbanov O. ED-P9
Zhukov N. ED-3, ED-5, NED-P25
Zielinski J. NED-P15, NED-P16
Zyryanov V. NED-6, NED-P9, NED-P10, NED-P11, NED-P12, DEA-11